THEORY OF SPHERICAL AND CYLINDRICAL LANGMUIR PROBES IN A COLLISIONLESS, MAXWELLIAN PLASMA AT REST

by

James G. Laframboise

JUNE 1966

UTIAS REPORT NO. 100

THEORY OF SPHERICAL AND CYLINDRICAL LANGMUIR PROBES IN A COLLISIONLESS, MAXWELLIAN PLASMA AT REST

by

James G. Laframboise

Manuscript received March 1966

JUNE 1966

UTIAS REPORT NO. 100

ACKNOWLEDGEMENTS

The author wishes to express his special thanks to Dr. J. H. de Leeuw, whose thoughtful supervision provided continuing guidance for this work.

Thanks for the opportunity to conduct this study are extended to the director and faculty of UTIAS.

I am indebted to the Institute of Computer Science, University of Toronto, for use of their IBM 7094 computer.

I would like to thank the many fellow students whose discussions contributed a number of valuable ideas to this project. In particular, I would like to thank K. A. Graf and A. A. Sonin who provided specific experimental information needed to insure that the results obtained were those of greatest possible value.

Thanks are due to Union Carbide Canada Ltd., who for two years provided assistance with fellowships.

This work was supported by the Defense Research Board of Canada, and by the U.S. Air Force Office of Scientific Research under grants AF-AFOSR-366-63, AF-AFOSR-366-64, and AF-AFOSR-366-65.

SUMMARY

A method has been developed and used to obtain theoretical predictions of the current collected from a collisionless, fully Maxwellian plasma at rest by an electrically conducting Langmuir probe having spherical or cylindrical symmetry. The probe characteristic, or functional relation between current and probe potential, has been determined for both geometries for probe radii up to 100 times the Debye shielding distance of the hotter species of charged particle, for a complete range of ion-to-electron temperature ratios and for probe potentials from -25 to +25 times the thermal energy of the hotter species. Each current collection result is computed to a relative accuracy of 0.002 or better in an average time of approximately two minutes on the IBM 7094.

Maxwellian velocity distributions and finite current collection are assumed for both ions and electrons. The infinite plasma is replaced by an outer boundary at a finite radius, beyond which a power-law potential is specified. The resulting nonlinear system of integral equations is solved by an iterative numerical scheme which incorporates an extension of the Bernstein and Rabinowitz method to provide charge densities for ions and electrons. No a priori separation into sheath and quasi-neutral regions is assumed.

Explicit comparison is made between the results for a completely Maxwellian plasma and those for a plasma mono-energetic in attracted particles, as treated by Bernstein and Rabinowitz, Lam, and Chen. It is shown that in certain cases, the mono-energetic plasma does not adequately simulate the Maxwellian plasma.

It is also shown that difficulties encountered by Bernstein and Rabinowitz in computing the ion current for the cylinder in the zero-ion-temperature limit are illusory, and that the computations of Chen for this case do not take into account the fact that the ion temperature acts as a singular perturbation.

Computed charge density and potential functions are presented graphically. Computed probe characteristics are presented in graphical and tabular form. A listing is included of the Fortran programs used to obtain these results.

TABLE OF CONTENTS

SYMBOLS

E	energy
e	one electronic charge
F	force on a particle
f	distribution function; density of particles in position-velocity space
g	inverse of number of particles in a Debye cube
$g(t)$	$= (\sqrt{\pi}/2)\ (1 - \mathrm{erf}(t)\ )\ \exp(t^2)$; function defined in Eq. (E.21)
I	collected current for a spherical probe; collected current per unit length for a cylindrical probe
i	$= I/I_o$; nondimensional collected current
i^*	nondimensional current defined in Eqs. (13.6)
J	angular momentum
k	Boltzmann's constant
$M(r)$	mixing function; Section V
m	particle mass
N	number density
p	momentum
q	charge on a particle
r	radius
R_p	probe radius
R_B	radius of outer boundary
$\underline{r}$	position vector
T	temperature
U	$= Ze\phi(r) + J^2/2mr^2$; effective potential
v	velocity
x	$= R_p/r$; nondimensional inverse radius
Z	number of electronic charges on a particle
z	longitudinal cylindrical coordinate

α	velocity variable; Section VII
α	"varies as"
β	$= E/kT$; nondimensional energy
β^*	$= (-Z_-/Z_+)(E_+/kT_-)$; nondimensional energy defined in Eq.(13.7)
θ	cylindrical coordinate
Φ	integral operator; Section V
ϕ	electric potential
ϵ	permittivity of space
λ_D	Debye shielding distance; $=(\epsilon kT/q^2N_\infty)^{1/2}$
ρ	charge density; $= ZeN$
η	$= \rho/\rho_\infty$; nondimensional charge density
χ	$= Ze\phi/kT$; nondimensional potential
Ω	$= J^2/2m\, R_p{}^2kT$; nondimensional square of probe radius
π_3	$= \chi_p$; nondimensional probe potential
π_6	$= -T_+Z_-/T_-Z_+$; effective temperature ratio
π_7	$= m_+Z_-/m_-Z_+$; effective mass ratio
ξ	$= r/\lambda_{D_-}$; nondimensional radius used in Sec. XIII

<u>Subscripts</u>

+	for positive ions
-	for electrons
+-	for positive ions, but referred to electron temperature; defined in Eq. (9.10b)
0	at plasma potential
∞	at infinite radius
p	at the probe
B	at the outer boundary
G	concerning locus of extrema of effective potentials
M	referring to energy of mono-energetic ions or corresponding absorption boundary

N	for the N'th iteration; Sections V and VI
net	result for ions less result for electrons
r	radial
SE	at the sheath edge; Section XIII
t	transverse
T	thermal
$v_r < 0$	referring to inbound particles
$v_r > 0$	referring to outbound particles

Symbols defined and used in Appendixes only

A,B,C	variables used in Appendix E
a,b,c,d,e,f	variables used in Appendix G
C_E	= 0.57721566....; Euler's Constant; Eq. (E.53)
$F_m(B)$, $H_1(\mu,B)$, $H_2(A)$	functions defined in Eqs. (E.51), (E.46), and (E.68), respectively
$h(\xi)$	function used in Appendix F
h,i,j,k,m,n	integer variables used in Appendices E,F, and G
I_o	zero-order Bessel function of imaginary argument; Eq. (E.75)
K	constant defined in Eq. (A.7); variable defined in Eq. (E.55)
K_0,K_1,K_2	functions used in Appendix D
K_0	zero-order modified Bessel Function of the second kind; Eq.(E.61)
$P(\mu,\lambda)$	two functions defined in Eqs. (E.60) and (E.74)
P,Q,R,T	variables used in Appendix E
S	distance; Appendix A
s	radial variable; Appendices D,E.
s	$= r/\lambda_D$; Appendix F
t	time; Appendix A
t	dummy variable; Appendix F
W	quantity defined in Eq. (E.84)

x,z	dummy variables; Appendix E
y,Y	functions used in Appendix D
y	nondimensional potential, separate definitions in Appendices F and G
b_o,t_c,t_d,S_s,S_d	quantities used in Appendix A
ξ	dummy variable; Appendices E,F
$\alpha,\alpha_G,\epsilon_G,\theta,\Phi,$ $\mu,\kappa,\tau,\lambda,\omega$	quantities used in Appendix E
$\dot{\Psi}$	quantity defined in Eq. (A.1)
$\psi_G(s,s')$	two functions defined in Eqs. (E.32) and (E.87)
σ_1,σ_2	functions used in Appendix F
1	subscript referring to field particles; Appendix A
c,d	subscripts referring to collisions and deflections, respectively; Appendix A.

1. INTRODUCTION

A method has been developed and used to calculate the electric potential and the space charge density near spherically and cylindrically symmetric electrostatic probes immersed in a hot, rarefied, fully Maxwellian plasma at rest, and thereby to calculate the current collected by such probes from the surrounding plasma.

An electrostatic or "Langmuir" probe is a piece of conducting material that is inserted into a plasma on a mechanical support which provides electrical connection from the probe to external circuitry (Fig. 1). The probe potential is varied, slowly enough to eliminate transient effects, over a range that normally includes the plasma potential. The electric current collected by the probe from the plasma is recorded as a function of probe potential. The shape of this curve, known as the "probe characteristic", depends on the composition and the thermodynamic state of the plasma, and is therefore potentially rich in information about the plasma. This fact has enabled the experimenter to use plasma probes as instruments to measure the state parameters of plasmas that exist either in the laboratory or in nature. Figure 2 shows the general appearance of a Langmuir probe characteristic.

Many examples of ionized gases, or plasmas, exist in nature as well as in man-made devices. The earth's ionosphere, the material of the sun and stars, and the interplanetary gas are all naturally occurring plasmas, and Langmuir probes are frequently carried by spacecraft in order to investigate their surroundings.

The local disturbances created in the ionosphere by the entire spacecraft can often be analysed using theories developed for Langmuir probes, since the vehicle itself constitutes a conducting object immersed in a plasma; in this case there is no external connection to allow current to drain off, and the spacecraft will arrive at an equilibrium or "floating" potential at which it collects no net current (Fig. 2). Man-made devices in which plasmas are produced include experiments in controlled thermonuclear fusion, communication devices used in electrical engineering, electric thrusters for space vehicles, and plasma generators for conversion of chemical into electrical power.

Another important type of device is the experimental chamber, often called a "plasma tunnel", designed for the study of the properties of the plasma itself. The study of plasmas in these chambers is in many cases of vital importance in obtaining the basic information necessary before the applications listed above can be carried out. One of the most important types of study carried on in this type of facility has been the development of various methods, including Langmuir probes, for measurement of state parameters, or "plasma diagnostics". The work described herein has been done as part of a combined activity at UTIAS, one aim of which has been to develop and compare the use of Langmuir probes, microwaves, and electron beams for diagnostic work. Details of some of the experimental work that has been done using UTIAS plasma tunnel facilities, closely related to the theoretical investigation of Langmuir probes reported here, are contained in Sec. XVII, and also in Refs. 1,2,3,4, and 19. Specific results obtained here have been used in carrying out experiments described in these reports.

A central problem in the use of plasma probes has been the extraction of the desired values of the thermodynamic state parameters from the information given by experimentally measured probe characteristics. Theoretical work, including that presented here, has centred around the solution of the inverse problem: if one has a plasma of given composition and state, what is the shape of the probe characteristic? Quantitative answers to this question have been obtained as a result of this research, for a range of plasma conditions of broad experimental importance.

A plasma probe which is charged to a potential different from that of the surrounding plasma, will create an electric field which attracts particles of opposite charge and repels those of like charge. If the probe potential is large enough, very few of the repelled particles will have sufficient kinetic energy to reach the probe surface, and a region adjacent to the probe will contain only attracted particles. The net space charge density thus created in this region will be of opposite sign to the charge on the probe, and will tend to prevent electric fields from penetrating into the plasma. This region of charge imbalance is known as a sheath. Beyond the sheath, the densities of repelled and attracted charge are very nearly equal, and the electric field is relatively weak, though still significant.

Any charge imbalance in an ionized plasma sets up electric fields that tend to limit its extent and neutralize it. It has been shown elsewhere (Ref. 1) that the sheath thickness is always related to a plasma parameter known as the Debye shielding distance, which depends on the temperatures and number densities of the various species of charged particles present. The ratio of probe radius to Debye distance is therefore one of the factors that governs the shape of the potential well that surrounds the probe. Since the flux of attracted particles reaching the probe can be strongly affected by the shape and extent of this well, the ratio of probe radius to Debye length has a strong influence on the collected current. Measurements of collected current will therefore contain information about the Debye lengths of the various species.

A charged particle that comes within the influence of the probe is affected in general not only by the macroscopic electric field surrounding the probe, but also by the scattering effect of encounters with other particles. There exists, however, a class of situations, of great importance in experimental work, in which a particle will, on the average, traverse a distance equal to many probe diameters before being appreciably deflected out of its collisionless trajectory by such events. It is then a good approximation to assume that all particles move only along collisionless trajectories, but their initial velocity distribution far from the probe is the Maxwell equilibrium distribution that normally exists when collisions dominate. It is this class of situations that has been considered here. Limits on the validity of the collisionless approximation are discussed in Sec. III and in Appendix A.

The surface of a plasma probe is always at a much lower temperature than the plasma. As a result, nearly all electrons that strike it are absorbed, and nearly all ions that strike it combine with electrons from the surface and move off as neutral atoms. These neutrals do not interact with electric fields and, in the collisionless approximation, are in effect removed from the problem.

At large probe potentials the attracted species strike the probe with sufficient kinetic energy to dislodge charged particles from the surface. Those having appropriate charge are repelled into the plasma and show up as a contribution to the measured probe current (Fig. 2). This phenomenon is called secondary emission. Another source of secondary current collection appears when electrons accelerated to high velocities by the field of the probe collide with neutrals and ionize them to produce extra electrons. Plasma probes are normally operated at potentials small enough to prevent these effects from occurring.

The plasma probes that are used in experimental measurements may have a great variety of shapes. Since the usefulness of such a probe to the experimenter is considerably increased if theoretical predictions of its characteristics are available, the most useful shapes are usually those possessing sufficiently high symmetry that the dynamics of particle motion in the electric fields near the probe are of simplified form. In particular, the cases considered here are those of a sphere or long cylinder in a stationary plasma, or a long cylinder in a plasma flowing parallel to the cylinder axis. In these cases, all particles move in central force fields.

A description of related work on the theoretical prediction of Langmuir probe characteristics is contained in Sec. V, including the pioneering work of Bernstein and Rabinowitz (Refs. 5 and 21) and its extensions by Lam (Refs. 7 and 27) and Chen (Ref. 8), as well as others.

II. STATEMENT OF THE PROBLEM

In order to define a mathematical model for the plasma, the following assumptions have been made:

1. The plasma consists of two species of charged particles, one positive and one negative. Far from the probe, the net charge density approaches zero. Maxwellian velocity distributions are assumed for both species in a reference frame at rest relative to the probe in the spherical case; at rest or in uniform motion parallel to the probe axis in the cylindrical case. The latter generalization is a trivial one, but it suggests that the calculations for the cylindrical probe may be used to measure the properties of a flowing plasma if the probe axis is parallel to the flow and if the probe is sufficiently long that end effects may be neglected. Cylindrical probes are in fact often used in flowing plasmas because of this analytical advantage (Refs. 1 to 4).

In many experimental situations, thermal contact between the two species is weak enough to allow significant temperature differences to exist between them if one of them acts as an energy source or sink. Therefore, an arbitrary temperature ratio is allowed in the theoretical model.

2. The plasma is assumed to be sufficiently hot and rarefied that near encounters between particles are of vanishing importance in comparison with collective phenomena, and each particle moves undisturbed in a macroscopic electric field determined by the Poisson equation. The conditions under which this approximation is valid are discussed in Sec. III and Appendix A.

3. Annihilation of both species of charged particles is assumed to occur at the probe surface. In the situation being considered, in which binary encounters are ignored, re-emitted neutralized particles do not interact significantly with the plasma. As Berstein and Rabinowitz (Ref. 5) have pointed out, their solution method, an extension of which is used here, is capable in principle of dealing with an arbitrary form of charge emission from the probe surface. This method could therefore be used to compute the large potential ends of the probe characteristics if an appropriate model for bombardment-induced secondary charge emission were provided. Such a calculation is beyond the scope of the present work.

4. Finite collection by the probe of both ions and electrons is allowed to occur. In combination with the assumption of Maxwellian velocity distributions for both species, this provision permits the entire probe characteristic to be obtained, in contrast with previous treatments (Refs. 5 to 8) which were applicable only to restricted ranges of probe potentials.

5. No magnetic fields are assumed present.

6. A steady state is assumed to exist.

7. All particle velocities are assumed to be much smaller than the speed of light.

8. In order to define a solution scheme, the infinite plasma surrounding the probe is replaced by a surface, concentric with the probe, at a finite radius. A linear relation between the electric potential and its radial derivative is assumed at this boundary, corresponding to a potential which varies as a specified negative power of radius beyond. Charged particles emitted inward from this boundary possess velocity distributions corresponding to particles Maxwellian at infinite radius, but disturbed by the presence of the given power-law potential.

9. Trapped orbits, if any, are assumed to be unpopulated. The conditions required for the existence of these orbits, which are defined as bounded orbits that do not strike the probe, are discussed in Sec. VIII, together with the resulting implications for the usefulness of results calculated on the basis of this assumption.

III. SCALING PARAMETERS

The net current I_{net} collected from a plasma at rest by a probe of radius R_p is a function of the following quantities:

i) The ion and electron temperatures T_+ and T_-. We define reference energies $E_{T_+} = kT_+$ and $E_{T_-} = kT_-$ where k is Boltzmann's constant.

ii) The ion and electron masses m_+ and m_-.

iii) The ion and electron charges $q_+ = Z_+e$ and $q_- = Z_-e$ where e is one electronic charge and Z is the number of electronic charges per particle.

iv) The number density at infinity of one of the two species, say N_{∞_+}. N_{∞_-} is not an independent quantity because of the plasma neutrality condition:

$$N_{\infty_+} q_+ + N_{\infty_-} q_- = 0 \qquad (3.1)$$

v) The probe radius R_p and probe potential ϕ_p, the latter defined relative to the potential of the plasma far from the probe.

vi) The permittivity of space ϵ .

The complete family of characteristics for either the spherical or the cylindrical probe is therefore a functional relation connecting the 11 quantities I_{net}, E_{T_+}, E_{T_-}, m_+, m_-, q_+, q_-, $N_{\infty+}$, R_p, ϕ_p and ϵ .

Since each of these quantities is expressible in terms of the four dimensions mass, length, time, and charge, there exist seven linearly independent dimensionless quantities such that the solution of the problem is a relation among them. These quantities may be found by inspection. The proof of the foregoing statements may be found in standard works on dimensional analysis, such as Ref. 9.

The complete set of characteristics for either the spherical or the cylindrical probe is therefore of the form F (i_{net}, π_1, π_2, π_3, π_4, π_5, ε_+)=0, where these quantities are defined, by inspection, as follows:

$$i_{net} = I_{net}/(I_+)_0 \quad ,$$

where $(I_+)_0$ is the current of ions that strikes the probe when it is at plasma potential, i.e., the current due to the random thermal ion motion in the absence of electric fields, which for a spherical probe, is given by:

$$(I_+)_0 = Z_+ e N_{\infty_+} R_p^2 \, (8\pi \, kT_+/m_+)^{\frac{1}{2}}, \text{ and for}$$

unit length of a cylindrical probe is given by:

$$(I_+)_0 = Z_+ e \, N_{\infty_+} \, R_p \, (2 \, \pi \, kT_+/m_+)^{\frac{1}{2}} \quad ;$$

$$\pi_1 = E_{T_+}/E_{T_-} = T_+/T_- \quad ;$$

$$\pi_2 = m_+/m_- \quad ;$$

$$\pi_3 = Z_+ \, e \, \phi_p/kT_+ = \chi_{p_+} \quad ;$$

$$\pi_4 = R_p(Z_+^2 \, e^2 \, N_{\infty_+}/\epsilon kT_+)^{\frac{1}{2}} = R_p/\lambda_{D+} = (\gamma_+)^{\frac{1}{2}} \quad ;$$

$$\pi_5 = q_+/q_- = Z_+/Z_- \quad ;$$

$$\varepsilon_+ = N_{\infty_+}{}^{-1} \, (kT_+/Z_+^2 \, e^2 \, N_{\infty_+})^{-3/2} \quad ;$$

The quantities i_{net} and π_3 may be thought of as the nondimensional current and nondimensional probe potential. The symbol $\lambda_D = (\epsilon kT/Z^2 \, e^2 \, N_\infty)^{\frac{1}{2}}$ denotes the

Debye shielding distance of a species of charged particle in the plasma. Therefore π_4 is the ratio of probe radius to the ion Debye distance. The value of g_+ represents the inverse of the number of ions in the volume λ_{D+}^3. The quantities γ_+ and χ_p are nondimensional variables used later in the text, in particular in Sec. IX. Their appearance in Eqs. (3.2) constitutes a definition of them.

It has been shown by Rostoker and Rosenbluth (Ref.10) that in the limit as $g \to 0$ for each species in the plasma, the Liouville equation governing the particle dynamics reduces to a form known as the Vlasov equation, a collisionless-Boltzmann equation in which the force term is obtained from the solution of the Poisson equation.

The limit $g \to 0$ is the limit of a hot, rarefied plasma; $N_\infty T^{-3} \to 0$. It is in this limit that near encounters between charged particles become of negligible importance in comparison with collective phenomena. For any finite value of g, a particle can, on the average, traverse only a certain distance in the plasma before being scattered out of its trajectory by near encounters. This fact sets an upper limit on the probe size for which results obtainable from the Vlasov equation will apply in any given case; in other words, it determines a Knudsen number, or ratio of mean free path to probe dimension, which is a function of R_p/λ_D and g (Appendix A).

By inspection of the equations for the system in their dimensionless form (Sections IX and XI), it can be shown that the ratio $\pi_2 = m_+/m_-$ enters into the computational scheme only when the net current is calculated. This ratio may therefore remain unspecified when the ion and electron currents are computed separately.

It can also be shown that the parameters $\pi_1 = T_+/T_-$ and $\pi_5 = Z_+/Z_-$ occur only as a quotient in the equations, except in the equation for net current. Therefore it is possible to treat these as one quantity for computational purposes. We accordingly define a new dimensionless parameter as follows:

$$\pi_6 = - \frac{T_+}{T_-} \frac{Z_-}{Z_+} \tag{3.3}$$

We therefore have, for either the ion or the electron current in the Vlasov limit:

$$i = i(\pi_6, \chi_p, \gamma_+) \tag{3.4}$$

Usually, $Z_+ = 1$ and $Z_- = -1$, so that π_6 becomes the ion to electron temperature ratio T_+/T_-. For this reason, we will call π_6 the "effective temperature ratio", bearing in mind that the results of the calculations, which are presented as functions of T_+/T_-, may be applied to the case of multiply charged ions by scaling this quantity.

Since the mass ratio π_2 may be left unspecified until net currents are calculated, no distinction exists between ions and electrons in formulating a scheme for calculating i_+ or i_- separately. The nondimensional ion current collected by a probe which is, for example, ion attracting, with given ratios of probe potential to ion energy, ion to electron effective temperature, and probe radius to ion Debye length, is equal to the nondimensional electron current collected by an electron-attracting probe with the same ratios of probe potential to electron energy, electron to ion effective temperature, and probe radius to electron Debye length. It is therefore possible to speak of the "attracted" or the "repelled" species without further identifying them.

Because the roles of ions and electrons can be interchanged in this manner, a complete set of values of $i(\pi_6, \chi_{p_+}, \gamma_+)$ can be used to provide values of both i_+ and i_-, and thereby to obtain the complete set of probe characteristics for a given ion to electron mass ratio. Since the relation between i_{net} and χ_{p_+} (or χ_{p_-}) constitutes a probe characteristic, the solution of the problem for either the spherical or the cylindrical probe is a two-parameter family of characteristic curves.

IV. EQUATIONS DESCRIBING THE COLLISIONLESS PLASMA

The system of equations to be solved is as follows (Ref. 5). Let $\underline{r}$ be the position vector in physical space and $\underline{p}$ be its canonically conjugate momentum vector (Ref. 11). Let $f_+(\underline{r},\underline{p})$ and $f_-(\underline{r}, \underline{p})$ be the distribution functions in position-momentum space for ions and electrons. Let $\underline{v}$ be the velocity vector and t be time. Let $\underline{F}_+$ and $\underline{F}_-$ be the forces exerted by the electric field on ions and electrons. Then the collisionless-Boltzmann equations for a steady-state situation are:

$$\frac{Df_+}{Dt} = \frac{\partial f_+}{\partial \underline{r}} \cdot \underline{v} + \frac{\partial f_+}{\partial \underline{p}} \cdot \underline{F}_+ = 0 \qquad (4.1)$$

$$\frac{Df_-}{Dt} = \frac{\partial f_-}{\partial \underline{r}} \cdot \underline{v} + \frac{\partial f_-}{\partial \underline{p}} \cdot \underline{F}_- = 0$$

The content of these equations is that the distribution functions f_+ and f_- are constant along particle trajectories in a space of canonical coordinates (Appendix B).

The electric forces on the ions and electrons are:

$$\underline{F}_+ = -Z_+ e \frac{\partial \phi}{\partial \underline{r}}$$

$$\underline{F}_- = -Z_- e \frac{\partial \phi}{\partial \underline{r}} \qquad (4.2)$$

Let ρ be the net density of electric charge, and let N_+ and N_- be the number densities of ions and electrons. Then Poisson's equation is:

$$\nabla^2\phi = -\rho/\epsilon \qquad (4.3)$$

where

$$\rho = e(Z_+ N_+ + Z_- N_-) \qquad (4.4)$$

Finally:

$$N_+ (\underline{r}) = \int f_+ (\underline{r},\underline{v}) \, d^3 \underline{v}$$
$$N_- (\underline{r}) = \int f_- (\underline{r},\underline{v}) \, d^3 \underline{v} \qquad (4.5)$$

V. SOLUTION SCHEME FOR COLLISIONLESS-BOLTZMANN EQUATIONS

The most difficult problem in finding a solution scheme for Eqs. (4.1) to (4.5) has been to obtain methods of calculating the number density $N(\underline{r})$ of the attracted species as a functional of potential $\phi(\underline{r})$.

In the case of a spherical probe immersed in a stationary plasma, Allen, Boyd, and Reynolds (Ref. 6) simplified the problem by assuming that the attracted particles had no thermal motion and fell radially inward toward the probe under the influence of the electric field. They also simplified the number density calculation for repelled particles by assuming that the probe was at a large enough potential to prevent any of them from reaching it. By means of this assumption and by invoking the continuity equation for the attracted particles, they obtained an ordinary differential equation which they were able to integrate numerically to give potential as a function of radius for any given value of collected current.

Bernstein and Rabinowitz (Refs. 5, 21) developed a more general scheme capable in principle of finding $N(\underline{r})$ as a functional of $\phi(r)$ for an arbitrary velocity distribution specified far from the probe, under one restriction; namely, that the situation be one possessing sufficiently high symmetry that there exist constants of the particle motion equal in number to the velocity coordinates of the particles. This requirement is satisfied if the particles move in a central force field. They then approximated the velocity distribution for attracted particles by a mono-energetic one in which all such particles far from the probe moved with the same speed, all directions of motion being equally probable. This assumption, toegether with that of zero collection of repelled particles, also gave them a differential equation, which they integrated numerically.

More recently, Lam (Ref. 7) has carried out an asymptotic analysis on the mono-energetic Bernstein and Rabinowitz differential equation in the limit $R_p \gg \lambda_D$, and has obtained probe characteristics valid in that limit, in the cases of very large and very small probe potentials. He has also obtained the leading correction term for expressing mono-energetic current collection as a power series in λ_D/R_p (Ref. 27)

The present treatment, in contrast with these previous ones, assumes a full poly-energetic, Maxwellian distribution for the attracted as well as for the repelled species. As a result, the charge density at any given radius can be shown to depend not only on the local value of the potential at that radius but on the value of the potential everywhere in the vicinity of the probe (Appendix E). The system is therefore not reducible to a differential equation, and a nonlinear system of integral equations results which has been solved numerically on the IBM 7094 digital computer at the University of Toronto. This more general procedure is capable of dealing with the mono-energetic assumption as a special case, and explicit comparison has been made in order to evaluate the errors introduced by this approximation.

The iterative procedure for the numerical solution of the equations is as follows. An initial trial function is assumed for the net charge density. Poisson's equation is integrated to provide the electric potential and its first two radial derivatives, as functions of radius. Using this information, the ion and electron collected currents and charge densities are calculated. The resulting net charge density function is mixed with the previous net charge density to provide a closer approximation to the solution. This process is repeated until sufficient accuracy is obtained.

The process of calculating the ion and electron charge densities from a given net density and subtracting them to give a new net density defines a non-linear integral operator Φ which acts on the N'th iterate $\rho_N(r)$ to give the next iterate $\rho_{N+1}(r)$. The solution to the system is a function which satisfies $\rho(r) = \Phi\rho(r)$. In general, the sequence of functions generated by the operator Φ diverges by overshooting the true solution and oscillating about it with increasing amplitude (Appendix C). We therefore define a mixing function $M(r)$ which has the property $0 < M(r) \leq 1$ for any r. We then define a new iterative scheme as follows:

$$\rho_{N+1}(r) = M(r)\Phi\, \rho_N(r) + (1 - M(r)\ )\ \rho_N(r) \tag{5.1}$$

Inspection of this equation shows that if $\rho_{N+1}(r) = \rho_N(r)$, then $\rho_N(r) = \Phi\rho_N(r)$ as required for a correct solution. An optimum form for the function $M(r)$ is found by computational experiment.

An iterative procedure which resembles in some respects the one developed here, has been developed by Hamza and Richley (Ref. 22) for use in a numerical solution of the Boltzmann-Vlasov equations in a multi-electrode, two dimensional ion-thruster geometry. In this procedure, zero charge density is initially assumed and the two-dimensional Laplace equation is solved numerically for the given boundary conditions. A steady, parallel beam of ions is then introduced. By numerically integrating ion trajectories, the resulting charge density is calculated; the Poisson equation is then solved to find a new potential configuration. If this new potential is then used as a basis for another iteration, and the procedure is repeated a number of times, it is found to diverge; convergence has been obtained by mixing each successive potential with the initial potential obtained by solving the Laplace equation. The mixing function is called a "suppression factor". There is one important difference between the procedure used here and that of Ref. 26: no solution of the Laplace equation is used here as part of a mixing scheme because such a potential at large radii has the wrong dependence on radius (Table 2) and would cause unacceptably large perturbations in charge densities.

A number of approaches to the problem of obtaining probe characteristics for a completely Maxwellian plasma have recently been published. Hall (Refs. 23, 24, and 25) has described a number of steps leading toward the development of a computation scheme based on an assumed form for the locus of extrema in energy vs angular momentum space (Sec. VIII); he approximates the locus of extrema by a pair of line segments and then iterates to find the best possible positions for these lines according to criteria which he has derived. Based on this method, he has obtained and graphically displayed the first two terms in an expansion for the ion current collected by a cylindrical probe in a Maxwellian plasma, valid in the limit of zero ion-to-electron temperature ratio (Ref. 25).

Maskalenko (Ref. 26) has formulated the general problem for the cylindrical probe, including expressions for charge density and flux for the Maxwellian case. He then specializes to the limiting case of large R_p/λ_{D_-} and outlines a computation scheme for this limit. At this date he has not yet published any computed results.

Walker (Ref. 28) has formulated the Maxwellian problem for an ion-attracting spherical probe at sufficiently large potential to assume negligible electron collection . He has published a single-parameter family of probe characteristics which depend only on R_p/λ_{D_-} and have apparently been done for an ion-to-electron temperature ratio of 1, although this point has not been specified. Few details are given concerning the computation scheme, which is said to involve no iterative procedure, but only an inward integration from a set of arbitrarily chosen conditions at some relatively large radius; as in the mono-energetic solutions of Bernstein and Rabinowitz (Refs. 5 and 21) the probe radius is left unspecified. From the point of view of this investigation, it is difficult to see how this can be done without introducing some unspecified approximation, since unlike the mono-energetic case, the charge density at any radius in the Maxwellian case depends on the form of the potential over a continuous range, in general, of both smaller and larger radii (Appendix E). Furthermore, in the Maxwellian case, unlike the mono-energetic case, there is no range of situations in which the specific value of the probe radius can be ignored, because there are always some energy levels in the distribution function for which the probe does not lie "hidden" inside the corresponding absorption radii (Sec. VIII).

Reference 29 contains analytic approximations constructed from the probe characteristics of Ref. 28 by a curve-fitting process.

Preliminary results of the computations described in the present treatment have been reported in Refs. 2 and 20.

VI. CALCULATION OF THE CHARGE DENSITIES

The solution of Eqs. (4.1) uses an extension of the method of Bernstein and Rabinowitz (Ref. 5). In situations possessing sufficiently high symmetry, such as those considered here, all particles move in a central force field, and there exist constants of the motion equal in number to the velocity coordinates of the particles. In this case, the integration over velocity space in Eqs. (4.5) can be transformed into an integration over the ranges of these constants. Velocity coordinates are thus eliminated from the problem and particle trajectories need not be calculated explicitly in order to find N_+ and N_- for a given potential function ϕ . The effect of the potential on the particle densities makes itself felt in the existence of forbidden regions in the phase space defined by the constants of the motion. In these regions, no particles can exist and the distribution functions vanish. This method is discussed in detail beginning with Sec. VII.

The elimination of explicit trajectory calculations in this manner is of crucial importance in formulating a scheme for calculating charge densities. A situation possessing less symmetry, and therefore requiring such trajectory calculations, for example, a sphere in a flowing Maxwellian plasma, would involve numerical trajectory computations of such magnitude as to appear prohibitive. This is particularly true for an iterative calculation such as this one, in which ϕ itself is only one member of a sequence of functions ϕ_N

which have the true solution as their limit, and N_+ and N_- must be determined anew during each iteration.

Furthermore each complete set of iterations defines a solution for only one value of nondimensional probe potential and one value of each nondimensional plasma parameter (Eq. 3.4); in a flowing plasma, the flow velocity itself would require the inclusion of additional parameters to describe a given case.

VII. SPHERICAL PROBE

The velocity of a particle passing through any point in a spherical coordinate system may be resolved into a radial component v_r and two transverse components which specify the projection of the velocity vector in a plane perpendicular to the radius. If we take polar coordinates t and α in this plane, then we obtain for either ion or electron number density, from Eq. (4.5):

$$N(\underline{r}) = \int f(\underline{r},\underline{v})dv_r\, dv_t\, v_t\, d\,\alpha \tag{7.1}$$

For all situations to be considered, the distribution function is isotropic at infinity and all electric fields are radial. Hence f depends only on r, v_r, and v_t, and not on α. We may immediately integrate Eq.(7.1) over α to obtain:

$$N(r) = \pi \int_{v_t=0}^{v_t=\infty} \int_{v_r=-\infty}^{v_r=\infty} f(r,v_r,\, v_t)\, dv_r\, d(v_t^2) \tag{7.2}$$

The appropriate constants of the motion are the total energy E and angular momentum J of a charged particle:

$$\begin{aligned} E &= Ze\phi(r) + \frac{m}{2}(v_r^2 + v_t^2) \\ J^2 &= m^2\, r^2\, v_t^2 \end{aligned} \tag{7.3}$$

The inverse relationships are:

$$\begin{aligned} v_r &= \pm \left[2/m\, (E - Ze\phi(r)) - J^2/m^2\, r^2 \right]^{\frac{1}{2}} \\ v_t^2 &= J^2/m^2\, r^2 \end{aligned} \tag{7.4}$$

The integration over velocity space in Eq. (7.2) may now be transformed into an integration over E and J^2.

$$N(r) = \pi \int_{J^2=0}^{J^2=\infty} \int_{\sqrt{E}=-\infty}^{\sqrt{E}=\infty} f(E,J)\, \frac{\partial(v_r,\, v_t^2)}{\partial(E,\, J^2)}\, dE\, dJ^2 \tag{7.5}$$

The limits on the integration over E represent the fact that E goes from 0 to ∞ once for positive values of v_r and again for negative values of v_r. This point is made clearer by the following discussion.

At a given radius in position space, the integration along v_r must be considered separately for incoming particles ($v_r < 0$) and outgoing particles ($v_r > 0$). In any central force field, the incoming and outgoing halves of a particle trajectory are mirror images of each other. Therefore, in any region of the (J^2, E) plane in which an outgoing particle may exist, i.e., which represents a particle trajectory that does not strike the probe, the particle must be counted twice at the radius r, since it appears once inbound and once outbound. Therefore,

$$f(E, J^2)_{v_r > 0} = f(E, J^2)_{v_r < 0} \text{ and } f = 2f_{v_r < 0} .$$

In any region of (J^2, E) space which represents trajectories that strike the probe no outbound particles exist at the radius r. We then have $f_{v_r>0} = 0$ and $f = f_{v_r<0}$. Finally, there exist regions of (J^2, E) space corresponding to particles which do not reach the radius r because they have turned back at larger radii. In these regions, f = 0. The integration may therefore be taken over incoming particles only, with $f = Kf_{v_r<0}$, where K = 0, 1, or 2.

We now examine a sequence of particle trajectories which correspond to a fixed value of E and increasing values of J^2. The trajectories belonging to such a sequence cross any given radius r in an increasingly tangential direction, as can be shown by inspection of Eq. (7.4). The distance of closest approach to the origin r = 0 for particles which come from infinity will always increase with increasing J^2. Therefore there will always be a largest angular momentum J_1 for which particles still strike the probe. (This does not always correspond to grazing incidence at the probe surface; see for example the set of particle trajectories shown in Fig. 4d.) For all values of J^2 from 0 to $J_1{}^2$, it follows that K = 1.

Similarly, for a fixed E, there will always be a largest angular momentum $J_2 \geq J_1$ for which particles still penetrate inward as far as any given radius r; at this radius, a particle with energy E and angular momentum greater than J_2 is forbidden. For values of J^2 between $J_1{}^2$ and $J_2{}^2$, we then have K = 2; for larger values of J^2, we have K = 0.

We evaluate the Jacobian in Eq. (7.5) to obtain:

$$N(r) = \frac{\pi}{m^3 r^2} \int_{E=0}^{E=\infty} \int_{J^2=0}^{J^2=\infty} K(E,J^2) f_{v_r<0}(E,J^2)\, dJ^2 \Big/ \left\{ 2/m(E-Ze\phi(r)) - J^2/m^2r^2 \right\}^{\frac{1}{2}} \tag{7.6}$$

If the velocity distribution does not depend on J, as is the case for all distributions to be considered, then f = f(E) and the integration over J may be immediately carried out over all ranges of J^2 in which the value of K does not change. The result will be the sum of a number of integrated terms, one for each end of each of these ranges. For compactness of notation, we define K_n as the value of K corresponding to all values of J between J_{n-1} and J_n where n = 1 or 2. For convenience we also define a zero value of angular momentum J_0. We note that by the definition of K_n we have K_1=1 and K_2 = 2. We then obtain:

$$N(r) = -\frac{2\pi}{m^2}\int_0^\infty dEf_{v_r<0}(E)\sum_{n=1}^{2} K_n \left\{2m(E-Ze\phi(r)) - J^2/r^2\right\}^{\frac{1}{2}} \Bigg|_{J_{n-1}(E,r)}^{J_n(E,r)} \tag{7.7}$$

The value J_1 is both the lower limit of the region in which $K = K_2 = 2$, and the upper limit of the region in which $K = K_1 = 1$. Accordingly, the summation indicated in Eq. (7.7) may be condensed by combining the corresponding pair of terms. In order to preserve compactness of notation, we define quantities K_0 and K_3, which are both zero, and then define the quantity $Q_n = K_{n-1}-K_n$; we then have $Q_1 = -1$, $Q_2 = -1$, and $Q_3 = 2$. Equation (7.7) then reduces to:

$$N(r) = -\frac{2\pi}{m^2}\int_0^\infty dEf_{v_r<0}(E)\sum_{n=1}^{3} Q_n \left\{ 2m\ (E-Ze\phi(r)\ ) - J_n^2/r^2\right\}^{\frac{1}{2}} \tag{7.8}$$

where

$$0 = J_0 \leq J_1\ (E) \leq J_2\ (E,r)$$

This formal way of expressing the number density N(r) will prove to be of advantage later in calculating specific values of this quantity. In a number of situations, it will be found that some or all of the quantities J_0, J_1, and J_2 will coincide in certain ranges of E, and the summation in Eq. (7.8) will consist of fewer than the indicated three terms in these same ranges of E. These points will become clear later (Appendix E).

We see that the integration over velocity space in Eq. (7.1) has been reduced to the calculation of a set of line integrals over paths $J_n^2(E)$ in the (J^2,E) plane. These paths are characterized by the fact that K takes on different values on either side of them. It is therefore necessary to consider within what regions of the (J^2,E) plane an incoming particle will strike the probe, within what regions it flies by the probe and within what regions its existence at a given radius is forbidden. This question is studied in Sec. VIII.

The current of a given species of particle in the plasma, collected by the probe, is given by:

$$I = \left[\ 4\pi r^2\ Ze \int f_{v_r<0}\ (r,\underline{v})\ \left|v_r\right|\ d^3\underline{v}\ \right]_{r=R_p} \tag{7.9}$$

This integration may be transformed in a manner similar to Eq. (7.5), into an integration over (J^2,E) space. Since we intend to study only situations in which $f_{v_r<0}$ does not depend on J^2, the result is:

$$I = \frac{4\pi^2\ Ze}{m^3}\int_0^\infty f_{v_r<0}\ (E)\ J_1^2\ (E)\ dE \tag{7.10}$$

The quantity of interest for experimental measurements is the net current I_{net}, which may be obtained as follows, after Eq. (7.10) has been evaluated for each of the species of charged particles:

$$I_{net} = I_+ + I_- = I_+ - \left| I_- \right| \qquad (7.11)$$

In this study the velocity distribution at infinity for each species is taken as a Maxwellian distribution function:

$$f(E) = N_\infty \left(\frac{m}{2\pi k T} \right)^{3/2} e^{-E/kT} \qquad (7.12)$$

For purposes of comparison with work by other authors who employed mono-energetic distributions for the attracted species (Sec. V), we define a mono-energetic velocity distribution corresponding to particles which have no preferred direction of motion and which each possess an equal amount of total energy which we call E_M. If $\delta(x)$ is the well-known Dirac delta function, then this distribution is:

$$f(E) = \frac{m^2 N_\infty}{4\pi} \frac{\delta(E - E_M)}{(2m E_M)^{\frac{1}{2}}} \qquad (7.13)$$

An energy E_M must now be chosen which will cause the mono-energetic distribution to best approximate the Maxwellian distribution which corresponds to the temperature T. In order to do this, we choose the value of E_M which will cause a low-order moment of the mono-energetic distribution to coincide with the same moment of the Maxwellian. It has been suggested by Chen (Ref. 8) that the most suitable moment is the random flux; this equates the current collected by a probe at plasma potential. Equating this for both distributions, we obtain, for the spherical probe:

$$E_M = \frac{4}{\pi} kT \qquad (7.14)$$

VIII. ANALYSIS OF PARTICLE ORBITS

If we eliminate v_t from Eqs. (7.3), we obtain:

$$E - (Ze\phi(r) + J^2/2mr^2) = m\, v_r^{\,2}/2 \qquad (8.1)$$

The term $J^2/2mr^2$ in this equation expresses the effect of angular momentum of circumferential motion of a particle on its radial motion. The form of this equation shows that this term is in effect a repulsive contribution to the potential energy. Accordingly, we define as follows an effective potential energy U for the motion of a particle possessing angular momentum $\pm$ J:

$$U = Ze\phi(r) + J^2/2mr^2 \qquad (8.2)$$

A particle with a particular J^2 and E can reach a particular r only if $E - U(r) \geq 0$. The relation E = U defines a straight line in the (J^2,E) plane, having a positive slope equal to $1/2mr^2$. Below this line, particles cannot exist. This line will therefore be called the "cutoff boundary" corresponding to the radius r.

It is also possible for a particle which is not prohibited from a particular r by the $E < U$ condition to be prevented from penetrating inward to this radius by a potential barrier at a larger radius. In other words, a particle corresponding to the values E and J^2 will exist at a particular r if and only if $E \geq U(r')$ for all $r' \geq r$.

Any particle able to exist at the probe surface will be absorbed by the probe. Therefore, unless potential barriers exist at larger radii, all particles will be absorbed by the probe above the line:

$$E = Ze\,\phi_p + J^2/2\,mR_p^{\,2} \tag{8.3}$$

The general appearance of the (J^2, E) plane is shown in Fig. 3a for an attracting probe ($Ze\,\phi_p < 0$ for the species under consideration) and in Fig. 3b for a repelling probe ($Ze\,\phi_p > 0$), unless potential barriers intervene.

These diagrams are drawn for some specific radius r. They show the location of the cutoff boundary corresponding to this radius; they also show the location of the line corresponding to Eq. (8.3), which represents the cutoff boundary corresponding to $r = R_p$. Values of the integer Q defined in Sec. VII, corresponding to these boundaries and to all other boundaries across which the integer K (Sec. VII) changes, are also shown. The quantities β and Ω shown in these diagrams are nondimensional equivalents of E and J^2 defined in Sec. IX. For an attracting probe, it can be shown that potential barriers do not intervene to alter these diagrams if potential falls off with increasing radius sufficiently slowly; for a repelling probe, the necessary condition is that the potential be monotonically decreasing. These statements are discussed in greater detail later in this section.

It is now necessary to examine the influence of potential barriers on these diagrams.

Figures 4a and 4b show families of curves of effective potential U as a function of r, sketched for various values of J^2, corresponding to attractive potentials $Ze\phi(r)$ which decay more rapidly or more slowly than an inverse square potential, respectively. Examination of the expression for U (Eq. 8.2) shows that if $\phi(r)$ decreases more steeply with increasing r than an inverse square law, then the term $J^2/2mr^2$ will dominate at large enough radii and the term $Ze\phi(r)$ will dominate at small radii. Since $J^2/2mr^2 > 0$ for any non-zero value of J, and $Ze\phi(r) < 0$ for an attractive potential, the effective potential will have a maximum at some value of r. For a larger value of J^2, this maximum will occur at a smaller radius. If $\phi(r)$ decreases more slowly than an inverse square potential, then the term $J^2/2mr^2$ will dominate at smaller radii, and the term $Ze\phi(r)$ will dominate at larger radii, producing a minimum in $U(r)$.

As Fig. 4a illustrates, if a maximum occurs in a curve of effective potential corresponding to a particular value of J^2, all particles coming from infinity whose trajectories correspond to that value of J^2 and to energies E less than the value of U at the maximum, are prevented from penetrating inward past the maximum and therefore do not reach the probe. Therefore, if an attractive potential $\phi(r)$ is a steeper function of r than an inverse square, potential barriers exist which decrease the current collected by the probe.

We now examine, with reference to Fig. 4a, a sequence of trajectories corresponding to some given energy E, and to increasing values of J^2. As J^2 is increased, the corresponding curve $U(r)$ moves upward until the maximum in this curve becomes equal to E. No trajectories corresponding to larger J^2 can reach the probe, or even penetrate inward as far as the radius at which the maximum of $U(r)$ is just equal to E; we will call this radius $r_M(E)$. We also see that any particle with energy E that does penetrate inward to this radius must have an angular momentum small enough that it will reach the probe and be absorbed by it; we therefore call $r_M(E)$ the absorption boundary corresponding to the energy E. Figure 4d shows such a sequence of trajectories, and also shows the location of $r_M(E)$. As E is increased, $r_M(E)$ is decreased, until for sufficiently large E, $r_M(E) = R_p$. For larger values of E, there exist no corresponding absorption radii, and the maximum value of J^2 for which such particles still strike the probe is given by Eq. (8.3). A sequence of trajectories corresponding to such a value of E, and increasing values of J^2, is shown in Fig. 4c. For such a sequence of trajectories, i.e. when no absorption radius $r_M(E)$ exists for the energy E, current collection is said to be "orbital-motion-limited" at the energy E.

The orbital-motion-limited current represents the maximum current of particles of energy E that can be collected for a given probe potential and given distribution of such particles at infinity, in the collisionless case. This is true because the presence of potential barriers can only decrease the number of particles of this energy which reach the probe. If the current is orbital-motion-limited for all values of E corresponding to particles which come from infinity, then it is simply described as orbital-motion-limited. This terminology has been used by previous authors, though it may be considered as not very illuminating.

We now examine a sequence of cases in which the probe potential and all other nondimensional parameters are held constant except that the ratio of probe radius to Debye length is increased. Since the thickness of the sheath adjacent to the probe is always of the order of a few Debye lengths (Sections XV and XVI) the potential well surrounding the probe will contract and steepen, and, in general, an increasing number of particles will be prevented by potential barriers from reaching the probe, so that the collected current will decrease. Since there is always a largest energy E for which there still exists outside the probe an absorption radius $r_M(E)$, we expect that this largest E, which we call E_H, will increase as R_p/λ_D is increased.

We may now infer some differences which we may expect to see in the collected current as R_p/λ_D is increased, depending on whether the distribution of attracted particles is Maxwellian or mono-energetic. First, the current collection for mono-energetic particles need only be orbital-motion-limited at one energy in order to be completely orbital-motion-limited, so we expect current collection in this case to remain orbital-motion-limited for larger values of R_p/λ_D. Also, we may expect current collection in this case to decrease more suddenly once it is no longer orbital-motion-limited, since in the Maxwellian case current collection is an integral over contributions from many energies, each of which will cease to be orbital-motion-limited at a different value of R_p/λ_D. Both of these expectations are borne out in the computed results (Sections XV and XVI); in fact, in the mono-energetic case, curves of current collection vs R_p/λ_D actually have a discontinuous slope at the value at which current becomes no longer orbital-motion-limited.

Another type of orbit which exists when absorption radii are present is shown in Fig. 4e; this diagram shows an orbit corresponding to the same values of J^2 and E as a particle coming from infinity, but which connects with it nowhere, and originates and ends at the probe surface. This orbit lies entirely inside $r_M(E)$ whereas the other orbit lies entirely outside $r_M(E)$. Such an orbit can only be populated by emission from the probe surface, which we have assumed does not occur, or momentarily, by a collision; the population of such orbits is a negligible problem in comparison with the more serious one of trapped orbits.

Such trapped orbits exist when minima of effective potential occur, such as those shown in Fig. 4b; an example of a trapped orbit is shown in Fig. 4f. Trapped orbits and their implications are discussed in detail later in this section.

A more complicated situation than those of Figs. 4a and 4b is shown in Fig. 5a, which shows a family of effective potential curves, corresponding to various values of J^2, for a case in which the dependence of $\phi(r)$ on r is steeper than an inverse square at some radii, and shallower at others. In this case, trapped orbits, orbits unpopulated because they originate at the probe, and potential barriers, are all present. This situation is typical of potential configurations actually found to exist in many cases; variations of this situation also occur, as discussed later in this section. We also note that in the situation shown, the smallest absorption radius that is present does not lie immediately adjacent to the probe surface but is at some distance from it.

We now proceed to derive a more quantitative manner of dealing with the effects of potential barriers; this formulation will be essential in constructing a calculation scheme.

Since $\nabla^2\phi = -\rho/\epsilon$ and ρ is finite everywhere, $\nabla\phi$ is continuous everywhere. Therefore, ϕ is a continuous, smooth function of r. By its definition, Eq. (8.2), U is therefore a continuous, smooth function of r. Since $\phi \to 0$ as $r \to \infty$, $U \to 0$ also. We also have $E \geq 0$ for any particle coming in from infinity. Therefore, if $U(r) \leq E$ and $U(r') > E$ for some $r' > r$, i.e. if the corresponding orbit is unpopulated at r, then U must have a maximum at some radius r″ larger than r. The maximal value $U(r'')$ must be greater than E.

In Figs. 4a, 4b, and 5a, all points $(r'', U(r''))$, where a maximum or a minimum occurs in a curve of effective potential versus radius, have been joined to generate a curve called a locus of extrema in the (r, U) plane. The orbit corresponding to a given J^2 and E will be unpopulated at the radius r if the locus of extrema attains a value of U greater than E, at the point where it crosses the curve $U(r)$ corresponding to J^2, for any r' greater than r.

The locus of extrema of the curves $U(r)$ is therefore of primary imporantance in the analysis of particle orbits and the determination of $J_1(E)$ and $J_2^2(E,r)$. Each point on this locus of extrema crosses a specific curve of effective potential, corresponding to a specific value of J^2. Furthermore, it crosses at a specific value of U which corresponds to a specific energy level $E = U$. Each point on this locus of extrema therefore corresponds to a particular J^2 and E as well as a particular r; therefore, for a given potential function $\phi(r)$, the locus of extrema iefines a curve in the (J^2,E) plane having r as its parameter. It will be shown below that this curve is a well-behaved function of ϕ and $d\phi/dr$ and always has a positive slope which decreases as r increases. It may, however, contain one or more cusps.

The foregoing statements may now be given a geometrical interpretation in the (J^2,E) plane; namely, any point in this plane will be unpopulated at a radius r if any portion of the locus of extrema corresponding to radii greater than r passes above it, i.e., attains a greater E for the same value of J^2.

The defining condition for the locus of extrema is

$$\left(\frac{dU}{dr}\right)_J = 0$$

If we define the subscript G as referring to the locus of extrema, we obtain:

$$J_G{}^2 = mr^3\, Ze\, \frac{d\phi}{dr} \tag{8.4}$$

Substituting this result in the relation:

$$E = Ze\phi(r) + J^2/2mr^2 \tag{8.5}$$

we obtain:

$$E_G = Ze\left(\phi(r) + \frac{r}{2}\frac{d\phi}{dr}\right) \tag{8.6}$$

If Eq. (8.5) is differentiated with respect to r and the resulting equation is solved together with Eq. (8.5) to obtain expressions for J^2 and E, these expressions are identical with Eqs. (8.4) and (8.6). The procedure just described is the standard technique for obtaining the parametric form of the curve which is the envelope of a family of straight lines whose generating parameter is r. This means that the curve $(J_G{}^2(r), E_G(r))$ is the envelope of all the straight lines represented by Eq. (8.5) in the (J^2, E) plane. The locus of extrema is therefore tangent to the straight line given by Eq. (8.5) at the point on the locus corresponding to the conditions at r. The slope of the locus of extrema must therefore decrease toward zero as r increases.

It is now possible to draw the (J^2,E) diagram corresponding to Fig. 5a. This diagram is shown in Fig. 5b. The integration paths $J_n{}^2(E)$ required to integrate Eqs. (7.8) and (7.10) or their cylindrical analogues Eqs. (10.6) and (10.8) can be seen on this diagram. It is instructive to trace in detail these integration paths, in order to obtain a clear picture of what is involved in the integration of these expressions. The integration path $J_0{}^2(E)$ corresponds in this diagram to the line that is labeled AB; the paths $J_1{}^2(E)$ and $J_2{}^2(E)$ correspond to the loci labeled CHF and CHLG, respectively. At larger values of r, the point of tangency of the cutoff boundary (8.5) slides along the locus of extrema. The path $J_2{}^2(E)$ must be modified qualitatively at these larger radii. Figures 6a to 6c show the resulting appearance of the (J^2,E) diagram for three successively larger values of r. In Fig. 6a, $J_2{}^2(E)$ corresponds to the locus labeled CHEG; in Figs. 6b and 6c, $J_2{}^2(E)$ corresponds to the loci labeled CDE and CD, respectively. Qualitative departures from the situation shown may also occur for potentials U(r) which have other shapes, so that the integration paths examined here are only a small sample of the many configurations that are possible.

Some further properties of the locus of extrema are of importance. Examination of Eq. (8.4) for J_G^2 and Eq. (8.6) for E_G shows that both of these quantities are able to take on negative values. For example, J_G^2 will actually do so in the case of either a repelling potential or an attracting one that is non-monotonic in form. It is therefore possible for the locus of extrema to enter any quadrant of the (J^2,E) plane, but since negative values of J^2 are physically meaningless and particles coming from infinity always have $E \geq 0$, this curve becomes of importance only when it enters the first quadrant. Since the locus of extrema is tangent to the cutoff boundary (8.5) at the point $(J_G^2(r), E(r))$, it always has a positive slope which decreases as r increases.

The locus of extrema itself possesses maxima and minima in the (r,U) plane. An extremum in the locus of extrema corresponds to extremal values of both E_G and J_G^2 simultaneously (Fig. 5a), and therefore has two defining conditions, both of which are equivalent. These are:

$$\frac{dE_G}{dr} = \frac{dJ_G^2}{dr} = 0 \tag{8.7}$$

The first relation gives:

$$Ze\left(\frac{3}{2}\frac{d\phi}{dr} + \frac{r}{2}\frac{d^2\phi}{dr^2}\right) = 0 \tag{8.8}$$

The expression for dE_G/dr, which is equated to zero in Eq. (8.8), represents the slope of the locus of extrema in the (r,U) plane. Positive or negative values of this slope correspond respectively to regions containing absorption boundaries or trapped orbits (Figs. 4a, 4b, 5a). Numerical tests of the sign of this quantity therefore provide essential information for the computation scheme by determining the nature of the potential generated during each iteration. This quantity will reappear later in nondimensional form in Eq. (E.29).

Since the locus of extrema always has a positive slope in the (J^2,E) plane, and since dE_G/dr and dJ_G^2/dr always change sign simultaneously, therefore an extremum of the locus of extrema in the (r,U) plane always produces a cusp in the (J^2,E) plane. Two such cusps are visible in Fig. 5b and in Figs. 6a to 6c.

A potential may be envisioned that would be sufficiently irregular in form to cause dE_G/dr and dJ_G^2/dr to change sign several times and therefore produce a locus of extrema having several cusps, corresponding to multiple systems of potential barriers. Situations of this type were in fact found to be generated as transient phenomena by the iterative scheme. In order to continue the calculations beyond this point, it therefore became necessary to incorporate into the program an ability to calculate charge density even in these situations. It was feared that the use of approximate calculations at this stage might disturb the computation enough to keep it from converging to the true solution. It was also considered dangerous to ignore the possibility that in some cases even the final solution might have such a configuration. The detailed study of these multiple-cusp or multiple-barrier potentials, such as that made here, has therefore been an essential part of this investigation.

Figure 7 shows some possible potential configurations, together with the resulting forms of the locus of extrema in the (r,U) plane, and its corresponding forms in the (J^2,E) plane. The 10 specific cases shown in Fig. 8 have been incorporated into the computation scheme.

The dotted curves in this figure represent segments of the locus of extrema which may enter the first quadrant but which do so in such a manner as not to influence any of the particles which strike the probe. For example, the presence of any of the dotted segments in cases 5 and 6 in this figure would represent situations in which the current collection was still orbital-motion-limited, but the charge density at certain radii was affected by potential barriers.

This examination of the behaviour of the locus of extrema has until now considered only the case of an infinite plasma. However, it has been pointed out earlier (Sec. II) that the calculation scheme defined here makes use of an outer boundary at finite radius. In general, the presence of any boundary of this type makes it necessary to modify the preceding discussion; however, it can be shown that no such changes are necessary for the particular boundary conditions specified here. To prove this will be the purpose of the following discussion.

The asymptotic potentials for large radius, $\phi \propto r^{-2}$ for a spherical probe and $\phi \propto r^{-1}$ for a cylindrical probe, derived by Bernstein and Rabinowitz (Ref. 5), lead to the relations:

$$\begin{aligned} d\phi/dr &= -2\phi/r \qquad &\text{spherical probe} \\ d\phi/dr &= -\phi/r \qquad &\text{cylindrical probe} \end{aligned} \tag{8.9}$$

These relations are used as boundary conditions on Poisson's equation at the outer edge $r = R_B$ of the computation net. Appendix D derives in detail the resulting method for integrating the Poisson equation.

Examination of Eqs. (8.4) and (8.6) for a power-law potential $\phi \propto r^{-n}$ shows that the locus of extrema does not enter the first quadrant of the (J^2,E) plane for $n \leq 2$. Since this condition is satisfied in both the spherical and cylindrical cases for the power-law potentials assumed beyond the boundary, the locus of extrema enters the first quadrant only for $r < R_B$. This fact is of advantage in devising the scheme for calculation of the charge densities for $r \leq R_B$. It means that the form of the potential beyond the boundary has no effect on the formulation of these calculations.

As a result, it is possible to calculate both the attracted and repelled charge densities while leaving the precise dependence of potential on radius beyond the boundary unspecified; this dependence enters the problem only as a boundary condition on the integration of the Poisson equation (Appendix D).

The introduction of this power-law boundary condition is of crucial importance in defining a workable computation scheme, because the fact that the assumed potential at and beyond the boundary is a close approximation to the actual potential in the infinite case means that the outer boundary can be placed much closer to the probe without significantly disturbing the computed results than would be possible for the more obvious assumption of a boundary held at zero potential. This matter is discussed in more detail in Appendix H.

It may be seen from Figs. 4b and 5a that if dE_G/dr is positive over some range of radii, a family of minima in curves of effective potential will exist in this range. These minima form potential wells which are capable of trapping particles in bounded orbits that do not strike the probe surface. An orbit of this type is illustrated in Fig. 4f. As Bernstein and Rabinowitz (Ref. 5) have point out, these orbits can be populated by collisions, no matter how infrequently such collisions occur. This effect occurs because these collisions are capable of changing the energy and angular momentum of a particle at some radius to values corresponding to those of any trapped orbits that exist at that radius. A particle thus "knocked into" a trapped orbit will remain in it until another collision knocks it out again. Appendix A imposes a modification on this argument; it is shown there that it is much more common in general for charged particles to be scattered out of their collisionless trajectories by numerous small-angle encounters than by large angle collisions. Thus particles will tend to "drift into" or out of trapped orbits instead of being knocked into them. In any case, the resulting contributions to charge density cannot be calculated by the collisionless theory used here.

Since the assumption has been made (Sec. II) that all such potential wells are unpopulated, the results of this investigation may be of restricted use to the experimenter in any situation where these results predict the existence of potential wells. An exception to this will occur if an experimental situation arises in which the population of these orbits can be shown to be negligible. It may be argued that this occurs for a cylindrical probe; even when the length-to-diameter ratio of the probe is large enough for the infinite-cylinder results obtained here to be useful, the trapped particles may still be expected to leak out of the ends of the geometry rapidly enough to prevent appreciable charge accumulation. Moreover, if the plasma is flowing parallel to the cylinder axis, nearly all trapped particles will be carried downstream by their longitudinal velocity.

This is a fortunate coincidence, because the cylindrical probe can be shown to be always surrounded by trapped orbits, which exist everywhere outside a certain radius. Substitution of $\phi \propto 1/r$, the asymptotic potential for large radii, into expression (8.6) gives a form for E_G whose radial derivative is always positive in the case of the attracted species. As the probe potential is increased, the innermost radius of these trapped orbits moves outward. At sufficiently large probe potentials, a second, inner family of trapped orbits forms adjacent to the probe. The outer boundary of this family then moves outward upon further increase of probe potential.

In contrast with this situation, the spherical probe, whose asymptotic potential $\phi \propto 1/r^2$ is steeper than that for a cylinder, develops only the inner family of trapped orbits. In both the spherical and cylindrical cases, the potential in the vicinity of the probe will be more shallow in form for smaller ratios of probe radius to Debye length, and the inner family of trapped orbits will begin to appear at smaller probe potentials.

It should be noted here that qualitative reasoning of the type presented above to argue for the non-population of trapped orbits around a cylindrical probe, is often dangerous. The final answer to this question must ultimately come from a more complete theory or from experiment.

Although the collisionless theory developed here cannot be used to predict the effect on the collected current of trapped-orbit population, an argument may be advanced to suggest whether the effect will be to increase or decrease the collected current in any given case. If trapped orbits near the probe are populated, the density of the attracted species will be locally increased. Examination of the Poisson equation (4.3) shows that the magnitude of $\nabla^2\phi$ near the probe will be increased, tending to increase the curvature of the potential well near the probe and hence to cause the potential well to steepen and contract. Particles which would otherwise have orbited into the probe will miss it and the collection of the attracted species will be decreased.

This argument is subject to the same warning as the preceding argument. However, it may be made more convincing by examination of a related effect. Calculations have been carried out in this investigation for the case in which the distribution for repelled particles is replaced by one corresponding to the simple "Boltzmann factor" law (Eq. 13.13). This situation corresponds to repelled particles which are not absorbed or annihilated at the probe surface but simply "reflected" by it. These calculations are discussed in greater detail in Sections XIII and XV; their relevance here is that they correspond to an increase in the density of the repelled rather than the attracted particles near the probe and therefore constitute the converse of the effect of populating the trapped orbits. As is shown in Sec. XV, the attracted-species current is in all such cases increased above corresponding values calculated for a completely absorptive probe. Therefore, if trapped-orbit population increases the attracted-species density near the probe, we may indeed suspect that the attracted-species current will decrease. In other words, the results presented here will in this case form an upper bound.

There is one respect in which the two situations discussed here will fail to be the converse of each other. In the "reflecting probe" situation, the increment in charge density will have its largest value at the probe surface, whereas if trapped orbits are populated, the maximum increment will occur at a certain distance from the probe. Furthermore, an increase in attracted-particle density will change the potential everywhere, and situations may be envisioned in which the change is such as to increase rather than decrease the current collection.

IX. NON-DIMENSIONAL EQUATIONS - SPHERICAL PROBE

In order to discard unnecessary groups of symbols and make easier the task of constructing a computation scheme, we now rewrite the expressions developed in Chapter VII in nondimensional form. We therefore introduce the following dimensionless quantities:

$$
\begin{aligned}
\beta &= E/kT & \eta &= \rho/\rho_\infty = N/N_\infty \\
\Omega &= J^2/2m\,R_p^{\,2}\,kT & \tilde{v} &= v\,(m/kT)^{\frac{1}{2}} \\
x &= R_p/r & \tilde{f} &= f/N_\infty\,(kT/m)^{3/2} \\
\chi &= Ze\phi/kT & \gamma &= R_p^{\,2}/\lambda_D^{\,2} \\
\pi_7 &= -\frac{m_+}{m_-}\,\frac{Z_-}{Z_+} & i &= I/(I)_{\phi_p = 0}
\end{aligned}
\qquad (9.1)
$$

The Maxwell velocity distribution (7.12) becomes

$$\tilde{f} = (1/2\pi)^{3/2}\, e^{-\beta} \tag{9.2}$$

The mono-energetic distribution (7.13) becomes:

$$\tilde{f} = \frac{\delta(\beta - \beta_M)}{4\pi\sqrt{2\,\beta_M}} \tag{9.3}$$

From (7.14), we have:

$$\beta_M = \frac{4}{\pi} \tag{9.4}$$

Equation (7.8) for the density of either species of charged particle, becomes:

$$\eta = -2^{3/2}\,\pi \int_0^\infty d\beta\, \tilde{f}(\beta) \sum_n Q_n \left\{ \beta - \chi - \Omega_n(\beta)\, x^2 \right\}^{\frac{1}{2}} \tag{9.5}$$

Poisson's equation (4.3) reduces to:

$$\frac{d^2\chi}{dx^2} = -\frac{\gamma\, \eta_{net}}{x^4} \tag{9.6}$$

Equation (4.4) becomes:

$$\eta_{net_+} = \rho/\rho_{\infty_+} = \eta_+ - \eta_- \tag{9.7}$$

Equations (8.4) and (8.6) become:

$$\Omega_G = -\frac{1}{2x}\frac{d\chi}{dx} \qquad \beta_G = \chi - \frac{x}{2}\frac{d\chi}{dx} \tag{9.8}$$

The above equations, (9.2) to (9.8), together with appropriate tests on the potential χ and its derivatives in order to find the proper values of $\Omega_n(\beta)$, define the iterative scheme necessary to carry out the calculations.

The current collection (7.10) becomes:

$$i = (2\pi)^{3/2} \int_0^\infty d\,\beta\, \tilde{f}\,(\beta)\, \Omega_1\,(\beta) \tag{9.9}$$

If electron current at plasma potential is used as a reference, the net current equation (7.11) becomes:

$$i_{net} = I_{net}/I_{0-} = i_- - i_+\,(\pi_6/\pi_7)^{\frac{1}{2}} \tag{9.10a}$$

A convenient reference current for the ions is that ion current which would be collected by a probe at plasma potential if the effective temperature of the ions were the same as that of the electrons. If we define the ion current nondimensionalized in this manner as i_{+-}, we obtain:

$$i_{+-} = i_+ (\pi_6)^{\frac{1}{2}}$$

The momentum-energy boundaries $\Omega_n(\beta)$ may take any one of four forms. is the nondimensional form of the cutoff boundary relation (8.5):

$$\Omega_n(\beta) = (\beta - \chi(x))/x^2$$

The second corresponds to the probe surface cutoff boundary

$$\Omega_n(\beta) = \beta - \chi_p \, .$$

The third and fourth correspond respectively to zero angular momentum and to the locus of extrema:

$$\Omega_n(\beta) = 0 \qquad (9.1\ldots)$$

$$\Omega_n(\beta) = \Omega_G(\beta) \qquad (9.1\ldots)$$

When these expressions are substituted into Eqs. (9.5) and (9.9), or their cylindrical analogues Eqs. (11.2) and (11.4), the first three of them produce integrals in β that may be evaluated analytically. Expression (9.14) produces integrals that must be evaluated numerically, but may first be transformed into integrations over radius.

These integrations are carried out in detail in Appendix E.

From the definitions of π_6 and χ, we obtain the following relation between the potential nondimensionalized in terms of ion energy and terms of electron energy:

$$\chi_- = -\chi_+ \pi_6$$

Finally, from the definitions of π_6 and γ, and making use of the plasma neutrality condition (3.1), we obtain the following relation between the ratios of probe radius to ion and electron Debye lengths:

$$\gamma_- = \left(\frac{\lambda_{D_+}}{\lambda_{D_-}}\right)^2 \gamma_+ = \frac{Z_-^2 N_{\infty_-} T_+}{Z_+^2 N_{\infty_+} T_-} \gamma_+ = \gamma_+ \pi_6 \qquad (9.16)$$

X. CYLINDRICAL PROBE

For the cylindrical probe, it is convenient to employ the usual coordinates r, θ, z. The number density of either species of particle is then given by:

$$N(\underline{r}) = \int f(\underline{r}, \underline{v}) \, dv_r \, dv_\theta dv_z \qquad (10.1)$$

The appropriate constants of the motion are the energy E and angular momentum J of transverse motion in the (r,θ) plane, and the velocity v_z of motion parallel to the cylinder axis. E and J are given in terms of v_r and v_θ by expressions similar to Eq. (7.3).

It is useful to define a reduced velocity distribution as follows:

$$\hat{f}(E, J) = \int_{-\infty}^{\infty} f(E, J, v_z)dv_z \tag{10.2}$$

We then proceed as in the spherical case, observing that the same discussion about the limits of integration on v_r and v_θ, and hence on E and J, applies once again:

$$N(r) = \int_{v_\theta=-\infty}^{v_\theta=\infty} \int_{v_r=-\infty}^{v_r=\infty} \hat{f}(E,J) \frac{\partial(v_r,v_\theta)}{\partial(E,J)} d\,E\,d\,J \tag{10.3}$$

$$= \frac{2}{m^2 r} \int_{v_\theta=0}^{v_\theta=\infty} \int_{v_r=-\infty}^{v_r=0} \frac{\hat{f}_{v_r<0}(E)K(J^2)d\,E\,dJ}{\left[\frac{2}{m}\left(E-Ze\phi(r)\right)-\frac{J^2}{m^2r^2}\right]^{\frac{1}{2}}} \tag{10.4}$$

$$\frac{2}{m}\int_{E=0}^{E=\infty} d\,E\,\hat{f}_{v_r<0}(E)\sum_n K_n(J^2)\,\text{arc sin}\left\{\frac{J^2}{2mr^2\,(E-Ze\phi(r))}\right\}^{\frac{1}{2}}\Bigg|_{J=J_{n-1}(E)}^{J=J_n(E)} \tag{10.5}$$

$$= \frac{2}{m}\int_{E=0}^{E=\infty} d\,E\,\hat{f}_{v_r<0}(E)\sum_n Q_n\,\text{arc sin}\left\{\frac{J_n^{\,2}}{2mr^2\,(E-Ze\phi(r))}\right\}^{\frac{1}{2}} \tag{10.6}$$

In Eqs. (10.4) to (10.6), the quantities K, K_n, and Q_n are as defined in Sec. VII.

The collected current per unit probe length is

$$I = \left[2\pi r\,Ze\int f_{v_r<0}\,(r,\underline{v})\left|v_r\right| d^3\underline{v}\right]_{r=R_p} \tag{10.7}$$

$$= \frac{4\pi Ze}{m^2}\int_{E=0}^{E=\infty}\hat{f}(E)J_1(E)\,d\,E \tag{10.8}$$

The velocity distribution that is Maxwellian in transverse motion is

$$\hat{f}(E) = N_\infty\,\frac{m}{2\pi kT}\,e^{-E/kT} \tag{10.9}$$

The velocity distribution that is mono-energetic in transverse motion is

$$\hat{f}(E) = \frac{m\, N_\infty}{2\pi} \quad \delta(E - E_M) \tag{10.10}$$

As before, we equate collected currents at plasma potential in order to fix E_M. We first observe that if $\bar{v}$ is the average velocity of particle motion transverse to the cylinder axis, rather than the average velocity of three-dimensional motion, then the number of particles striking the probe surface per unit area per unit time is $N\bar{v}/\pi$ rather than $N\bar{v}/4$.

Equating currents, we obtain:

$$E_M = \frac{\pi}{4} kT \tag{10.11}$$

for the cylindrical probe.

XI. NON-DIMENSIONAL EQUATIONS - CYLINDRICAL PROBE

We define a non-dimensional velocity distribution in terms of the reduced distribution (10.2):

$$\tilde{f} = \frac{\hat{f}}{N_\infty} \frac{kT}{m} \tag{11.1}$$

Equation (10.6) becomes:

$$\eta = 2\int_0^\infty d\beta\ \tilde{f}(\beta) \sum_n Q_n \arcsin\left\{\frac{\Omega_n x^2}{\beta - \chi}\right\}^{\frac{1}{2}} \tag{11.2}$$

Poisson's equation becomes:

$$\frac{d}{dx}\left(x \frac{d\chi}{dx}\right) = - \frac{\gamma\ \eta_{net}}{x^3} \tag{11.3}$$

The current collection equation (10.8) becomes:

$$i = 4(\pi)^{\frac{1}{2}} \int_0^\infty d\beta\ \tilde{f}(\beta)\ (\Omega_1(\beta))^{\frac{1}{2}} \tag{11.4}$$

The Maxwell distribution (10.9) becomes:

$$\tilde{f} = \frac{1}{2\pi} e^{-\beta} \tag{11.5}$$

The mono-energetic distribution (10.10) becomes:

$$\tilde{f} = \frac{\delta(\beta - \beta_M)}{2\pi} \tag{11.6}$$

where:

$$\beta_M = \frac{\pi}{4} \tag{11.7}$$

XII. THE LIMIT OF ZERO-TEMPERATURE REPELLED PARTICLES

A frequently occurring experimental situation is one in which the ion-to-electron temperature ratio is very small compared to unity. In such situations, the positive half or electron collection part of the probe characteristic becomes very difficult to calculate. The ions, which in this case are the repelled species, have relatively little thermal energy and are turned back by a correspondingly small rise in potential. The ion density falls to zero very rapidly as the sheath is entered, and the sheath edge tends to become very sharply defined. Calculations of electron current were found to become very sensitive in these cases. Since these calculations were considered to be of substantial value, it was decided to consider the limiting case of zero repelled-species temperature and modify the computation scheme to obtain the corresponding attracted-species current results. These would then form end-point data for results obtained at progressively decreasing repelled-species temperatures. This modified computation scheme is described here.

We first examine certain expressions for number density $N(r)$ as a function of potential $\phi(r)$, derived in detail in Appendix E. For the repelled species ($Ze\phi_p>0$), these expressions are given by Eq. (E.39) for the spherical probe and by Eq. (E.92) for the cylinder. Examination of these expressions shows that for probe potentials much larger than the repelled-species thermal energy, they both reduce to:

$$N/N_\infty = e^{-Ze\phi/kT} \tag{12.1}$$

This dependence is of the same form as that prediced in general by equilibrium thermodynamics. In the limit $T \to 0$, the value of N given by Eq. (12.1) is zero for $Ze\phi$ positive, and indeterminate for $Ze\phi$ zero. The region outside the probe is therefore split by a sharply defined sheath edge into two regions: a plasma in which ϕ vanishes exactly everywhere and the density of repelled particles is exactly equal to the density of attracted particles; and a sheath where ϕ rises to its value at the probe and from which repelled particles are completely excluded. The density of repelled particles falls discontinuously to zero as the sheath is entered. The electric field is continuous across the sheath edge since no mechanism exists which can produce an infinite charge density there or anywhere else outside the probe. Therefore ϕ and $d\phi/dr$ both vanish at the sheath edge; the inward flux of attracted particles at this radius is entirely due to their random thermal motion. The density of the attracted species outside the sheath is affected by the depletion of these particles by the probe, but since electric fields are zero in this region, this density no longer influences the rest of the problem. The flux of attracted particles reaching the probe is therefore dependent only on the potential distribution in the sheath, and not on conditions outside it. Computations of potential and charge density therefore need to be carried out only inside the sheath. The sheath edge radius is not known in advance, but since no electric fields may penetrate past the sheath edge into the plasma, its position must adjust itself until the total space charge within the sheath exactly cancels the charge on the probe. This condition is equivalent to the vanishing of $d\phi/dr$ at the sheath edge.

These considerations serve to define a boundary value problem in which not only the potential and charge density distributions but also the position of one boundary, the sheath edge, must be found as part of the solution. This problem is solved here in order to calculate the collected current in the limit of zero-temperature repelled particles. Figure 9 shows qualitatively the forms of potential and charge densities as functions of radius. The subscript B is here defined as referring to the sheath edge radius.

The modified solution scheme used to calculate the collected currents is as follows. The boundary condition for $(d\phi/dr)_B$ is relaxed. For a given charge distribution, the boundary conditions $\phi \to \phi_p$ as $r \to R_p$ and $\phi_B = 0$ then serve to define a well-posed two-point boundary value problem for Poisson's equation. (The solution is derived in detail in Appendix D.) An initial trial value is assumed for the sheath edge radius R_B. An iterative procedure is carried out, as in the general case, to obtain the potential as a function of radius, and the collected current. The value thus obtained for the sheath edge potential gradient $(d\phi/dr)_B$ is used to decide whether the assumed sheath edge radius is too large or too small. A second trial value of R_B is computed and the process is repeated. When a sheath edge position is found which produces a sufficiently small sheath edge potential gradient, the calculation is stopped.

The method for calculating the density of attracted particles must be modified in the presence of the zero-potential sheath edge. In order to examine why this is so, we substitute the sheath edge boundary condition $\phi(R_B) = 0$ into the cutoff boundary expression given by Eq. (8.5) and use Eqs. (9.1) to convert the resulting expression into non-dimensional form. We then obtain the following expression for the sheath edge cutoff boundary in the (Ω, β) plane:

$$\beta = \Omega x_B^2 \tag{12.2}$$

This boundary appears in Fig. 10 as a straight line having positive slope and passing through the origin. No particles coming from infinity can reach the sheath edge having an angular momentum and energy corresponding to any point below this line. Therefore, in order to influence the current and charge density, the locus of extrema must now not only enter the first quadrant of the (Ω, β) plane, but must also rise above this line. Figure 10 shows the resulting changes that will occur in Figs. 3a and 6c. As in Sec. VIII, it is instructive to identify the integration paths $J_1(E)$ and $J_2(E)$ with the corresponding loci in Fig. 10. In Figs. 10a and 10b, $J_1(E)$ is represented by the loci ACF and ACHF, respectively; $J_2(E)$ is represented by the paths ABG and ACBG, respectively. Once again, it should be noted that these particular configurations are only a small sample of the many that are possible.

Using Fig. 10a and the notation developed in Appendix E, we obtain the following expression for the maximum current of collisionless attracted particles that may be collected by a probe in the presence of the zero-potential sheath edge at the location $x = x_B$:

$$i = i_2\,(\beta_C) + i_1\,(\beta_C) \tag{12.3}$$

where β_C is the value of β corresponding to the intersection between the lines $\beta = \Omega x_B^2$ and $\beta = \chi_p + \Omega$, which is therefore given by:

$$\beta_C = - \frac{\chi_p}{\frac{1}{x_B^2} - 1} \tag{12.4}$$

For the spherical probe, we substitute Eqs. (E.34) and (E.35) into Eq. (12.3) to obtain:

$$i = \frac{1}{x_B^2}\left(1 - (\beta_C + 1)\, e^{-\beta_C}\right) + (\beta_C - \chi_p + 1)e^{-\beta_C} \tag{12.5}$$

For the cylindrical probe, we substitute Eqs. (E. 89) and (E.90) to obtain:

$$i = \frac{1}{x_B}\left[1 - \frac{2}{\sqrt{\pi}}\, e^{-\beta_C}\left(\sqrt{\beta_C} + g\,(\sqrt{\beta_C})\right)\right] + \frac{2}{\sqrt{\pi}}\, e^{-\beta_C}\left[\sqrt{\beta_C - \chi_p} + g\left(\sqrt{\beta_C - \chi_p}\right)\right] \tag{12.6}$$

These expressions give the maximum values of collected current that can be drawn from a concentric outer boundary for a given boundary radius and potential difference between the inner and outer boundary, when the outer boundary emits collisionless Maxwellian particles inward. An expression equivalent to Eq. (12.5) has been derived by Medicus (Ref. 30). For large values of R_B/R_p expressions (12.5) and (12.6) approach the orbital-motion-limited current expressions (E.43a) and (E.94a), respectively. For values of R_B/R_p only slightly greater than 1, they reduce to the usual expressions for current increase as a function of sheath edge radius in which it is assumed that all particles entering the sheath strike the probe. Large values for R_B/R_p may be expected to occur if the probe diameter is small compared to the attracted-species Debye length ($R_p << \lambda_D$) and the probe potential is large; R_B/R_p will be close to 1 if $R_p >> \lambda_D$.

The currents given by Eqs. (12.5) and (12.6) in terms of sheath edge location are upper bounds for the current values calculated here by the solution scheme described above. These upper bounds are never actually attained (for a given sheath edge location) because barriers of effective potential are always present within the sheath. This is because there will always be a region just inside the sheath edge in which the potential varies more steeply with radius than an inverse square law. (This happens in spite of the fact that the potential gradient approaches zero at the sheath edge.) This is equivalent to the statement that the locus of extrema always enters the region $\Omega > 0$, $\beta > \Omega\, x_B^2$. The latter may be proven by noting that at $x = x_B$, $\chi = d\chi/dx = 0$ and $d^2\chi/dx^2 < 0$, and substituting this information into Eqs. (9.8) for Ω_G and β_G.

In the limit of large R_p/λ_D, the sheath lies close to the probe surface and is well approximated by a planar situation in which all particles entering the sheath strike the probe. The collected current can then be calculated if the sheath edge radius alone is known, and the sheath edge radius can be obtained from the solution of the planar Poisson equation. This solution is derived in Appendix F for the case in which the particles being attracted into the sheath are Maxwellian. At large probe potentials the form of the solution curve is asymptotic to the familiar Child-Langmuir sheath relation. Since this relation does not correctly predict the form of the sheath potential at small potentials, a finite difference between the sheath edge radii predicted by the Child-Langmuir and the exact solutions will persist even at large probe potentials.

If either the spherical or cylindrical mono-energetic distributions (Eqs. (9.3) and (11.6), respectively) are substituted in place of the Maxwellian in Appendix F, and the corresponding calculations are repeated, sheath potentials will result which are different than the one derived there. These can also be shown to be asymptotic to the Child-Langmuir result, so that the above remarks apply once again.

These spherical and cylindrical mono-energetic distributions will produce sheath potential shapes, even in the large-probe limit, that differ from each other as well as from the Maxwellian result. This is because the cylindrical distribution of Eq. (11.6) is mono-energetic in transverse motion only. The spherical distribution of Eq. (9.3) forms a spherical shell in velocity space; on the other hand the distribution corresponding to Eq. (11.6) forms a cylindrical shell. No distribution of longitudinal velocity exists which can make the two equivalent.

XIII. MONO-ENERGETIC ATTRACTED PARTICLES; THE PLASMA APPROXIMATION

It has been indicated earlier (Sec. IV) that other authors have substituted a mono-energetic model for the velocity distribution of the attracted species, in place of the more realistic Maxwellian, in order to reduce the problem from a system of integral equations to an ordinary differential equation and make the task of obtaining numerical results substantially easier. Since one of the goals of this research has been to display explicitly the effects of this approximation by comparing the results with those for the Maxwellian case, a routine for calculation of the density of mono-energetic attracted particles has been incorporated into the computing program. This subprogram operates within the iterative scheme designed for the Maxwellian case. One practical benefit that has resulted has been the use of this subprogram to provide a very good first approximation for the Maxwellian case, which is much more expensive in computation time. This has resulted in a substantial reduction in the total computation time required to obtain the Maxwellian results.

Furthermore, the Maxwellian and mono-energetic distributions coalesce in the zero-temperature limit, so that the zero-temperature mono-energetic results provide an end point for curves of collected current vs attracted-species temperature for either distribution.

We therefore include here a brief derivation of the expressions for the density of mono-energetic attracted particles. Apart from notation, many of these expressions are substantially the same as those developed in Ref. 5.

For the spherical probe, substitution of Eq. (9.3) into Eqs. (9.5) and (9.9) gives:

$$\eta = -\frac{1}{2\sqrt{\beta_M}} \sum_n Q_n \left\{ \beta_M - \chi - \Omega_n (\beta_M) x^2 \right\}^{\frac{1}{2}}$$

$$i = \frac{1}{2} \sqrt{\frac{\pi}{\beta_M}} \; \Omega_1 (\beta_M) \tag{13.1}$$

where $$\beta_M = \frac{4}{\pi}$$

For the cylindrical probe, substitution of Eq. (11.6) into Eqs. (11.2) and (11.4) gives:

$$\eta = \frac{1}{\pi} \sum_n Q_n \text{ arc sin} \left\{ \frac{\Omega_n(\beta_M)x^2}{\beta_M - \chi} \right\}^{\frac{1}{2}}$$

$$i = \frac{2}{\sqrt{\pi}} \sqrt{\Omega_1(\beta_M)}$$

$$\beta_M = \frac{\pi}{4}$$

In both the spherical and the cylindrical cases, the locus of extrema normally has the general appearance shown in Figs. 5b and 6, with two exceptions: first, the upper cusps shown in these diagrams are generally absent for small probe potentials or large probe radii because the potential in these cases will remain steeper than an inverse square law near the probe (no inner family of trapped orbits); second, for the spherical probe the lower cusp usually vanishes, because in contrast with the cylinder, the potential will remain steeper than an inverse square as radius increases. In this case the locus of extrema corresponding to large radii becomes tangent to the Ω axis as shown in Fig. 7a.

As is shown in Fig. 6, as the radius increases, the cutoff line (shown as DE in Fig. 6b) moves downward and to the right, and its point of tangency D (Fig.6b) moves downward along the locus of extrema. Two cases may be distinguished: at smaller radii, D is above the energy level β_M. This energy level would appear as a fixed horizontal line in Fig. 5b and Figs. 6a to 6c but is not included since these diagrams have not been drawn for a specific distribution function. This line would then intersect the segment CD of the locus of extrema in Fig. 6b. Corresponding to this situation it is evident from the definitions of $\Omega_1(\beta)$ and $\Omega_2(\beta)$ that we have $\Omega_1(\beta_M) = \Omega_2(\beta_M) = \Omega_G(\beta_M)$. At larger radii, D goes below the energy level β_M. In this case, a line representing this energy level would intersect both the segment DH of the locus of extrema and the cutoff boundary DE in Fig. 6. Corresponding to this situation we have $\Omega_1(\beta_M) = \Omega_G(\beta_M)$ and $\Omega_2(\beta_M) = (\beta_M - \chi)/x^2$. In both cases, $\Omega_0 = 0$, $Q_0 = Q_1 = -1$ and $Q_2 = 2$. If we define x_M as the value of x at which the point of tangency is at energy β_M, we then obtain for the sphere, from Eq. (13.1):

$$\eta = \frac{1}{2} \left\{1 - \frac{\chi}{\beta_M}\right\}^{\frac{1}{2}} \mp \frac{1}{2}\left\{ 1 - \frac{\chi}{\beta_M} - \frac{\Omega_G(\beta_M)}{\beta_M} x^2 \right\}^{\frac{1}{2}} ; \; x \gtrless x_M \tag{13.3}$$

$$i = \frac{1}{2} \sqrt{\frac{\pi}{\beta_M}} \; \Omega_G(\beta_M)$$

Similarly, for the cylinder we obtain from Eq. (13.2):

$$\eta = \frac{1}{\pi} \arcsin \left\{ \frac{\Omega_G(\beta_M) x^2}{\beta_M (1 - \chi/\beta_M)} \right\}^{\frac{1}{2}} \; ; \; x > x_M$$

$$= 1 - \frac{1}{\pi} \arcsin \left\{ \frac{\Omega_G(\beta_M) \, x^2}{\beta_M (1 - \chi/\beta_M)} \right\}^{\frac{1}{2}} \; ; \; x < x_M \qquad (13.4)$$

$$i = \frac{2}{\sqrt{\pi}} \sqrt{\Omega_G(\beta_M)}$$

The radial coordinate x_M may be given a physical interpretation by noting that for radii smaller than the one corresponding to this value, $\Omega_1(\beta_M) = \Omega_2(\beta_M)$; in other words, all particles that exist at these radii strike the probe. The quantity x_M therefore corresponds to an absorption radius for the mono-energetic attracted particles; any of these particles that have small enough angular momentum to allow them to come inside this radius are collected by the probe (Fig. 4a). If the distribution function is poly-energetic, a continuum of such radii exists, one for each energy level in the distribution. These radii decrease as the corresponding energy increases. For particles possessing sufficiently high energies, no absorption radius exists; collection of these particles is orbital-motion-limited. In situations such as that of Figs. 5 and 6, where the locus of extrema goes through a maximum and an inner family of trapped orbits exists near the probe, there also exists near the probe a region containing no absorption radii.

The cutoff boundary $\beta = \chi(x_M) + \Omega x_M^2$ corresponding to the radial coordinate x_M is tangent to the locus of extrema $\Omega_G(\beta)$ at the point $(\Omega_G(\beta_M), \beta_M)$; therefore, at $x = x_M$, we have:

$$\Omega_G(\beta_M) - \frac{\beta_M - \chi(x)}{x^2} = 0$$

$$\frac{d}{dx}\left(\Omega_G(\beta_M) - \frac{\beta_M - \chi(x)}{x^2}\right) = 0 \qquad (13.5)$$

$$\frac{d^2}{dx^2}\left(\Omega_G(\beta_M) - \frac{\beta_M - \chi(x)}{x^2}\right) < 0$$

The first of these conditions implies that the second bracketed quantity in Eq. (13.3) vanishes at $x = x_M$, and that the bracketed quantities in Eq. (13.4) are equal to unity at $x = x_M$.

In order to derive the Bernstein and Rabinowitz differential quations for potential as a function of radius, we identify the attracted species with the ions, and we define new non-dimensional radii and ion currents. We assume that the probe potential is negative, or ion attracting, and that it is much greater in magnitude than the electron energy. We use as reference radius the electron Debye length $\lambda_{D_-} = (\epsilon kT_-/q_-^2 N_{-\infty})^{\frac{1}{2}}$ and as reference current, the ion current that would be collected by a sphere, or by unit length of cylinder, having a radius of one electron Debye length if the ions were Maxwellian and their effective temperature (Sec. III) were equal to that of the electrons. For the sphere and cylinder, respectively, the non-dimensional currents i^* referred to these reference currents are:

$$i^* = I_+(Z_+ \, e \, N_{\infty +} \, \lambda_{D-}{}^2)^{-1} \left(\frac{8\pi k T_-}{m_+}\right)^{-\frac{1}{2}} \left(-\frac{Z_+}{Z_-}\right)^{-\frac{1}{2}} = i_+ \;\; \gamma_- \; \sqrt{\pi_6}$$

$$i^* = I_+(Z_+ \, e \, N_{\infty +} \, \lambda_{D-})^{-1} \left(\frac{8\pi k T_-}{m_+}\right)^{-\frac{1}{2}} \left(-\frac{Z_+}{Z_-}\right)^{-\frac{1}{2}} = i_+ \; \sqrt{\gamma_- \pi_6} \tag{13.6}$$

We note that Eqs. (13.3) and (13.4) contain the expression χ_+/β_M. This becomes:

$$\frac{\chi_+}{\beta_M} = - \frac{\chi_-}{\pi_6 \, \beta_M} = \frac{-\chi_-}{\left(-\frac{Z_-}{Z_+}\frac{E_+}{kT_-}\right)} = - \frac{\chi_-}{\beta^*} \tag{13.7}$$

The new quantity β^* defined by Eq. (13.7) represents non-dimensional energy for the mono-energetic ions, now referred to the temperature of Maxwellian electrons rather than to the temperature of a corresponding distribution of Maxwellian ions as in earlier Sections. The quantity β_M, which is the ratio E_+/kT_+, is therefore not contained in the definition of β^*. For singly charged ions, as is usually the case, β^* is identical to the quantity β used in Ref. 5.

We also note that $\chi_- > 0$ for all x.

We define a new radial variable ξ as follows:

$$\xi = \frac{r}{\lambda_{D-}} = \frac{r}{R_p} \; \frac{R_p}{\lambda_{D-}} = \frac{\sqrt{\gamma_-}}{x} \tag{13.8}$$

We substitute Eqs. (13.6) to (13.8) into Eqs. (13.3) and (13.5) to obtain for the spherical case:

$$\eta_+ = \frac{1}{2}\left\{1 + \frac{\chi_-}{\beta^*}\right\}^{\frac{1}{2}} \mp \frac{1}{2}\left\{1 + \frac{\chi_-}{\beta^*} - \frac{2}{\sqrt{\pi}} \; \frac{i^*}{\sqrt{\beta^*}\,\xi^2}\right\}^{\frac{1}{2}} ; \quad \xi \lessgtr \xi_M$$

$$1 + \frac{\chi_-(\xi_M)}{\beta^*} - \frac{2}{\sqrt{\pi}} \; \frac{i^*}{\sqrt{\beta^*}\,\xi_M{}^2} = 0 \tag{13.9}$$

For the cylinder, we obtain from Eqs. (13.4) and (13.5):

$$\eta_+ = \frac{1}{\pi} \text{ arc sin}\left\{\frac{\pi}{4} \; \frac{i^*}{\xi^2(\beta^* + \chi)}\right\}^{\frac{1}{2}} ; \quad \xi < \xi_M$$

$$\eta_+ = 1 - \frac{1}{\pi} \text{ arc sin}\left\{\frac{\pi}{4} \; \frac{i^{*2}}{\xi^2(\beta^* + \chi_-)}\right\}^{\frac{1}{2}} ; \quad \xi > \xi_M \tag{13.10}$$

$$\frac{\pi}{4} \; \frac{i^{*2}}{\xi_M{}^2\,(\beta^* + \chi_-(\xi_M))} = 1$$

Expressions (13.9) and (13.10) are in a form equivalent to those derived by Bernstein and Rabinowitz (Ref. 5) for ion density. By comparing Eqs. (13.9) and (13.10) with their Eqs. (34) and (51), it is possible to obtain expressions for their nondimensional current ι in terms of the quantities defined here. For the sphere and cylinder, respectively, these are:

$$\iota = \frac{2}{\sqrt{\pi}} \; i^* \qquad\qquad (13.11)$$
$$\iota = \frac{\pi}{4} \; \frac{i^{*2}}{\beta^*}$$

The second expression in Eq. (13.11) illustrates the reason why Bernstein and Rabinowitz were unable to display solution curves for the cylindrical probe for the case $\beta^* = 0$, which is a nonsingular limit of Eq. (13.10); they nondimensionalized their ion current using a reference current which is a function of β^*. As $\beta^* \rightarrow 0$, their nondimensional current ι becomes infinite for a given probe potential χ_{-p} and probe radius ξ_p, whereas the actual current collected is finite.

In terms of the radial variable ξ, Poisson's equation (4.3) becomes, for the sphere and cylinder, respectively:

$$\frac{1}{\xi^2} \; \frac{d}{d\xi}\left(\xi^2 \; \frac{d\chi_-}{d\xi}\right) = \eta_+ - \eta_- \qquad\qquad (13.12)$$
$$\frac{1}{\xi} \; \frac{d}{d\xi}\left(\xi \, \frac{d\chi_-}{d\xi}\right) = \eta_+ - \eta_-$$

From Eqs. (E.39) and (E.92), we obtain for $\chi_{-p} \gg 1$, the following expression for electron density:

$$\eta_- \simeq e^{-\chi_-} \qquad\qquad (13.13)$$

This approximation together with Eqs. (13.9) to (13.12) constitutes the Bernstein and Rabinowitz differential equations for potential vs radius, for the sphere and cylinder. This expression for the electron density would also be correct for small repelling probe potentials in the hypothetical case of a probe which reflected all electrons which struck it, because the electrons would then not be depleted by the probe and would be in thermodynamic equilibrium; Eq. (13.13) coincides with the well-known distribution corresponding to this condition.

If the limit of zero ion temperature, $\beta^* \rightarrow 0$, is taken in Eq. (13.9), the result diverges for $\xi > \xi_M$; for $\xi < \xi_M$, we obtain:

$$\eta_+ = \frac{1}{2\sqrt{\pi}} \; \frac{i^*}{\xi^2 \sqrt{\chi_-}} \qquad\qquad (13.14)$$

This result implies that $\xi_M \rightarrow \infty$ as $\beta^* \rightarrow 0$: this can also be proven by letting $\beta^* \rightarrow 0$ in Eq. (13.9b); we obtain the result $\chi_-(\xi_M) \rightarrow 0$; this in turn implies $\xi_M \rightarrow \infty$. As Bernstein and Rabinowitz have pointed out, Eq. (13.14), apart from notation, is identical to the form which Allen, Boyd, and

Reynolds (Ref. 6) derived by assuming that the ions had no thermal motion and fell radially inward from infinity under the influence of the electric field.

The form of Eq. (13.14) indicates that the solution scheme developed here for the general case will break down for the spherical probe in the limit of zero ion temperature. This may be seen by noting that as $\xi \to \infty$, we require $\eta_+ \to 1$; we observe that Eq. (13.14) specifies the collected current i^* in terms of the limiting behaviour of the potential χ_- at infinite radius. Since the present calculation scheme replaces the infinite plasma by a finite outer boundary, it is clear that the scheme will fail to work in the limit $\beta^* \to 0$. In fact, it may be expected that the calculation scheme for finite ion temperature will become progressively more ill-behaved as ion temperature decreases because the form of the potential at large radii will become relatively more important. This expectation has been borne out in computations for the spherical probe in both the Maxwellian and the mono-energetic cases (Sec. XV; Appendix H).

The Bernstein and Rabinowitz and Allen, Boyd and Reynolds calculations do not have this difficulty because they extend to infinite radius. Neither of these, however, is able to deal with a Maxwellian plasma or a small probe potential. Therefore, no method exists at present to adequately treat these cases when the ion temperature is small. However, for large probe potentials, the Allen, Boyd and Reynolds equation is the zero-ion-temperature limit for the Maxwellian as well as for the mono-energetic case. Solutions of this equation may therefore be expected to provide an end point for curves of ion current vs ion temperature, and thereby enable graphical determination of ion current in the complete range of temperatures extending to zero.

Accordingly, a numerical solution of the Allen, Boyd and Reynolds equation has been carried out here (Appendices G and I) in order to provide these limiting values. This is in spite of the fact that this task has already been carried out by three other authors (Refs. 5, 6 and 8); none of these has carried out calculations in the complete range required here, and none of them has published his computer program.

A qualitatively different situation is obtained for the cylindrical probe if the limit $\beta^* \to 0$ is taken in Eq. (13.10); we note that ξ_M does not become infinite, and that the expression for η_+ does not approach the expression that may be derived by assuming that the ions move radially inward (Ref. 8). This anomaly has been a source of concern to several previous authors (Refs. 6 and 8); some light may be shed on it by studying the behaviour of the electric potential at large radii.

For the sphere, we assume $\xi > \xi_M$, $\xi \to \infty$ and $\chi_- \to 0$, and approximate the set of Bernstein and Rabinowitz differential equations (13.9), (13.12) and (13.13) to obtain:

$$\frac{d^2 \chi_-}{d\xi^2} + \frac{2}{\xi}\frac{d\chi_-}{d\xi} \simeq \chi_- \left(1 + \frac{1}{2\beta^*}\right) - \left(\frac{1}{2\sqrt{\pi}} \quad \frac{i^*}{\sqrt{\beta^*}}\right)\xi^{-2} \qquad (13.15)$$

If $\chi_- \alpha\ \xi^{-N}$, the left side of Eq. (13.15) $\alpha\ \xi^{-(N+2)}$ and vanishes to order N; neither bracketed term on the right side vanishes; therefore, $N = 2$, and we obtain, to second order in ξ :

$$\chi_- \simeq \frac{1}{2\sqrt{\pi}} \quad \frac{i^*}{\sqrt{\beta^*} + \frac{1}{2\sqrt{\beta^*}}} \quad \xi^{-2} \tag{13.16}$$

Apart from notation, this result is the same as that obtained by Bernstein and Rabinowitz using the plasma approximation.

If $\beta^* \rightarrow 0$, the coefficient of ξ^{-2} in Eq. (13.16) vanishes, and the leading term in the potential for large radii may be found from Eq. (13.14) by noting that as $\xi \rightarrow \infty$, $\eta_+ \rightarrow 1$; this gives:

$$\chi_- \simeq \frac{i^{*2}}{4\pi} \quad \xi^{-4} \tag{13.17}$$

For the cylinder, we combine Eqs. (13.10), (13.12) and (13.13) and approximate as before to obtain:

$$\frac{d^2\chi_-}{d\xi^2} + \frac{1}{\xi}\frac{d\chi_-}{d\xi} \simeq \chi_- - \frac{1}{2\sqrt{\pi}} \quad \frac{i^*}{\sqrt{\beta^* + \chi_-}} \tag{13.18}$$

For finite β^*, χ_- vanishes in comparison with β^* in the limit of large radii; once again, if $\chi_- \propto \xi^{-N}$, the left side vanishes to order N; we obtain, to first order in ξ:

$$\chi_- \simeq \frac{1}{2\sqrt{\pi}} \quad \frac{i^*}{\sqrt{\beta^*}} \quad \xi^{-1} \tag{13.19}$$

To obtain the leading term in the case $\beta^* = 0$, we proceed to this limit in Eq. (13.18) before letting $\chi_- \longrightarrow 0$; we then obtain:

$$\chi_- \simeq \left(\frac{i^*}{2\sqrt{\pi}}\right)^{\frac{2}{3}} \quad \xi^{-\frac{2}{3}} \tag{13.20}$$

Examination of these asymptotic potentials shows that in the case of the sphere, the potential becomes a steeper function of radius in the limit of zero ion temperature, whereas for the cylinder, it becomes shallower. Furthermore, for sufficiently small ion temperatures and large radii, the dependence of potential on radius will always be steeper than an inverse square law for the sphere, and shallower for the cylinder.

In order to illustrate the significance of this difference, we consider an ion of zero total energy and zero angular momentum, which suffers a small deflection while falling radially inward toward the probe under the influence of the electric field. We assume that this ion is deflected in angle but that its speed is unchanged; i.e., its total energy remains zero but it acquires a finite angular momentum. It is possible to show (Fig. 4) that if it is moving in a potential steeper than an inverse square, it will always continue to fall inward to the probe, but if the potential is shallower than an inverse square, and the ion has acquired sufficient angular momentum, there exists a turning point in its orbit. It will miss the probe and move back out into the plasma; it will fail to be collected.

In any physical situation all of the ions are scattered to some extent by the presence of other particles (Appendix A) and will in general acquire a non-zero distribution of angular momenta. If this distribution corresponds to one isotropic at infinite radius, and if the total energy of each ion remains unchanged, the results computed here for the cylinder, which are based on the zero-ion-temperature limit of Eq. (13.10), will correctly predict the current. Chen (Ref. 8) has carried out zero-ion-temperature cylindrical-probe calculations based on the assumption that the ions have zero angular momentum and move radially inward. His results may be expected to overestimate the current collection.

Since the cold-ion limit gives a result that disagrees with the zero-ion-temperature assumption of radially inward motion, the ion temperature β^* plays the role of a singular perturbation, similar to that of the inverse Reynolds number in continuum fluid mechanics. It is this fact that Chen has not taken into account.

Of some interest in studying the behaviour of the potential is the "plasma approximation" or "quasi-neutral solution". This solution is obtained by observing that outside the sheath the ion and electron charge densities approach each other very rapidly, so that the difference between the two rapidly becomes much smaller than the magnitude of either. Therefore, the potential obtained by making the approximation of equal charge densities, $\eta_+ = \eta_-$, is a close approximation to the actual potential.

Using this approximation, together with Eqs.(13.9), (13.10) and (13.13), and solving for the radius ξ, we obtain, for the sphere and cylinder, respectively:

$$\frac{i^*}{2\sqrt{\pi}\,\xi^2} = e^{-\chi_-}\sqrt{\beta^* + \chi_-} - \sqrt{\beta^*}\; e^{-2\chi_-}$$

$$\frac{\sqrt{\pi}}{2}\,\frac{i^*}{\xi} = (\beta^* + \chi_-)^{\frac{1}{2}} \sin\left(\pi e^{-\chi_-}\right) \tag{13.21}$$

We observe that in both cases, the radius ξ becomes large as the potential χ_- becomes small, as expected, but that ξ also becomes large for large χ_-. This means that for a certain value of χ_-, ξ goes through a minimum, and the potential slope $d\chi_-/d\xi$ becomes infinite. This suggests that the corresponding radius ξ is a lower limit for radii at which the plasma approximation will hold.

It is of interest to compare the value of χ_- at which $d\chi_-/d\xi$ becomes infinite, with a prediction derived by Bohm (Ref. 12) that at the sheath edge $\chi_- \geq 1/2$ for a stable sheath.

By differentiating ξ^{-2} and ξ^{-1} with respect to χ_- in Eqs. (13.21a) and (13.21b) respectively, and equating the result to zero, we obtain the following expressions for the sheath edge potential χ_{SE}:

$$\frac{1}{2} - (\beta^* + \chi_{SE}) + 2\, e^{-\chi_{SE}} \sqrt{\beta^* (\beta^* + \chi_{SE})} = 0$$

$$\tan \left(\pi e^{-\chi_{SE}}\right) - 2\pi\, e^{-\chi_{SE}} (\beta^* + \chi_{SE}) = 0 \tag{13.22}$$

Solving Eqs. (13.22) numerically for the value of χ_{SE} associated with a given β^* shows that Bohm's criterion is fulfilled in all cases. For the sphere, $\chi_{SE} = 1/2$ when $\beta^* = 0$; as β^* increases χ_{SE} first increases, then maximizes for β^* somewhat less than unity, then decreases toward $\ln 2 = 0.693...$ as β^* becomes large. For the cylinder, χ_{SE} is slightly less than unity for $\beta^*=0$, and decreases to $\ln 2$ as β^* becomes large. Therefore, another qualitative difference between the sphere and the cylinder is seen to exist; for moderately small β^*, the rate of change of sheath edge potential with β^* is positive for the sphere and negative for the cylinder.

Expressions for the absorption boundary potential and radius may be obtained by substituting the expressions for ξ_M in Eqs. (13.9) and (13.10) into Eq. (13.21). For the sphere, this procedure gives:

$$4e^{-2\chi_M} = 1 + \frac{\chi_M}{\beta^*}$$

$$\xi_M^2 = \frac{e^{2\chi_M}}{2\sqrt{\pi}} \frac{i^*}{\sqrt{\beta^*}} \tag{13.23}$$

For the cylinder:

$$\chi_M = \ln 2$$

$$\xi_M^2 = \frac{\pi}{4} \frac{i^{*2}}{\beta^* + \ln 2} \tag{13.24}$$

Expressions (13.23) and (13.24) show once again that for the sphere, the absorption boundary moves out to infinity as the ion temperature becomes small, whereas for the cylinder, it remains finite. By allowing β^* to become large in Eq. (13.23a) we obtain $\chi_M \rightarrow \ln 2$; for the cylinder, $\chi_M = \ln 2$ for any β^*. Therefore, in both cases, as β^* becomes large, $\chi_M \rightarrow \chi_{SE}$; if the attracted species is much hotter than the repelled species, the absorption boundary and sheath edge radius tend to coincide.

Many of the results obtained here may be expected to agree qualitatively with the Maxwellian case, for which it is impossible to use these methods to obtain similar expressions.

XIV. ORBITAL-MOTION-LIMITED COLLECTED CURRENT EXPRESSIONS

The orbital-motion-limited current (Sec. VIII) is that collected by a probe when none of the particles which come from infinity and are capable of penetrating inward to the probe are excluded from it by intermediate barriers of effective potential. In other words, all particles which lie above the probe cutoff boundary of Eq. (8.3) in the (J^2,E) plane actually reach the probe. For the attracted species, it is the collected current in the limit $R_p/\lambda_D \to 0$, and, in certain cases, it is the collected current within a finite neighbourhood of this limit (Appendix E; Sections XV and XVI). We summarize here the expressions for orbital-motion-limited current derived in other sections. From Eqs. (E.43) and (E.94), we have for Maxwellian particles:

For the spherical probe:

$$\begin{aligned} i &= 1 - \chi_p \quad ; \quad \chi_p \le 0 \\ i &= e^{-\chi_p} \quad ; \quad \chi_p \ge 0 \end{aligned} \qquad (14.1)$$

and for the cylindrical probe:

$$\begin{aligned} i &= \frac{2}{\sqrt{\pi}} \left(\sqrt{-\chi_p} + g\left(\sqrt{-\chi_p}\right) \right) ; \quad \chi_p \le 0 \\ i &= e^{-\chi_p} \quad ; \quad \chi_p \ge 0 \end{aligned} \qquad (14.2)$$

From Eqs. (13.1) and (13.2), setting $\Omega_1(\beta_M) = \beta_M - \chi_p$, we obtain for mono-energetic particles, for the sphere and cylinder, respectively:

$$\begin{aligned} i &= 1 - \frac{\pi}{4}\chi_p \quad ; \quad \chi_p \le \frac{4}{\pi} \\ i &= \sqrt{1 - \frac{4}{\pi}\chi_p} \; ; \quad \chi_p \le \frac{\pi}{4} \end{aligned} \qquad (14.3)$$

It is often useful to non-dimensionalize the ion current by dividing by its value when the ions are at electron temperature and the probe is at plasma potential. We substitute expressions (9.10b) and (9.15) into Eqs. (14.1) to (14.3) to obtain the following ion current expressions. For Maxwellian ions collected by a spherical probe, we have:

$$\begin{aligned} i_{+-} &= \sqrt{\tau_6} + \frac{\chi_{p-}}{\sqrt{\tau_6}} \quad ; \quad \chi_{p-} \ge 0 \\ i_{+-} &= \sqrt{\tau_6}\, e^{\chi_{p-}/\tau_6} \quad ; \quad \chi_{p-} \le 0 \end{aligned} \qquad (14.4)$$

For Maxwellian ions collected by a cylindrical probe:

$$i_{+-} = \frac{2}{\sqrt{\pi}} \left(\sqrt{\chi_{p-}} + \sqrt{\pi_6}\; g\left(\sqrt{\chi_{p-}/\pi_6}\right) \right); \quad \chi_{p_-} \geq 0$$
$$i_{+-} = \sqrt{\pi_6}\; e^{\chi_{p-}/\pi_6} \qquad ; \quad \chi_{p-} \leq 0 \tag{14.5}$$

For mono-energetic ions, we obtain from Eq. (14.3) the following expressions for the sphere and cylinder, respectively:

$$i_{+-} = \sqrt{\pi_6} + \frac{\pi}{4} \frac{\chi_{p-}}{\sqrt{\pi_6}} \quad ; \quad \chi_{p-} \geq -\frac{4}{\pi}\; \pi_6$$
$$i_{+-} = \frac{2}{\sqrt{\pi}} \sqrt{\chi_{p-} + \frac{\pi}{4}\pi_6}\; ; \quad \chi_{p-} \geq -\frac{\pi}{4}\; \pi_6 \tag{14.6}$$

Examination of Eqs. (14.4) to (14.6) shows that in general, the mono-energetic expression approximates the Maxwellian much more closely for the cylindrical case. For the sphere, the two do not approach each other at large probe potentials as they do for the cylinder. It is also noteworthy that as the ion temperature becomes zero, the orbital-motion-limited current becomes infinite for the sphere, but remains finite for the cylinder.

Computations of current for a cylindrical probe in the general case show that in certain ranges of R_p/λ_D, the differences between the Maxwellian and the mono-energetic results are considerably greater than in the orbital-motion-limited case (Sec. XV).

We also note once again that the roles of ions and electrons in expressions (14.4) to (14.6) are completely interchangeable.

XV. RESULTS AND DISCUSSION - SPHERICAL PROBE

Before beginning discussion of the relevant features of the calculated results, a brief description is given of where can be found the various items of background material in this report. The Fortran II programs that have been developed and used to obtain the numerical results presented here are listed in Appendix I. Table 3 identifies the most important Fortran variables and formulas in these programs with their text equivalents. Representative samples of printed output obtained from the University of Toronto IBM 7094 digital computer using these programs are shown in Appendix J. Computed current collection results are presented in Table 5 for the spherical probe and in Table 6 for the cylindrical probe. Appendix H contains a discussion of the accuracy of these results. Current collection results, potential and charge density distributions, and trapped-orbit and orbital-motion-limited-current boundaries are shown in Figs. 13 to 31 for the spherical probe and in Figs. 32 to 51 for the cylindrical probe.

It is common usage to employ the electrons as the reference species in any discussion of Langmuir probes; this convention is followed in presenting these results. The electrons are also the hotter species in the majority of situations of laboratory interest; accordingly, results are presented here for the range $0 \leq T_+/T_- \leq 1$.

For brevity of presentation, we also assume in presenting all results that $Z_+ = 1$ and $Z_- = -1$. As pointed out in Sec. III, this assumption involves no real loss of generality since the results may be applied to the case of multiply charged ions by scaling the temperature ratio T_+/T_-. Since the nondimensional probe potential χ_{p_-} referred to electrons always has the opposite sign to the probe potential ϕ_p, it is also common practice to use as a nondimensional probe potential the quantity $-\chi_{p_-}$; since $Z_- = -1$, we have $-\chi_{p_-} = e\phi_p/kT_-$.

It has already been pointed out (Sec. III) that the roles of ions and electrons are interchangeable for purposes of this discussion; also that these results may be applied to the case of multiply charged particles by scaling the quantity T_+/T_-. It is also note-worthy that if the need arises to use the colder species as reference, these results may be expressed in terms of nondimensional probe potential relative to the colder species, and the ratio of probe radius to colder-species Debye length, by using Eqs. (9.15) and (9.16) to scale the quantities χ_p and γ.

Furthermore, the nondimensional probe potential referred to the colder species is always larger than that referred to the hotter species so that these results, which are computed for values of χ_p, referred to the hotter species, from -25 to 25, will always cover a range larger than this when referred to the colder species. By identifying the colder species with the electrons, it is possible by the above reasoning to apply the results presented here to cases in which T_+/T_- is greater than unity.

The results of these calculations therefore apply to a considerably larger range of situations than those evident at first glance.

The preceding remarks in this Section apply not only to the results for the spherical probe but also those for the cylindrical probe presented in Sec. XVI. The remainder of this section is devoted to a discussion of the computed results for the spherical probe which appear in Figs. 13 to 31. The current collection results plotted in Figs. 20 to 29 are also presented in Table 5.

Figure 13 shows potential vs distance from probe surface in electron (or ion) Debye lengths for a probe at a fixed potential $e\phi_p/kT_- = \pm 25$, for equal ion and electron temperatures and a range of ratios of probe radius to either Debye length from 1 to 100. Figure 14 shows corresponding ion and electron charge densities. In both cases the influence of the probe may be seen extending a greater number of Debye lengths into the plasma as R_p/λ_{D-} is increased. The local rise in attracted-species charge density near the probe for the smaller values of R_p/λ_{D-} shown is due to two causes. First, the potential in this region is of a form which allows particles having certain values of angular momentum and energy to orbit the probe many times before falling into it or moving back out to infinity; the presence of these particles in this region therefore produces a rise in charge density because of their long dwell time. The second reason is that because of the spherical geometry, the particles moving toward the probe are concentrated into a smaller volume as they approach it; their density must rise accordingly.

A situation in which the ions and electrons are at different temperatures is shown in Fig. 15. In this diagram potential is plotted against radius for various values of probe potential for the values $T_+/T_- = 0.1$ and $R_p/\lambda_{D-} = 10$. The marked asymmetry between the cases of positive and negative probe potentials is due to the fact that in these two ranges the colder and hotter species, respectively, are repelled. As discussed in Sec. XIII, the amount of electric field that penetrates past the sheath edge into the plasma is nearly proportional to the thermal energy of the repelled species; therefore, shielding by the ions at positive probe potentials is nearly complete, whereas electron shielding at negative probe potentials allows a much larger amount of electric field to penetrate into the plasma.

A related set of charge distributions is plotted in Fig. 16, which shows ion and electron densities for a probe at positive potentials for the same range of cases as those shown for a positive probe in Fig. 15. The progressive increase in charge separation associated with sheath formation and growth is evident here. If the results corresponding to $e\phi_p/kT_- = -25$ and $R_p/\lambda_{D-} = 10$ are compared in Figs. 14 and 16, the difference between them is that in Fig. 16, the repelled species, i.e. the ions, is no longer at the same temperature as the attracted species but only at a tenth of it. Comparison of these results shows the sharpening of the sheath edge as the repelled-species temperature is reduced with attracted-species parameters held constant. The dotted curve in Fig. 16 showing the corresponding result for $T_+/T_- = 0$ shows this trend carried to completion.

Figures 17 and 18 show potential and charge densities, respectively, plotted as functions of radius for the case of zero attracted-particle temperature and large probe potential, obtained by numerical solution of the Allen, Boyd, and Reynolds equation (Ref. 6) as treated in Sec. XIII and Appendix G, and carried out by Program 4 (Appendix I). Figure 17 also shows as a dotted curve the trapped-orbit boundary. If some particular situation involving zero attracted-species (ion, in this case) temperature has values of probe potential and R_p/λ_{D-} corresponding to values of potential and r/λ_{D-} in Fig. 17 which lie above this boundary, then the form of the potential adjacent to the probe will be such that trapped orbits of the type discussed in Section VIII exist. The results plotted above this boundary are therefore subject to the qualifications noted in that Section, namely, that the population of such orbits must be negligible. In Fig. 17 and in all later diagrams in which trapped-orbit boundaries appear, it is to be understood that they refer only to a fully Maxwellian plasma, and not to one with a mono-energetic distribution for the attracted species; zero-temperature attracted particles are included in this definition as a limiting case of the Maxwellian distribution.

The increasing concentration of the attracted particles as they move radially inward toward the probe is again visible in Fig. 17, as in Fig. 14; in this case the particles do not orbit the probe and the increase in their density is due only to the decrease in the volume that they occupy as they approach the probe.

If the probe potential is now changed in sign so that the particles which are at zero temperature are now the repelled ones, then the situation is as described in Sec. XII. In particular, the sheath edge radius in this case is now a sharply defined location at which the repelled-species density falls discontinuously from its value outside the sheath to zero within it. Computed values of this sheath edge radius are plotted in Fig. 19 as a function of probe potential and ratio of electron, i.e. attracted species, Debye length to probe radius. The results for non-zero values of λ_{D-}/R_p have been computed using Program 2 (Sec. XII; Appendix I); the curve for $\lambda_{D-}/R_p = 0$ has been computed using Program 3, which calculates the probe characteristic in the planar-sheath limit (Appendices F,I). The smooth transition in the result from the non-zero case to the limit may be regarded as a check on the correctness of both programs; on the other hand, the steep variation of sheath edge radius with λ_{D-}/R_p near this limit at larger probe potentials is an indication that the more complete description deviates rapidly from the planar-sheath approximation as λ_{D-}/R_p increases. The trapped-orbit boundary is also shown in this diagram.

The trapped-orbit boundaries shown in Fig. 19 and subsequent diagrams have been obtained from the computed results by the following method. Corresponding to each set of values of the three parameters T_+/T_-, $e\phi_p/kT_-$, and R_p/λ_{D-} is a maximum radius at which the shape of the potential allows trapped orbits to exist. Table 3 identifies this quantity in the output of the computer programs. The ratio T_+/T_- and either one of the two quantities $e\phi_p/kT_-$ or R_p/λ_{D-} are held constant and this maximum radius is obtained as a computed result for several values of the other. It is then extrapolated back to zero distance from the probe as a function of this quantity.

Figure 20 shows attracted-species (ion or electron) current collection as a function of probe potential for the case $T_+/T_- = 1$ for various values of R_p/λ_{D-}. The result for $R_p/\lambda_{D-} = 0$, the orbital-motion-limited current, is obtained from Eq. (14.1); the remaining curves are computed results appearing in Table 5c.

Figure 20 also shows the trapped-orbit boundary for $T_+/T_- = 1$; as in Figs. 17 and 19, this boundary corresponds to the smallest probe potential for a given value of R_p/λ_{D-}, or equivalently the largest value of R_p/λ_{D-} for a given probe potential, for which the form of the potential adjacent to the probe is shallow enough so that trapped orbits exist. The question of whether these trapped orbits, when they exist, will be populated, has been discussed in Sec. VIII. In that section it is pointed out that if these orbits are populated, the probable effect will be a decrease in current collection below the values shown in Fig. 20. All results in this diagram corresponding to points above this boundary are therefore subject to this qualification.

Ion current results for the case $T_+/T_- = 0$ are shown in Fig. 21, plotted as functions of probe potential for various values of R_p/λ_{D-}. These results correspond to the potentials and charge densities of Figs. 17 and 18 and are therefore based on the simplified electron density model of Eq. (13.13). Accordingly, for values of $-e\phi_p/kT_-$ smaller than about 5, they can be expected to deviate significantly from current collection values corresponding to the more realistic model of an absorbing probe (i.e. one that collects every charged particle that strikes it), and should therefore be used with caution. In contrast with the case of finite ion temperature (Fig. 20) the ion current at zero ion temperature increases without limit as R_p/λ_{D-} is decreased, for any fixed probe potential. Figure 21 also shows the trapped-orbit boundary corresponding to $T_+/T_- = 0$. The current collection results shown in this diagram appear in Table 5a.

Figure 22 shows electron current as a function of probe potential for various values of R_p/λ_{D-}, for the case $T_+/T_- = 0$, i.e. for the case of zero-temperature repelled particles. The results for non-zero values of R_p/λ_{D-}

have been computed using Program 2 (Appendix I); the result for $R_p/\lambda_{D-} = 0$ is the same as that for Fig. 20. Once again, the trapped-orbit boundary is shown.

Comparison of Fig. 22 with Fig. 20 shows that the electron current decreases more rapidly as R_p/λ_{D-} increases when the ions are at zero temperature than when they are at electron temperature. This effect is brought out more clearly in Fig. 26; the reasons for it are discussed in connection with that diagram. The current collection results in Fig. 22 correspond to the same cases as the sheath edge radii shown in Fig. 19.

Ion collection as a function of λ_{D-}/R_p is shown in Fig. 23 for $e\phi_p/kT_- = -25$ and values of T_+/T_- of 0, 0.5 and 1. This diagram has been plotted in this manner in order to best illustrate the behaviour of the collected current as λ_{D-}/R_p becomes small. This diagram shows that for smaller values of λ_{D-}/R_p the ion collection is not a monotonic function of ion temperature; this behaviour is brought out more clearly in Figs. 27a and 28. This diagram also shows the corresponding results for mono-energetic ions. The curve shown for the case $T_+/T_- = 0$ is a member of both the Maxwellian and mono-energetic families of curves in this diagram since, as pointed out in Sec. XIII, the mono-energetic and Maxwellian distributionsare the same in this limit.

The kink in the mono-energetic curve for $T_+/T_- = 1$ is caused by the fact that current collection for mono-energetic ions becomes orbital-motion-limited at this point. It may also be noted that no such feature appears in the corresponding Maxwellian result. The reasons for this behaviour have been discussed in Sec. VIII; this section also defines what is meant by orbital-motion-limited current when the attracted species is Maxwellian. The results for ion and electron collection are of course the same for the case $T_+/T_- = 1$.

None of these curves extend to $\lambda_{D-}/R_p = 0$ since the computation scheme has been defined only for finite values of R_p/λ_{D-}. An exception to this occurs in Figs. 25 and 45 for the case where the repelled particles are at zero temperature.

The trapped-orbit boundary for the Maxwellian case is also shown in Fig. 23. As mentioned in connection with Fig. 17, all trapped-orbit boundaries shown in this and other diagrams refer to a fully Maxwellian plasma only.

In order to display more clearly the behavior of the ion current at small values of R_p/λ_{D-}, the same results as those of Fig. 23 are shown again in Fig. 24, plotted as functions of R_p/λ_{D-} instead of λ_{D-}/R_p. Here the results shown for non-zero values of T_+/T_- indicate that in the Maxwellian case, the current collection for non-zero values of R_p/λ_{D-} approaches the result for $R_p/\lambda_{D-} = 0$ only as a limit. In contrast, the mono-energetic results show a finite range of values of R_p/λ_{D-} in which the current has a constant value. In Sec. XVI, it will be seen that the corresponding Maxwellian results for the cylindrical probe, unlike those for the sphere, also show such a region of constant current level. Appendix E contains a discussion of the reasons for this difference in behavior. Since it was impractical to use the computation scheme arbitrarily close to zero R_p/λ_{D-} (the smallest value of R_p/λ_{D-} for which computations were done was 0.2) the question of whether the current collection becomes orbital-motion-limited, i.e. reaches this maximum value, for any non-zero values of R_p/λ_{D-} cannot be definitely settled without an asymptotic analysis of the problem for small R_p/λ_{D-}; such an analysis is beyond the scope of this research. Moreover, this question is of academic interest only since the result for zero R_p/λ_{D-} is known and the residual uncertainty for very small R_p/λ_{D-} is extremely small.

Figure 25 shows electron current as a function of λ_{D-}/R_p for $e\phi_p/kT_- = 25$ and values of T_+/T_- of 0, 0.5, and 1. Once again, the trapped-orbit boundary is shown. The corresponding mono-energetic current results are also shown. The planar-sheath approximation to the result for large R_p/λ_{D-} and $T_+/T_- = 0$ (Appendices F, J) is also shown; in spite of the fact that the Maxwellian and mono-energetic curves for $T_+/T_- = 0$ are indistinguishable in this diagram for small values of λ_{D-}/R_p, it should be noted that only the Maxwellian curve has the planar-sheath approximation as an asymptote. The curves for $T_+/T_- = 0$ include the end point at $\lambda_{D-}/R_p = 0$ since the limiting result $i_- = 1$ is known (Sec. XII).

The electron current results of Fig. 25 are shown again in Fig. 26, plotted as functions of R_p/λ_{D-} instead of λ_{D-}/R_p. As noted earlier in connection with Fig. 22, the electron current decreases more rapidly as R_p/λ_{D-} increases when the ions are at a lower temperature. This occurs because the ions are in this case the repelled species; for lower values of their temperature a smaller amount of the field of the probe is able to penetrate past the sheath edge into the plasma (Sec. XIII) and attract electrons to the probe. As noted earlier in connection with Figs. 14 and 16, if the temperature of the repelled species is lowered while the attracted-species parameters are held constant, the sheath edge tends to sharpen since the repelled particles are now turned back by a smaller rise in potential. As a result, the potential well surrounding the probe steepens and contracts; fewer particles enter this well; current collection decreases.

Once again, as mentioned in connection with Fig. 24, the precise dependence of current on R_p/λ_{D-} for values near zero cannot be determined without an asymptotic analysis for cases near this limit. In particular, when $T_+/T_- = 0$, the behaviour of the sheath edge radius as $R_p/\lambda_{D-} \to 0$ is a very involved question. As before, the answers to these questions are of very minor importance in determining current collection since the limiting result is known.

Figure 27a shows ion and electron currents as functions of T_+/T_- for various attracting probe potentials and $R_p/\lambda_{D-} = 10$. Mono-energetic results with finite collection of the repelled particles, and the simplified case based on the assumption of zero collection of these particles, are both shown; the latter corresponds to the use of the simplified relation (13.13) for electron density. Current collection values for $e\phi_p/kT_- = -10$ obtained from the tabulated results of Bernstein and Rabinowitz (Ref. 21) are shown circled for comparison. They are seen to join smoothly on to the mono-energetic results computed here for larger values of ion temperature. The most striking feature of these results is that as ion to electron temperature ratio T_+/T_- is decreased, the ion collection passes through a minimum, then increases very rapidly as T_+/T_- approaches zero. The reason for this behaviour is that as ion temperature decreases, the dominant influence is at first the decrease of ion thermal motion and therefore ion random flux; as ion temperature decreases further, the absorption radii discussed in Sections VIII and XIII move outward to infinity, slowly at first, then very rapidly, so that the increase in ion collection volume becomes the dominant influence. The reason why this behaviour occurs has also been discussed in Sec. XIII. On the other hand the electron collection for positive probe potentials is seen to be a smoothly increasing function of T_+/T_-. Since the points corresponding to $T_+/T_- = 0$ are calculated using a different solution scheme (Program 2; Appendix I) than those corresponding to non-zero values of T_+/T_-, these results also furnish a check on the correctness of both programs.

Figure 27b shows ion or electron collection as a function of probe potential for $T_+/T_- = 1$ and $R_p/\lambda_{D_-} = 100$. This diagram has been plotted for the cases of Maxwellian attracted particles and mono-energetic attracted particles with and without collection by the probe of repelled particles. In the latter case the distribution of repelled particles again corresponds to the simplified model of Eq. (13.13). The difference between these results for mono-energetic attracted particles is typical of all corresponding results obtained for both the spherical and cylindrical probes, though it is smaller at lower values of R_p/λ_{D_-}. The reason why the current in the case of non-collection is increased relative to its values in the case of collection has been discussed in Sec. VIII. It is due to the fact that the assumption of zero collection results in an increase in the density of the repelled particles adjacent to the probe and decreases the steepness of the potential near the probe, allowing more of the attracted particles to reach it.

In order to illustrate more clearly the behaviour of the ion current, this quantity is plotted again in Fig. 28, as a function of both T_+/T_- and probe potential for $R_p/\lambda_{D_-} = 10$. As explained in connection with Fig. 21, the zero-temperature result is of the required accuracy for the completely absorptive probe assumed in this research only in the range $e\phi_p/kT_- \lesssim -5$. Accordingly, this curve is not drawn for probe potentials closer to zero. The non-monotonic nature of the dependence on ion temperature is again visible, as in Fig. 27a. The curve for $T_+/T_- = 0.1$ extends only to $e\phi_p/kT_- = -10$ since the computation scheme proved unable to carry out these calculations at larger probe potentials (Sec. XIII; Appendix H) Accordingly, the regions between $T_+/T_- = 0$ and 0.25 of the curves corresponding to values of $-e\phi_p/kT_-$ of 15,20, and 25, have been plotted on the basis of the expected behaviour of these curves, using as guides the curves shown for smaller values of $-e\phi_p/kT_-$, as well as the mono-energetic curve shown for $-e\phi_p/kT_- = 25$. Results for mono-energetic ions are shown for $T_+/T_- = 1$ and for $e\phi_p/kT_- = -25$. The trapped-orbit boundary is also shown.

Figure 29 shows electron current as a function of probe potential for $R_p/\lambda_{D_-} = 10$ and values of T_+/T_- from 0 to 1. The manner in which the curves for decreasing values of T_+/T_- depart at progressively lower probe potentials from the result for $T_+/T_- = 1$ is because of the progressively smaller probe potentials at which the electron sheath begins to form as T_+/T_- decreases. Again, the trapped-orbit boundary is shown; as indicated earlier, the location of this boundary corresponds to the smallest probe potential for which trapped orbits exist, for given values of T_+/T_- and R_p/λ_{D_-}.

The trapped-orbit boundary locations plotted in the preceding diagrams have been summarized in Figs. 30 and 31 for negative and positive probe potentials, respectively, for values of T_+/T_- from 0 to 1. The boundary for $T_+/T_- = 0$ in Fig. 30 is shown as a dotted line in the range $0 < -e\phi_p/kT_- < 5$ since this curve is based on solutions of the Allen, Boyd, and Reynolds equation (Appendices G, I) corresponding to the equilibrium distribution (13.13) for electrons. Also, in Fig. 30, it is evident that the trapped-orbit boundary location, like the ion current, is not a monotonic function of T_+/T_-. The fact that some of the boundaries shown in Figs. 30 and 31, as well as those for the cylinder in Figs. 50 and 51, are not extended to zero probe potential is because only enough computer runs were carried out in these ranges of parameters to obtain complete information about the quantity of primary importance, the current collection.

This completes the discussion of the results computed for the spherical probe.

XVI. RESULTS AND DISCUSSION - CYLINDRICAL PROBE

This section is devoted to a discussion of the computed results for the cylindrical probe which are shown in Figs. 32 to 52. The general remarks made at the beginning of Sec. XV also apply to the presentation of these results. The current collection results plotted in Figs. 39 to 49 are also presented in Table 6.

The potential and charge density distributions shown in Figs. 32 to 35 correspond, respectively, to those of Figs. 13 to 16 for the sphere. In comparison with the spherical probe, all of these diagrams show the larger extent of the disturbances in both potential and charge density created by the presence of the cylindrical probe. Figure 33 in comparison with Fig. 14 shows a smaller concentration of the attracted particles near the probe at low values of R_p/λ_{D-}; this is because the volume occupied by the inward-moving particles decreases more slowly in the cylindrical geometry as they move toward the probe.

Figure 36 shows potential vs radius for $R_p/\lambda_{D-} = 10$, for values of T_+/T_- of 0 and 1, and for values of $e\phi_p/kT_-$ of -1, -3, -10 and -25. It has been shown in Sec. XIII that for mono-energetic ions the form of the potential at large radius becomes more shallow in the limit as $T_+/T_- \to 0$. These results for a fully Maxwellian plasma show the same effect. Corresponding charge densities are plotted as functions of radius in Fig. 37, for the same values of R_p/λ_{D-} and T_+/T_-, and for values of $e\phi_p/kT_-$ of -0.1, -3, and -25. The charge densities are also observed to have a more gradual dependence on radius when $T_+/T_- = 0$.

Sheath edge thickness is shown in Fig. 38 as a function of both probe potential and λ_{D-}/R_p for $T_+/T_- = 0$ and positive values of probe potential, i.e. for the case of zero-temperature repelled particles, corresponding to Fig. 19 for the sphere. Comparison of these two diagrams shows that the sheath edge always lies farther from the probe in the cylindrical case for the same values of probe potential and λ_{D-}/R_p. One reason for this is that, as shown in Sec. XII, if the repelled particles are at zero temperature, none of the electric field due to the probe's presence can penetrate past the sheath edge into the plasma. This means that the total net space charge in the sheath must exactly cancel the charge on the probe. In the cylindrical case, the sheath volume per unit probe surface area is smaller for a given sheath thickness because of the geometry. The sheath edge must therefore tend to lie farther from the probe.

Figure 38 also shows part of the trapped-orbit boundary. The portion of this boundary corresponding to smaller values of λ_{D-}/R_p is not shown because the computer program was unable to produce results in this region (Appendix H). This trapped-orbit boundary, and all others shown on diagrams which refer to the cylindrical probe, refer only to the inner family of trapped orbits discussed in Sec. VIII.

Ion or electron current is plotted in Fig. 39 as a function of probe potential for $T_+/T_- = 1$ and various values of R_p/λ_{D_-}, corresponding to Fig. 20 for the sphere. In comparison, the current collection for the cylinder increases considerably more slowly with increasing probe potential. In contrast with the sphere, it remains orbital-motion-limited at non-zero values of R_p/λ_{D_-}. For instance, the curve for $R_p/\lambda_{D_-} = 2$ in Fig. 39 coalesces with the orbital-motion-limited result (Eq. 14.5a with $\pi_6 = 1$) at $e\phi_p/kT_- = \pm 2.9$. Figure 50b may be used to verify this value. Figure 39 also shows the trapped orbit boundary.

Figure 40 shows ion collection as a function of probe potential for $T_+/T_- = 0$ and various values of R_p/λ_{D_-}. This diagram corresponds to Fig. 21 for the sphere, except that the correct form of the electron distribution for small probe potentials has been used in the cylindrical case. Another difference between the two diagrams is that current collection for the cylinder remains finite in the limit $R_p/\lambda_{D_-} \to 0$ and becomes orbital-motion-limited for non-zero values of R_p/λ_{D_-} as this limit is approached. The result in Fig. 40 corresponding to $R_p/\lambda_{D_-} = 0$ is that of either Eq. (14.5a) or Eq. (14.6b) with π_6 set equal to zero.

Electron collection is shown in Fig. 41 as a function of probe potential for various values of R_p/λ_{D_-} and for $T_+/T_- = 0$, i.e. for the case of zero-temperature repelled particles, corresponding to Fig. 22 for the sphere. Part of the trapped-orbit boundary is shown. The reason why a section of it is not shown has been discussed in connection with Fig. 38 which corresponds to the same cases as those of Fig. 41. As in the spherical case, for increasing values of R_p/λ_{D_-} the electron collection initially decreases more rapidly when the ions are at zero temperature than when they are at electron temperature. In contrast to the results shown in Figs. 39 and 40, current collection in Fig. 41 is equal to the orbital-motion-limited result only in the limit as $R_p/\lambda_{D_-} \to 0$. The reason for this is that the orbital-motion-limited current cannot be attained in the presence of a zero-potential sheath edge at any finite radius (Sec. XII).

In order to display more clearly the behaviour of the current at small Debye lengths, the ion or electron collection has been plotted in Fig. 42 as a function of λ_{D_-}/R_p for $T_+/T_- = 1$ and various values of probe potential. Trapped-orbit and orbital-motion-limited current boundaries are shown. The method of obtaining the location of the orbital-motion-limited current boundary from the computed results is described later in connection with Fig. 50a. As is the case with the trapped-orbit boundaries, all orbital-motion-limited current boundaries shown in this and subsequent diagrams refer to a fully Maxwellian plasma, with the understanding that zero-temperature attracted particles are included as a special case.

The corresponding dependence of ion collection on λ_{D_-}/R_p for $T_+/T_- = 0$ is shown in Fig. 43 for various probe potentials. In comparison with Fig. 42, both the trapped-orbit and orbital-motion-limited current boundaries in general lie at larger values of R_p/λ_{D_-} for any given probe potential. Figure 50a and 50b also show these boundaries. The kink in the current-collection curves of Fig. 43 occurs because when the attracted species is at zero temperature, it is mono-energetic, and the discussion in Sec. VIII applies.

Figure 44 shows ion collection as a function of λ_{D-}/R_p for $e\phi_p/kT_- = -25$ and values of T_+/T_- of 0, 0.5, and 1. In contrast with Fig. 23, which shows the corresponding results for the sphere, the ion current is bounded at large values of λ_{D-}/R_p and small values of T_+/T_-, for any given probe potential. Current results for mono-energetic ions are shown for comparison; once again, the result for $T_+/T_- = 0$ is a member of both the Maxwellian and mono-energetic families of results. There is seen to be a range of values of λ_{D-}/R_p in which the current collection at fixed λ_{D-}/R_p is not a monotonic function of T_+/T_-. A detailed comparison of Figs. 42 and 43 shows that this occurs only for values of $-e\phi_p/kT_-$ greater than about 10. The trapped-orbit boundary is also shown.

Electron collection results have been plotted in Figs. 45 and 46 as functions of λ_{D-}/R_p and R_p/λ_{D-}, respectively, in order to illustrate the behaviour of the current collection for both small and large Debye lengths. These results are plotted for $e\phi_p/kT_- = 25$ and values of T_+/T_- of 0, 0.5, and 1. These diagrams correspond to Figs. 25 and 26 for the sphere. Figure 45 shows the trapped-orbit boundary in incomplete form since its location for $T_+/T_- = 0$ is not available, as discussed in connection with Fig. 38. As in Fig. 25, the results for $T_+/T_- = 0$ in Fig. 45 include the end point for $R_p/\lambda_{D-} = 0$ since the limiting result $i_- = 1$ is known. Current collection for Maxwellian electrons based on the planar-sheath approximation is also shown again in Fig. 45. Figures 45 and 46 also show corresponding current collection results for mono-energetic electrons. In contrast to the spherical case of Fig. 26, current collection for non-zero values of T_+/T_- in Fig. 46 is seen to be orbital-motion-limited, i.e. not a function of R_p/λ_{D-}, over a non-zero range of R_p/λ_{D-}.

Figure 47 shows ion collection for $e\phi_p/kT_- = -25$ and electron collection for $e\phi_p/kT_- = 25$, as functions of T_+/T_-, for $R_p/\lambda_{D-} = 10$. Results for mono-energetic attracted particles are shown for comparison. The Maxwellian and mono-energetic ion current results are seen to coalesce as $T_+/T_- \rightarrow 0$, as must be the case (Sec. XIII). Since the electron collection result for a positive probe in the limiting case $T_+/T_- = 0$ is calculated by a different program (Appendix I) than the results for non-zero values of T_+/T_-, the fact that these results are seen to join smoothly in Fig. 47 serves to verify the operation of both programs. We also note that the ion current for the negative probe is equal to the electron current for the positive probe when $T_+/T_- = 1$, as it must be (Sec. III).

Ion collection is shown in Fig. 48 for $R_p/\lambda_{D-} = 10$ as a function of both T_+/T_- and probe potential. This diagram corresponds to Fig. 28 for the sphere. The trapped-orbit boundary is shown, as well as the current collection for mono-energetic ions for $T_+/T_- = 1$ and for $e\phi_p/kT_- = -25$. In contrast with Fig. 28, the ion collection is seen to be a monotonic function of ion temperature for the cylinder for $R_p/\lambda_{D-} = 10$; the fact that this is not true for some values of R_p/λ_{D-} has been noted in connection with Fig. 44. The curve for $T_+/T_- = 0$ is seen to be complete in the cylindrical case, unlike that for the sphere.

Figure 49 shows electron current as a function of probe potential for $R_p/\lambda_{D-} = 10$ and values of T_+/T_- from 0 to 1. This diagram corresponds to Fig. 29 for the sphere. In comparison, the increase in current collection with probe potential is smaller in all cases, and the inner family of trapped orbits (Sec. VIII) occurs at smaller probe potentials in the cylindrical case than trapped orbits occur in the spherical case.

Trapped-orbit and orbital-motion-limited current boundaries are plotted in Fig. 50a for an ion-collecting probe for values of T_+/T_- of 0, 0.5, and 1. This diagram corresponds to Fig. 30 for the sphere; in contrast, the trapped-orbit boundary position is for nearly all values of probe potential seen to be a monotonic function of T_+/T_- in the cylindrical case. In this case, trapped orbits also exist at larger values of R_p/λ_{D-} than in the corresponding spherical case; this is because the potential in the cylindrical case is generally more shallow in form (Sec. VIII). Another difference between Figs. 30 and 50a is that in the spherical case, no orbital-motion-limited current boundaries are shown since there are no non-zero values of R_p/λ_{D-} for which this amount of current is actually collected; a discussion of the reasons for this difference appears in Appendix E. These boundaries have been obtained in the cylindrical case by obtaining as computer output for a sequence of cases the value of the maximum energy level for which current collection is not orbital-motion-limited (Sec. VIII; Table 3) and extrapolating this result to zero as a function of either probe potential or R_p/λ_{D-}. Figure 50b shows the data of Fig. 50a plotted on a larger scale in R_p/λ_{D-} to show more clearly the location of the orbital-motion-limited current boundaries.

Figure 51 shows the same boundaries as those of Fig. 50 in the case of an electron-collecting probe. This diagram corresponds to Fig. 31 for the sphere. The trapped-orbit boundary for $T_+/T_- = 0$ is incomplete as in Figs. 38 and 41. The boundaries for $T_+/T_- = 1$ are the same as those for ion collection in Fig. 50, as they must be (Sec. III).

It is clear from examination of the preceding diagrams that much of the information computed here for both the spherical and the cylindrical probes is in the region where trapped orbits exist. The fact that populating these orbits in any particular case is likely to cause a decrease in the attracted-species current has been pointed out in Sec. VIII. Since no quantitative predictions exist of the magnitude of these effects, it is evident that theoretical or experimental investigation of them would be of great value in finding out whether in any given situation they appreciably affect the current collection.

It is noteworthy that Bernstein and Rabinowitz (Refs. 5 and 21) were sufficiently concerned about this problem to forego carrying out their mono-energetic calculations in the trapped-orbit region. However, important cases are believed to exist in which the population of these orbits will be negligible (Sec. VIII); the obtaining of these results was accordingly considered to be a worthwhile task.

This completes the discussion of the computed results of this investigation. As noted in Sec. XV, these results may be applied by scaling of the appropriate parameters to situations involving multiply charged ions and values of T_+/T_- greater than 1.

XVII. COMPARISON WITH EXPERIMENTAL WORK AT U.T.I.A.S.

The theory and numerical calculations which form the subject of this investigation have been carried out as part of a coordinated project in the development of plasma diagnostic techniques at U.T.I.A.S. As part of this project, experimental work closely related to the work described herein has been performed by Graf (Ref. 3) and Sonin (Ref. 4). Results of this combined investigation have also been reported in Ref. 19.

Reference 3 reports the results of a comparison made between Langmuir probe and microwave measurements on the subsonic portion of a free-expansion argon plasma jet. Figure 52, which has been obtained from the results of Ref. 3 as they appear in Ref. 19, shows a comparison of electron number density results obtained using these two techniques. The Langmuir probe measurements used in constructing this diagram were made using a cylindrical probe of large length-to-diameter ratio aligned parallel to the local flow direction; numerical results which appear in Table 6 were used in calibrating this probe.

Reference 4 reports the results of experiments undertaken to compare the experimentally measured current collection of cylindrical probes with the results of this investigation (Table 6) and with results obtained from other theoretical formulations (Sections I, V, XIII). These probes were used under essentially similar conditions to those mentioned above in connection with Ref. 3. Figure 53 is reproduced from Ref. 4. This diagram corresponds to a situation in which the ion to electron temperature ratio was nearly zero and shows ion current I_i measured at 10 dimensionless units below the floating potential χ_f, plotted as a function of $(R_p/\lambda_D)^2\ I_i(\chi_f-10)$ where R_p/λ_D is in Fig. 53 the ratio of probe radius to electron Debye length. Numerical results of this investigation, and results calculated by Chen (Ref. 8) are shown for comparison. It is seen that at larger values of the abscissa in this diagram, the experimental results give good agreement with the theoretical results obtained here rather than with those of Ref. 8, which are based on the zero-angular-momentum or radially-inward-motion assumption for zero-temperature ions. The implications of this assumption have been discussed in Sec. XIII; the experimental data shown in Fig. 53 therefore amount to a verification of the assumption made here in this investigation that the zero energy ions have a uniform distribution of angular momentum far from the probe. In other words, their distribution is correctly predicted by the zero-energy limit of the mono-energetic distribution (Sec. XIII).

It is also seen in this diagram that the experimental points depart from the theory at the point where the theory predicts that the current becomes orbital-motion-limited and no longer increases. This effect must almost certainly be a collisional one; it means that a significant number of ions presumably undergo collisions while orbiting by the probe and are deflected so as to strike it when they would otherwise miss it. The purpose of this investigation has been to explore the implications of a collisionless theory, and calculations involving collisions are beyond its scope. However, this diagram illustrates the fact that it is possible to find some situations in which the collisionless results are much more sensitive to the presence of collisions than in other cases.

The foregoing questions are discussed in more detail in Refs. 3 and 4, which also contain complete descriptions of the experimental procedures involved. Reference 19 has been written as a summary of some of the results of this combined research program; it also contains further information on the relationships between this theory and the experiments just described.

XVIII. CONCLUDING REMARKS

A method has been developed and used to obtain theoretical predictions of the current collected from a collisionless, fully Maxwellian plasma at rest by an electrically conducting Langmuir probe having spherical or cylindrical symmetry; the results for the cylinder have the advantage of being applicable to an aligned probe in a flowing plasma. The probe characteristic has been determined for both spherical and cylindrical geometries for probe radii up to 100 times the Debye shielding distance of the hotter species of charged particle, for a complete range of ion-to-electron temperature ratios, and for probe potentials from -25 to 25 times the thermal energy of the hotter species. Results have been presented explicitly for temperature ratios in the range $0 \leq T_+/T_- \leq 1$, and it has been indicated (Sections IX, XV) that results for greater values of T_+/T_- may be obtained from these by scaling the appropriate nondimensional parameters. Each current collection result has been computed to a relative accuracy of 0.002 or better in an average time of approximately two minutes on the IBM 7094 at the University of Toronto.

Maxwellian velocity distributions and finite current collection have been assumed for both ions and electrons. The key to the construction of a workable computation scheme has been the replacement of the infinite plasma by an outer boundary at a finite radius, beyond which a power-law potential is specified. Experience with the computer program has in most cases shown that the computed results are remarkably insensitive to the precise location of this boundary, so that it may be placed relatively close to the probe surface, at a major gain in computation economy without appreciably disturbing the results.

The problem defined by these assumptions is expressible as a nonlinear system of integral equations, which has been solved numerically by an iterative scheme involving a sequence of successive approximations to potential and charge density distributions. An extension of the method of Bernstein and Rabinowitz (Refs. 5, 21) has been used to provide charge densities for ions and electrons at each step in the iterative process. The iteration has been found to be divergent in general, and convergence has been forced by modifying the computation scheme to provide mixing of each successive charge density result with its predecessor. The procedure does not assume any a priori separation into sheath and quasi-neutral regions.

Calculations based on the assumption of a mono-energetic distribution for the attracted particles have been made within the framework of this computation scheme, in order to provide explicit comparison with the results for a fully Maxwellian plasma, and to provide an efficient first approximation for computations with the Maxwellian plasma. In general, the results based on the mono-energetic model have been found to be a good approximation to those for the Maxwellian plasma for values of R_p/λ_{D-} greater than about 5 but show marked deviation from them for smaller values of R_p/λ_{D-} (Figs. 23 to 26, 44 to 46).

It has also been shown that the difficulties encountered by Bernstein and Rabinowitz (Ref. 5) in computing the ion current for the cylinder in the zero-ion-temperature limit are illusory, and that the computations of Chen (Ref. 8) for this case do not take into account the fact that the ion temperature acts as a singular perturbation.

Experimental results by Sonin (Ref. 4), using a cylindrical probe have been cited in Sec. XVII to indicate that even in the zero-ion-temperature limit, the current collection appears to be correctly predicted by the assumption of a uniform distribution in angular momentum as made here, rather than by the radially inward motion assumption made by Chen (Ref. 8). It is also pointed out in Sec. XVII that an exception to this occurs for values of R_p/λ_{D_-} in the orbital-motion-limited range, where the ion collection rises above the orbital-motion-limited value and hence disagrees with either theory, apparently because of collisional effects (Fig. 53).

Although the computation scheme used in this investigation to obtain results in the general case has been found to break down in certain extreme ranges of the plasma parameters, modifications or simpler theories have been found to give end-point data at nearly all of these limits, particularly when either the repelled or attracted species is at zero temperature (Sections XII, XIII, Appendix H). In the case of zero-temperature repelled particles, the modifications involved a major effort and allowed results to be obtained in an area in which up to now, even for the simplified case of mono-energetic ions, no results exist in the literature.

Computed charge density and potential distributions, as well as trapped-orbit and orbital-motion-limited boundaries and certain other information, have been presented graphically. Computed probe characteristics have been presented in both graphical and tabular form (Sections XV and XVI, Tables 5 and 6). A listing is included of the Fortran programs used to obtain these results (Appendix I).

REFERENCES

1. French, J.B. — Langmuir Probes in a Flowing Low Density Plasma. Institute for Aerospace Studies, Univ. of Toronto, UTIAS Report No. 79 (1961).

2. de Leeuw, J.H. — Electrostatic Plasma Probes. Fifth Biennial Gas Dynamics Symposium, 1963.

3. Graf, K.A. — The Determination of Spatially Non-Uniform Electron Density Distribution. Institute for Aerospace Studies, Univ. of Toronto, UTIAS Report No. 108 (1965).

4. Sonin, A.A. — The Behaviour of Free Molecule Cylindrical Langmuir Probes in Supersonic Flows, and Their Application to the Study of the Blunt Body Stagnation Layer. Institute for Aerospace Studies, Univ. of Toronto, UTIAS Report No. 109 (1965).

5. Bernstein, I.B., Rabinowitz, I.N. — Theory of Electrostatic Probes in a Low Density Plasma. Phys. of Fluids, Vol. 2, p. 112 (1959).

6. Allen, J.E., Boyd, R.L.F., Reynolds, P. — The Collection of Positive Ions by a Probe Immersed in a Plasma. Proc. Phys. Soc. B., Vol. 70, p. 297 (1957).

7. Lam, S.H. — The Langmuir Probe in a Collisionless Plasma. Princeton Univ., Gas Dynamics Lab. Rep. 681, (1964).

8. Chen, F.F. — Numerical Computations for Ion Probe Characteristics in a Collisionless Plasma. Princeton Univ., Plasma Phys. Lab. A.E.C.R. & D. Rep. MATT-252 (1964).

9. Langhaar, H.L. — Dimensional Analysis and Theory of Models, John Wiley & Sons, 1951.

10. Rostoker, N., Rosenbluth, M.N. — Test Particles in a Completely Ionized Plasma. Phys. of Fluids, Vol. 3, p. 1 (1960).

11. Goldstein, H. — Classical Mechanics. Addison-Wesley, 1959.

12. Bohm, D. — Minimum Ionic Kinetic Energy for a Stable Sheath. In: Characteristics of Electrical Discharges in Magnetic Fields. Ed. Guthrie and Wakerling, McGraw-Hill, 1949.

13. Spitzer, L., Jr. — Physics of Fully Ionized Gases, Interscience Publishers Inc., New York, 1956.

14. Chapman, S., Cowling, T.G. — The Mathematical Theory of Non-Uniform Gases, Cambridge Press, 1961.

15. Sundaresan, M.K.; Wu, T.Y. — Thermal Conductivity of a Fully Ionized Gas. Can. J. Phys., Vol. 42, No. 4, p. 794, 1964.

16. Pierce, B.O.; Foster, R.M. — A Short Table of Integrals, Ginn and Company, 1956.

17. Hastings, C., Jr. — Approximations for Digital Computers. Princeton, 1955.

18. McLachlan, N.W. — Bessel Functions for Engineers, Oxford, 1948.

19. Sonin, A.A.; Graf, K.A.; Laframboise, J.G.; de Leeuw, J.H. — The Ion Collection of Free Molecular Cylindrical Langmuir Probes in Flowing Plasmas. Seventh International Conference on Phenomena in Ionized Gases, August 1965. Gradevinska Knjiga Publishing House. Beograd, Yugoslavia.

20. Laframboise, J.G. — Theory of Cylindrical and Spherical Langmuir Probes in a Collisionless Plasma at Rest. Fourth International Symposium on Rarefied Gas Dynamics, Toronto, July 14-17, 1964. In: Rarefied Gas Dynamics, J. H. de Leeuw, Ed., Academic Press, New York (1965)

21. Bernstein, I.B.; Rabinowitz, I.N. — Theory of Electrostatic Probes in a Low Density Plasma. Princeton Univ., Plasma Phys. Lab. A.E.C.R.&D. Rep. PM-S-38 (1959).

22. Hamza, V.; Richley, E.A. — Numerical Solution of Two-Dimensional Poisson Equation: Theory and Application to Electrostatic-Ion-Engine Analysis. NASA Tech. Note D-1323 (1962).

23. Hall, L.S. — Probes and Magnetic Pumping in Plasma. Univ. of California, Lawrence Radiation Lab. Rep. No. UCRL-6535 (1961).

24. Hall, L.S. — The Computation of Self-Consistent Potential Distributions in a Collisionless Plasma. Univ. of California, Lawrence Radiation Lab. Rep. No. UCRL-7660-T (1964).

25. Hall, L.S.; Freis, R.P. — Theory of the Electrostatic Probe and Its Improved Use as a Diagnostic Tool. Univ. of California, Lawrence Radiation Lab. Rep. No. UCRL-12480 (1965).

26. Moskalenko, A.M. — Concentration and Flux of Particles Near a Cylindrical Body in a Plasma. XVth International Astronautical Congress, Warsaw, Poland, Sept. 7-12, 1964.

27. Lam, S.H. — Plasma Diagnostics with Moderately Large Langmuir Probes. Phys. of Fluids, Vol. 8, p. 1002 (1965).

28. Walker, E.H. — Plasma Sheath and Screening Around A Stationary Charged Sphere and a Rapidly Moving Charged Body. In: Interactions of Space Vehicles with an Ionized Atmosphere, S.F. Singer, Ed., Pergamon Press, London (1965).

29. Bettinger, R.T. Walker, E.H. — Relationship for Plasma Sheaths About Langmuir Probes. Phys. of Fluids, Vol. 8, Page 748 (1965).

30. Medicus, G. — Theory of Electron Collection of Spherical Probes. Journal of Applied Physics, Vol. 32, p. 2512 (1961).

TABLE 1

Maximum Number Density $N_{max.}$ of a Species of Charged Particles Whose Scattering Distance S_d is to be Larger Than One Probe Diameter, As a Function of R_p/λ_D and T

R_p/λ_D	$g_{max.}$	$T = 10^3\,°K$	$T = 2 \times 10^4\,°K$
2.5	6.34	4.3×10^{15}	3.5×10^{19}
10	0.712	5.5×10^{13}	4.4×10^{17}
100	0.0415	1.85×10^{11}	1.48×10^{15}

TABLE 2

Asymptotic Potentials at Large Radius

	Spherical Symmetry	Cylindrical Symmetry
Unshielded Coulomb Potential	$\phi \; \alpha \; r^{-1}$	Logarithmic Divergence
Debye Shielded Potential	$\phi \; \alpha \; \dfrac{e^{-r/\lambda_D}}{r}$	$\phi \; \alpha \; \dfrac{e^{-r/\lambda_D}}{\sqrt{r}}$
Current-Collecting Probe	$\phi \; \alpha \; r^{-2}$	$\phi \; \alpha \; r^{-1}$
Current-collecting Probe; Attracted Particles at Zero Temperature	$\phi \; \alpha \; r^{-4}$	$\phi \; \alpha \; r^{-2/3}$

TABLE 3a

Partial List of Correspondences Between Text Symbols and Fortran Variable Names

Text Reference	Text Symbol	Fortran Variable Name	Program Reference
Eq. (9.1)	x	X	Main Programs 1 and 2 and Related Subprograms
	x^2	XSQ	"
Eq. (D.2)	s	S	"
Eq. (D.2)	dx/ds	DXDS	"
	r/R_p	ROP	FFN 362*, 256*
	$\sqrt{1-x^2}$	SCOT	FFN 18*, 255*
Eq. (5.1)	$M(r)$	COOK	Function COOKIE
Eq. (9.1)	χ	XI	Main Programs 1 and 2 and Related Subprograms
Eq. (D.2)	$d\chi/ds$	DXIDS	"
Eq. (9.1)	η	ETA	"
Eq. (9.7)	η_+	ETAPS	Subprograms Charge, Chamon, Cal
Eq. (9.7)	η_-	ETANG	"
Eq. (E.28)	Ω_G	OMGAG	"
"	β_G	BETAG	"
Eq. (E. 29)	α_G	ALFAG	"
Eq. (E.31)	ϵ_G	EPSG	FUNCTIONS CHARGE, CAL
APPENDIX D	y, K_0, K_1	Y	Main Programs 1 and 2, FFN 33,38, 34
APPENDIX D	y	Y	Function CAL, FFN 290
Eqs. (D.21)	Y	Z	Main Programs 1 and 2, FFN 34, 35

FFN- Fortran Formula Number   * Nearest Numbered Formula

TABLE 3a
(continued)

Text Reference	Text Symbol	Fortran Variable Name	Program Reference
Figure 5; If the value of s at point D is the value of the Fortran Variable S(I), Then the value of S at Point L is the value of SH(I). It follows that s_H is Stored in SH(1)	s_H, s_L	SH	Subroutine Charge, FFN 320
	π	PI	Main Programs 1 and 2, FFN 101
	$\sqrt{\pi}$	SQTPI	
	$1/\pi$	VIPI	
	$1/\sqrt{\pi}$	SAY	
Eq. (D.21)	Δs	DELTS	Main Programs 1 and 2, FFN 16*
Eqs. (3.2), (9.1)	γ_+	GAMMA	Main Programs 1 and 2
	π_3	PI3	
	π_6	PI6	
	s_B	P	
	i_+	YPOS	
	i_-	YNEG	
Figure 5b, 6a,10b	β_H	BETH	
Figure 10a	β_C	BETH	
	$e^{-\beta_H}$ OR $e^{-\beta_C}$	EXY	
Smallest and Largest Values of s at Which Locus of Extrema Enters First Quadrant		SW, SWA	Subroutine Charge

TABLE 3a
(concluded)

Text Reference	Text Symbol	Fortran Variable Name	Program Reference
Values of β corresponding to above values of s		BETAW, BETAWA	Subroutine Charge
Smallest and largest values of s at which maxima occur in locus of extrema		SCRIT, SCRITA	Subroutine Charge
Coordinate indices corresponding to smallest values of s, if any, for which the point H in Figs. 5 and 6, corresponding to the cutoff boundary tangent at s, is not in the first quadrant		LK, LKA	
Eqs. (E.45),(E.67)	μ	AMU	Fuctions DYO, TRY
Eqs. (E.45),(E.67)	θ	THETA	Functions DYO, TRY
Eqs. (9.4),(11.7)	β_M	ENG	Subroutine Chamon, FFN 535, 536
Eq. (9.10b)	i_{+-}	YPN	Main Program 1, FFN 357
Eq. (13.6a)	i^*	CURRNT	Main Program 4
Appendix D	$(d\chi/dx)_{s=0}$	EDGE	Main Programs 1 and 2
Fig. 8	Case Number	LINK	Subroutines Charge, First, Second, Third, Fourth (Sphere and Cylinder)
Eq. (E.3)	κ	CAPPA	Functions DUO, DYO
Eq. (E.5)	β_B	AMDA BH	Function TRE Function TRY
Ratio of largest Trapped-orbit radius to R_p		RKRIT RTRAP	Subroutine Charge, FFN 234 Subroutine Charge, FFN 241, Subroutine Chamon, FFN 481*
Ratio of largest Trapped-orbit radius to λ_{D-}		STRAP	Main Program 4, FFN 99*

TABLE 3b

Partial List of Correspondences Between Text Equations and Fortran Formula Numbers

Text Equation	Fortran Formula Number	Program Reference
(9.4),(13.1c)	535	Subroutine CHAMON
(5.1),(9.7)	40	Main Programs 1 and 2
(9.8)	103* 402*	Subroutine CHARGE Subroutine CHAMON
(9.10b)	357	Main Program 1
(9.16)	16* 102	Main Program 1 Subroutine CHARGE
(9.15)	706*, 712* 331*, 328*	Subroutine CHARGE Subroutine CHAMON
(11.7),(13.2c)	536	Subroutine CHAMON
(12.5)	750	Subroutine THIRD (Sphere)
(12.6)	108*, 746*	Subroutine THIRD (Cylinder)
(13.1a)	438, 440, 444, 446, 452, 454	Subroutine CHAMON
(13.16)	456	Subroutine CHAMON
(13.2a)	439, 441, 445, 447, 453, 455	Subroutine CHAMON
(13.2b)	530	Subroutine CHAMON
(13.3a)	446, 452	Subroutine CHAMON
(13.4a)	447, 453	Subroutine CHAMON
(13.13), (13.14)	27*, 42*, 48*, 177*	Main Program 4
(14.1),(E.43)	751, 204	Subroutine THIRD (Sphere)
(14.2),(E.94)	180*, 204	Subroutine THIRD (Cylinder)
(D.2)	33	Main Programs 1 and 2
(D.7),(D.8)	39*, 39	Main Programs 1 and 2
(D.10)	326	Main Program 1
(D.11)	325	Main Programs 1 and 2
(D.12)	281	Main Programs 1 and 2
(D.15),(D.16)	285*, 285	Main Programs 1 and 2
(D.18)	331	Main Program 1
(D.19)	330	Main Programs 1 and 2

* Nearest Numbered Formula

TABLE 3b
(continued)

Text Equation	Fortran Formula Number	Program Reference
(D.21)	34, 35 25, 32	Main Programs 1 and 2 Main Program 3
(D.22)	332 to 337	Function CAL
(E.3)	501* 205*	Function DUO Function DYO
(E.5)	401* 35*	Function TRE Function TRY
(E.1)		Function UNO
(E.2)		Function DUO
(E.4)		Function TRE
(E.10)		Function DYO
(E.11)		Function TRY
(E.17),(E.42)	176, 751	Subroutine THIRD (Sphere)
(E.17)	176,745,180*	Subroutine THIRD (Cylinder)
(E.18)	177*,571,204 177 , 571, 204	Subroutine THIRD (Sphere) Subroutine THIRD (Cylinder)
(E.19)	552*,552 , 551 , 560*	Subroutine FIRST (Sphere or Cylinder)
(E.20)	552*, 556, 560*, 562	Subroutine FIRST (Sphere)
	552*, 556, 571, 573, 560*, 575*	Subroutine FIRST (Cylinder)
(E.21), (E.22)		Function COEFT
(E.23)	305	Function UNO
(E.25)	506	Function DUO
(E.27)	406	Function TRE
(E.30)	126* 126	Subroutine CHARGE Subroutine CHAMON
(E.31)	126	Subroutine CHARGE
(E.32),(E.33)	221, 292	Function CAL
(E.34),(E.89)	560* 540* 750,180* 320*	Subroutines FIRST Subroutines SECOND Subroutines THIRD Subroutines FOURTH

TABLE 3b
(concluded)

Text Equation	Fortran Formula Number	Program Reference
(E.35),(E.90)	562*,575*	Subroutines FIRST
	750 , 746*	Subroutines THIRD
	370, 375*	Subroutines FOURTH
(E.36),(E.91)	226, 310	Function CAL
(E.39)	177, 177*	Subroutine THIRD (Sphere)
(E.44)	200,190,84	Function DYO
(E.52)	10*	Function DYO
(E.53)	50	Function DYO
(E.57)	125*	Function DYO
(E.58)	116*	Function DYO
(E.59)	102*	Function CDO
(E.60) to (E.65)	199 to 216	Function DYO
(E.66)	19, 72, 73	Function TRY
(E.69) to (E.72)	40 to 16	Function TRY
(E.73)	22*	Function TRY
(E.76) to (E.78)	41 to 501	Function TRY
(E.82)	508, 509	Function TRY
(E.84), (E.85)	525 to 510	Function TRY
(E.86)	316*	Subroutine CHARGE
	317	Subroutine CHAMON
(E.87),(E.88)	221, 294	Function CAL
(E.92)	177, 571	Subroutine THIRD (Cylinder)
(F.9)	30*	Main Program 3
(F.15)	25,32	Main Program 3
(F.16)	23	Main Program 3
(G.14)		Subroutine POWERS
(G.15)	140 to 152	Main Program 4

TABLE 4

Suggested Computation Net Spacings and Outer Boundary Radii for Use With Program 1

Sphere: $T_+/T_- = 1$; $\chi_{p_-} = \pm 25$

R_p/λ_{D_-}	Δs	Points Per λ_D at Probe	$\left(\frac{ds}{dx}\right)_{r=R_p}$	s_B	$\frac{R_B}{R_p}$	$\frac{R_B - R_p}{\lambda_D}$
0.5	.0667	30	-1	2.8	16.44	7.7
1	.05	20	-1	2.4	11.02	10.0
2	.0333	15	-1	2.0	7.39	12.8
5	.0133	15	-1	0.80	5.00	20.0
10	.01	10	-1	0.72	3.57	25.7
20	.005	10	-1	0.56	2.27	25.5
50	.005	10	-2.5	0.56	1.64	31.8
100	.005	10	-5	0.50	1.40	40.3

Cylinder: $0 \leq T_+/T_- \leq 1$; $\chi_{p_-} = 25$

R_p/λ_{D_-}	Δs	Points Per λ_D at Probe	$\left(\frac{ds}{dx}\right)_{r=R_p}$	s_B	$\frac{R_B}{R_p}$	$\frac{R_B - R_p}{\lambda_D}$
1	.025	40	-1	2.9	18.17	17.2
2	.025	20	-1	2.3	9.97	17.9
5	.01	20	-1	0.80	5.00	20.0
10	.01	10	-1	0.72	3.57	25.7
20	.0067	7.5	-1	0.60	2.50	30.0
50	.01	5	-2.5	0.56	1.64	31.8
100	.01	5	-5	0.56	1.53	53.4

TABLE 5a

Spherical Probe; Ions at Zero Temperature; Electrons Not Collected by Probe Surface; Ion Currents Obtained from Solution of the Allen, Boyd and Reynolds Equation

$R_p/\lambda_{D-} = 0.5$

$e\phi_p/kT_-$	i_{+-}
0.3136	4.0000
0.8115	8.0000
1.4094	12.0000
2.0770	16.0000
2.8011	20.0000
3.5843	24.0000
5.2656	32.0000
7.0923	40.0000
10.56	54.0000
12.15	60.0000
17.8113	80.0000
23.9553	100.0000
30.4775	120.0000

$R_p/\lambda_{D-} = 0.75$

$e\phi_p/kT_-$	i_{+-}
0.1250	1.7778
0.3575	3.5556
0.6540	5.3333
0.9970	7.1111
1.3787	8.8889
1.8017	10.6667
2.7292	14.2222
3.7614	17.7778
5.77	24.0000
6.69	26.6667
10.0603	35.5556
13.7698	44.4444
17.7467	53.3333
26.4155	71.1111

$R_p/\lambda_{D-} = 1.0$

$e\phi_p/kT_-$	i_{+-}
0.0563	1.0000
0.1767	2.0000
0.3393	3.0000
0.5339	4.0000
0.7557	5.0000
1.0076	6.0000
1.5718	8.0000
2.2163	10.0000
3.50	13.5000
4.10	15.0000
6.3338	20.0000
8.8363	25.0000
11.5497	30.0000
17.5429	40.0000
24.1979	50.0000
31.3254	60.0000

$R_p/\lambda_{D-} = 1.5$

$e\phi_p/kT_-$	i_{+-}
0.0145	0.4444
0.0525	0.8889
0.1088	1.3333
0.1807	1.7778
0.2663	2.2222
0.3678	2.6667
0.6035	3.5556
0.8865	4.4444
1.482	6.0000
1.769	6.6667
2.8855	8.8889
4.1972	11.1111
5.6611	13.3333
9.0028	17.7778
12.8173	22.2222
16.9775	26.6667
26.3051	35.5556

$R_p/\lambda_{D-} = 2.0$

$-e\phi_p/kT_-$	i_{+-}
0.0191	0.5000
0.0411	0.7500
0.0708	1.0000
0.1075	1.2500
0.1522	1.5000
0.2594	2.0000
0.3932	2.5000
0.688	3.3750
0.833	3.7500
1.4259	5.0000
2.1616	6.2500
3.0136	7.5000
5.0479	10.0000
7.4572	12.5000
10.1480	15.0000
16.3272	20.0000
23.3638	25.0000
28.1026	28.1250
33.0521	31.2500

$R_p/\lambda_{D-} = 2.5$

$-e\phi_p/kT_-$	i_{+-}
0.0180	0.4800
0.0316	0.6400
0.0488	0.8000
0.0693	0.9600
0.1214	1.2800
0.1882	1.6000
0.340	2.1600
0.415	2.4000
0.7366	3.2000
1.1550	4.0000
1.6575	4.8000
2.9250	6.4000
4.5001	8.0000
6.3168	9.6000
10.6207	12.8000
15.6457	16.0000
19.0763	18.0000
22.6842	20.0000
26.5548	22.0000
30.5252	24.0000

$R_p/\lambda_{D-} = 3.0$

$-e\phi_p/kT_-$	i_{+-}
0.0157	0.4444
0.0246	0.5556
0.0347	0.6667
0.0617	0.8889
0.0967	1.1111
0.179	1.5000
0.219	1.6667
0.3964	2.2222
0.6359	2.7778
0.9313	3.3333
1.7171	4.4444
2.7478	5.5556
3.9872	6.6667
7.0478	8.8889
10.7385	11.1111
13.3015	12.5000
16.0195	13.8889
18.9623	15.2778
21.9963	16.6667
25.0659	18.0000
28.8479	19.5556

$R_p/\lambda_{D-} = 4.0$

$-e\phi_p/kT_-$	i_{+-}
0.0111	0.3750
0.0202	0.5000
0.0317	0.6250
0.058	0.8438
0.073	0.9375
0.1322	1.2500
0.2150	1.5625
0.3191	1.8750
0.6164	2.5000
1.0381	3.1250
1.5921	3.7500
3.1198	5.0000
5.1487	6.2500
6.6316	7.0313
8.2427	7.8125
10.0306	8.5938
11.9001	9.3750
13.8188	10.1250
16.2165	11.0000
20.5608	12.5000
25.2359	14.0000
30.6338	15.6250

TABLE 5a (concluded)

$R_p/\lambda_{D-} = 5.0$

$-e\phi_p/kT_-$	i_{+-}
0.0128	0.4000
0.024	0.5400
0.029	0.6000
0.0541	0.8000
0.0855	1.0000
0.1271	1.2000
0.2455	1.6000
0.4148	2.0000
0.6493	2.4000
1.3553	3.2000
2.4107	4.0000
3.2467	4.5000
4.1936	5.0000
5.2873	5.5000
6.4589	6.0000
7.6883	6.4800
9.2571	7.0400
12.1543	8.0000
15.3356	8.9600
19.0671	10.0000
26.9644	12.0000

$R_p/\lambda_{D-} = 7.5$

$-e\phi_p/kT_-$	i_{+-}
0.0104	0.3556
0.0163	0.4444
0.0236	0.5333
0.0431	0.7111
0.0696	0.8889
0.1046	1.0667
0.2081	1.4222
0.3680	1.7778
0.5137	2.0000
0.6912	2.2222
0.9244	2.4444
1.2009	2.6667
1.5221	2.8800
1.9801	3.1289
2.9282	3.5556
4.0977	3.9822
5.5930	4.4444
9.0476	5.3333
13.1432	6.2222
17.8576	7.1111
23.0113	8.0000
28.6300	8.8889

$R_p/\lambda_{D-} = 10$

$-e\phi_p/kT_-$	i_{+-}
0.0129	0.4000
0.0207	0.5000
0.0299	0.6000
0.0562	0.8000
0.0929	1.0000
0.1209	1.1250
0.1589	1.2500
0.2009	1.3750
0.2546	1.5000
0.3139	1.6200
0.4024	1.7600
0.6000	2.0000
0.8772	2.2400
1.2889	2.5000
2.4710	3.0000
4.1858	3.5000
6.4377	4.0000
9.0921	4.5000
12.1481	5.0000
19.2713	6.0000
27.4560	7.0000

$R_p/\lambda_{D-} = 15$

$-e\phi_p/kT_-$	i_{+-}
0.0100	0.3556
0.0162	0.4444
0.0211	0.5000
0.0260	0.5556
0.0315	0.6111
0.0376	0.6667
0.0452	0.7200
0.0532	0.7822
0.0716	0.8889
0.0942	0.9956
0.1220	1.1111
0.1966	1.3333
0.3104	1.5556
0.4922	1.7778
0.7682	2.0000
1.2052	2.2222
2.7249	2.6667
5.1857	3.1111
8.5188	3.5556
17.2951	4.4444

$R_p/\lambda_{D-} = 20$

$-e\phi_p/kT_-$	i_{+-}
0.0112	0.3750
0.0134	0.4050
0.0160	0.4400
0.0211	0.5000
0.0258	0.5600
0.0336	0.6250
0.0496	0.7500
0.0703	0.8750
0.0961	1.0000
0.1283	1.1250
0.1686	1.2500
0.2924	1.5000
0.5198	1.7500
0.9526	2.0000
3.0830	2.5000
7.2985	3.0000
13.2897	3.5000
20.6601	4.0000
24.8126	4.2500

$R_p/\lambda_{D-} = 50$

$-e\phi_p/kT_-$	i_{+-}
0.0131	0.4000
0.0190	0.4800
0.0266	0.5600
0.0346	0.6400
0.0396	0.6800
0.0959	1.0000
0.6781	1.7000
1.0751	1.8000
3.0099	2.0000
7.0263	2.2000
12.8249	2.4000
20.0797	2.6000

$R_p/\lambda_{D-} = 100$

$-e\phi_p/kT_-$	i_{+-}
0.0148	0.4250
0.0167	0.4500
0.0207	0.5000
0.0253	0.5500
0.0303	0.6000
0.0363	0.6500
0.0493	0.7500
0.0964	1.0000
0.3579	1.5000
1.1372	1.7000
2.9558	1.8000
12.5135	2.0000
19.6093	2.1000
27.8552	2.2000

TABLE 5b

Ion-Attracting Spherical Probe: Computed Values of Ion Current i_{+-}

For Values of T_+/T_- Between 0 and 1

$\frac{e\phi_p}{kT_-}$	$\frac{T_+}{T_-}$	$\frac{R_p}{\lambda_{D-}}$	i_{+-} Ions Maxwellian	i_{+-} Ions Mono-Energetic	i_{+-} Ions Mono-Energetic, Electrons Not Collected by Probe Surface
-25	0.75	10	5.938	5.826	
-20	"	"	5.350	5.249	
-15	"	"	4.708	4.620	
-10	"	"	3.978	3.902	
- 5	"	"	3.067	3.006	3.008
- 1	"	"	1.728	1.688	1.727
-25	0.5	10	5.838	5.709	
-20	"	"	5.263	5.145	
-15	"	"	4.634	4.527	
-10	"	"	3.919	3.827	
- 5	"	"	3.026	2.948	2.950
- 1	"	"	1.683	1.633	1.691
-25	0.25	10	5.810	5.659	
-20	"	"	5.236	5.102	
-15	"	"	4.615	4.498	
-10	"	"	3.911	3.803	
- 5	"	"	3.030		2.940
- 1	"	"	1.669	1.607	1.693
-25	0.1	10		5.795	
-10	"	"	4.018	3.911	
- 7	"	"	3.51		
- 5	"	"	3.1[illegible]		
-3	"	"	2.62		
- 2	"	"	2.27		
- 1.5	"	"	2.039	1.973	2.045
- 1.0	"	"	1.725	1.663	1.777
- 0.7	"	"	1.47		
- 0.5	"	"	1.242		
- 0.3	"	"	0.965		
- 0.1	"	"	0.586		
- 1	0.05	10		1.741	1.875
-25	0.75	1	24.166	23.536 (OML)	
- 5	"	"	6.186	5.400 (OML)	5.400 (OML)
-25	0.5	"	27.631	28.475 (OML)	
- 5	"	"	7.025	6.261 (OML)	6.261 (OML)
-25	0.25	"	34.1[illegible]	36.953	
- 5	"	"	8.77[illegible]	8.354 (OML)	8.354 (OML)
-25	0.5	2	19.263	19.643	
"	"	3	14.290	14.148	
"	"	5	9.627	9.459	
"	"	20	3.798	3.698	

(OML) - Orbital Motion Limited

TABLE 5c

Spherical Probe: Computed Values of Attracted-Species Current i_+ or i_- for $T_+/T_- = 1$

Both Species Maxwellian.

$\pm \frac{e\phi_p}{kT_-}$ ↓ \ R_p/λ_D →	0	0.2	0.3	0.5	1	2	3	5	7.5	10	15	20	50	100
0	1.0													1.0
0.1	1.1				1.0999			1.099		1.098		1.097	1.095	1.094
0.3	1.3				1.299		1.293	1.288		1.280		1.269	1.255	1.245
0.6	1.6				1.595	1.584	1.572	1.552		1.518		1.481	1.433	1.402
1.0	2.0				1.987	1.955	1.922	1.869		1.783		1.694	1.592	1.534
1.5	2.5			2.493	2.469	2.399	2.329	2.219		2.050		1.887	1.719	1.632
2.0	3.0			2.987	2.945	2.824	2.709	2.529		2.266		2.030	1.803	1.694
3.0	4.0			3.970	3.878	3.632	3.406	3.068		2.609		2.235	1.910	1.762
5.0	6.0			5.917	5.687	5.126	4.640	3.957		3.119		2.516	2.037	1.833
7.5	8.5			8.324	7.871	6.847	6.007	4.887	4.094	3.620		2.779	2.148	1.891
10.0	11.0			10.704	9.990	8.460	7.258	5.710	4.658	4.050		3.002	2.241*	1.938*
15.0	16.0			15.403	14.085	11.482	9.542	7.167	5.645	4.796		3.383	2.397	2.022
20.0	21.0			20.031	18.041	14.314	11.636	8.473	6.518	5.453	4.318	3.716	2.532*	2.097*
25.0	26.0	25.763	25.462	24.607	21.895	17.018	13.603	9.676	7.318	6.053	4.719	4.018	2.658	2.166

* Obtained By Graphical Interpolation

Table 5d

Spherical Probe: Computed Values of Attracted-Species Current i_+ or i_- For $T_+/T_- = 1$; Attracted Species Mono-Energetic. Results for the Case of Repelled Particles Not Collected By Probe Surface are Shown in Brackets

$\pm \frac{e\phi_p}{kT_-}$ ↓ / R_p/λ_{D-} →	0	1	2	3	5	7.5	10	15	20	50	100
0	1.0										1.0
0.1	1.0785									1.0785 (1.0785)	1.078 (1.0785)
0.3	1.2356								1.2356 (1.2356)	1.227 (1.2356)	1.216 (1.2356)
0.6	1.4712				1.4712 (1.4712)		1.4708 (1.4712)		1.446 (1.4712)	1.395 (1.468)	1.362 (1.464)
1.0	1.7854				1.7854 (1.7854)		1.748 (1.773)		1.655 (1.710)	1.546 (1.627)	1.486 (1.581)
[illegible]	[illegible]				[illegible]		2.019 ([illegible])		1.843 (1.885)	[illegible]	[illegible]
[illegible]	[illegible]				[illegible]		[illegible]		[illegible] (2.009)	[illegible]	[illegible]
[illegible]	[illegible]			[illegible]	[illegible]		[illegible] (2.582)		2.183 (2.193)	1.851 (1.863)	[illegible]
[illegible]	[illegible]			[illegible]	3.984 (3.985)		3.076 (3.077)		2.458 (2.459)	1.976 (1.979)	1.773 (1.775)
7.5	6.89[illegible]		6.890	6.245	4.910	4.059	3.569		2.719	2.087	1.828
10.0	8.854		8.854	7.565	5.730	4.614	3.991		2.933		
15.0	12.781		12.763	9.931	7.173	5.536	4.725		3.310	2.327	1.954
20.0	16.708	16.708	15.985	12.089	8.459	6.445	5.370	4.232	3.633		
25.0	20.635	20.635	19.008	14.066	9.642	7.232	5.957	4.628	3.930	2.583	2.080

TABLE 5e

Electron-Attracting Spherical Probe: Computed Values of Electron Current For Values of T_+/T_- Between 0 and 1

(Repelled Species Colder)

$\frac{e\phi_p}{kT_-}$	$\frac{T_+}{T_-}$	$\frac{R_p}{\lambda_{D-}}$	i_- Electrons Maxwellian	i_- Electrons Mono-Energetic	i_- Electrons Mono-Energetic, Ions Not Collected by Probe Surface
25	0.75	10	5.629	5.555	
25	0.5	10	5.156	5.102	
20	"	"	4.641	4.592	
15	"	"	4.077	4.041	
10	"	"	3.446	3.418	
5	"	"	2.675	2.660	
3	"	"	2.276	2.268	2.268
1	"	"	1.679	1.672	1.683
0.6	"	"	1.473	1.457	1.467
25	0.25	10	4.614	4.580	
25	0.1	10	4.233	4.216	
20	"	"	3.798	3.790	
15	"	"	3.329	3.326	
10	"	"	2.806	2.808	
7.5	"	"	2.511	2.517	
5	"	"	2.180	2.190	
3	"	"	1.868	1.882	
2	"	"	1.681	1.698	
1.5	"	"	1.574		
1.0	"	"	1.451		
0.7	"	"	1.364		
0.5	"	"	1.296		
0.3	"	"	1.212		
0.1	"	"	1.090		
25	0.5	1	20.412	20.635 (OML)	
"	"	2	15.261	17.324	
"	"	3	11.992	12.549	
"	"	5	8.397	8.423	
"	"	20	3.378	3.317	

(OML) - Orbital Motion Limited

TABLE 5f

Electron-Attracting Spherical Probe: Computed Values of Electron Current i_- for $T_+/T_- = 0$ (Repelled Species at Zero Temperature). Electrons Maxwellian; Results for Mono-Energetic Electrons are Shown in Brackets

$\frac{e\phi_p}{kT_-}$ ↓ \ R_p/λ_{D-} →	0	0.5	1	2	3	5	10	15	20	∞
0	1.0									1.0
0.1	1.1 (1.0785)	1.097	1.094	1.089	1.085	1.077 (1.0785)	1.063 (1.075)			
0.3	1.3 (1.2356)	1.287	1.273	1.249	1.230	1.198 (1.234)	1.147 (1.171)			
0.6	1.6 (1.4712)	1.566	1.529	1.469	1.421 (1.4712)	1.349 (1.422)	1.242 (1.270)			
1.0	2.0 (1.7854)	1.930	1.858	1.740 (1.7854)	1.650 (1.781)	1.522 (1.620)	1.345 (1.374)		1.202 (1.206)	
1.5	2.5 (2.178)	2.378	2.253	2.056 (2.178)	1.911 (2.120)	1.712 (1.828)	1.454 (1.482)			
2.0	3.0 (2.571)	2.819	2.637	2.356 (2.571)	2.154 (2.419)	1.885 (2.011)	1.551 (1.578)			
3.0	4.0 (3.356)	3.687	3.379	2.920 (3.356)	2.602 (2.949)	2.196 (2.335)	1.721 (1.746)			
5.0	6.0 (4.927)	5.379	4.791 (4.927)	3.956 (4.817)	3.408 (3.858)	2.738 (2.887)	2.009 (2.030)			
7.5	8.5 (6.890)	7.437	6.466 (6.890)	5.147 (6.316)	4.312 (4.847)	3.330 (3.483)	2.317 (2.334)	1.919 (1.919)		
10.0	11.0 (8.854)	9.448	8.073 (8.854)	6.262 (7.673)	5.146 (5.742)	3.866 (4.018)	2.592 (2.606)	2.105 (2.103)	1.848 (1.843)	
15.0	16.0 (12.781)	13.370	11.150 (12.781)	8.347 (10.143)	6.682 (7.361)	4.834 (4.981)	3.082 (3.090)	2.436 (2.430)	2.100 (2.091)	
20.0	21.0 (16.708)	17.195	14.098 (16.708)	10.303 (12.404)	8.102 (8.838)	5.713 (5.853)	3.523 (3.526)	2.733 (2.723)	2.326 (2.313)	
25.0	26.0 (20.635)	20.945	16.956 (20.635)	12.171 (14.527)	9.444 (10.218)	6.534 (6.665)	3.930 (3.930)	3.006 (2.994)	2.53 (2.518)	1.0

TABLE 6a

Ion-Attracting Cylindrical Probe; Computed Values of Ion Current for $T_+/T_- = 0$

$\frac{e\phi_p}{kT_-}$ ↓ \ R_p/λ_{D_-} →	0	2	2.7	2.9	3	4	5	10	20	30	40	50	60	100
0	0													0
-0.1	0.3568							0.3568						0.3555
-0.3	0.618							0.6167						0.5986
-0.6	0.874							0.8579						0.794
-1.0	1.128						1.123	1.069	1.015			0.961		0.936
-1.5								1.246						
-2.0	1.596					1.588	1.536	1.369	1.239			1.127		1.079
-3.0	1.955					1.902	1.802	1.535	1.347			1.191		1.124
-5.0	2.525					2.338	2.164	1.742	1.468			1.252		1.160
-7.5	3.090				3.090	2.732	2.490	1.922	1.564			1.296		1.185
-10.0	3.568				3.505	3.052	2.753	2.067	1.644			1.329		1.201
-15.0	4.370		4.370	4.252	4.173	3.573	3.185	2.306	1.774	1.569		1.389		1.231
-20.0	5.04				4.730	4.007	3.546	2.504	1.885	1.648	1.520	1.438		1.260
-25.0	5.642	5.642			5.213	4.384	3.857	2.680	1.983	1.718	1.575	1.481	1.418	1.281

TABLE 6b

Ion-Attracting Cylindrical Probe:
Computed Values of Ion Current i_{+-} For Values of T_+/T_- Between 0 and 1

$\frac{e\phi_p}{kT_-}$	$\frac{T_+}{T_-}$	$\frac{R_p}{\lambda_{D-}}$	i_{+-} Ions Maxwellian	i_{+-} Ions Mono-Energetic	i_{+-} Ions Mono-Energetic, Electrons Not Collected by Probe Surface
-25	0.75	10	3.238	3.182	
"	0.5	"	3.075	3.026	
"	0.25	"	2.891	2.856	
"	0.1	"	2.768	2.753	
-20	0.1	10	2.587	2.574	
-15	"	"	2.383	2.369	
-10	"	"	2.138		
- 7	"	"	1.957		
- 5	"	"	1.805		
- 3	"	"	1.594		
- 2	"	"	1.425		
- 1.5	"	"	1.304		
- 1.0	"	"	1.131		
- 0.6	"	"	0.9283		
- 0.3	"	"	0.7066		
- 0.1	"	"	0.4926		
-20	0.5	10	2.875	2.832	
-15	"	"	2.650	2.611	
-10	"	"	2.380	2.345	
- 5	"	"	2.014	1.988	1.989
- 1	"	"	1.326	1.306	1.331
-25	0.5	2	5.588	5.686 (OML)	
"	"	3	5.231	5.686 (OML)	
"	"	5	4.317	4.298	
"	"	20	2.311	2.266	
"	"	50	1.757	1.718	
"	"	100	1.537	1.500	

OML - Orbital Motion Limited

TABLE 6c

Cylindrical Probe: Computed Values of Attracted-Species Current i_+ or i_- For $T_+/T_- = 1$

Both Species Maxwellian

$\pm \frac{e\phi_p}{kT_-}$ ↓ \ R_p/λ_{D_-} →	0	1	1.5	2	2.5	3	4	5	10	20	30	40	50	100
0	1.0													1.0
0.1	1.0804								1.0803					
0.3	1.2101							1.2100	1.208	1.205			1.198	1.194
0.6	1.3721							1.371	1.362	1.348			1.327	1.314
1.0	1.5560						1.554	1.549	1.523	1.486			1.439	1.409
1.5	1.7551					1.754	1.747	1.735	1.677	1.605			1.523	1.478
2.0	1.9320					1.928	1.913	1.893	1.798	1.689			1.576	1.518
3.0	2.2417			2.2417	2.237	2.226	2.192	2.151	1.98	1.801			1.638	1.561
5.0	2.7555			2.750	2.731	2.701	2.626	2.544	2.22	1.940			1.703	1.599
7.5	3.2846			3.266	3.227	3.174	3.050	2.920	2.442	2.060			1.756	1.628
10.0	3.7388		3.735	3.703	3.645	3.567	3.402	3.231	2.622	2.157			1.798	1.650
15.0	4.5114		4.493	4.439	4.342	4.235	3.990	3.749	2.919	2.319	2.082		1.868	1.686
20.0	5.1695	5.1695	5.141	5.060	4.936	4.789	4.489	4.183	3.166	2.455	2.177	2.025	1.929	1.719
25.0	5.7526	5.7525	5.711	5.607	5.462	5.291	4.926	4.565	3.384	2.576	2.262	2.092	1.983	1.747

TABLE 6d

Cylindrical Probe: Computed Values of Attracted-Species Current i_+ or i_- For $T_+/T_- = 1$; Attracted Species Mono-Energetic. Results For the Case of Repelled Particles Not Collected by Probe Surface Are Shown in Brackets

$\pm \frac{e\phi_p}{kT_-}$ ↓ / R_p/λ_{D-} →	0	3	4	5	10	20	30	40	50	100
0	1.0									1.0
0.1	1.0618				1.0618 (1.0618)					
0.3	1.1756				1.1756 (1.1756)					
0.6	1.3281				1.3281 (1.3281)					
1.0	1.5077			1.5077 (1.5077)	1.500 (1.5077)					
1.5	1.7058									
2.0	1.8832			1.8832 (1.8832)	1.785 (1.802)					
3.0	2.1954			2.190 (2.193)	1.964 (1.971)					
5.0	2.7141			2.623 (2.624)	2.201 (2.202)					
7.5	3.2480		3.2480	3.016	2.415					
10.0	3.7057		3.644	3.335	2.589					
15.0	4.4831		4.279	3.857	2.876	2.270	2.031		1.818	1.638
20.0	5.1444		4.805	4.291	3.117	2.400	2.124	1.972	1.879	1.668
25.0	5.7298	5.7298	5.268	4.670	3.328	2.518	2.207	2.040	1.931	1.697

TABLE 6e

Electron-Attracting Cylindrical Probe:

Computed Values of Electron Current For Values of T_+/T_- Between 0 and 1

$\frac{e\phi_p}{kT_-}$	$\frac{T_+}{T_-}$	$\frac{R_p}{\lambda_{D_-}}$	i_- Electrons Maxwellian	i_- Electrons Mono-Energetic	i_- Electrons Mono-Energetic, Ions Not Collected by Probe Surface
25	0.75	10	3.166	3.108	
"	0.5	"	2.915	2.861	
"	0.25	"	2.628	2.583	
"	0.1	"	2.424	2.393	
20	0.1	10	2.263	2.237	
15	"	"	2.083	2.061	
10	"	"	1.870		
7	"	"	1.724		
5	"	"	1.610		
3	"	"	1.471		
2	"	"	1.384		
1.5	"	"	1.333		
1.0	"	"	1.273		
0.6	"	"	1.212		
0.3	"	"	1.147		
0.1	"	"	1.071		
20	0.5	10	2.727	2.678	
15	"	"	2.517	2.473	
10	"	"	2.266	2.233	
5	"	"	1.940	1.919	
1	"	"	1.453	1.445	1.455
25	0.75	1	5.730	5.7298 (OML)	
"	0.5	1	5.667	5.7298 (OML)	
"	0.75	2	5.480	5.7298 (OML)	
"	0.25	2	4.980	5.7298 (OML)	
"	0.5	3	4.826	5.436	
"	"	5	4.012	4.062	
"	"	20	2.204	2.152	
"	"	50	1.692	1.644	
"	"	100	1.491	1.448	
"	0.5	2	5.287	5.7298 (OML)	

(OML) - Orbital Motion Limited

TABLE 6f

Electron-Attracting Cylindrical Probe: Computed Values of Electron Current i_- For $T_+/T_- = 0$ (Repelled Species at Zero Temperature). Electrons Maxwellian; Results for Mono-Energetic Electrons are Shown in Brackets. * - Obtained by Graphical Interpolation

$\frac{e\phi_p}{kT_-}$ ↓ \ R_p/λ_{D_-} →	0	0.5	1	2	3	5	10	20	∞
0	1.0								
0.1	1.0804 (1.0618)	1.076	1.072	1.064	1.059	1.051 (1.0618)	1.038 (1.047)	1.025 (1.028)	1.0
0.3	1.2101 (1.1756)	1.198	1.185	1.163	1.145 (1.1756)	1.120 (1.154)	1.083 (1.095)	1.050 (1.053)	
0.6	1.3721 (1.3281)	1.351	1.326	1.283	1.249 (1.3281)	1.200 (1.247)	1.131 (1.144)	1.075 (1.078)	
1.0	1.5560 (1.5077)	1.524	1.485	1.418 (1.5077)	1.364 (1.483)	1.286 (1.341)	1.182 (1.194)	1.104 (1.104)	
2.0	1.9320 (1.8832)	1.878	1.810	1.689 (1.8832)	1.594 (1.765)	1.457 (1.518)	1.281 (1.290)	1.155 (1.155)	
3.0	2.2417 (2.1954)	2.170	2.076	1.910 (2.1954)	1.780 (1.981)	1.595 (1.657)	1.360 (1.366)	1.198 (1.196)	
5.0	2.7555 (2.7141)	2.652	2.516	2.275 (2.7141)	2.085 (2.328)	1.820 (1 882)	1.489 (1.491)	1.268 (1.265)	
7.5	3.2846 (3.2480)	3.151	2.971	2.652 (3.2480)	2.402 (2.679)	2.051 (2.112)	1.622 (1.621)	1.341 (1.337)	
10.0	3.7388 (3.7057)		3.36*	2.975 (3.7057)	2.673 (2.979)	2.250 (2.310)			
15.0	4.5114 (4.4831)	4.308	4.029 (4.4831)	3.530 (4.438)	3.136 (3.490)	2.588 (2.647)	1.933 (1.925)	1.513 (1.507)	
20.0	5.1695 (5.1444)		4.61* (5.1444)	4.008 (5.049)	3.538 (3.929)	2.880 (2.938)			
25.0	5.7526 (5.7298)	5.485	5.113 (5.7298)	4.436 (5.5964)	3.897 (4.322)	3.142 (3.198)	2.254 (2.241)	1.697 (1.687)	1.0

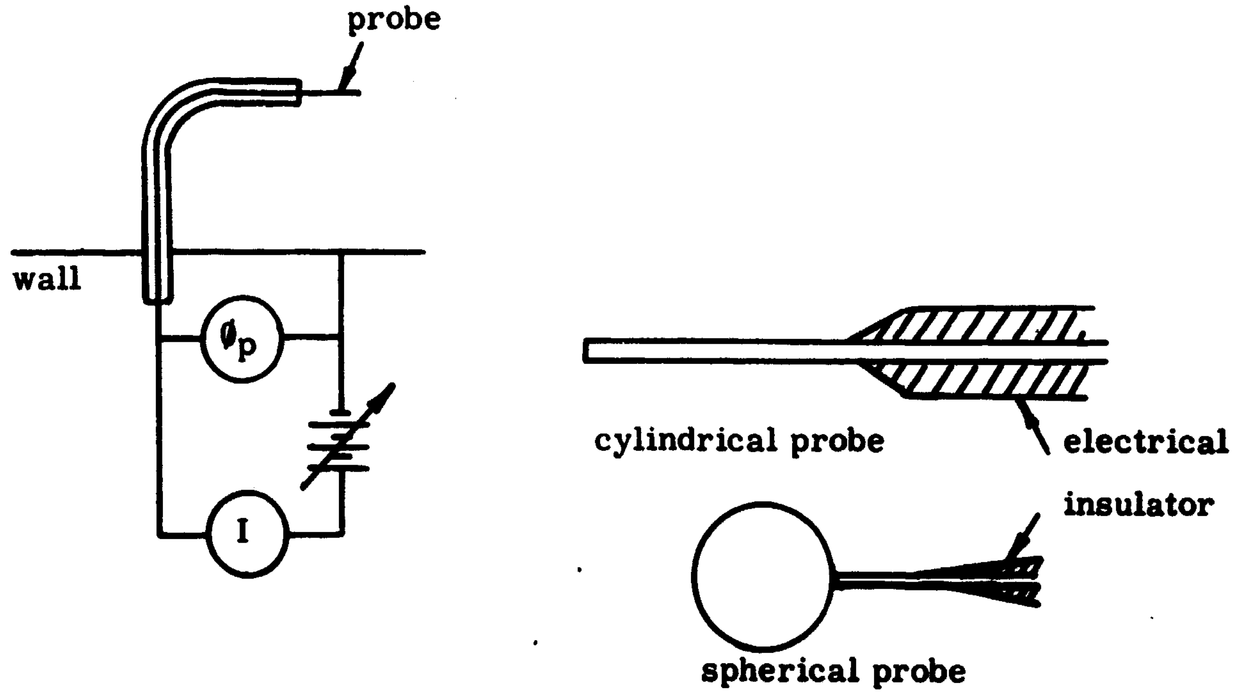

FIGURE 1

PROBES AND BASIC CIRCUIT

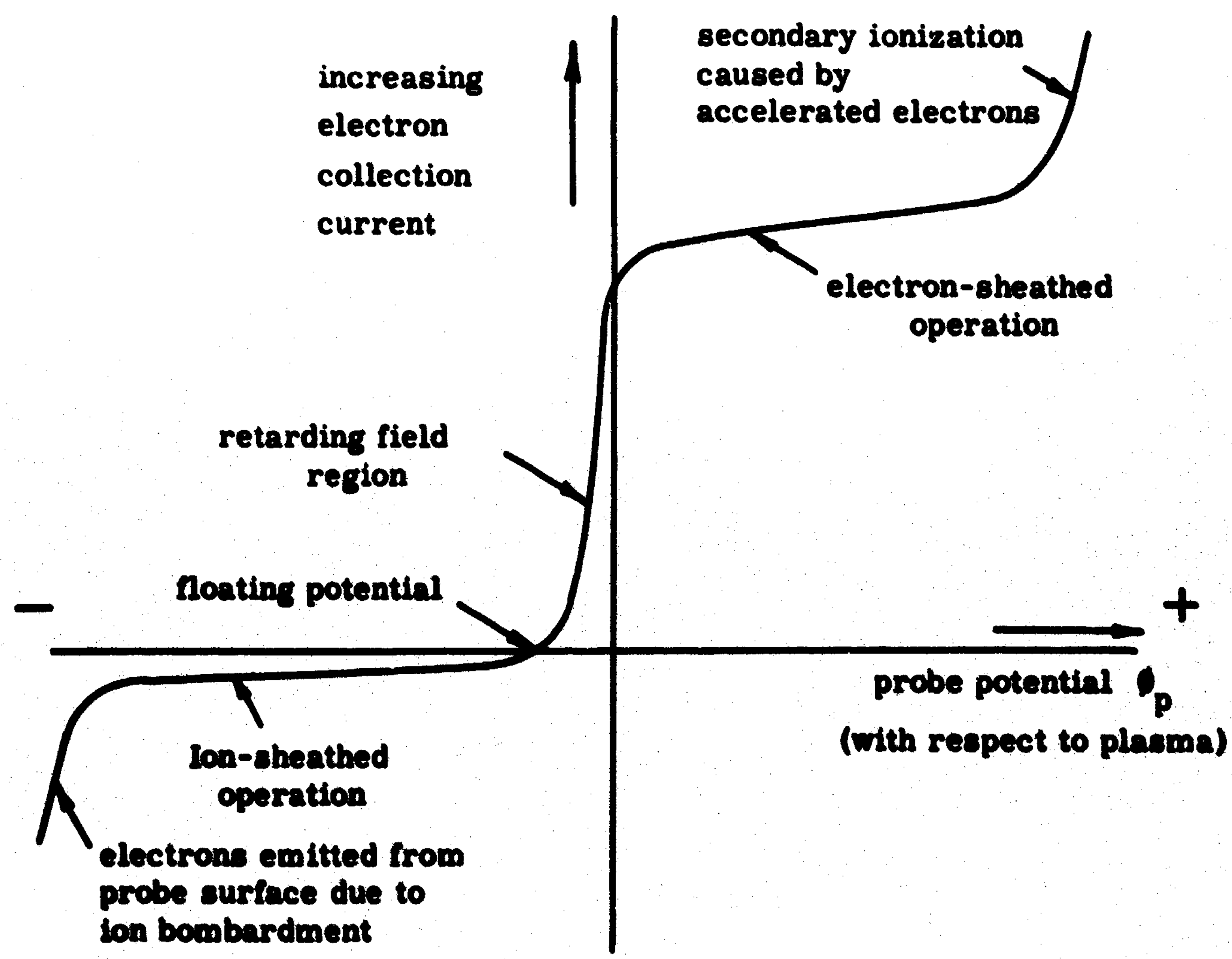

FIGURE 2

COMPLETE LANGMUIR PROBE CHARACTERISTIC.
(AFTER REF. 2) ION CURRENT EXAGGERATED.

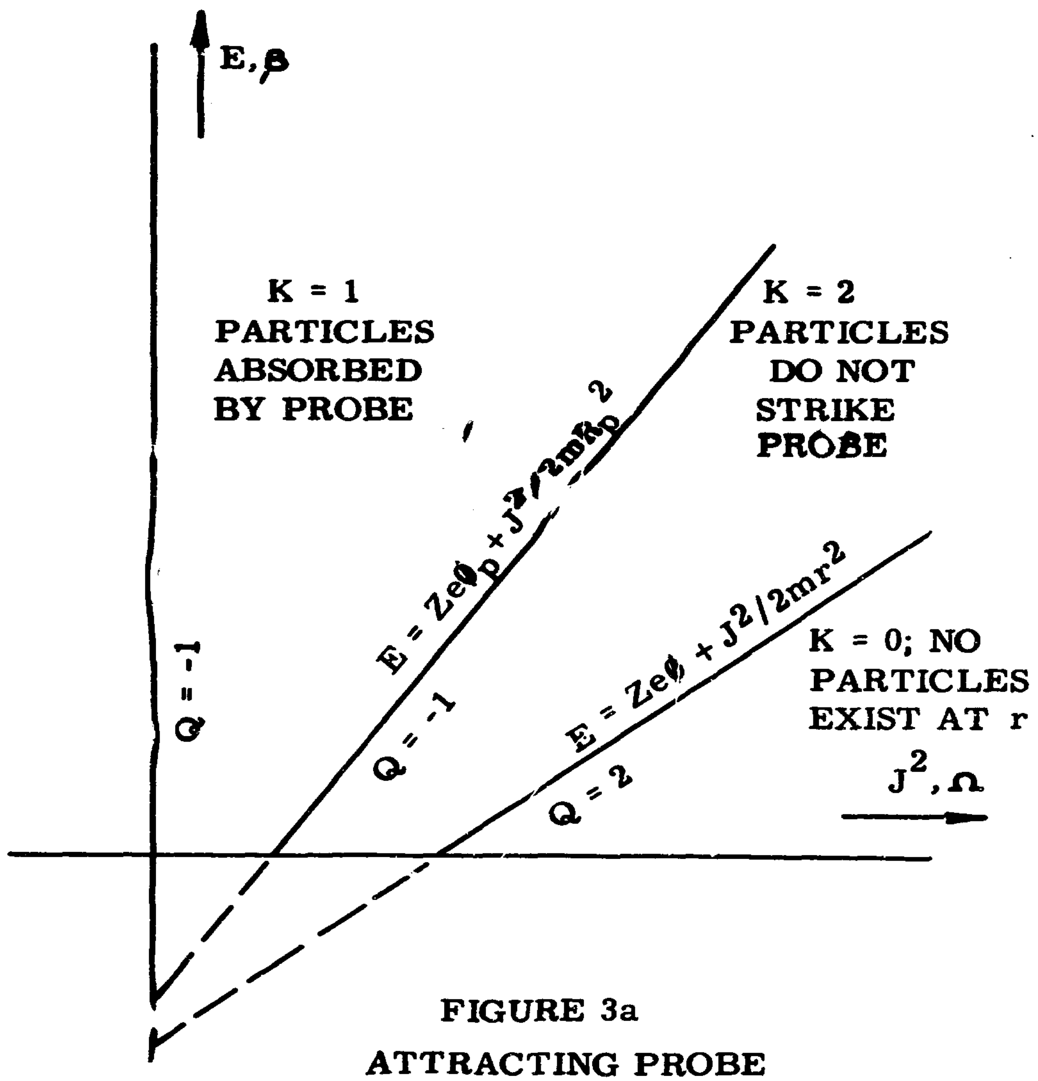

FIGURE 3a

ATTRACTING PROBE

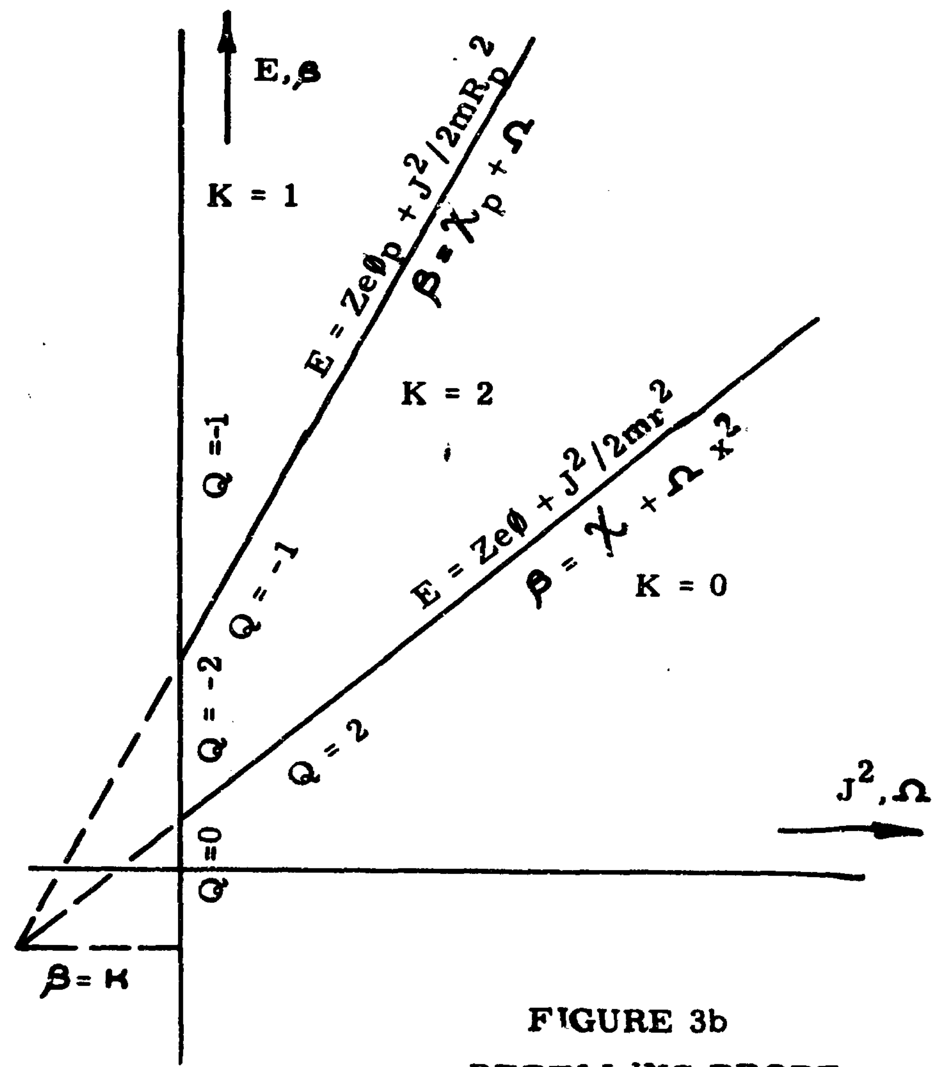

FIGURE 3b

REPELLING PROBE

FIGURE 3: PHASE SPACE OF ENERGY E AND ANGULAR MOMENTUM J CORRESPONDING TO ATTRACTING OR REPELLING PROBE IN THE CASE WHERE POTENTIAL BARRIERS DO NOT INTERVENE. THE QUANTITIES β AND Ω ARE THE NONDIMENSIONAL EQUIVALENTS OF E AND J^2 AS DEFINED IN SEC. IX.

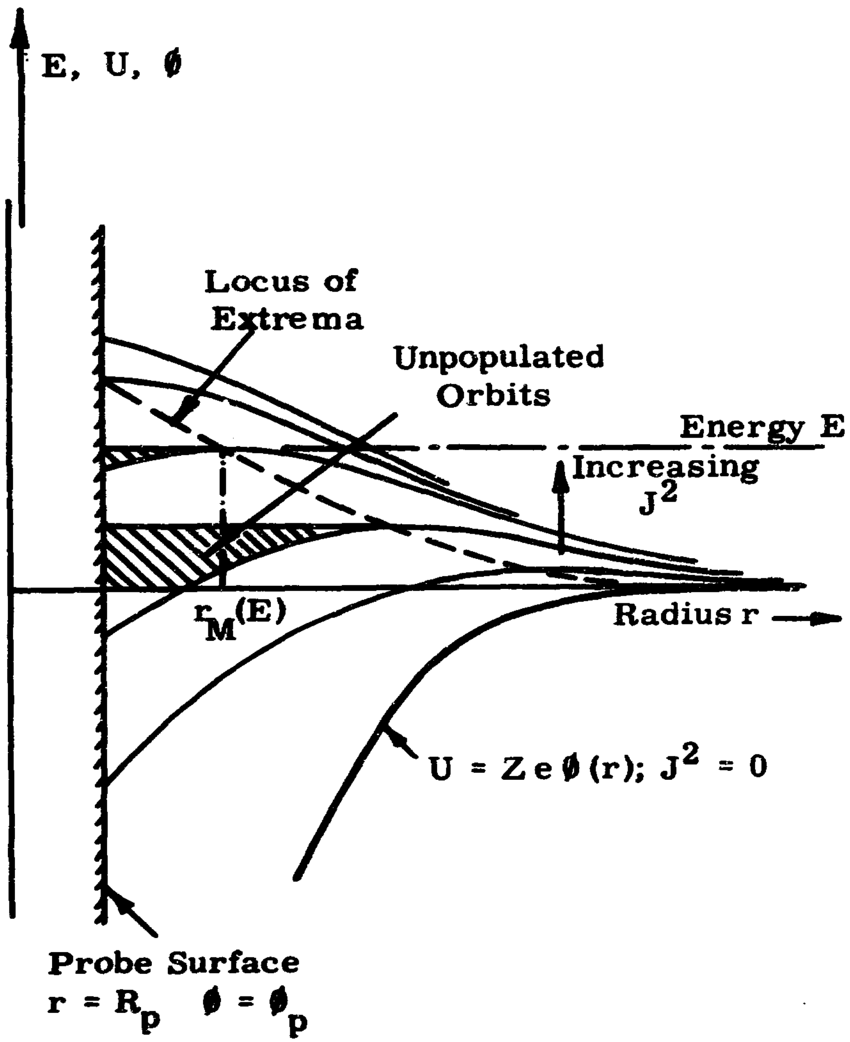

FIGURE 4a

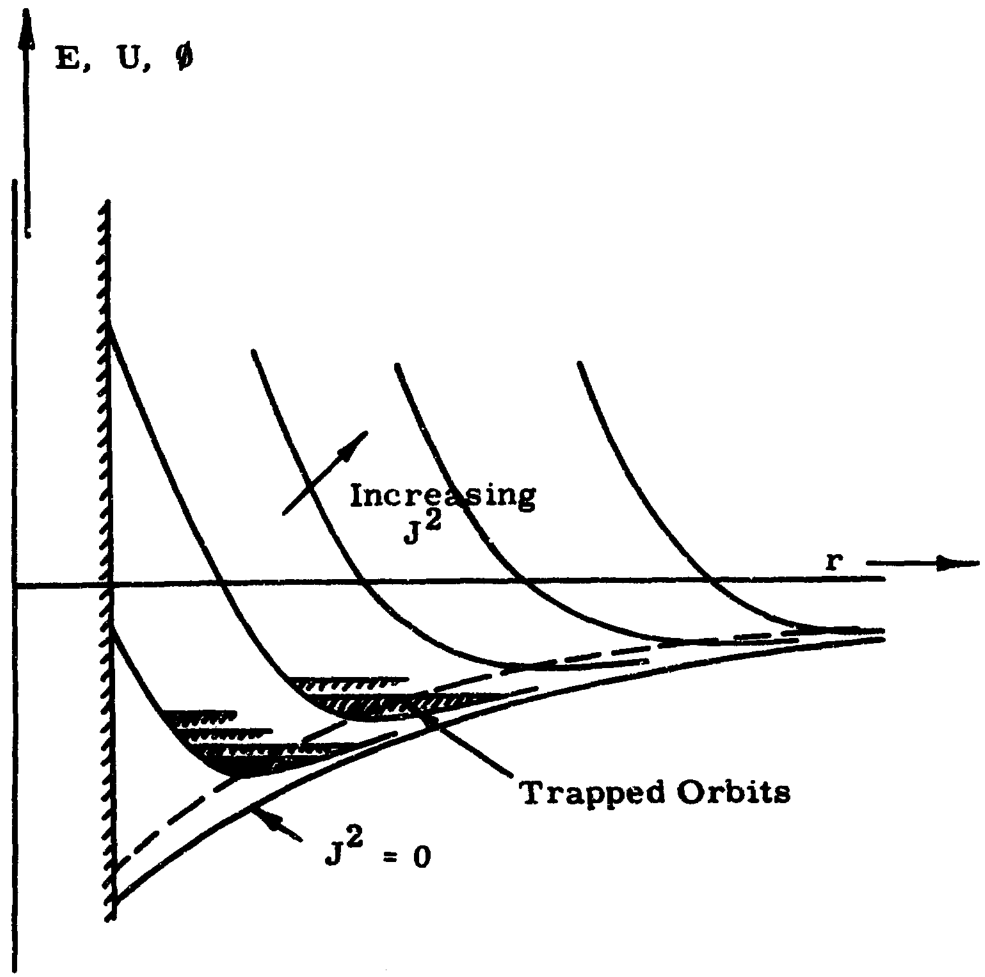

FIGURE 4b

FIGURES 4a AND 4b: EFFECTIVE POTENTIAL VS RADIUS, PLOTTED FOR VARIOUS VALUES OF J^2, CORRESPONDING TO ATTRACTIVE POTENTIALS $\phi(r)$ WHICH DECAY MORE RAPIDLY THAN AN INVERSE SQUARE POTENTIAL OR MORE SLOWLY, RESPECTIVELY.

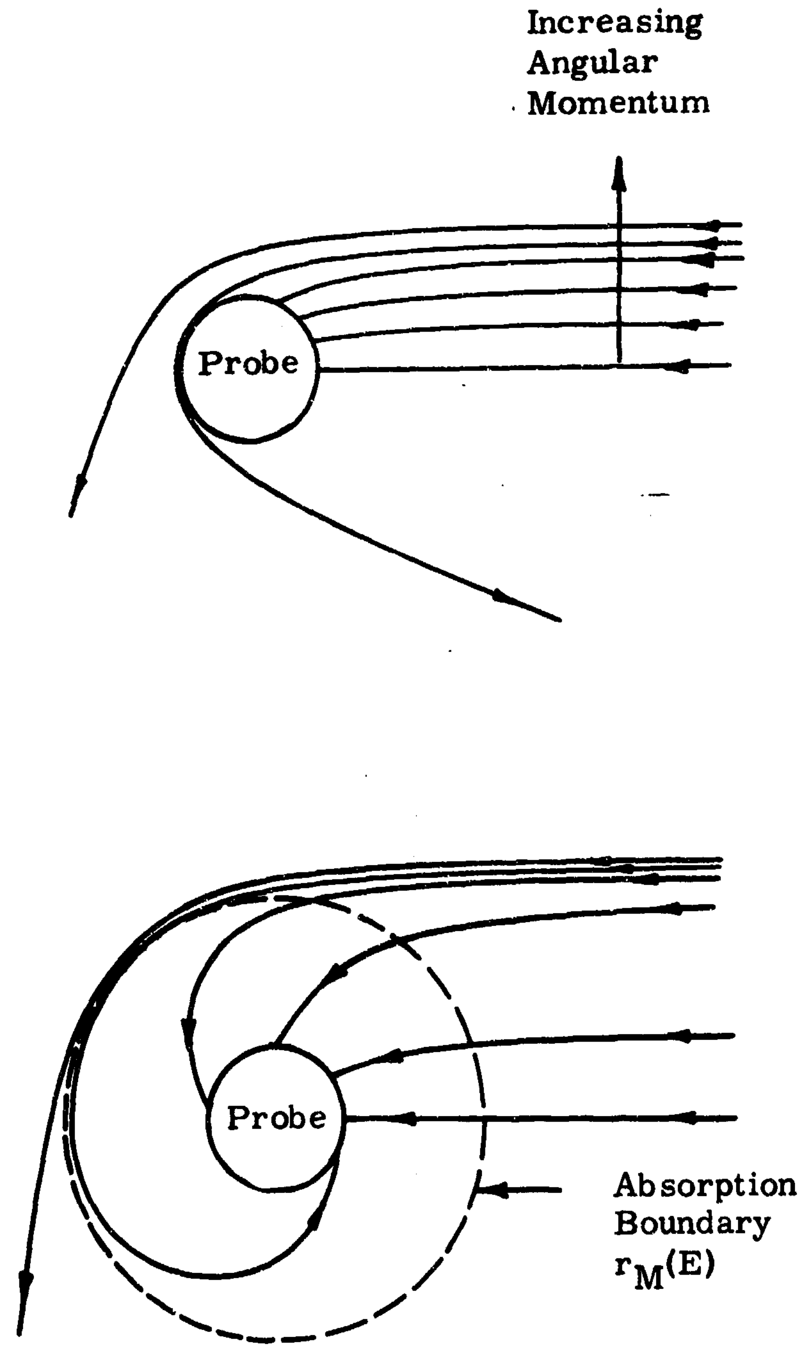

FIGURES 4c and 4d: FAMILIES OF ATTRACTED-PARTICLE ORBITS CORRESPONDING TO THE SAME TOTAL ENERGY E AND VARIOUS VALUES OF ANGULAR MOMENTUM J, SHOWN FOR SITUATIONS WHERE AN ABSORPTION BOUNDARY CORRESPONDING TO THE ENERGY E DOES NOT OR DOES EXIST, RESPECTIVELY.

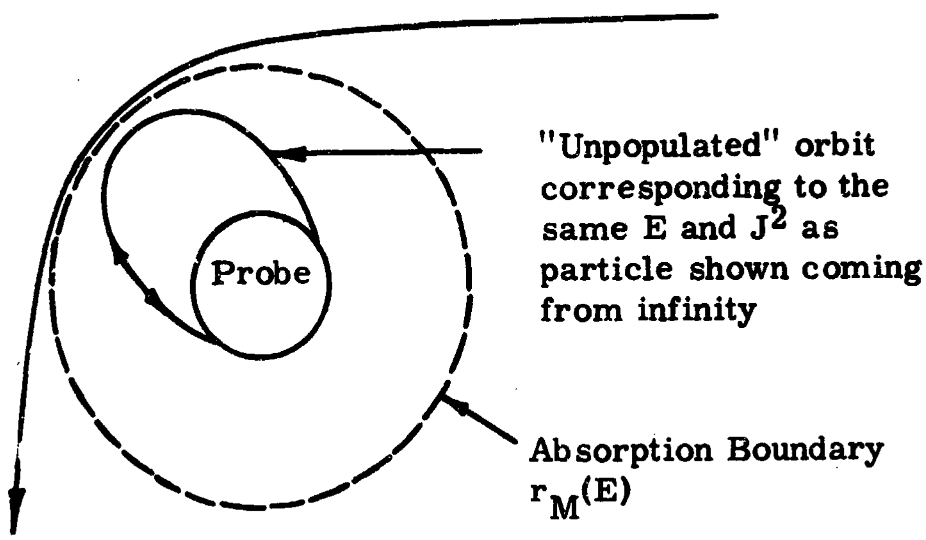

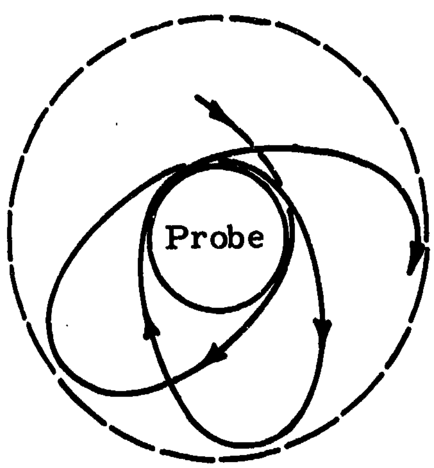

FIGURES 4e and 4f: FIGURE 4e SHOWS THE ORBIT OF A PARTICLE PREVENTED FROM REACHING THE PROBE BECAUSE OF THE EXISTENCE OF AN ABSORPTION BOUNDARY. FIGURE 4f SHOWS A TRAPPED ORBIT OF THE TYPE WHICH EXISTS WHENEVER THE DEPENDENCE OF POTENTIAL ON RADIUS IS LOCALLY SHALLOWER THAN AN INVERSE SQUARE POTENTIAL, CREATING MINIMA IN EFFECTIVE POTENTIAL FOR SOME VALUES OF J.

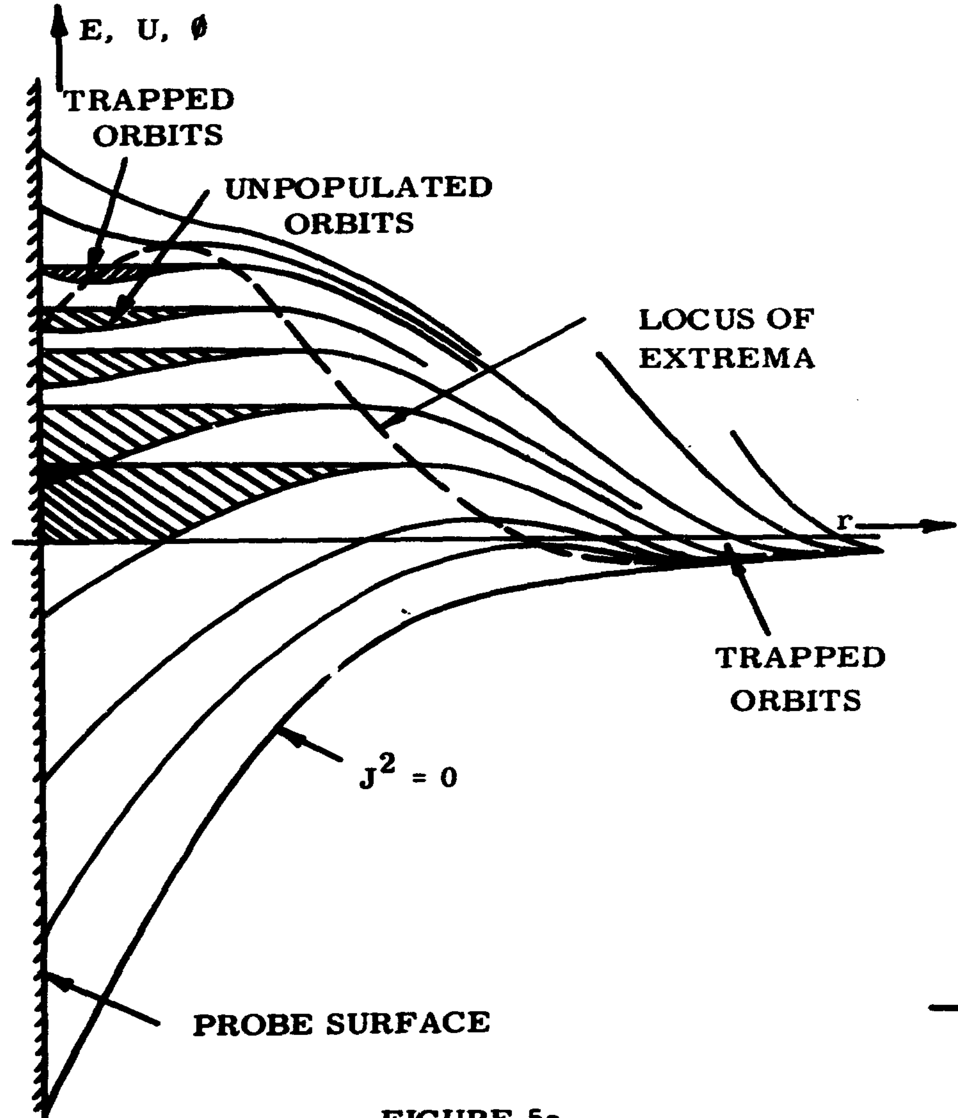

FIGURE 5a

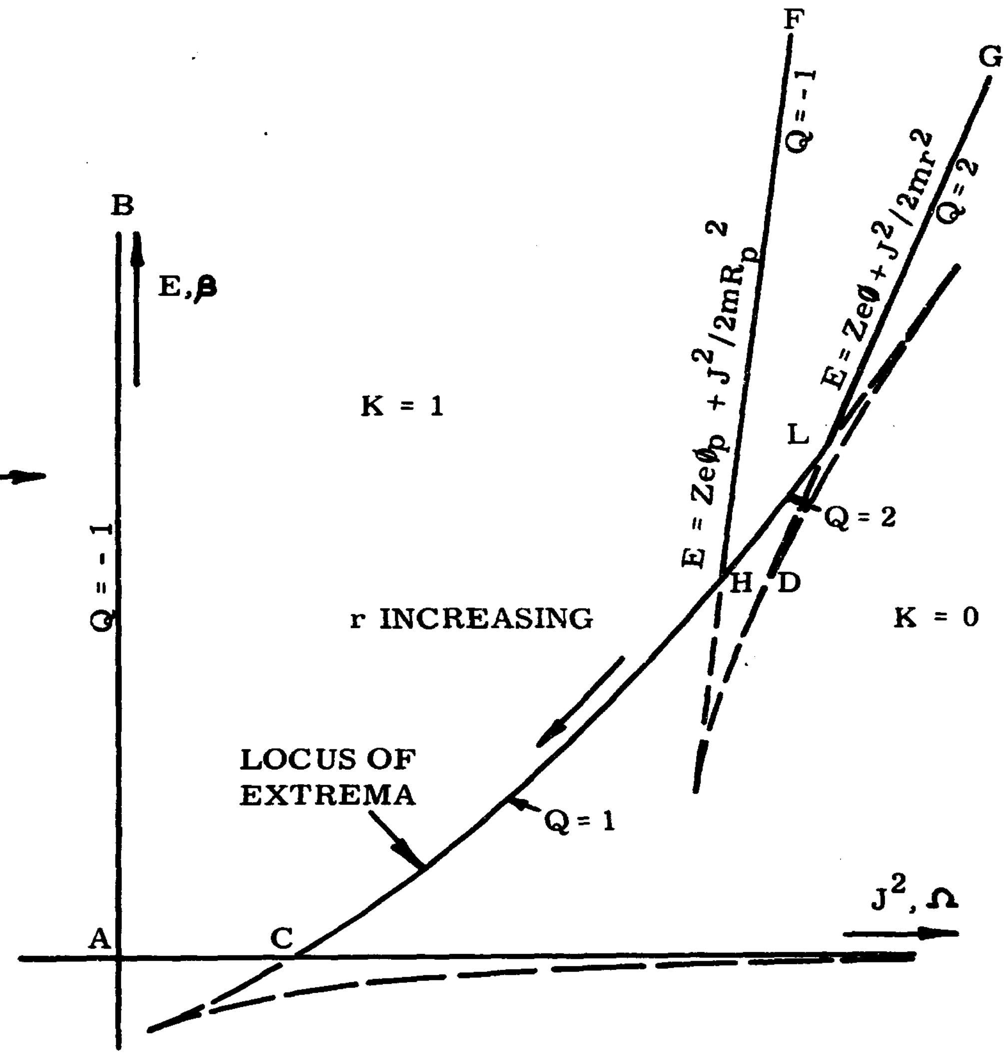

FIGURE 5b

FIGURE 5: INFLUENCE OF POTENTIAL BARRIERS ON PARTICLE TRAJECTORIES FOR A CYLINDRICAL PROBE AT LARGE ATTRACTIVE POTENTIAL

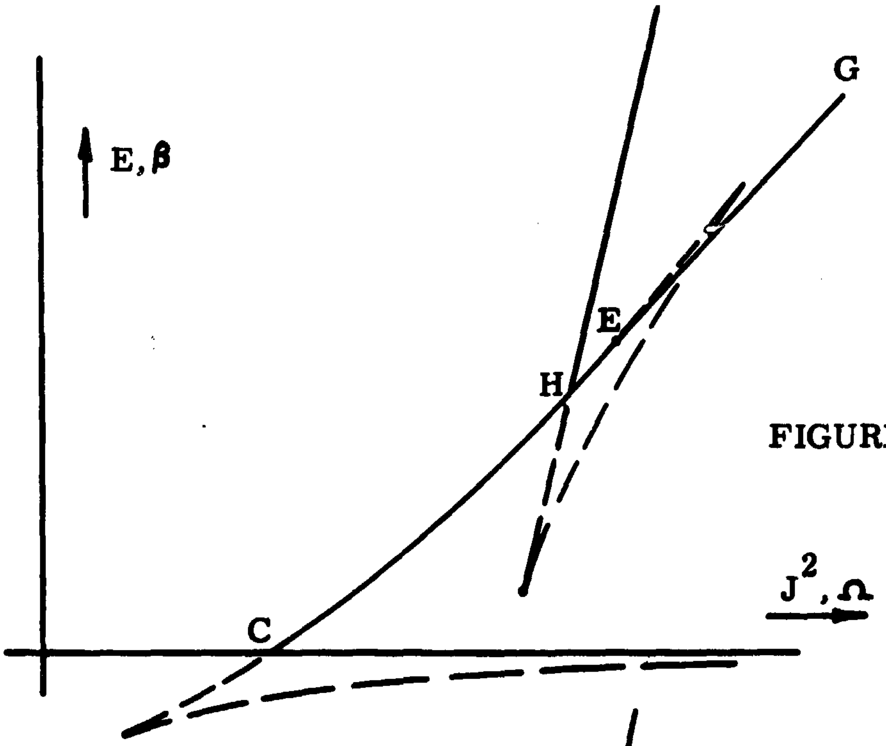

FIGURE 6a

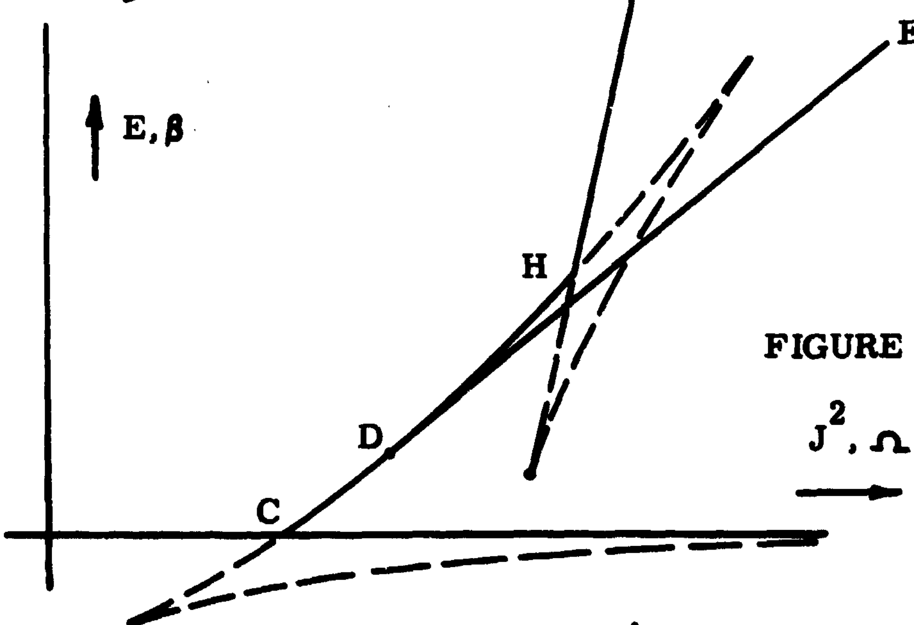

FIGURE 6b

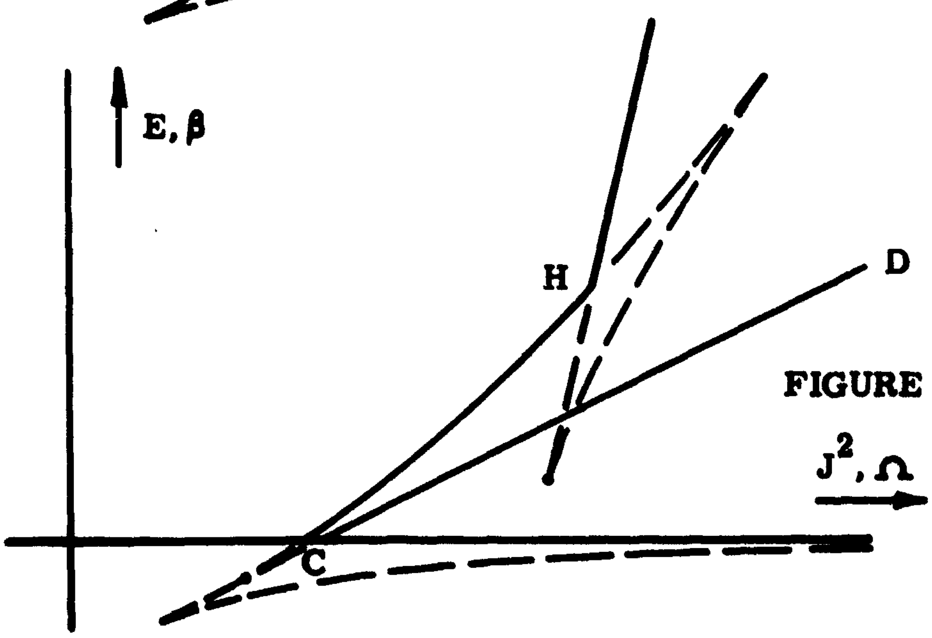

FIGURE 6c

FIGURE 6 QUALITATIVE CHANGES IN THE PATH $J^2{}_2(E)$ CORRESPONDING TO 3 SUCCESSIVELY INCREASING VALUES OF RADIUS r LARGER THAN THE VALUE CORRESPONDING TO FIG. 5b.

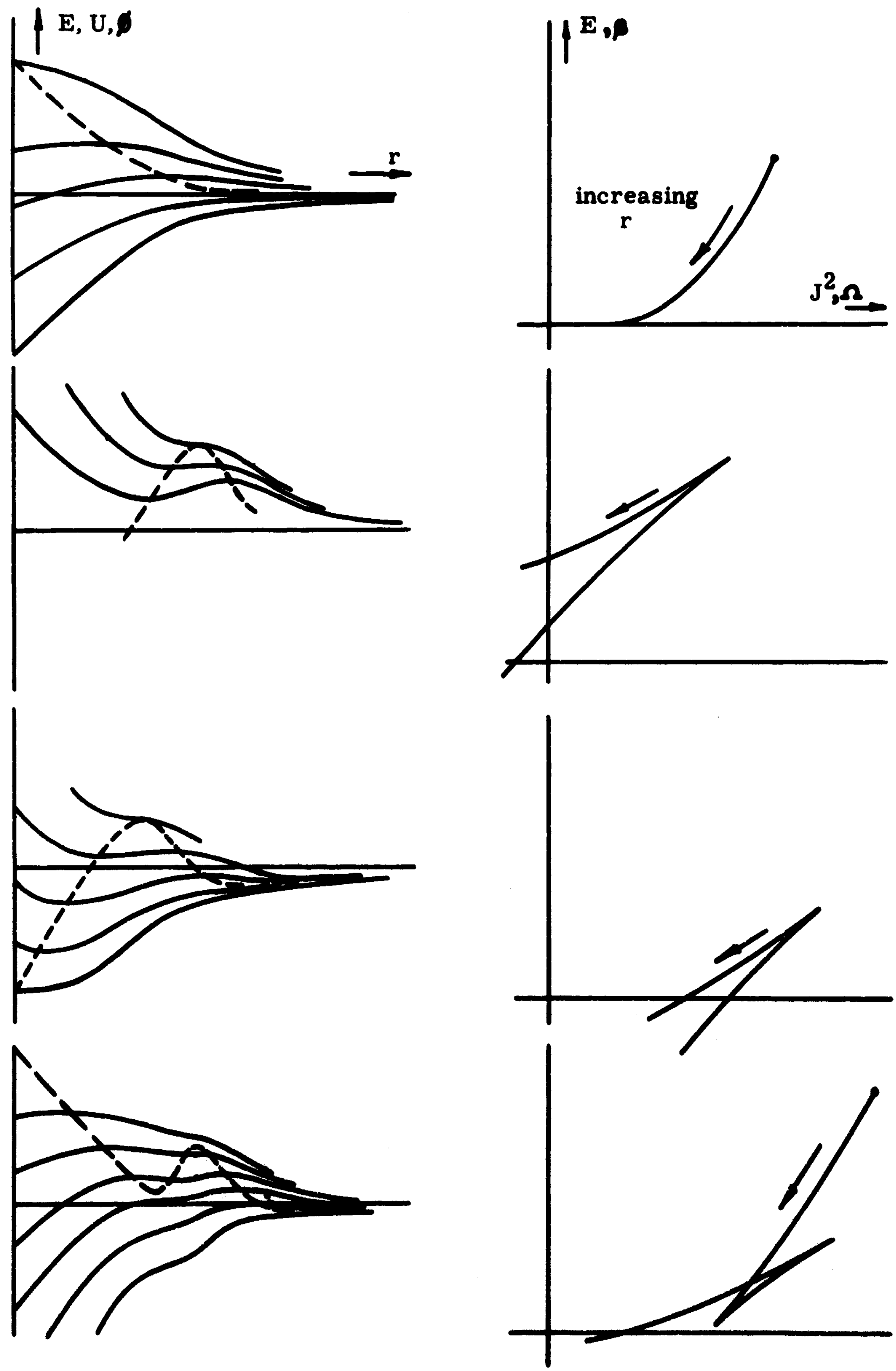

FIGURE 7 LOCI OF EXTREMA IN THE (r, U) AND (J^2, E) PLANES, SHOWING EFFECTS OF IRREGULARLY SHAPED POTENTIAL WELLS

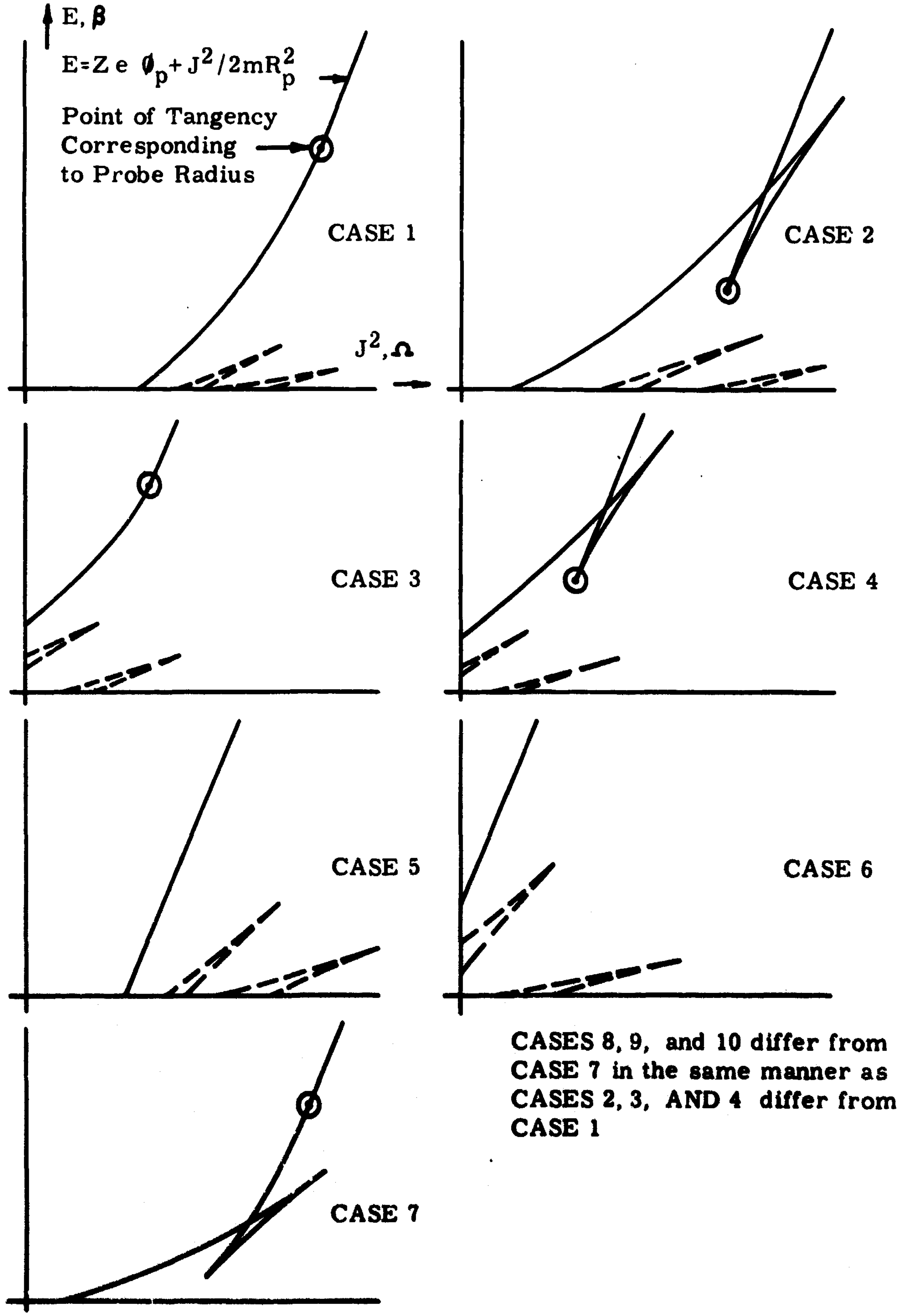

FIGURE 8: LOCI OF EXTREMA IN THE (J^2, E) PLANE, SHOWING THE 10 CASES FOR WHICH COMPUTATION OF CHARGE DENSITY HAS BEEN PROGRAMMED.

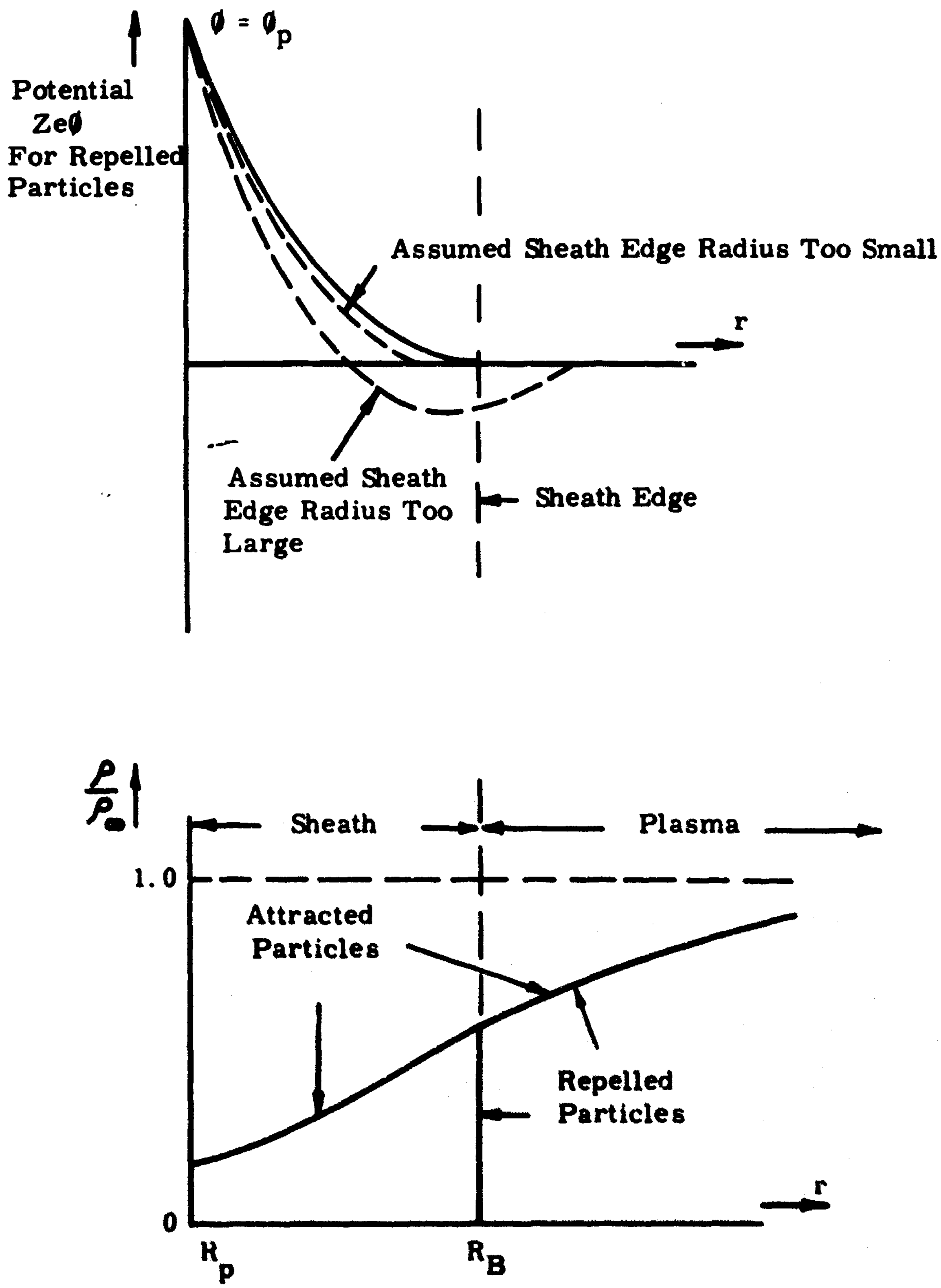

FIGURE 9: POTENTIAL AND CHARGE DENSITIES NEAR A PROBE SURFACE IN THE LIMIT OF ZERO-TEMPERATURE REPELLED PARTICLES

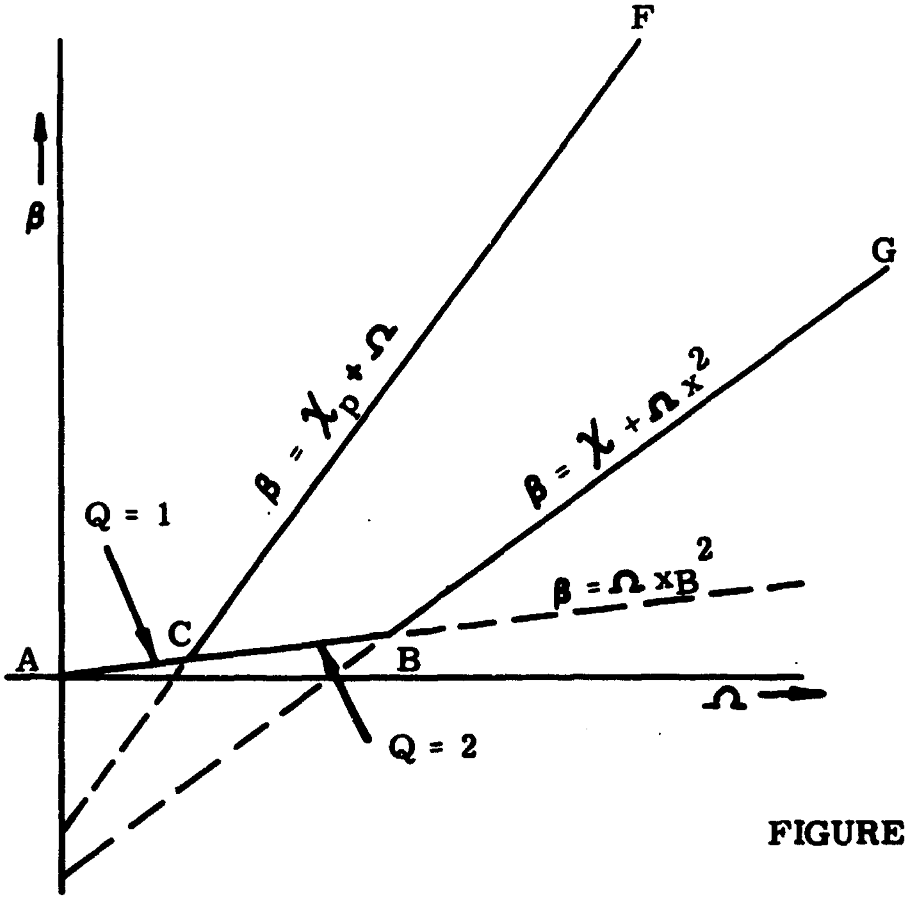

FIGURE 10a

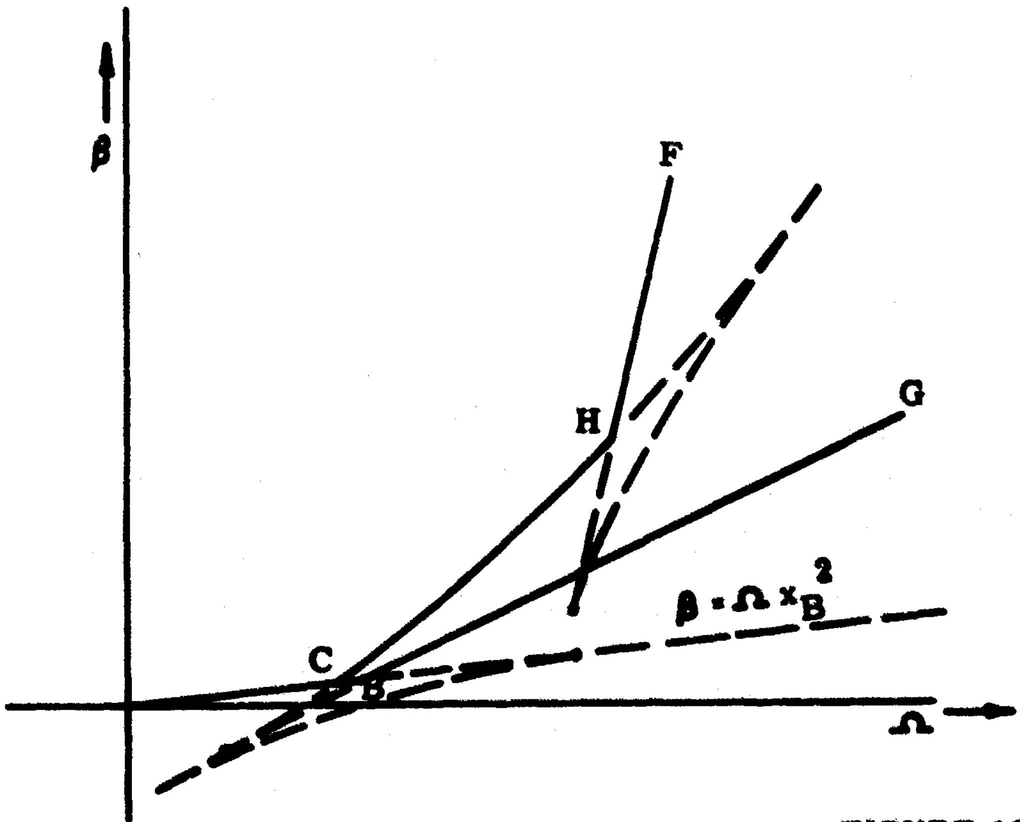

FIGURE 10b

FIGURE 10: MODIFICATION OF THE FUNCTIONS $\Omega_1(\beta)$ AND $\Omega_2(\beta)$ CAUSED BY THE PRESENCE OF A ZERO-POTENTIAL OUTER BOUNDARY AT A FINITE RADIUS. FIGURE 10a CORRESPONDS TO FIGURE 3a ; FIGURE 10b CORRESPONDS TO FIGURE 6c .

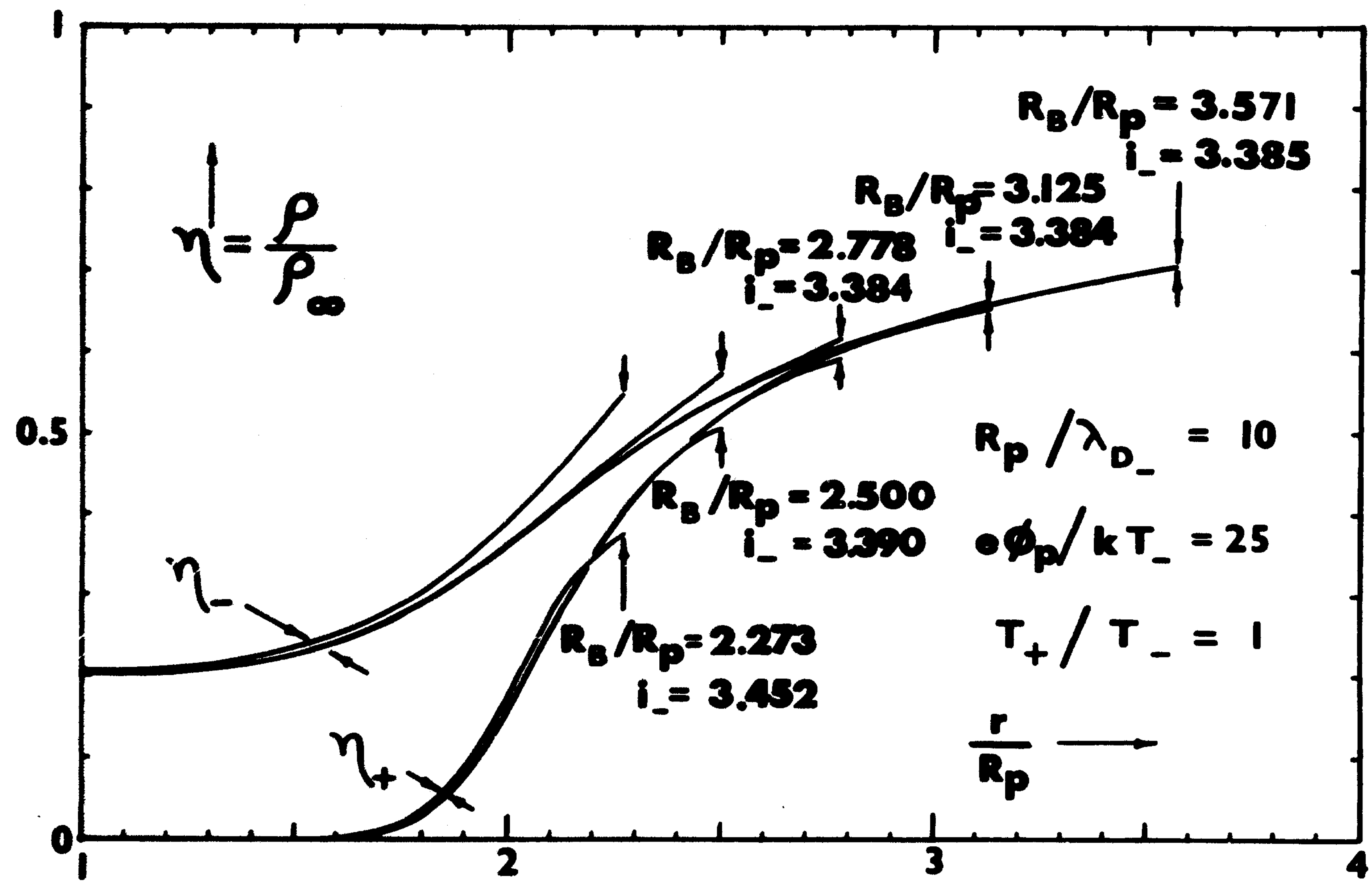

FIGURE 11: EFFECT OF OUTER BOUNDARY POSITION UPON COMPUTED RESULT: ION AND ELECTRON CHARGE DENSITIES AS FUNCTIONS OF RADIUS FOR SEVERAL VALUES OF R_B/R_p FOR A CYLINDRICAL PROBE WITH $R_p/\lambda_{D_-} = 10$; $e\phi_p/kT_- = 25$; $T_+/T_- = 1$.

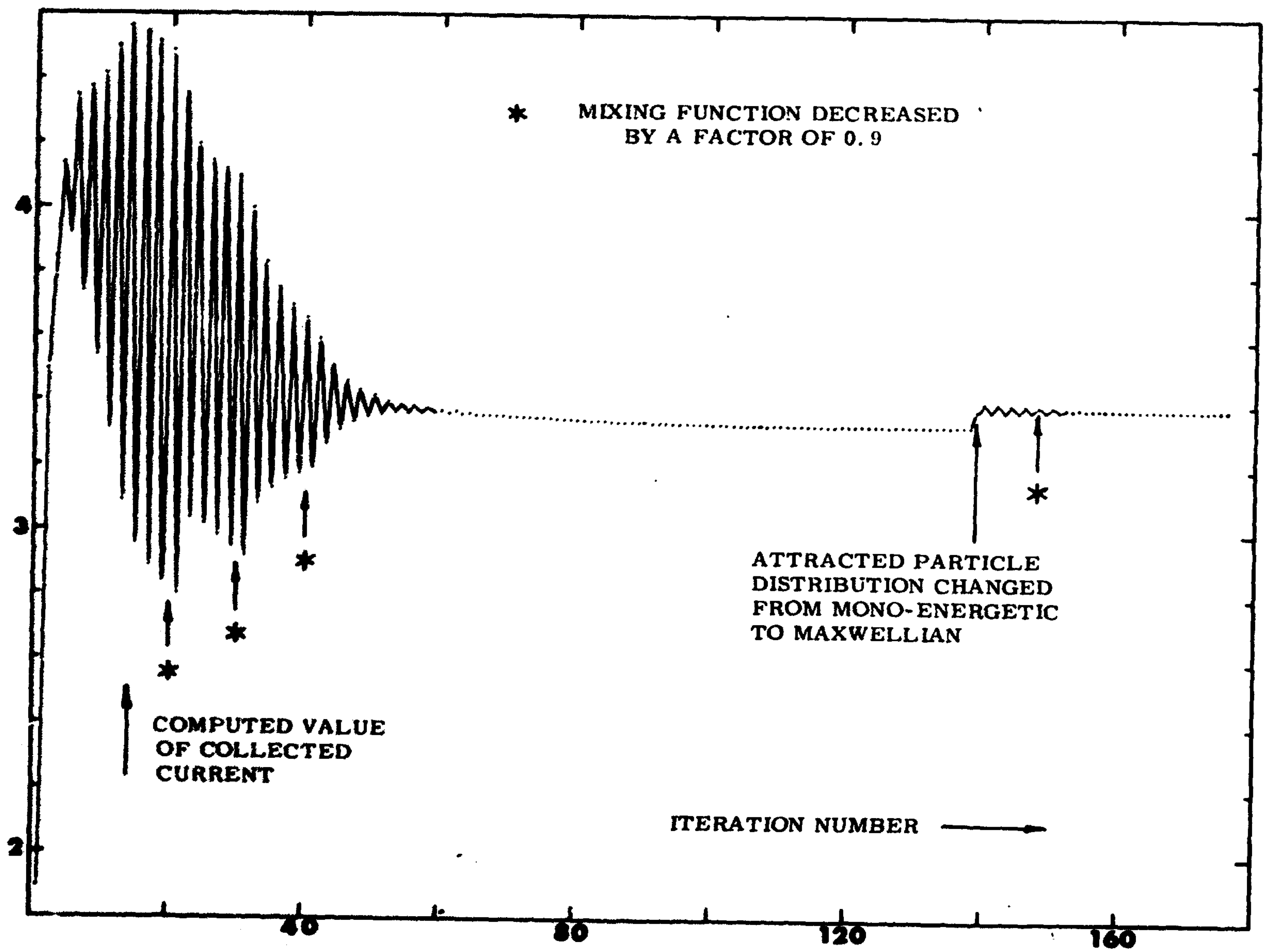

FIGURE 12: BEHAVIOR OF THE ITERATIVE SOLUTION SCHEME: COMPUTED VALUE OF ATTRACTED-SPECIES CURRENT AS A FUNCTION OF ITERATION NUMBER FOR A REPRESENTATIVE CASE WITH R_B/R_p = 3.57 AND OTHER PARAMETERS THE SAME AS FOR FIG. 11.

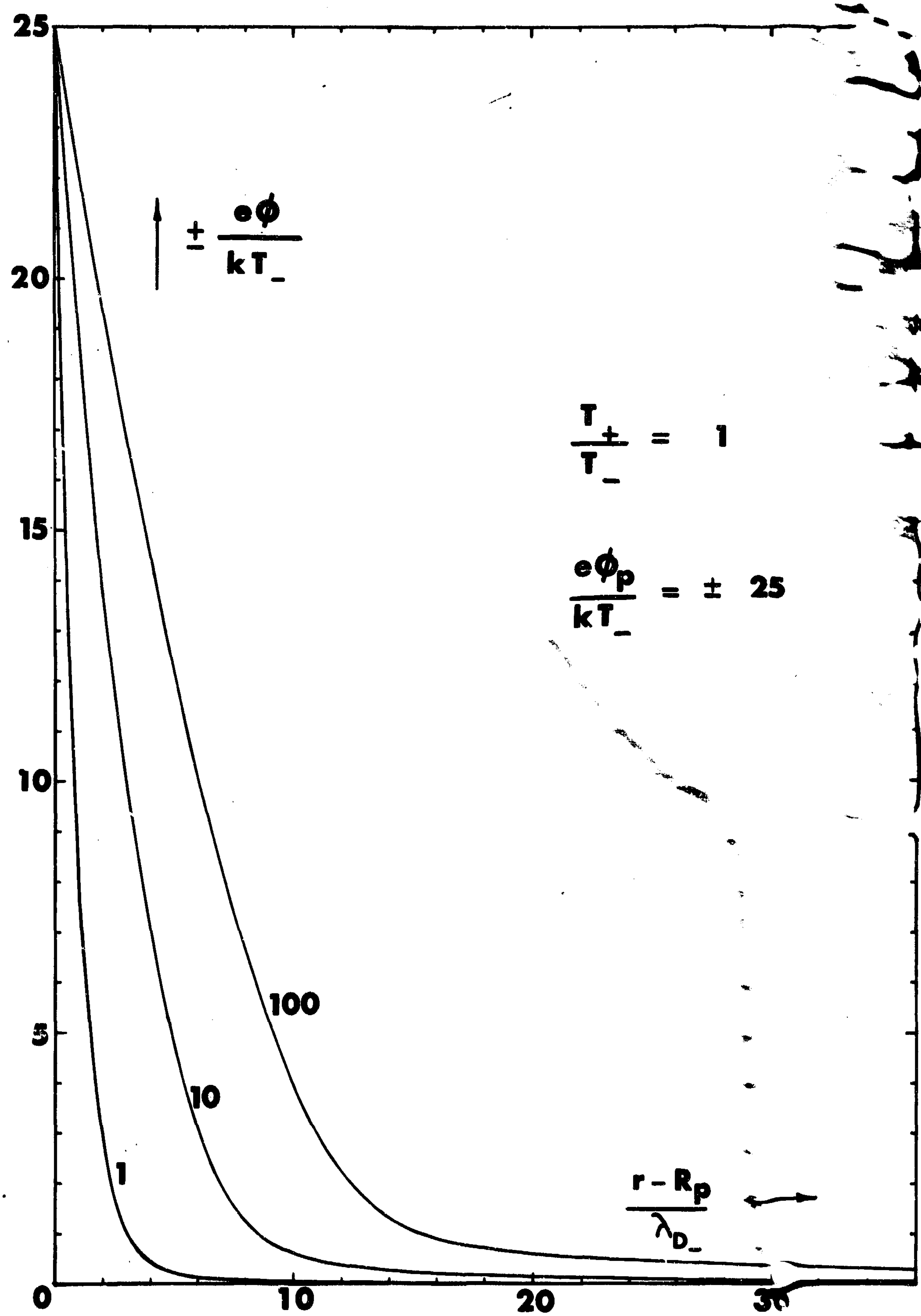

FIGURE 13 POTENTIAL VS DISTANCE FROM PROBE SURFACE IN TERMS OF EITHER DEBYE LENGTH. SPHERICAL PROBE; $e\phi_p/kT_- = \pm 25$; $T_+/T_- = 1$; PLOTTED FOR VARIOUS RATIOS OF PROBE RADIUS TO ION OR ELECTRON DEBYE LENGTH.

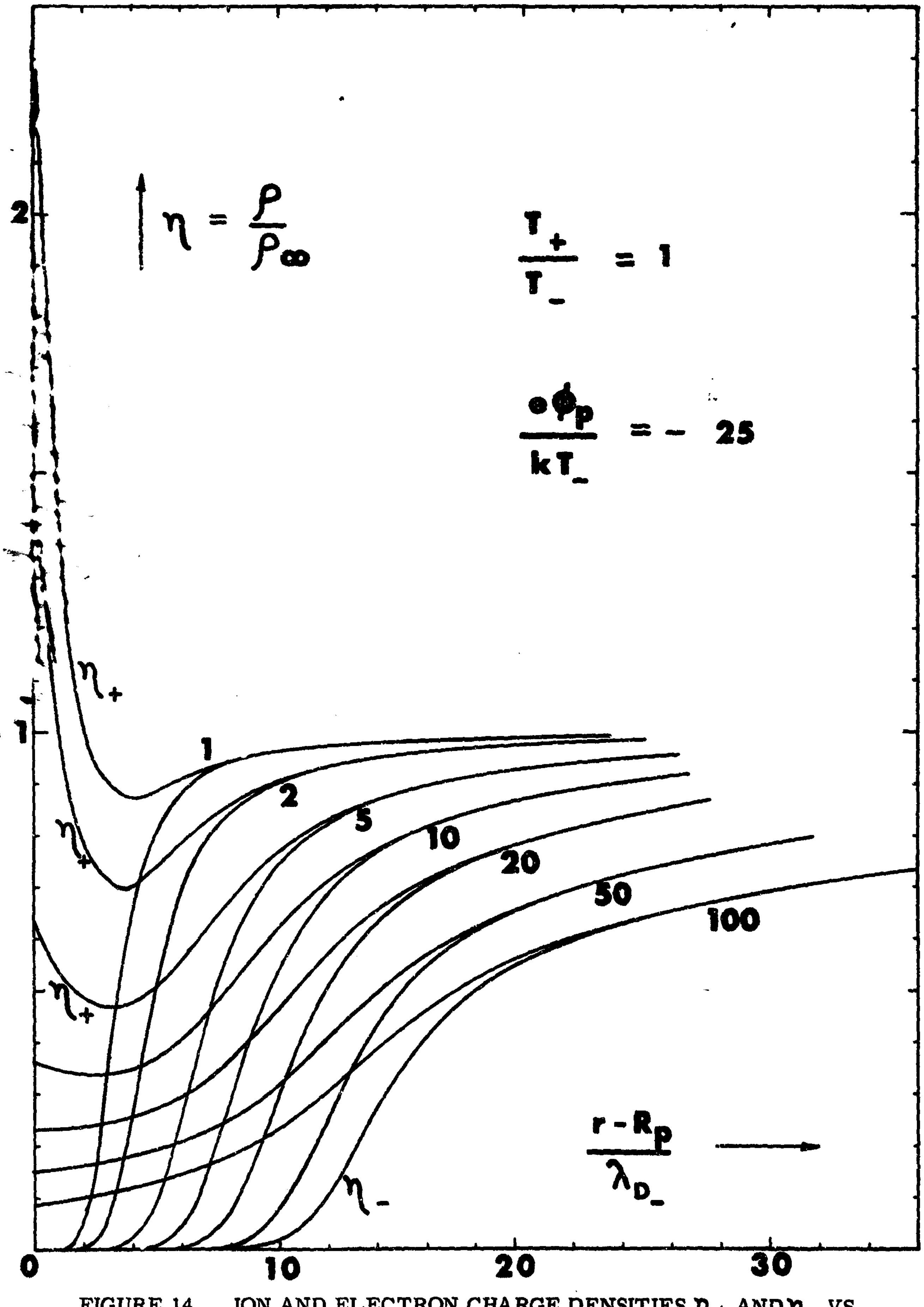

FIGURE 14 ION AND ELECTRON CHARGE DENSITIES η_+ AND η_- VS DISTANCE FROM PROBE SURFACE IN DEBYE LENGTHS; SPHERICAL PROBE; $e\phi_p/kT_- = 25$; $T_+/T_- = 1$; PLOTTED FOR VARIOUS RATIOS OF PROBE RADIUS TO ION OR ELECTRON DEBYE LENGTH

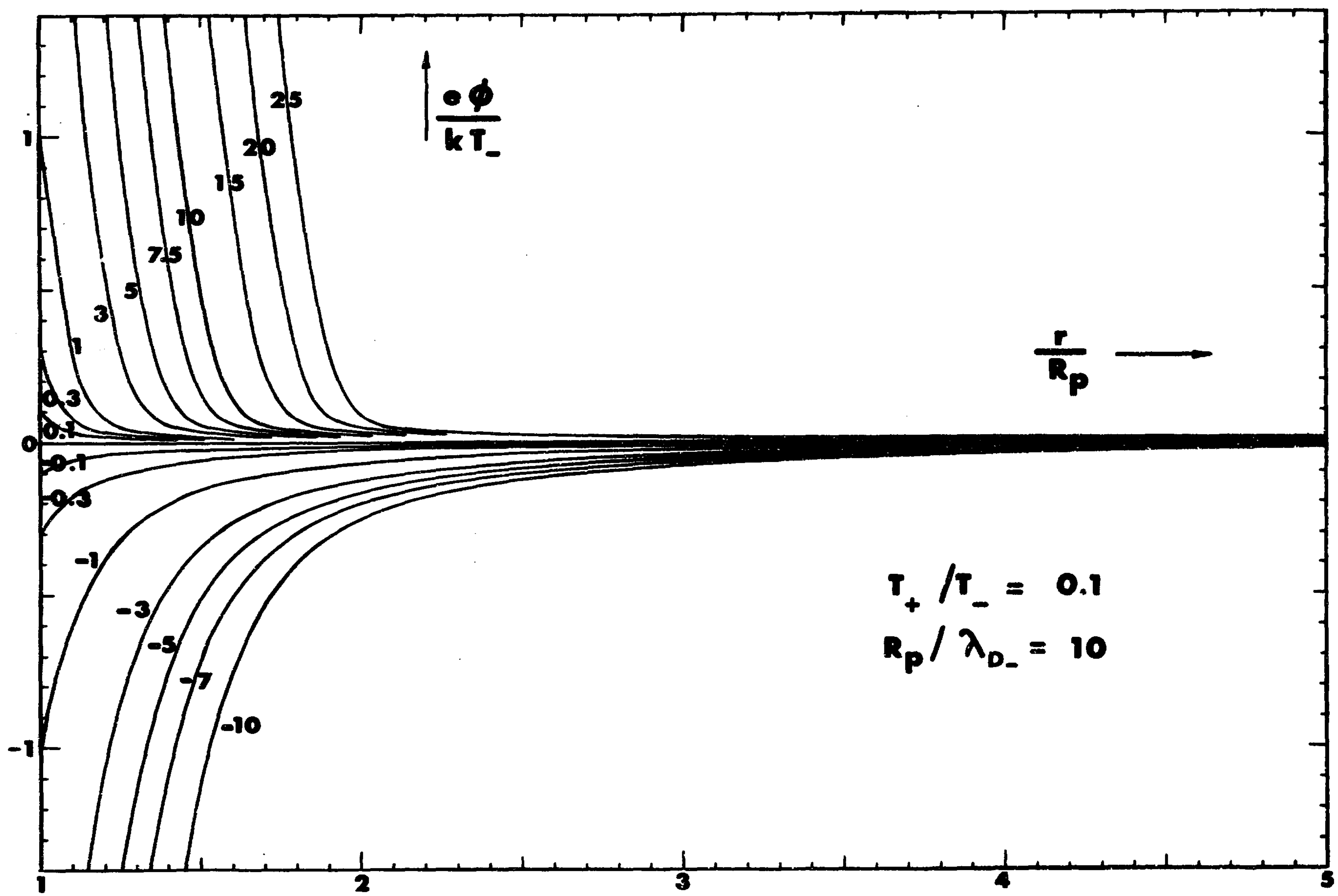

FIGURE 15 POTENTIAL VS RADIUS FOR VARIOUS VALUES OF NON-DIMENSIONAL PROBE POTENTIAL $e\phi_p/kT_-$; SPHERICAL PROBE; $T_+/T_- = 0.1$; $R_p/\lambda_{D_-} = 10$.

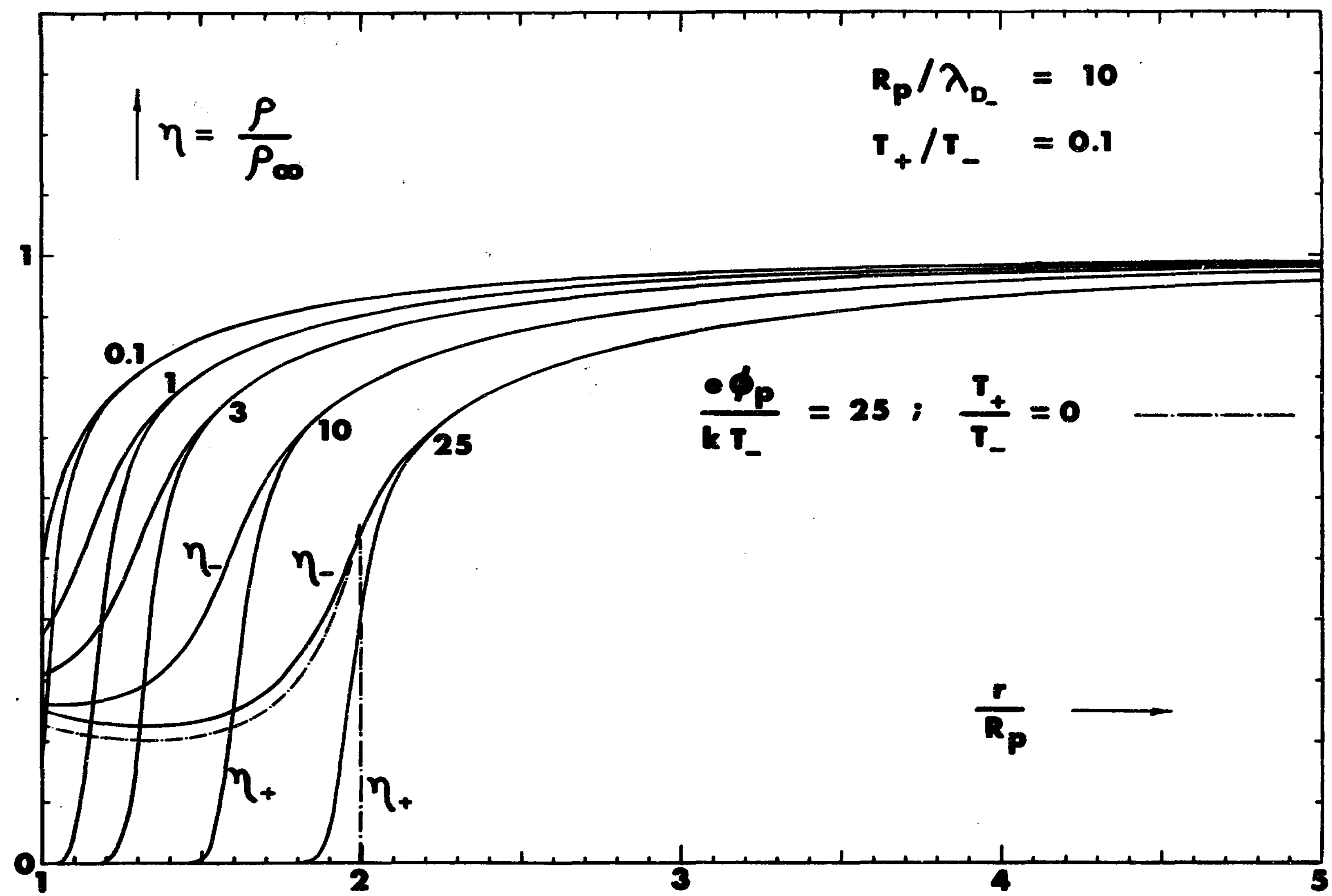

FIGURE 16 ION AND ELECTRON CHARGE DENSITIES η_+ AND η_- VS RADIUS FOR VARIOUS VALUES OF NONDIMENSIONAL PROBE POTENTIAL $e\phi_p/kT_-$; ELECTRON-ATTRACTING SPHERICAL PROBE; $T_+/T_- = 0.1$; $R_p/\lambda_{D_-} = 10$. DOTTED CURVES SHOW η_+ AND η_- WITHIN SHEATH FOR THE CASE $e\phi_p/kT_- = 25$, $T_+/T_- = 0$, $R_p/\lambda_{D_-} = 10$.

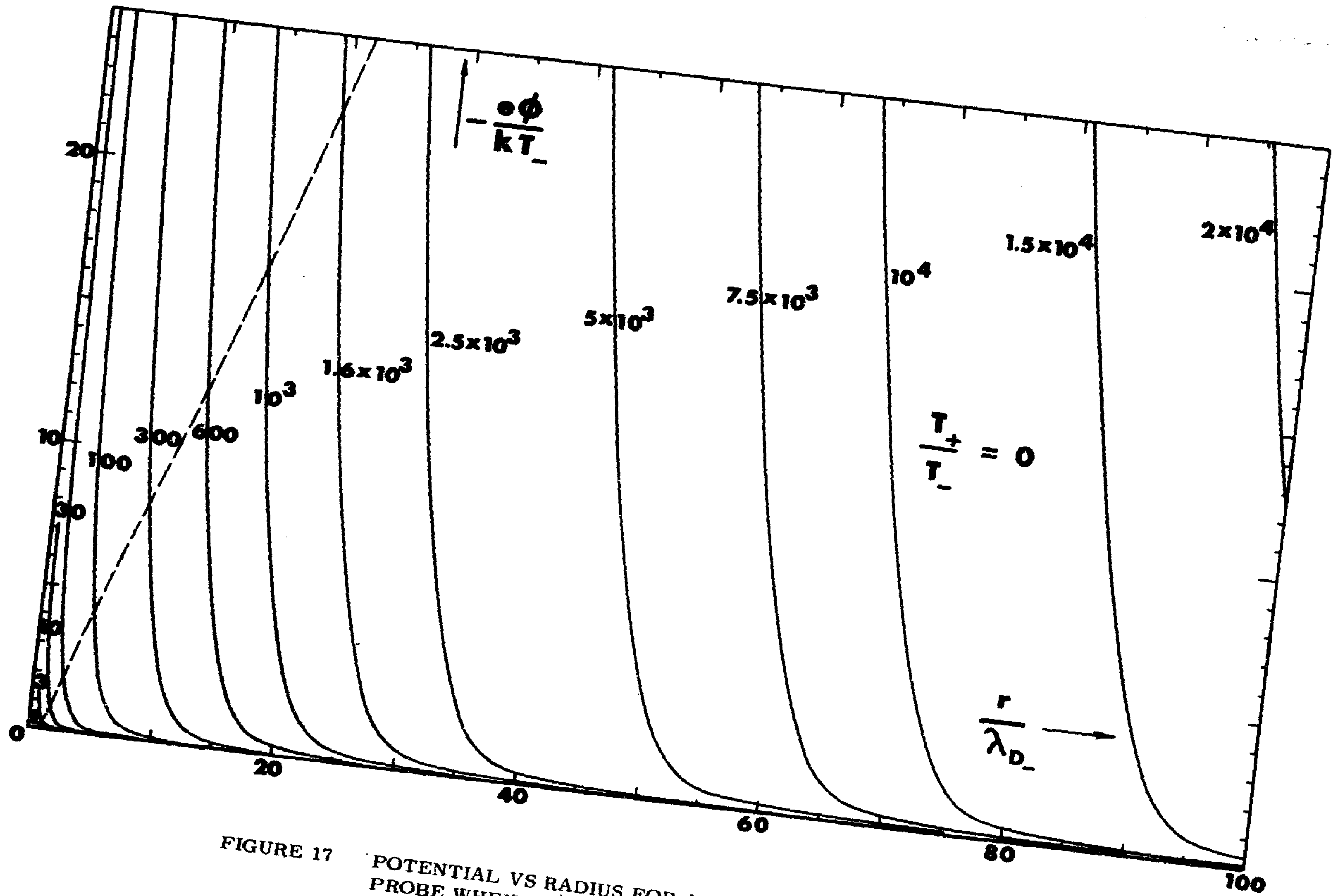

FIGURE 17 POTENTIAL VS RADIUS FOR AN ION-ATTRACTING SPHERICAL PROBE WHEN IONS ARE AT ZERO TEMPERATURE AND ELECTRONS ARE REFLECTED BY PROBE SURFACE; OBTAINED BY NUMERICAL SOLUTION OF ALLEN, BOYD, AND REYNOLDS EQUATION; PLOTTED FOR VARIOUS VALUES OF THE NONDIMENSIONAL CURRENT i^* DEFINED IN EQ. (13.6a). DOTTED CURVE SHOWS TRAPPED-ORBIT BOUNDARY.

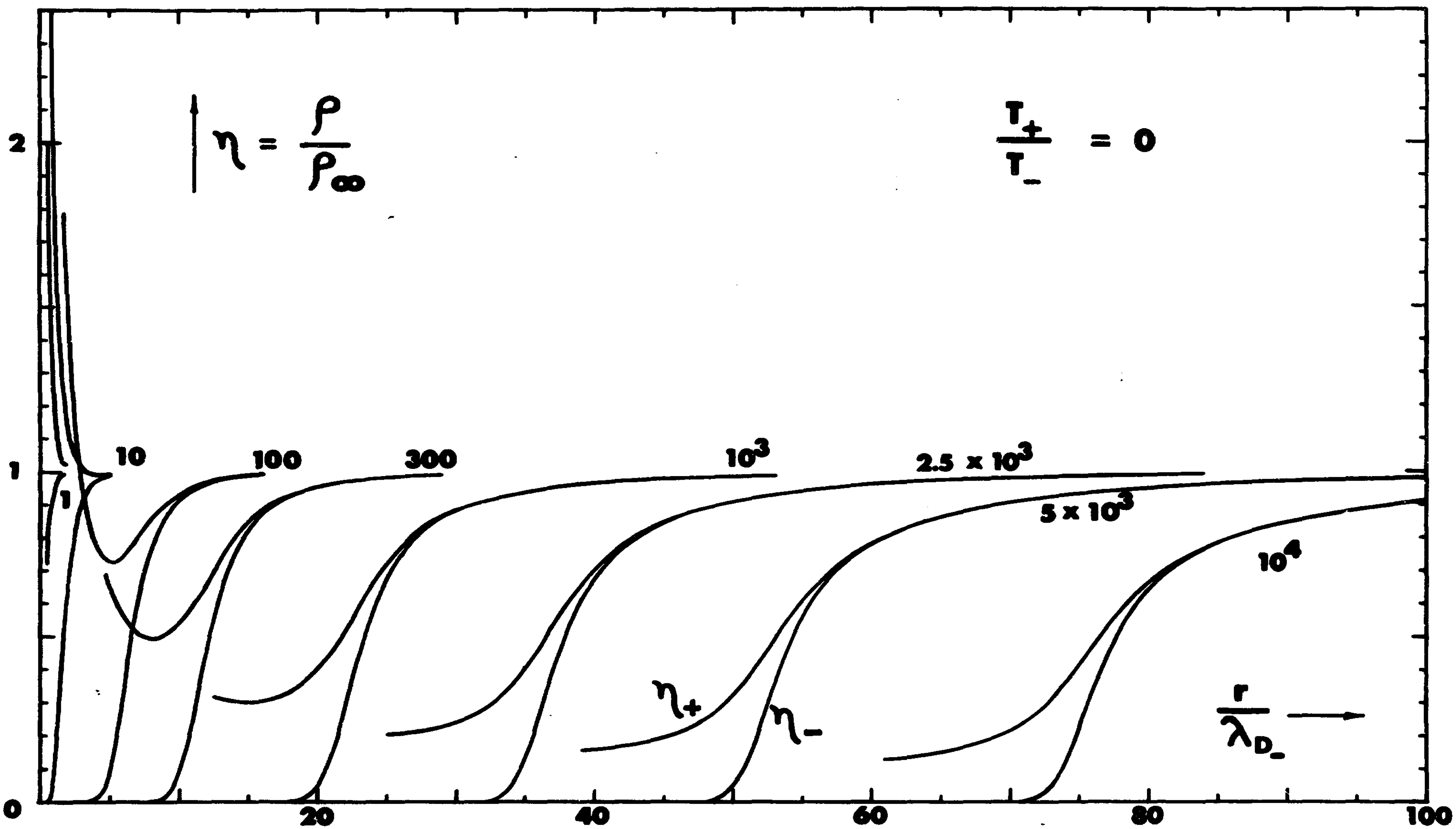

FIGURE 18 ION AND ELECTRON CHARGE DENSITIES VS RADIUS CORRESPONDING TO THE SAME SITUATION AS THAT OF FIG. 17.

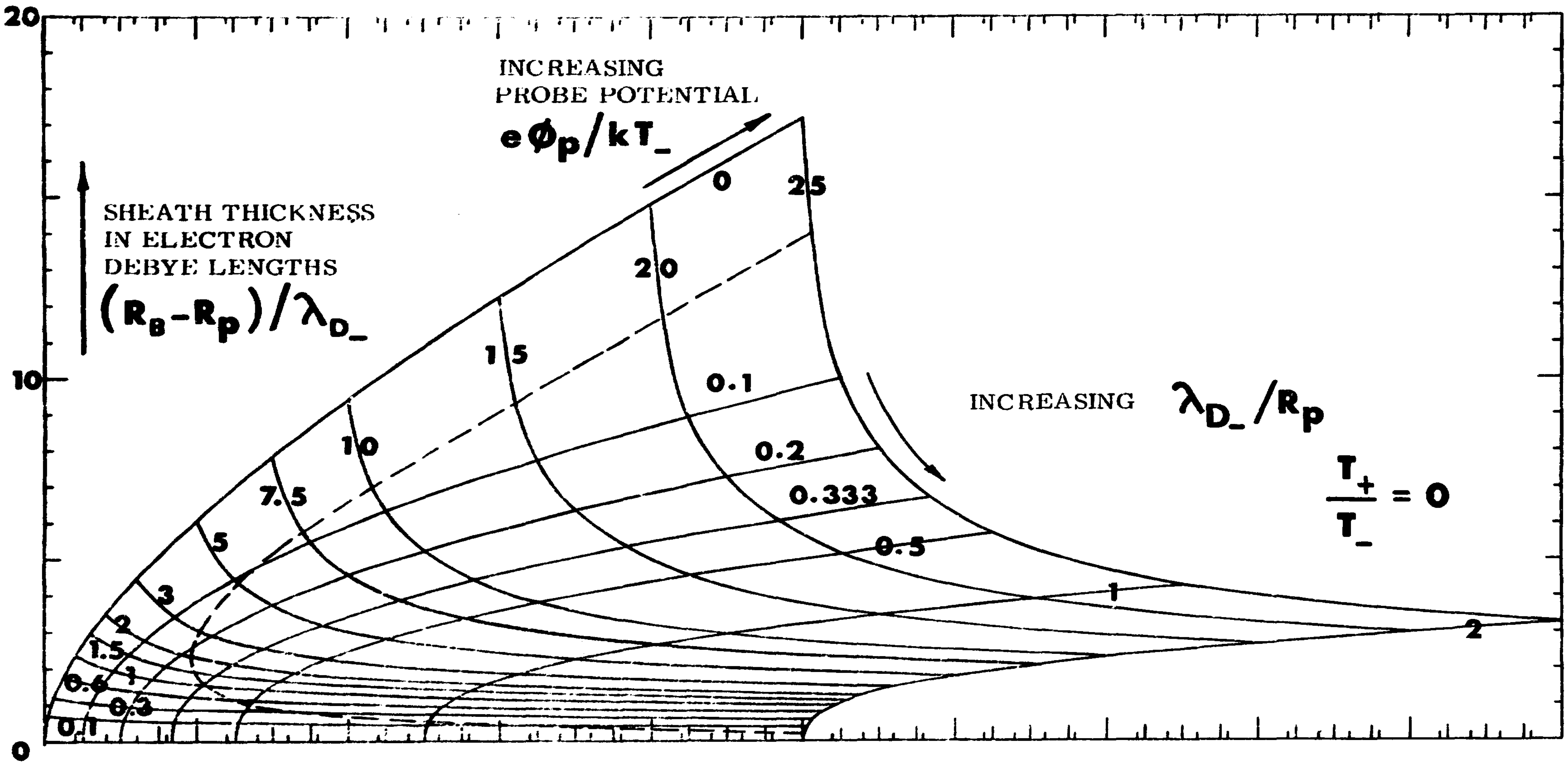

FIGURE 19 SHEATH THICKNESS IN ELECTRON DEBYE LENGTHS. ELECTRON-ATTRACTING SPHERICAL PROBE; $T_+/T_- = 0$ (REPELLED SPECIES AT ZERO TEMPERATURE); PLOTTED FOR VARIOUS VALUES OF NONDIMENSIONAL PROBE POTENTIAL AND λ_{D-}/R_p. DOTTED CURVE SHOWS TRAPPED-ORBIT BOUNDARY.

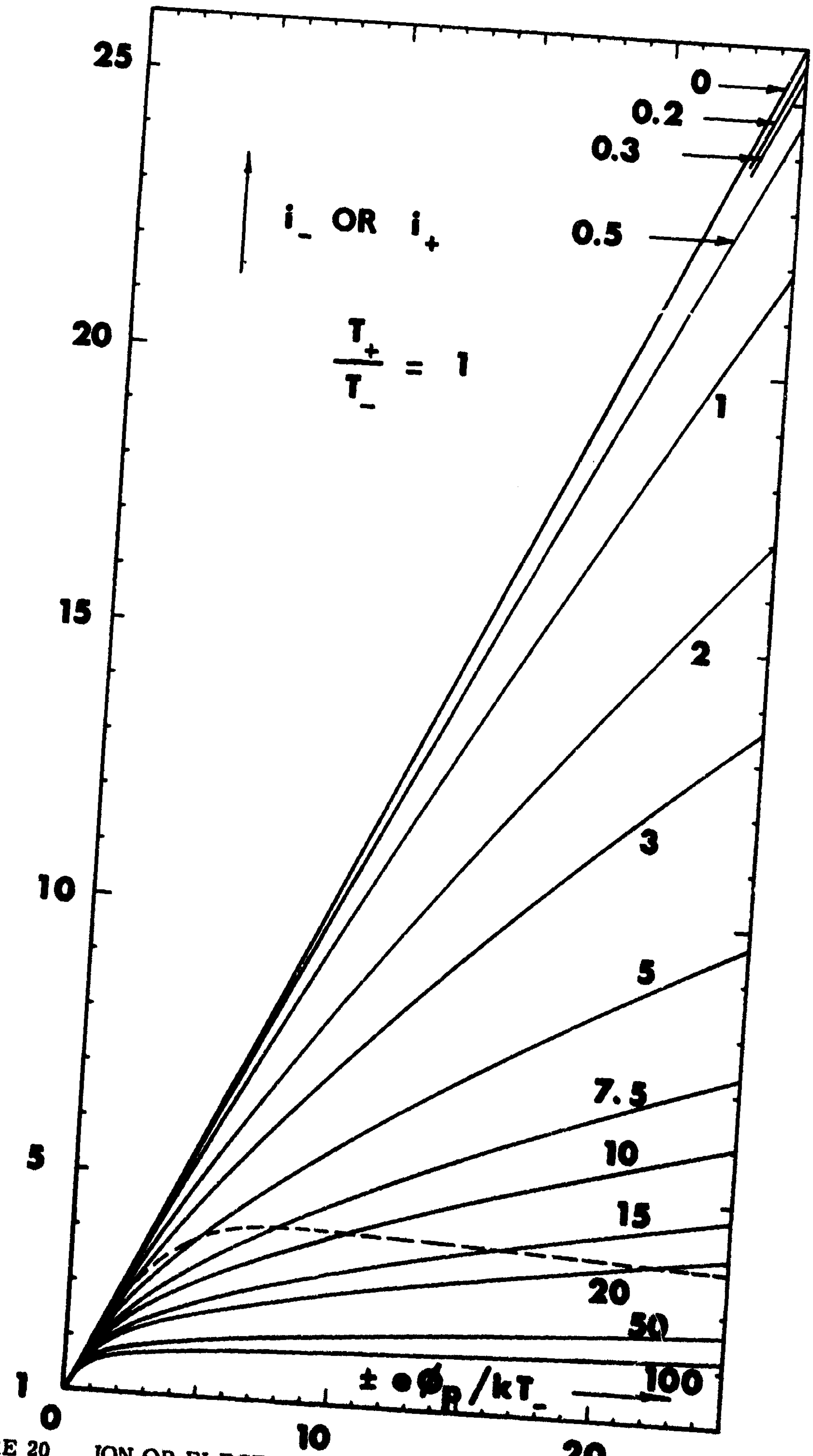

FIGURE 20 ION OR ELECTRON CURRENT VS PROBE POTENTIAL FOR VARIOUS RATIOS OF PROBE RADIUS TO ION OR ELECTRON DEBYE LENGTH; SPHERICAL PROBE; $T_+/T_- = 1$. DOTTED CURVE SHOWS TRAPPED-ORBIT BOUNDARY.

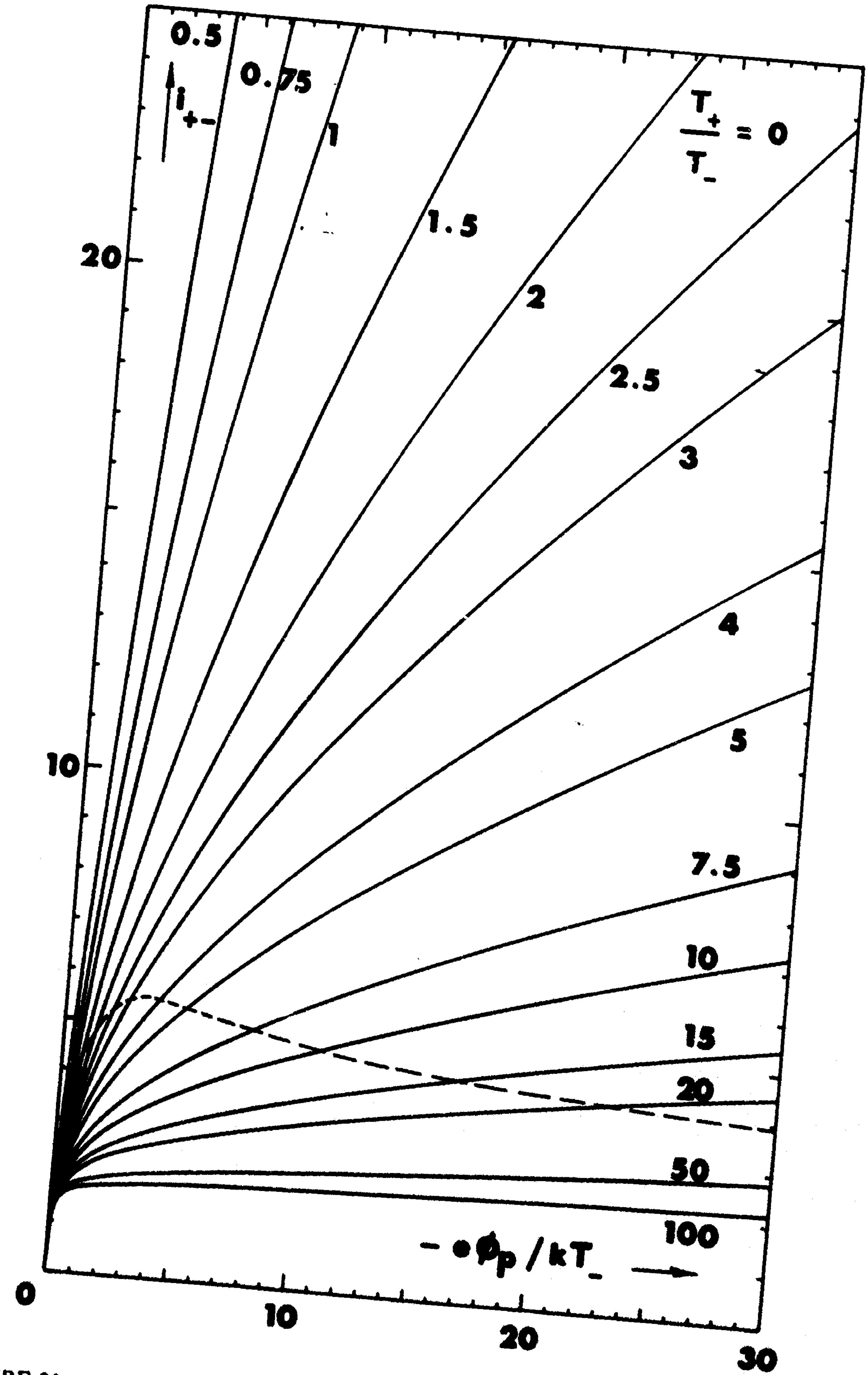

FIGURE 21 ION CURRENT i_{+-} VS PROBE POTENTIAL FOR VARIOUS RATIOS OF PROBE RADIUS TO ELECTRON DEBYE LENGTH; ION-ATTRACTING SPHERICAL PROBE; $T_+/T_- = 0$; ELECTRONS REFLECTED BY PROBE SURFACE; OBTAINED FROM NUMERICAL SOLUTION OF THE ALLEN, BOYD, AND REYNOLDS EQUATION. DOTTED CURVE SHOWS TRAPPED-ORBIT BOUNDARY.

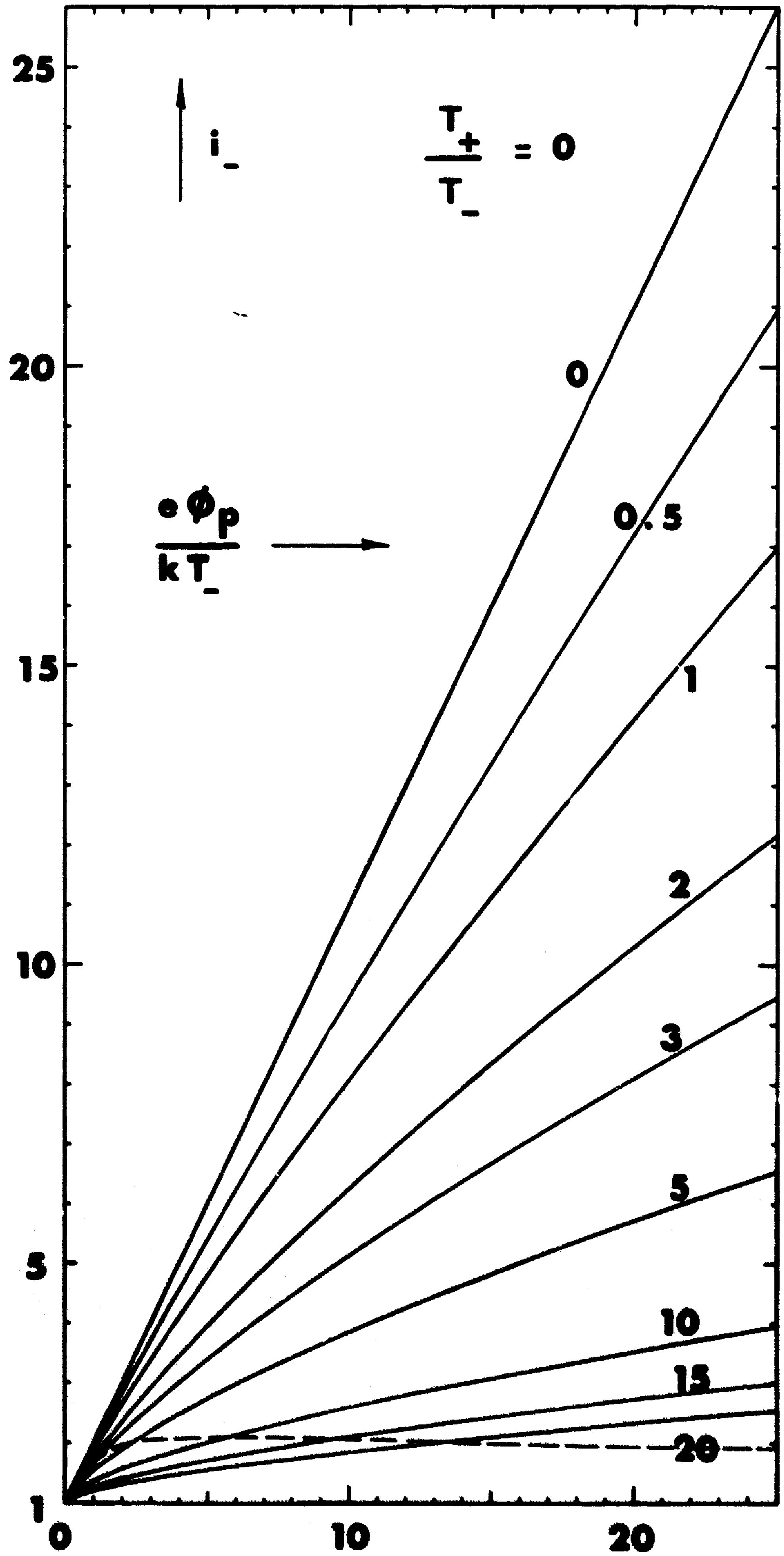

FIGURE 22 ELECTRON CURRENT i_- VS PROBE POTENTIAL FOR VARIOUS RATIOS OF PROBE RADIUS TO ELECTRON DEBYE LENGTH; ELECTRON-ATTRACTING SPHERICAL PROBE; $T_+/T_- = 0$ (REPELLED SPECIES AT ZERO TEMPERATURE). DOTTED CURVE SHOWS TRAPPED-ORBIT BOUNDARY.

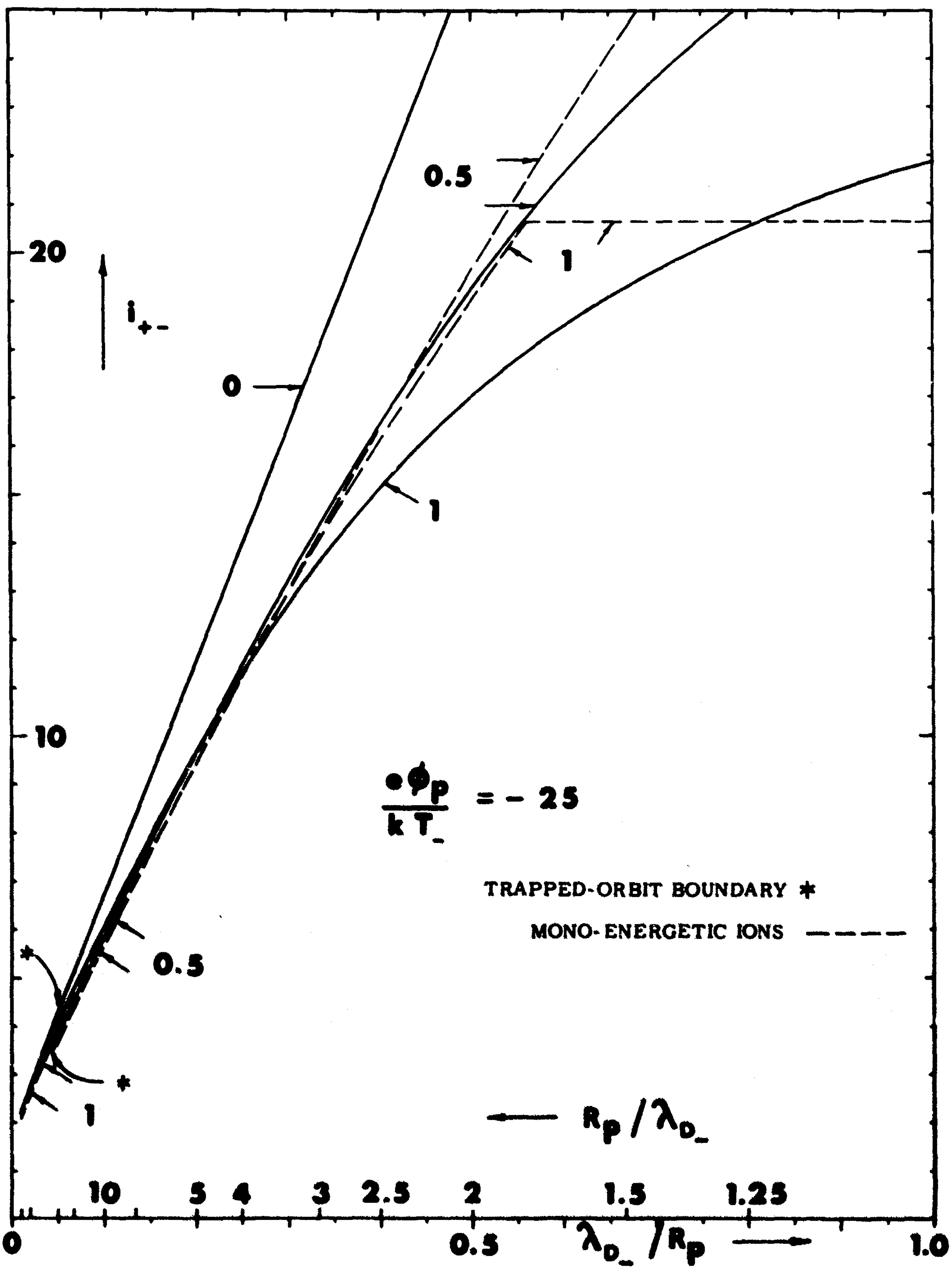

FIGURE 23 ION CURRENT i_{+-} VS λ_{D_-}/R_p FOR VALUES OF T_+/T_- OF 0, 0.5 AND 1; SPHERICAL PROBE; $e\phi_p/kT_- = -25$.

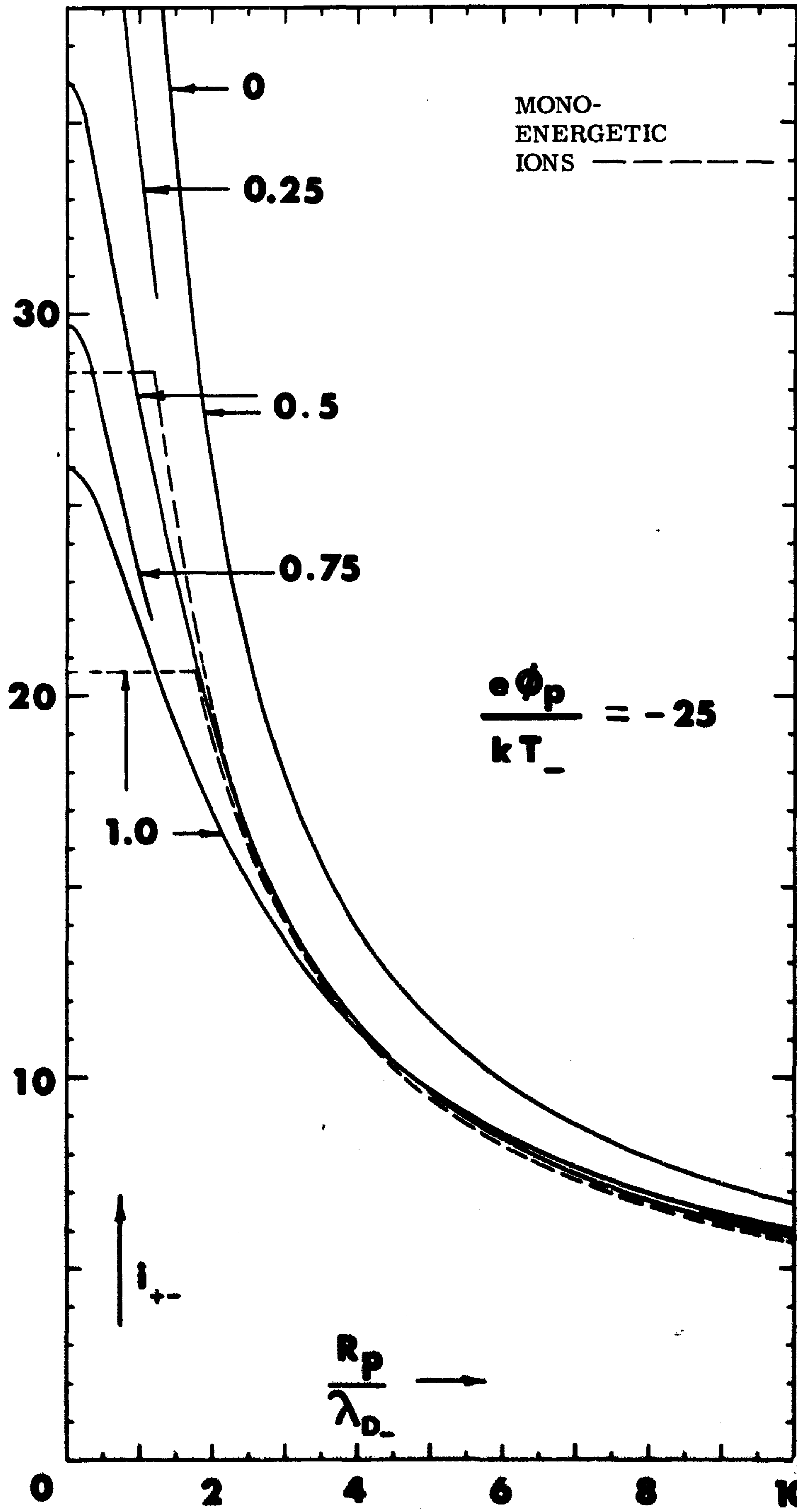

FIGURE 24 ION CURRENT i_{+-} VS R_p/λ_D FOR VARIOUS VALUES OF T_+/T_- FROM 0 TO 1; SPHERICAL PROBE; $e\phi_p/kT_- = -25$.

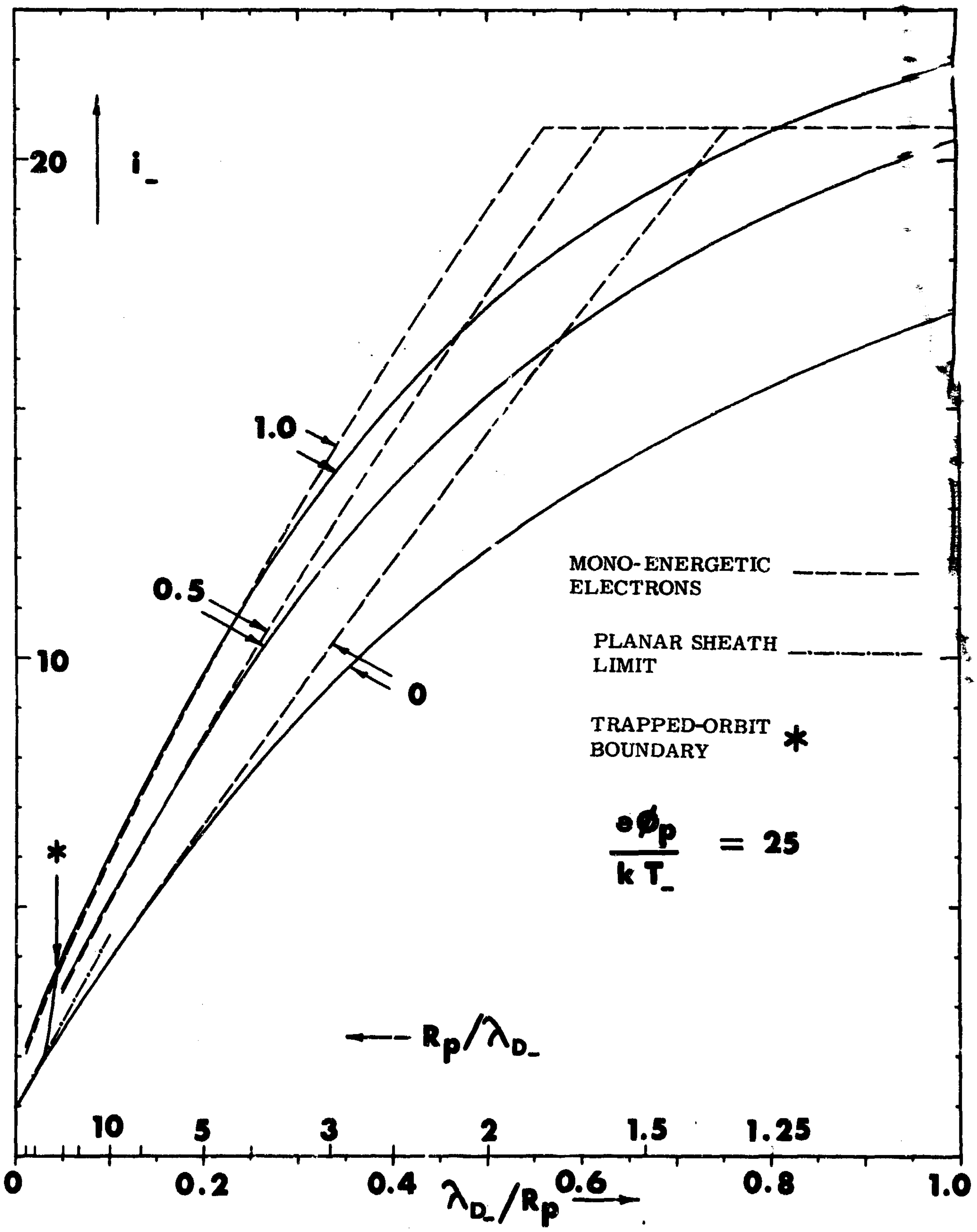

FIGURE 25: ELECTRON CURRENT i_- VS λ_D/R_p FOR VALUES OF T_+/T_- OF 0, 0.5 AND 1; SPHERICAL PROBE; $e\phi_p/kT_- = 25$.

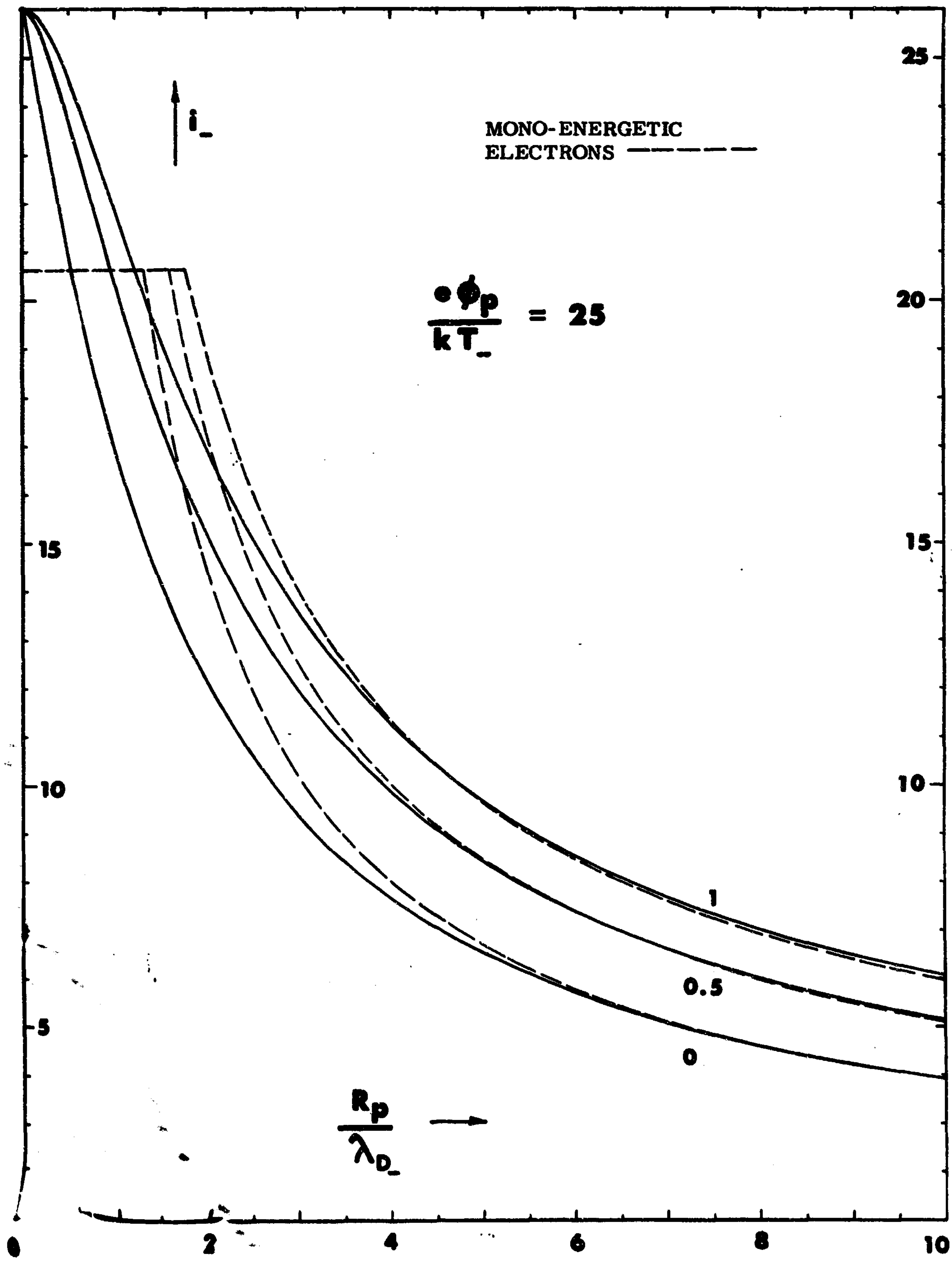

FIGURE 26 ELEC[illegible]N CURRENT i_- VS R_p/λ_{D_-} FOR VALUES OF T_+/T_- OF 0, [illegible] A[illegible]1; SPHERICAL PROBE; $e\phi_p/kT_- = 25$.

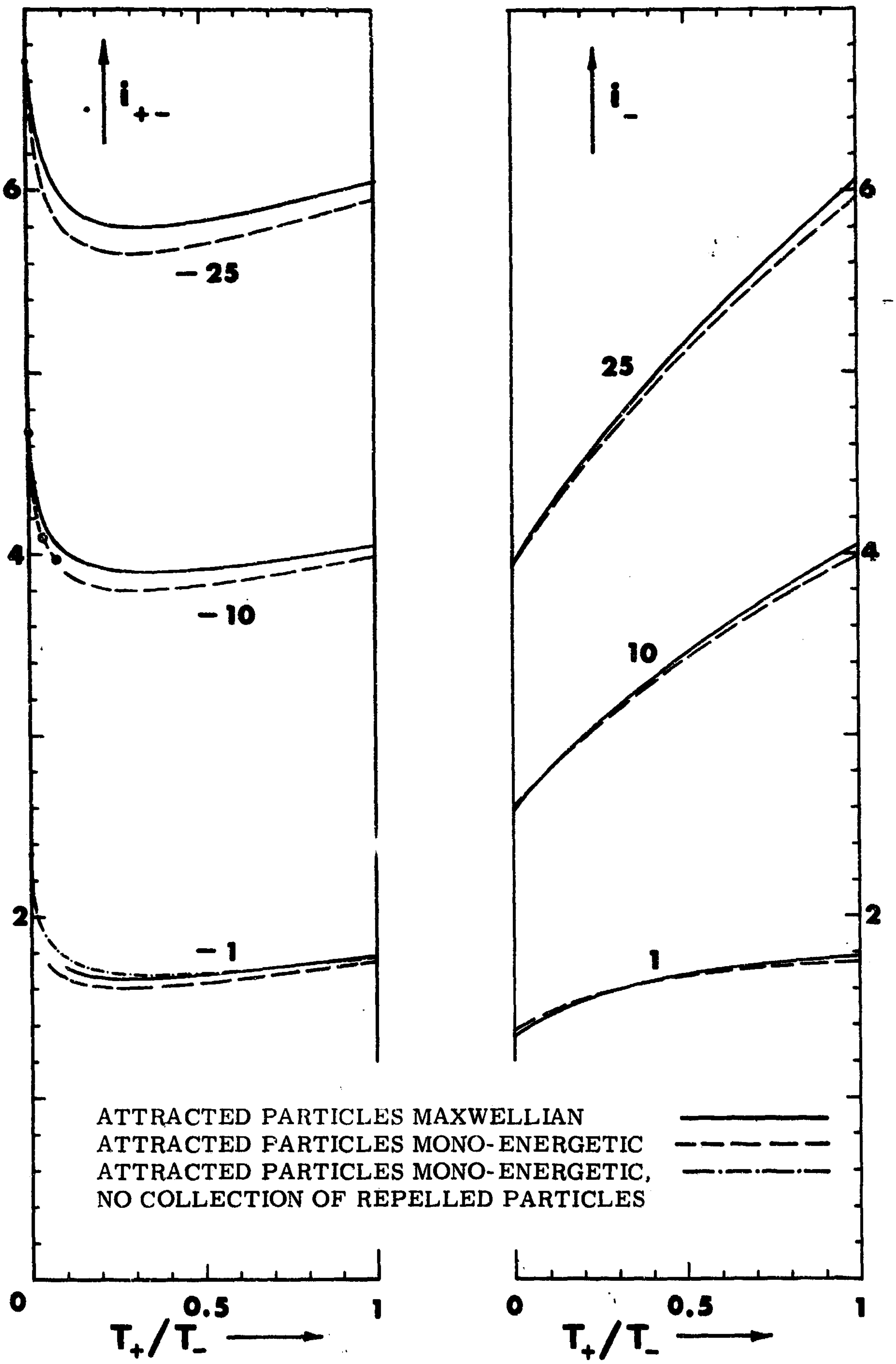

FIGURE 27a ION AND ELECTRON CURRENTS COLLECTED BY ION - AND ELECTRON-ATTRACTING SPHERICAL PROBE, RESPECTIVELY, AS FUNCTIONS OF T_+/T_-, FOR R_p/λ_{D-} = 10 AND VALUES OF $e\phi_p/kT_-$ OF -25, -10, -1, 1, 10 and 25. RESULTS FOR MONO-ENERGETIC ATTRACTED SPECIES WITH AND WITHOUT REPELLED-SPECIES COLLECTION BY PROBE SURFACE SHOWN FOR COMPARISON.

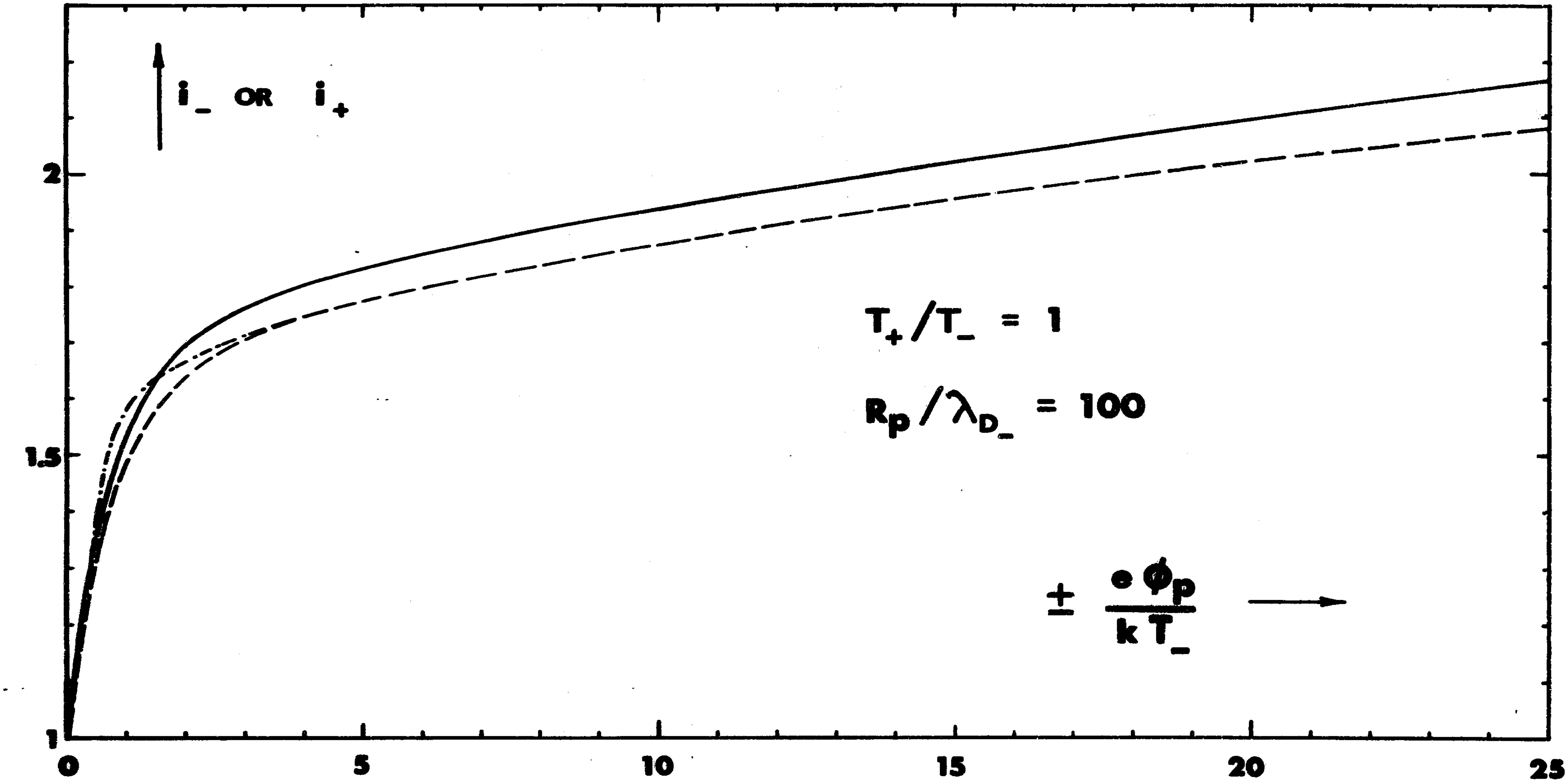

FIGURE 27b ATTRACTED-SPECIES CURRENT COLLECTED BY A SPHERICAL PROBE AS A FUNCTION OF PROBE POTENTIAL FOR $T_+/T_- = 1$ AND $R_p/\lambda_{D_-} = 100$. RESULTS FOR MONO-ENERGETIC ATTRACTED SPECIES LABELLED AS IN FIG. 27a.

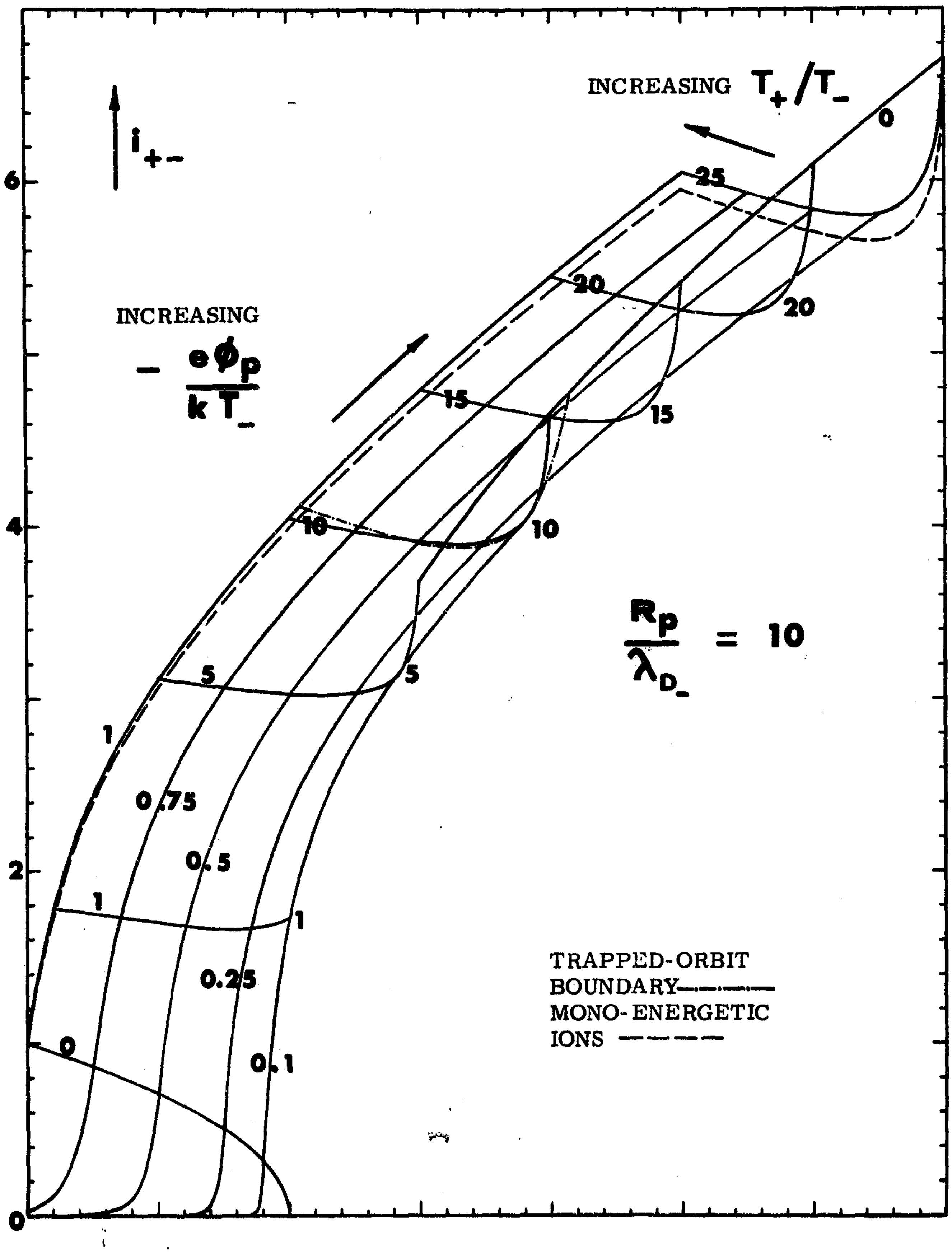

FIGURE 28 ION CURRENT i_{+-} AS A FUNCTION OF $e\phi_p/kT_-$ AND T_+/T_- FOR A SPHERICAL PROBE WITH $R_p/\lambda_{D_-} = 10$. MONO-ENERGETIC RESULTS SHOWN FOR $T_+/T_- = 1$ AND FOR $e\phi_p/kT_- = -25$ FOR COMPARISON.

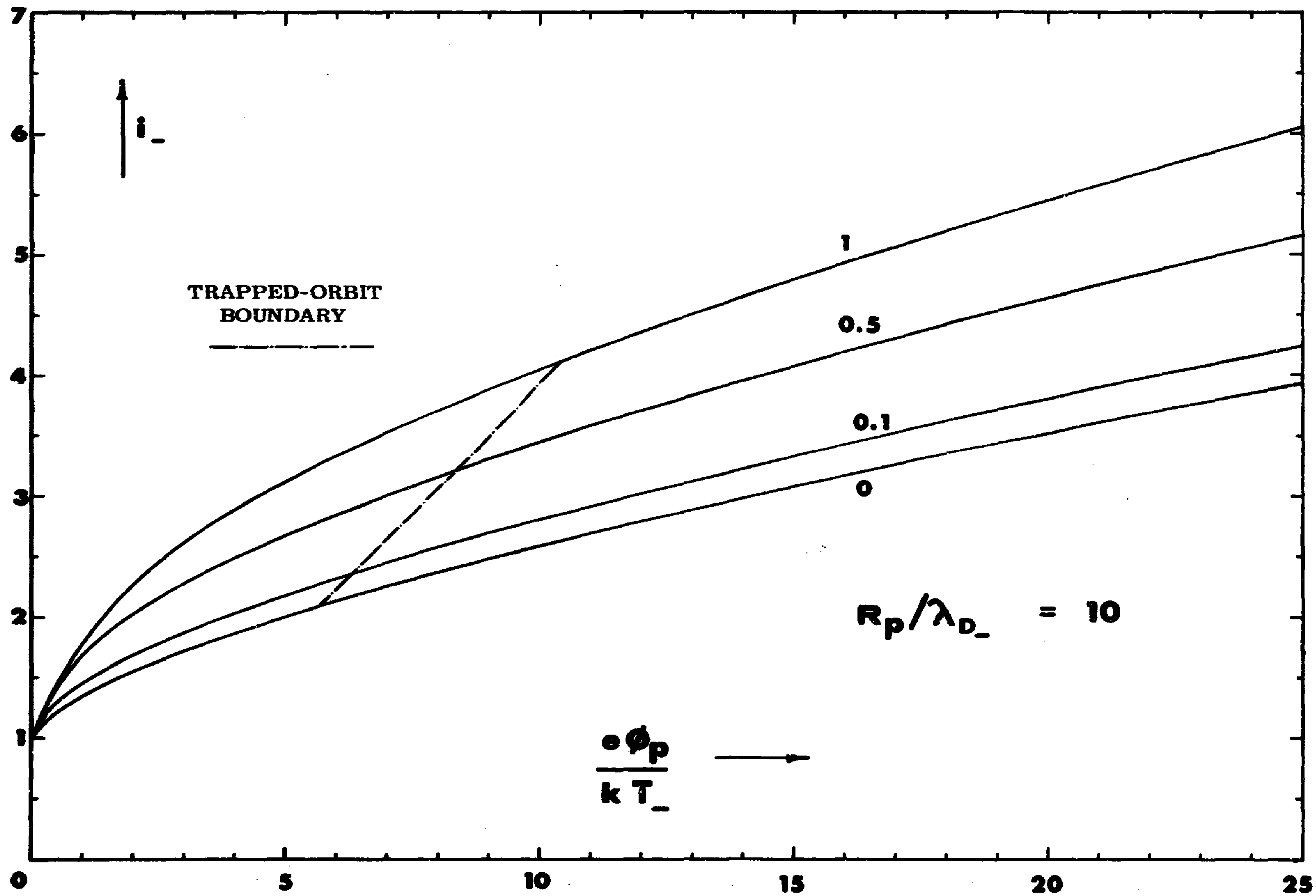

FIGURE 29 ELECTRON CURRENT i_- AS A FUNCTION OF $e\phi_p/kT_-$; PLOTTED FOR VALUES OF T_+/T_- FROM 0 TO 1. SPHERICAL PROBE: $R_p/\lambda_{D_-} = 10$.

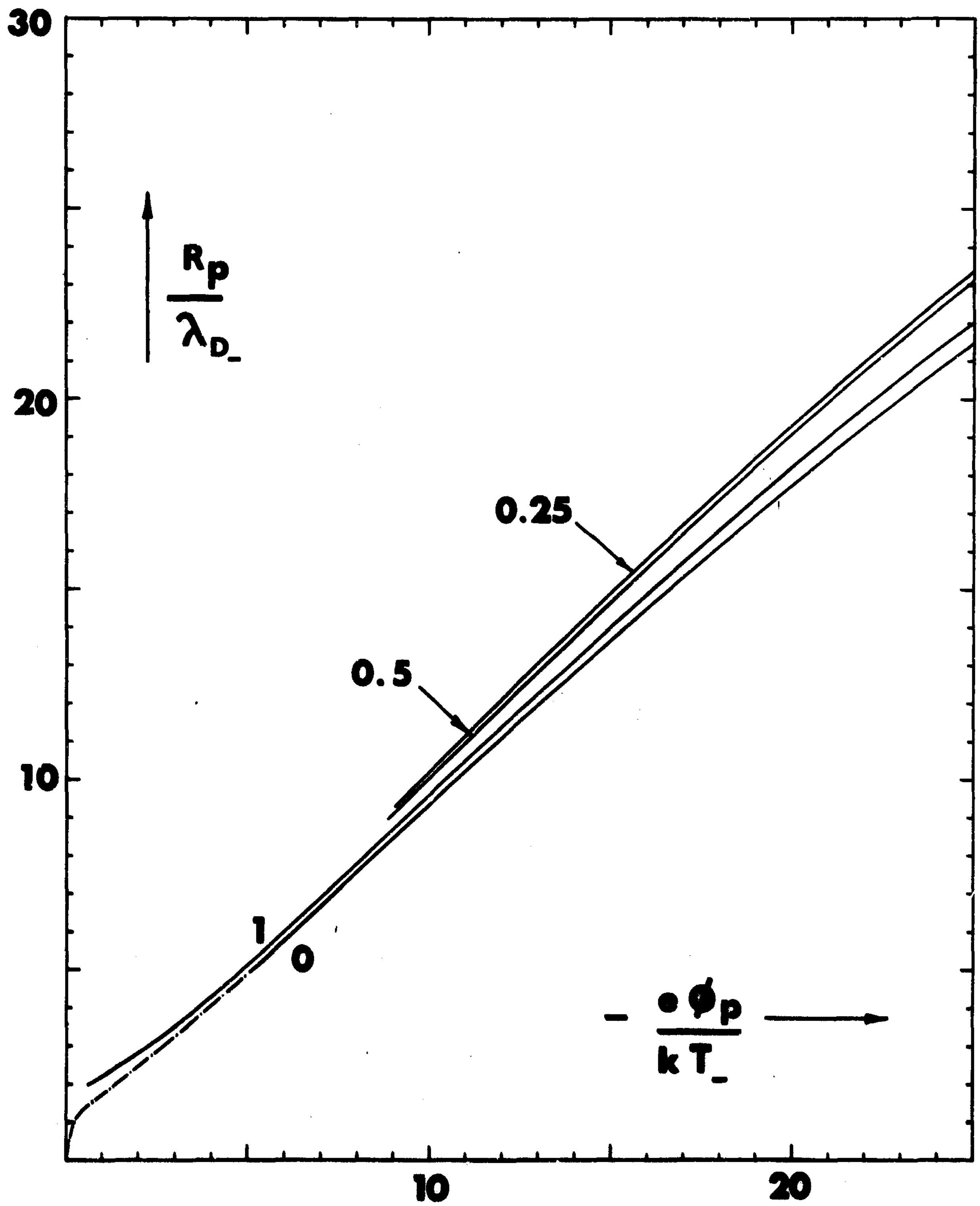

FIGURE 30 TRAPPED-ORBIT BOUNDARY: UPPER LIMIT OF R_p/λ_{D-} FOR WHICH TRAPPED ORBITS EXIST; PLOTTED AS A FUNCTION OF $e\phi_p/kT_-$, FOR VALUES OF T_+/T_- OF 0, 0.25, 0.5 AND 1.0. ION-ATTRACTING SPHERICAL PROBE.

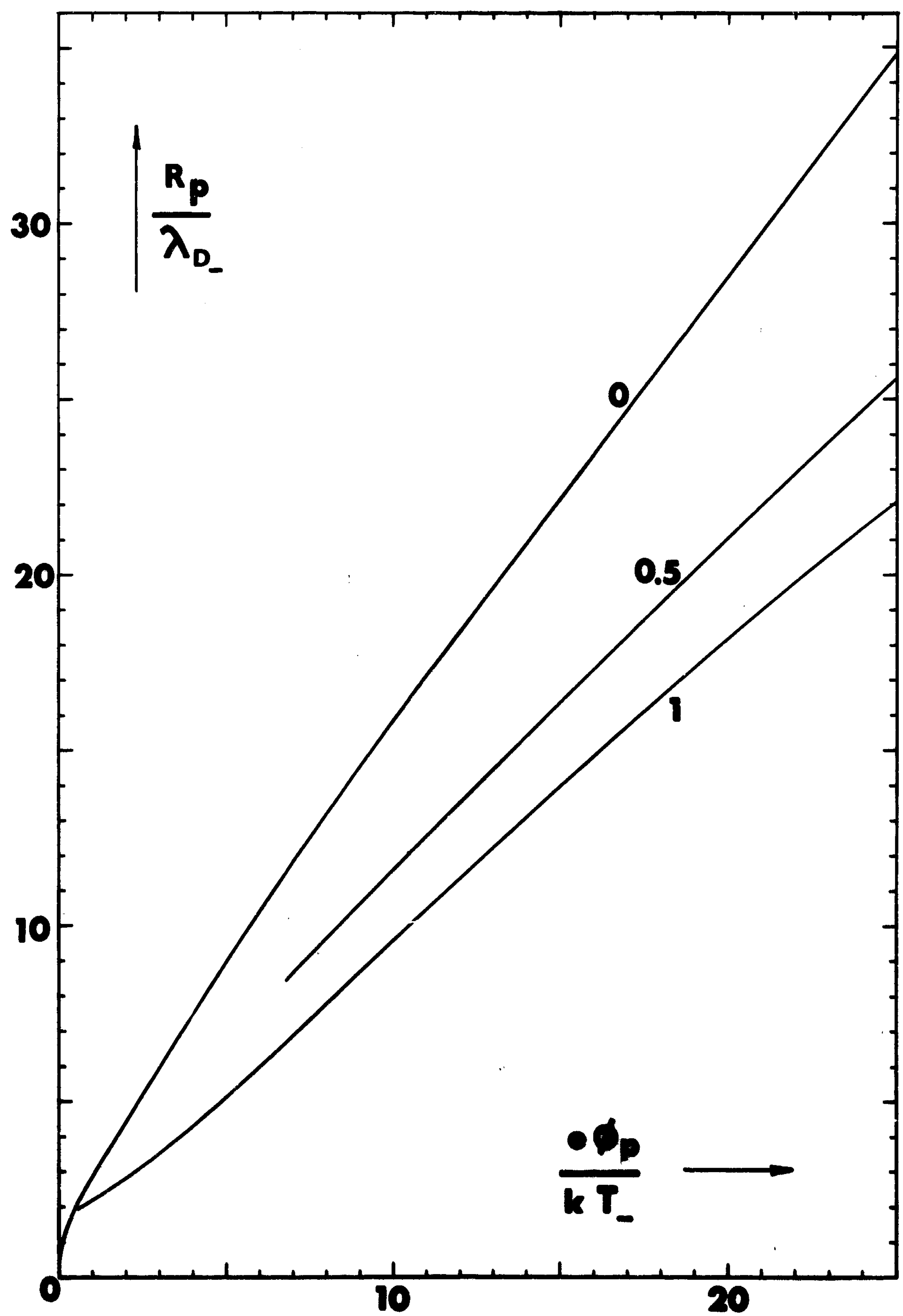

FIGURE 31 TRAPPED-ORBIT BOUNDARY: UPPER LIMIT OF R_p/λ_{D-} FOR WHICH TRAPPED ORBITS EXIST; PLOTTED AS A FUNCTION OF $e\phi_p/kT_-$ FOR VALUES OF T_+/T_- OF 0, 0.5, AND 1.0. ELECTRON-ATTRACTING SPHERICAL PROBE.

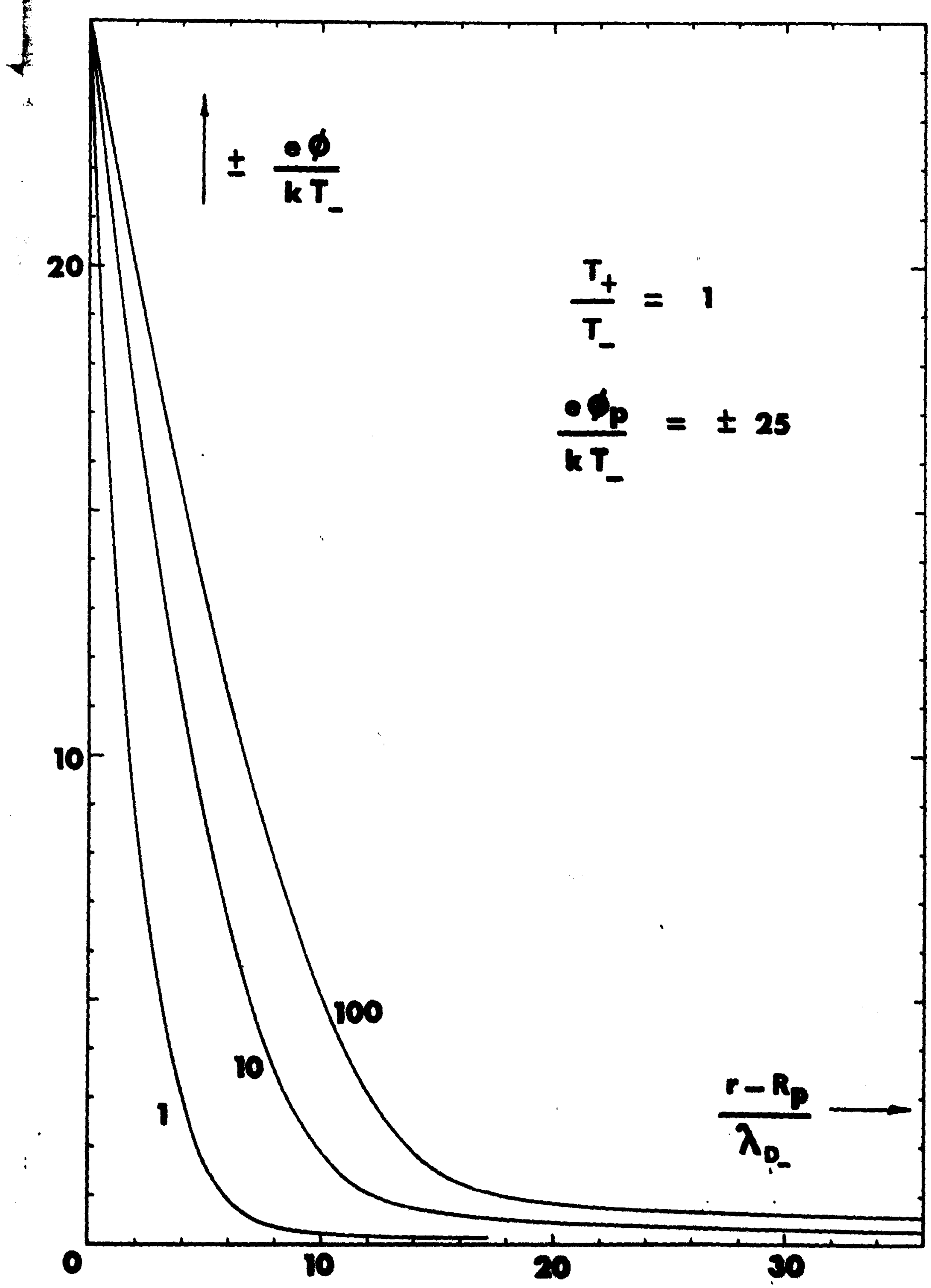

FIGURE 32 POTENTIAL VS DISTANCE FROM PROBE SURFACE IN DEBYE LENGTHS; CYLINDRICAL PROBE; $e\phi_p/kT_- = \pm 25$; $T_+/T_- = 1$; PLOTTED FOR VARIOUS RATIOS OF PROBE RADIUS TO ION OR ELECTRON DEBYE LENGTH.

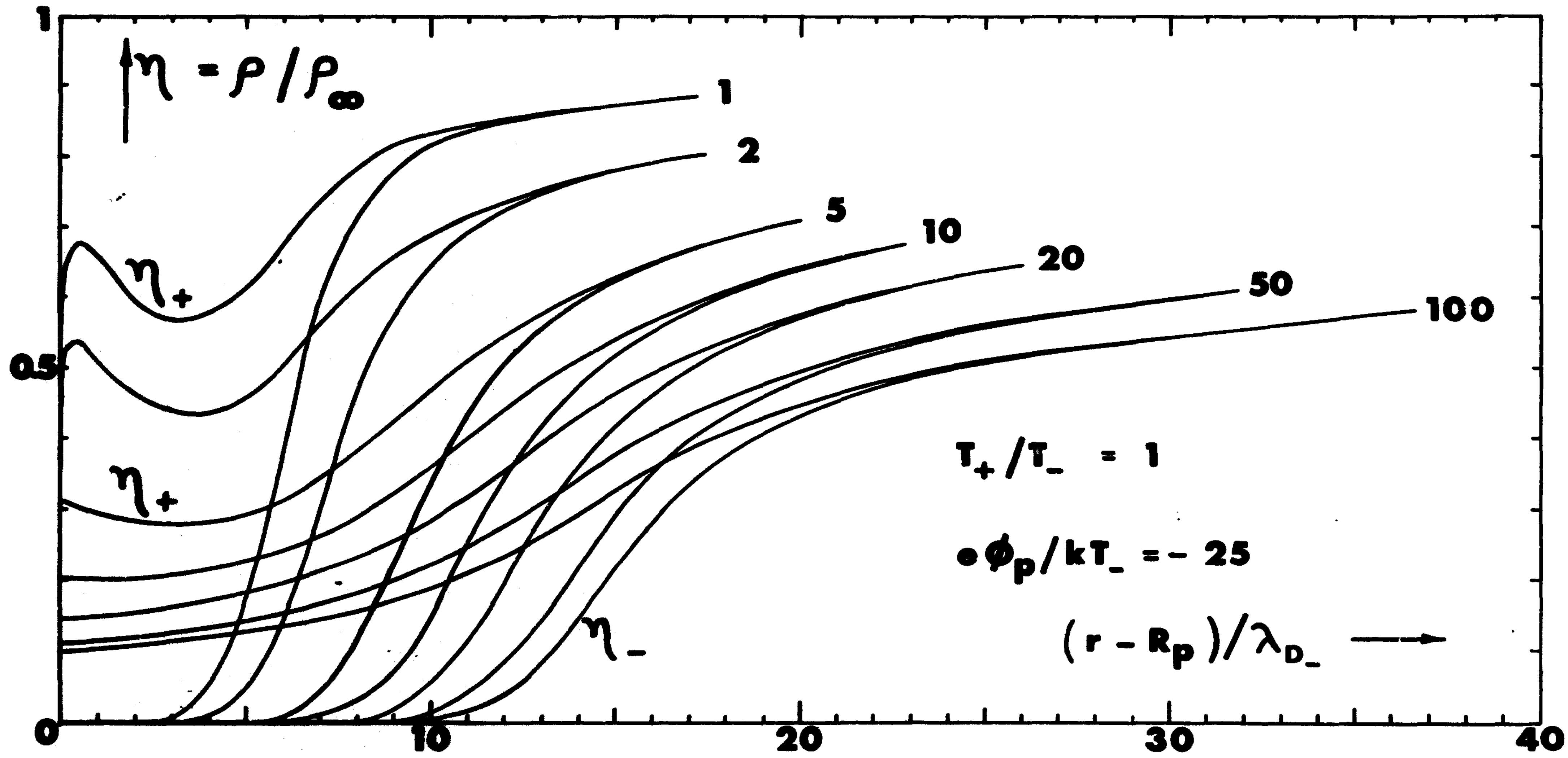

FIGURE 33 ION AND ELECTRON CHARGE DENSITIES η_+ AND η_- VS DISTANCE FROM PROBE SURFACE IN DEBYE LENGTHS; CYLINDRICAL PROBE; $e\phi_p/kT_- = -25$; $T_+/T_- = 1$; PLOTTED FOR VARIOUS RATIOS OF PROBE RADIUS TO ION OR ELECTRON DEBYE LENGTH.

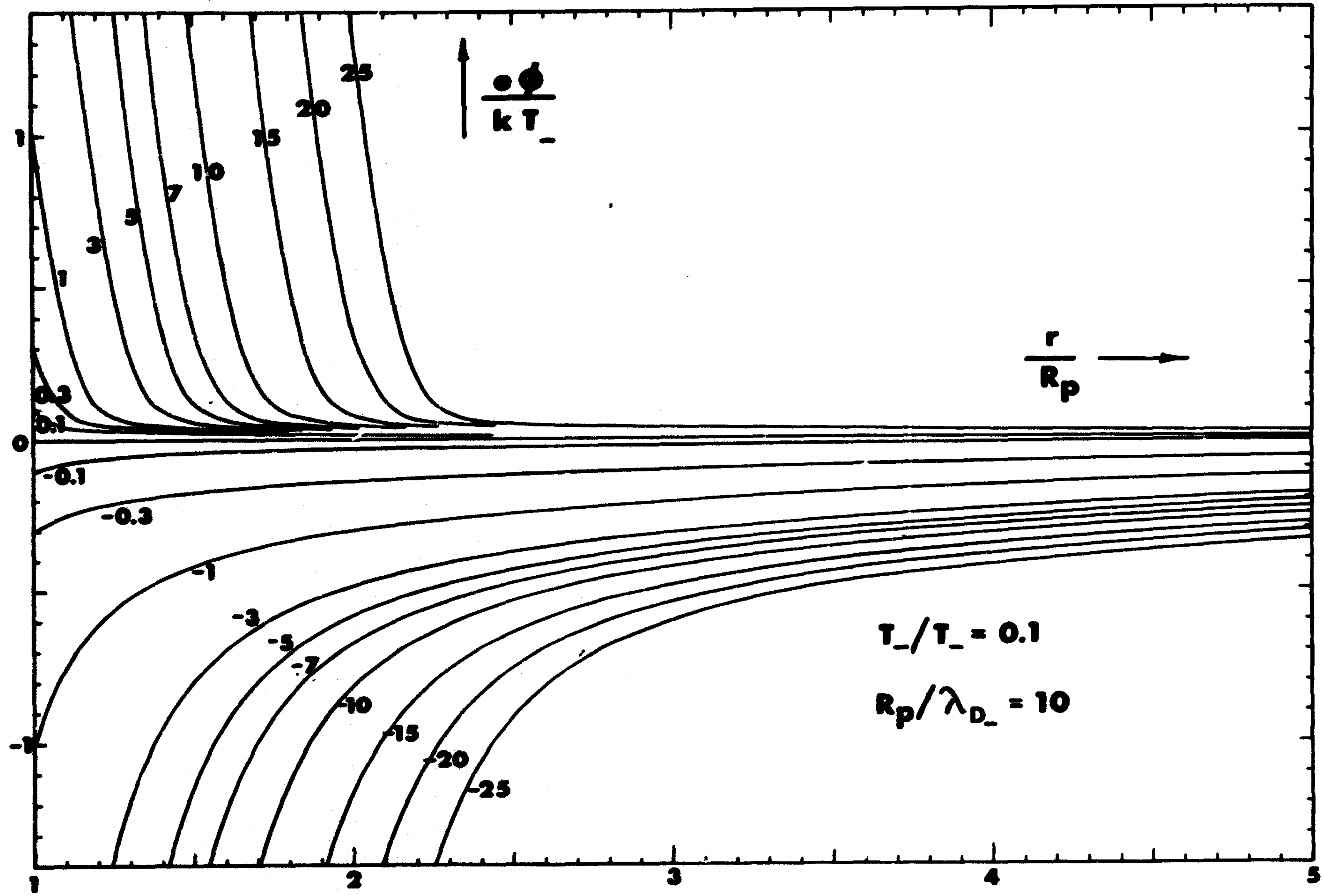

FIGURE 34 POTENTIAL VS RADIUS FOR VARIOUS VALUES OF NONDIMENSIONAL PROBE POTENTIAL $e\phi_p/kT_-$. CYLINDRICAL PROBE; $T_+/T_- = 0.1$; $R_p/\lambda_{D_-} = 10$.

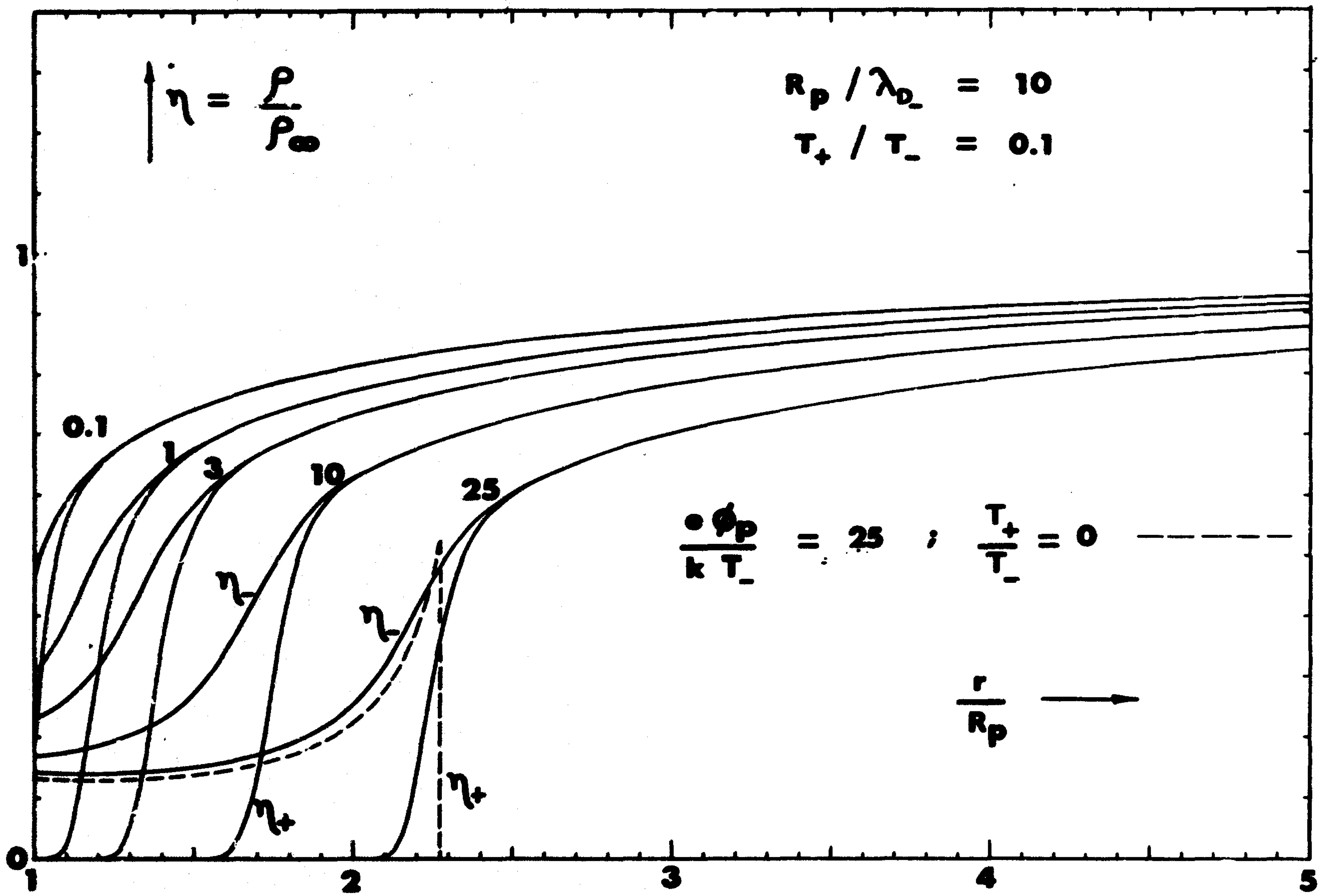

FIGURE 35 ION AND ELECTRON CHARGE DENSITIES η_+ AND η_- VS RADIUS FOR VARIOUS VALUES OF NONDIMENSIONAL PROBE POTENTIAL $e\phi_p/kT_-$. ELECTRON-ATTRACTING CYLINDRICAL PROBE; $T_+/T_- = 0.1$; $R_p/\lambda_{D_-} = 10$. DOTTED CURVES SHOW η_+ AND η_- WITHIN SHEATH FOR THE CASE $e\phi_p/kT_- = 25$; $T_+/T_- = 0$; $R_p/\lambda_{D_-} = 10$.

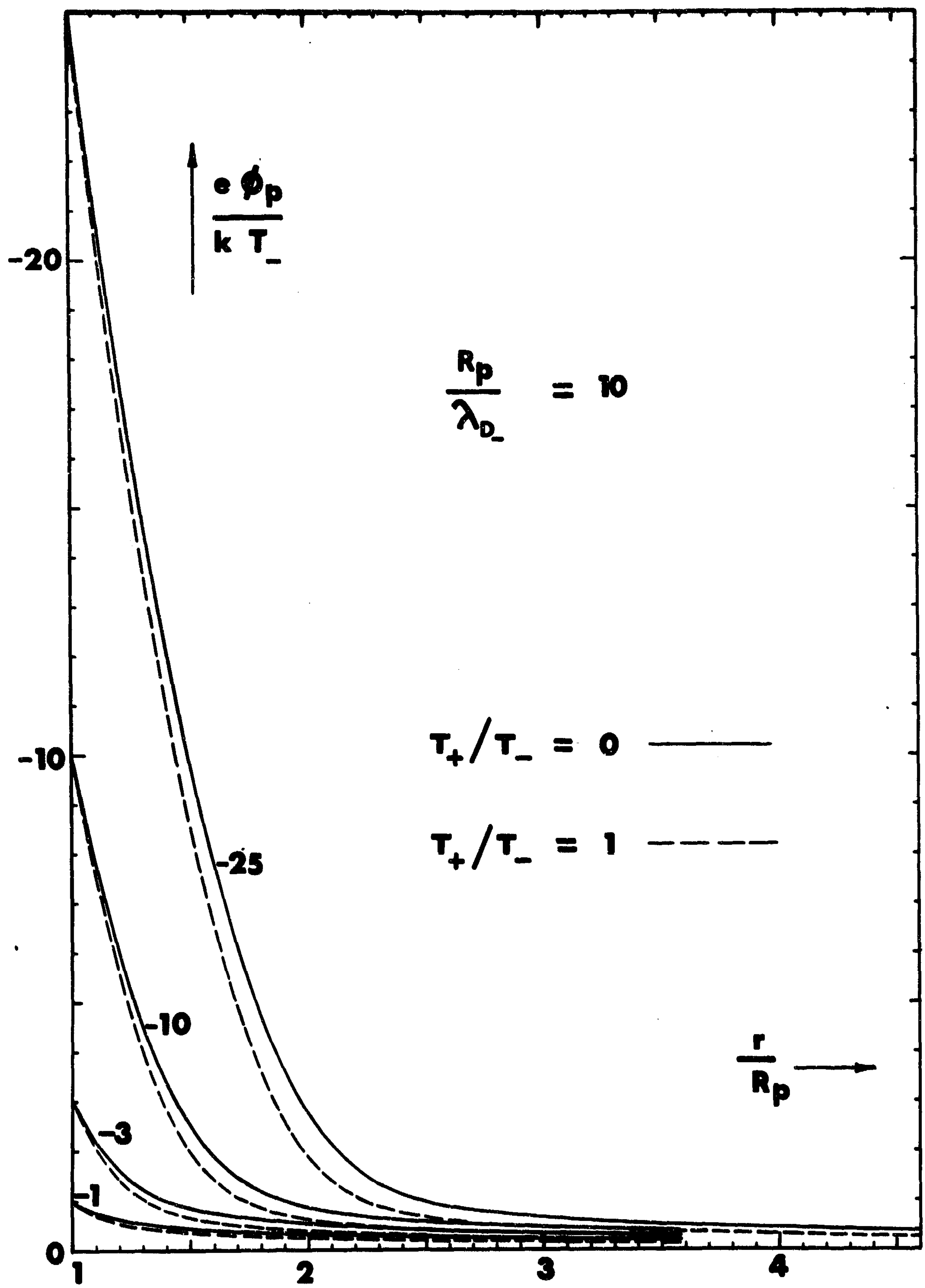

FIGURE 36 POTENTIAL VS RADIUS FOR VALUES OF T_+/T_- OF 0 AND 1; ION-ATTRACTING CYLINDRICAL PROBE; $R_p/\lambda_{D-} = 10$.

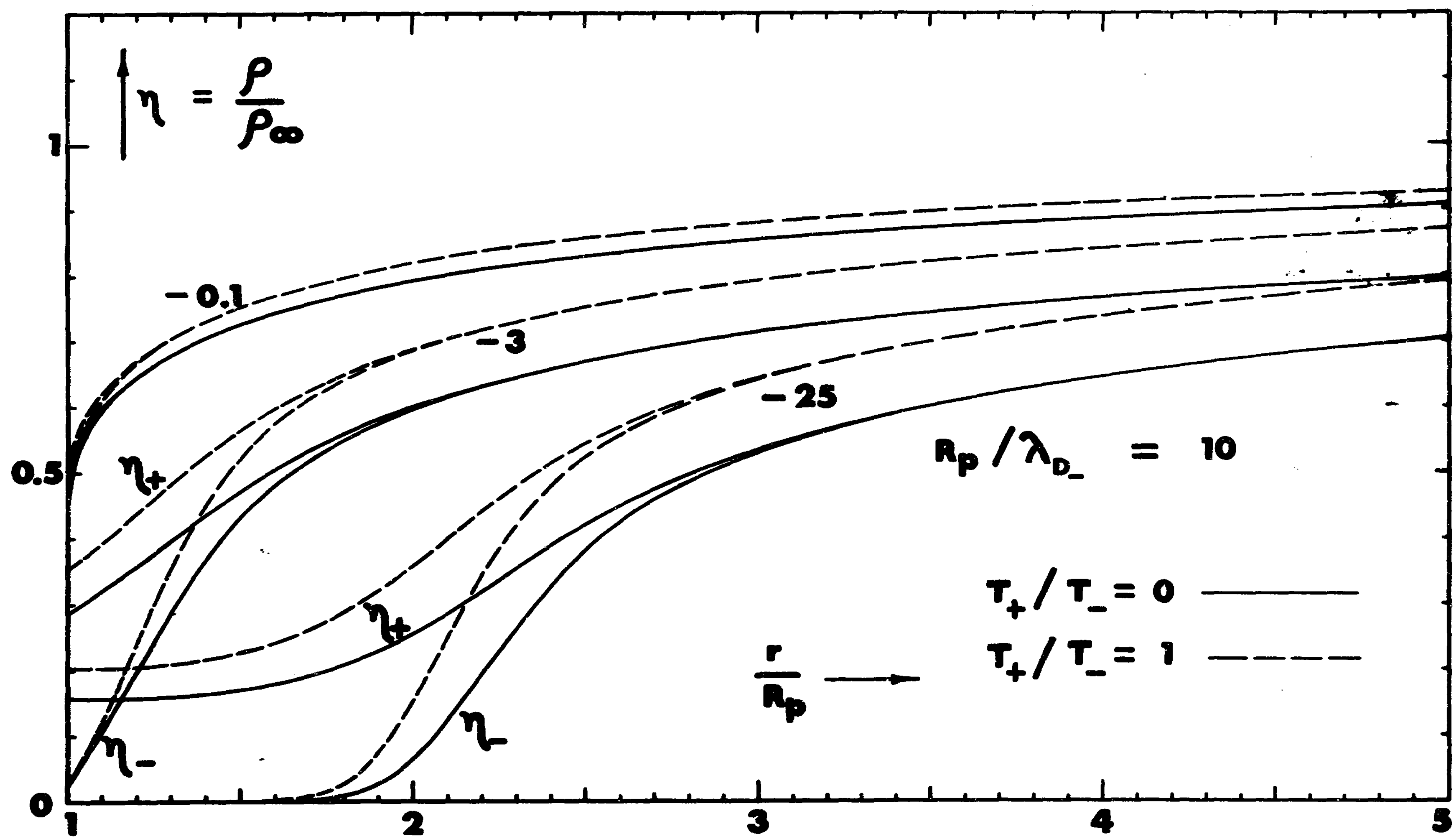

FIGURE 37 ION AND ELECTRON CHARGE DENSITIES η_+ AND η_- VS RADIUS FOR VARIOUS VALUES OF NONDIMENSIONAL PROBE POTENTIAL $e\phi_p/kT_-$. ION-ATTRACTING CYLINDRICAL PROBE; $T_+/T_- = 0$; $R_p/\lambda_{D_-} = 10$.

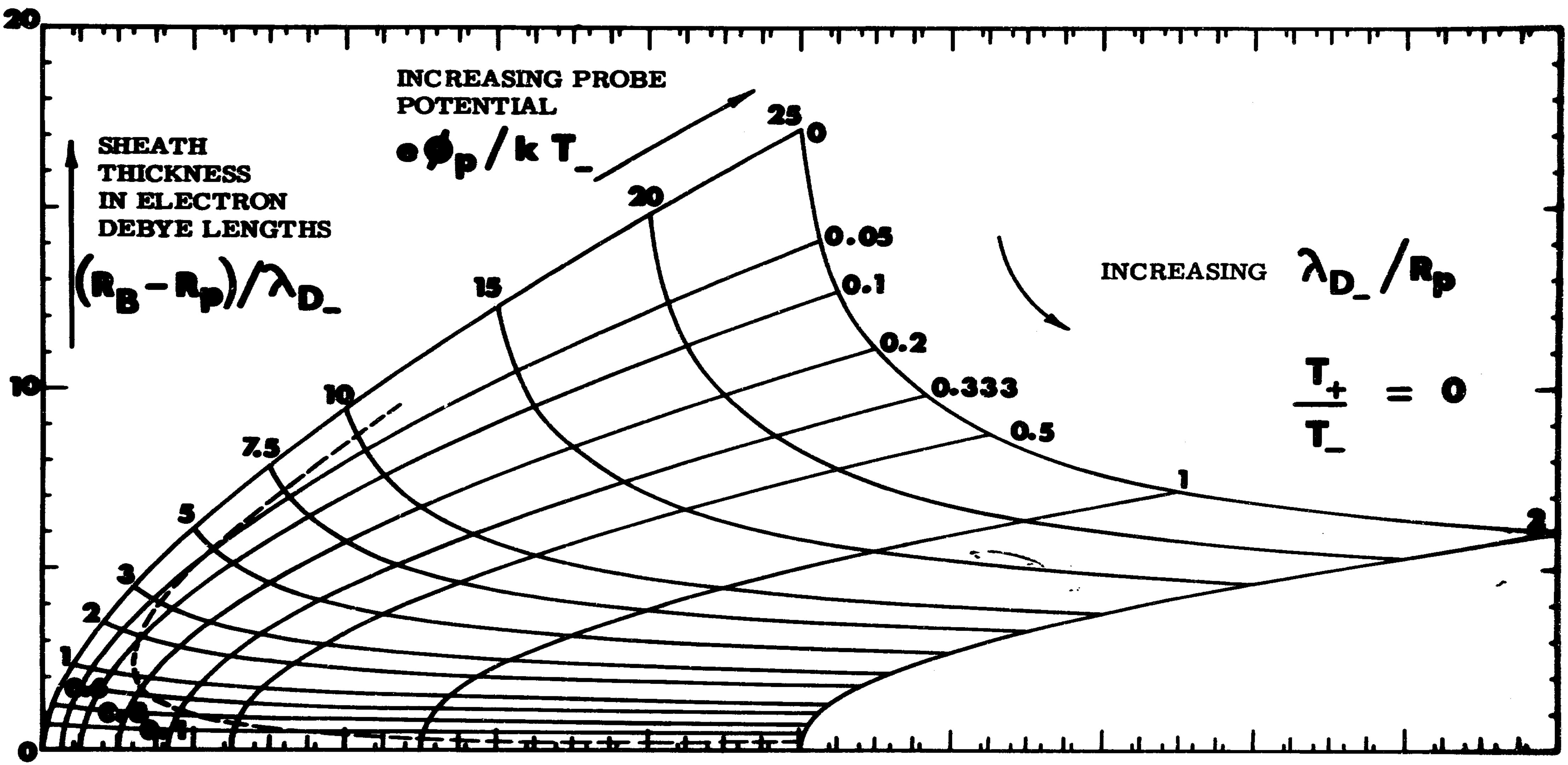

FIGURE 38 SHEATH THICKNESS IN ELECTRON DEBYE LENGTHS. ELECTRON-ATTRACTING CYLINDRICAL PROBE; $T_+/T_- = 0$ (REPELLED SPECIES AT ZERO TEMPERATURE); PLOTTED FOR VARIOUS VALUES OF NONDIMENSIONAL PROBE POTENTIAL AND λ_{D-}/R_p. DOTTED CURVE SHOWS TRAPPED-ORBIT BOUNDARY.

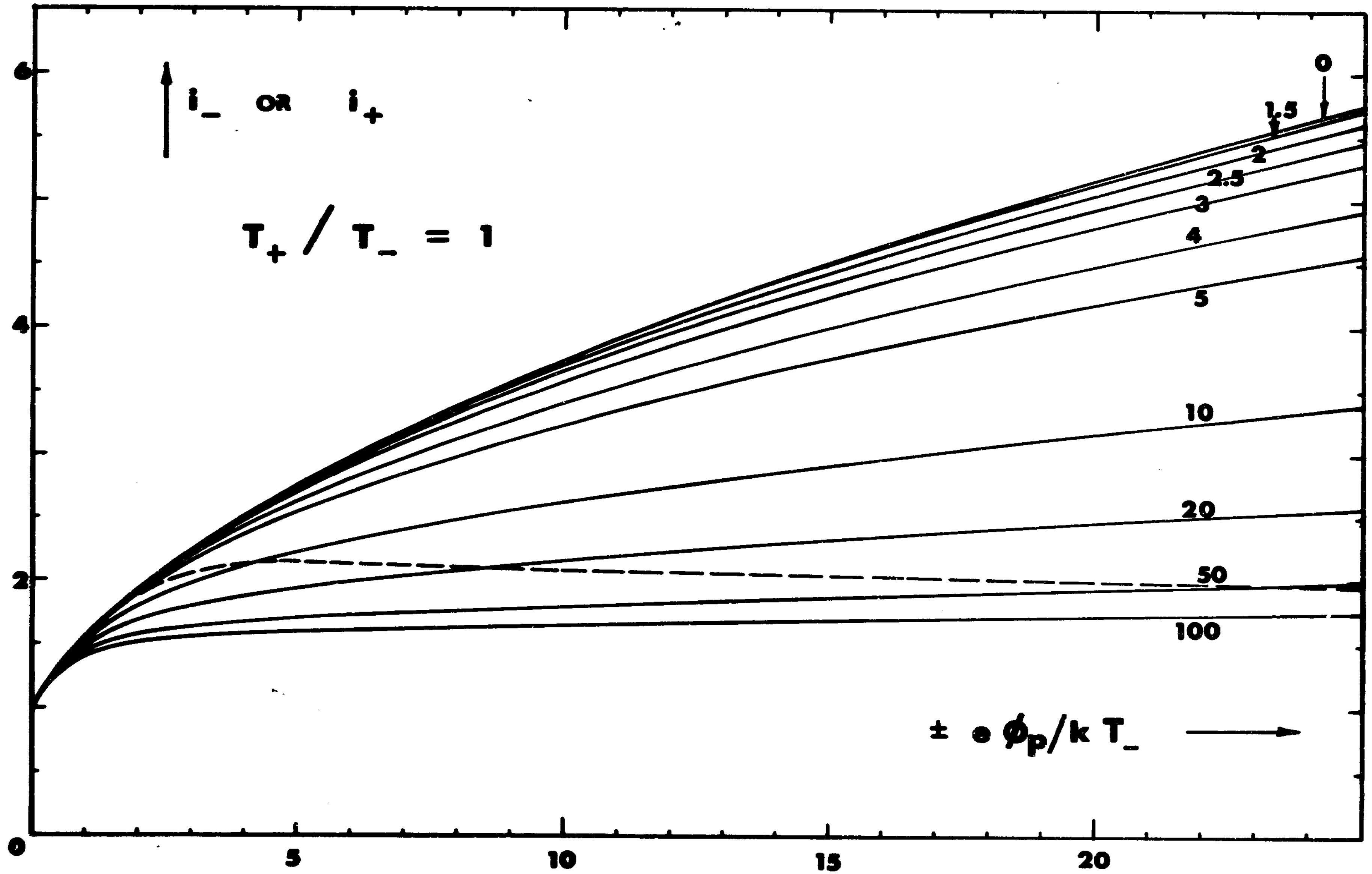

FIGURE 39 ION OR ELECTRON CURRENT VS PROBE POTENTIAL FOR VARIOUS RATIOS OF PROBE RADIUS TO ION OR ELECTRON DEBYE LENGTH; CYLINDRICAL PROBE; $T_+/T_- = 1$. DOTTED CURVE SHOWS TRAPPED-ORBIT BOUNDARY.

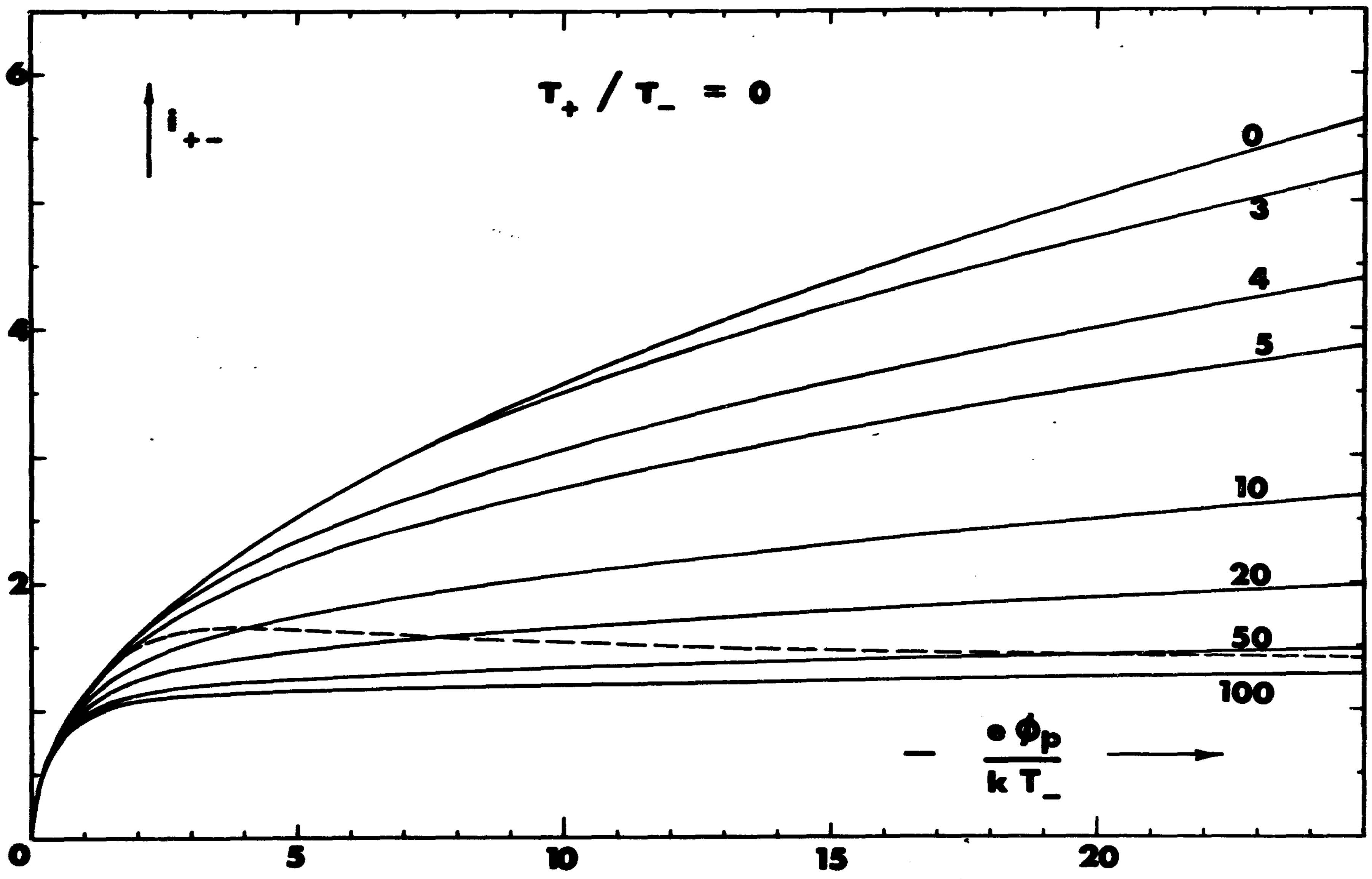

FIGURE 40 ION CURRENT i_{+-} VS PROBE POTENTIAL FOR VARIOUS RATIOS OF PROBE RADIUS TO ELECTRON DEBYE LENGTH. ION-ATTRACTING CYLINDRICAL PROBE; $T_+/T_- = 0$. DOTTED CURVE SHOWS TRAPPED-ORBIT BOUNDARY.

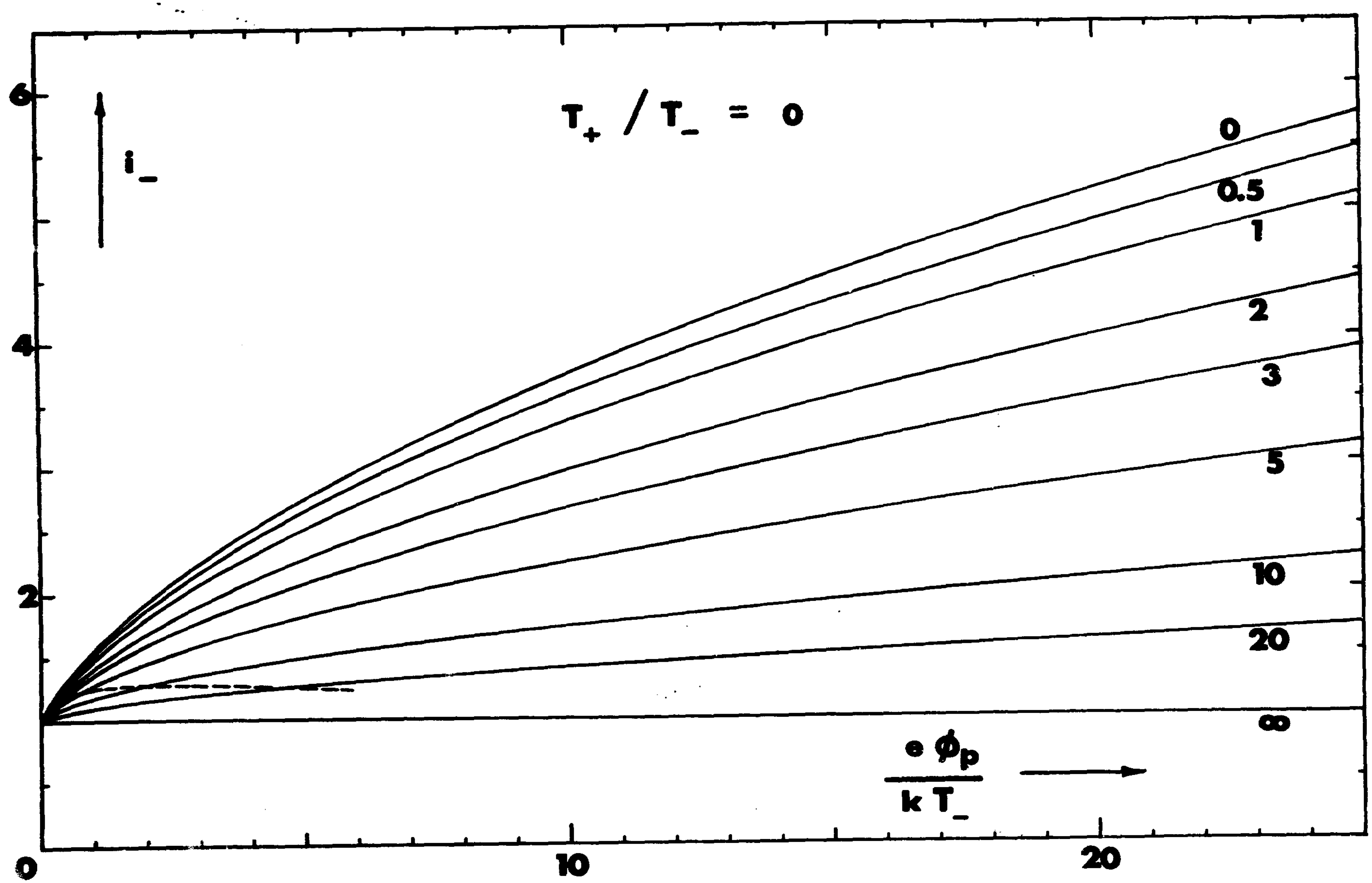

FIGURE 41 ELECTRON CURRENT i_- VS PROBE POTENTIAL FOR VARIOUS RATIOS OF PROBE RADIUS TO ELECTRON DEBYE LENGTH. ELECTRON-ATTRACTING CYLINDRICAL PROBE; $T_+/T_- = 0$ (REPELLED SPECIES AT ZERO TEMPERATURE). DOTTED CURVE SHOWS TRAPPED-ORBIT BOUNDARY.

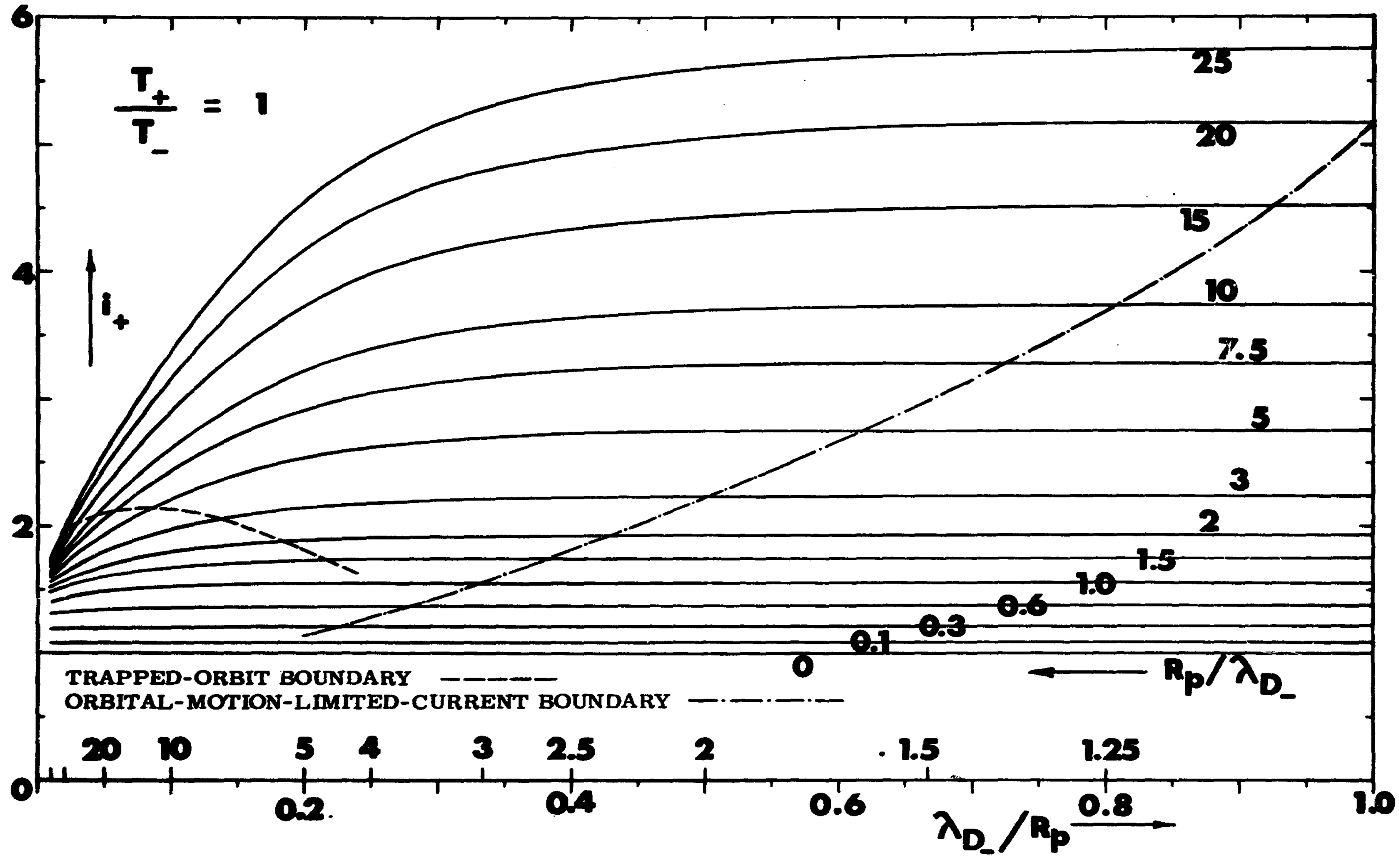

FIGURE 42 ION OR ELECTRON CURRENT VS λ_{D_+}/R_p OR λ_{D_-}/R_p FOR VARIOUS VALUES OF $\pm\, e\phi_p/kT_-$; CYLINDRICAL PROBE; $T_+/T_- = 1$.

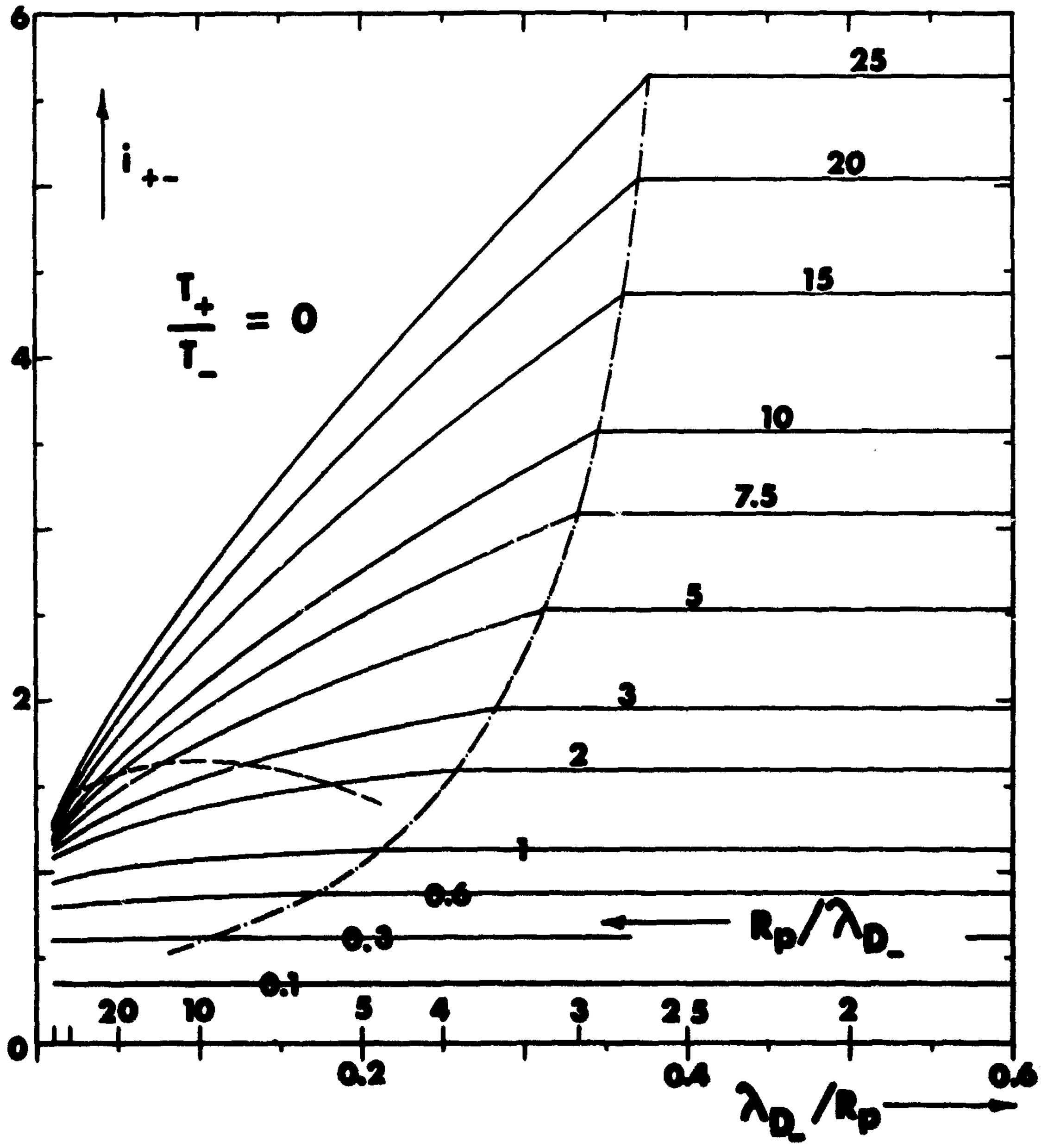

FIGURE 43 ION CURRENT VS λ_{D_-}/R_p FOR VARIOUS VALUES OF $-e\phi_p/kT_-$; CYLINDRICAL PROBE; $T_+/T_- = 0$. ORBITAL-MOTION-LIMITED-CURRENT AND TRAPPED-ORBIT BOUNDARIES LABELLED AS IN FIGURE 42.

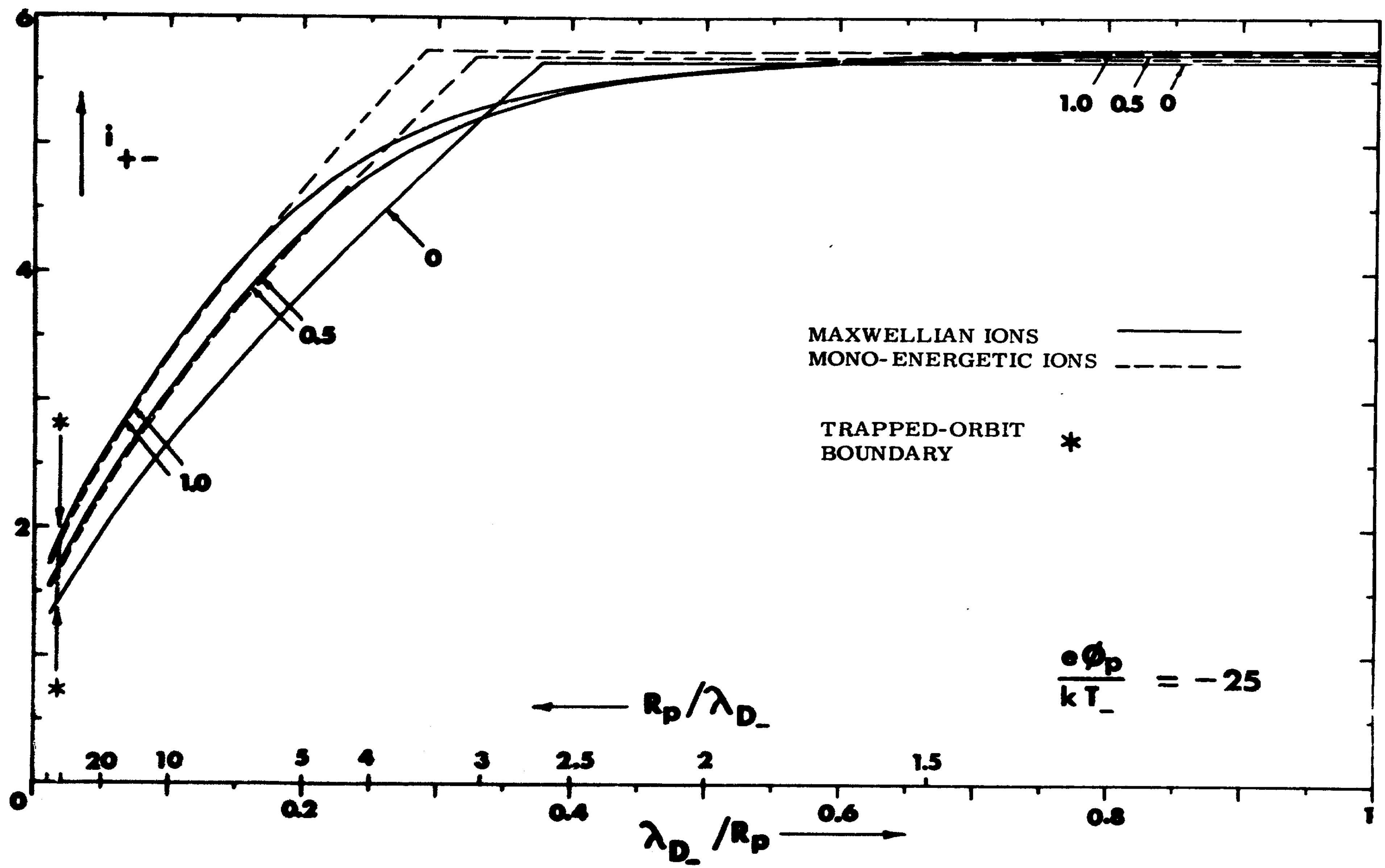

FIGURE 44 ION CURRENT i_{+-} VS λ_{D-}/R_p FOR VALUES OF T_+/T_- OF 0, 0.5 AND 1; CYLINDRICAL PROBE; $e\phi_p/kT_- = -25$.

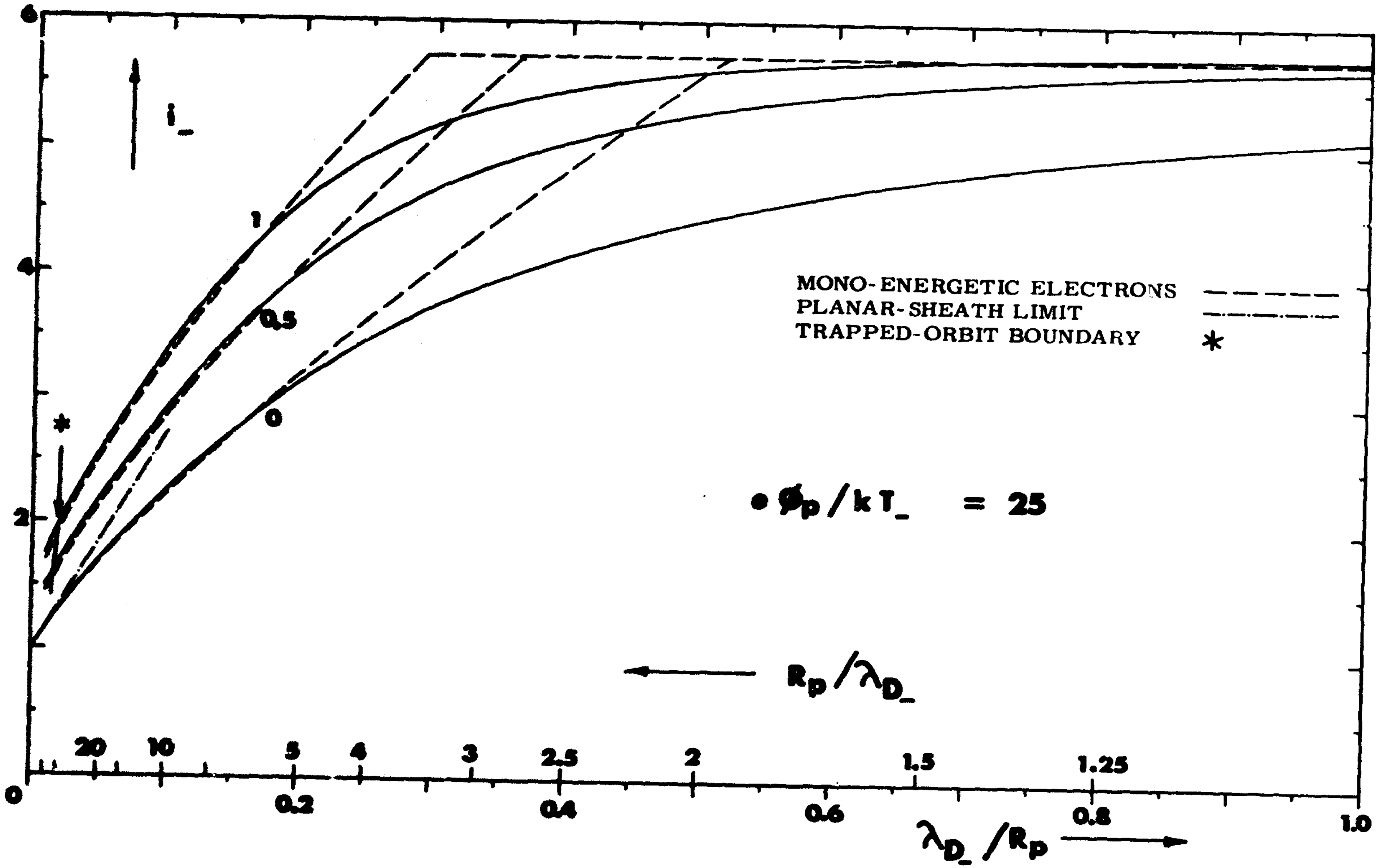

FIGURE 45 ELECTRON CURRENT i_- VS λ_{D-}/R_p FOR VALUES OF T_+/T_- OF 0, 0.5 AND 1; CYLINDRICAL PROBE; $e\phi_p/kT_- = 25$.

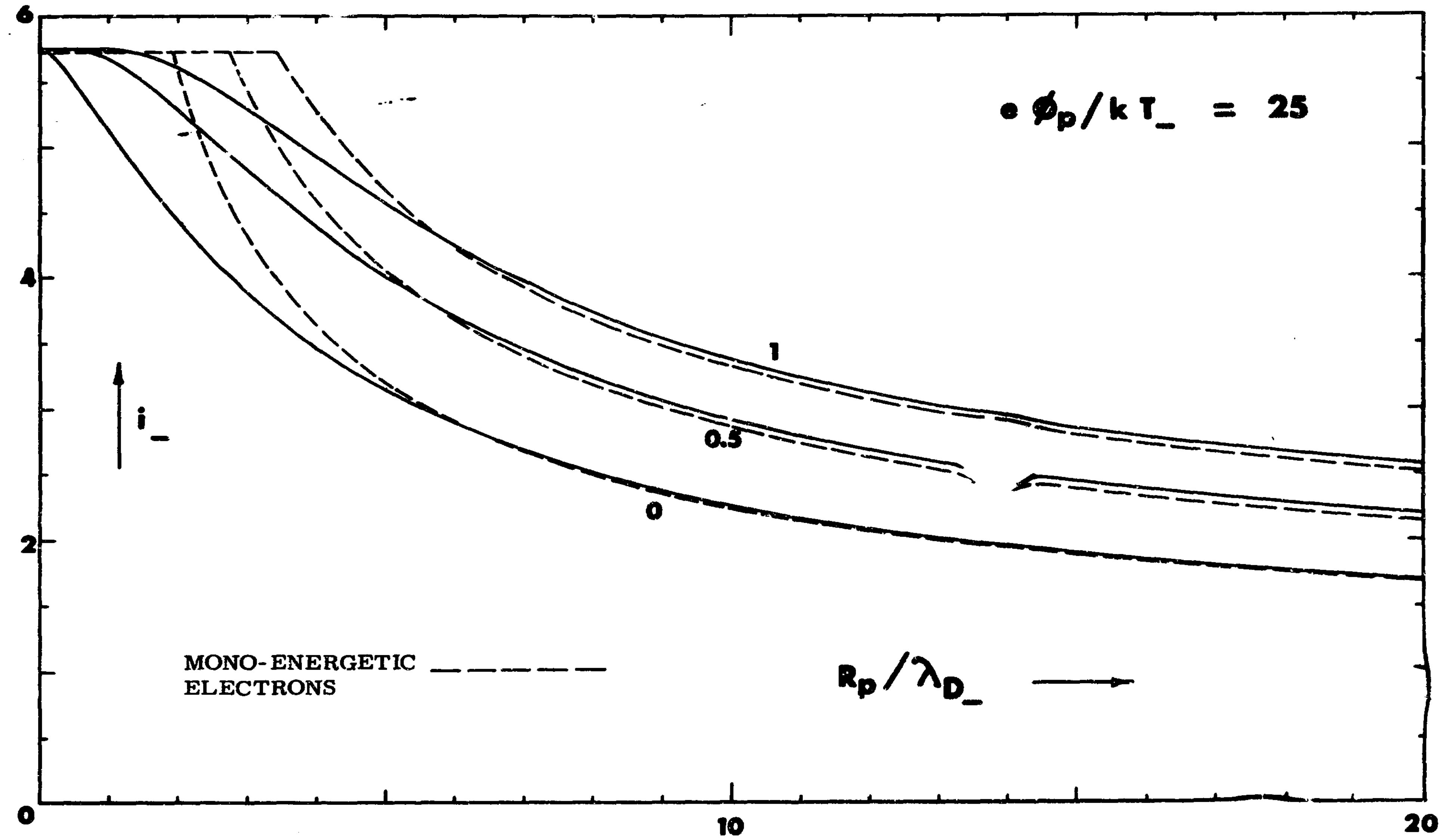

FIGURE 46 ELECTRON CURRENT i_- VS R_p/λ_{D-} FOR VALUES OF T_+/T_- OF 0, 0.5 AND 1; CYLINDRICAL PROBE; $e\phi_p/kT_- = 25$.

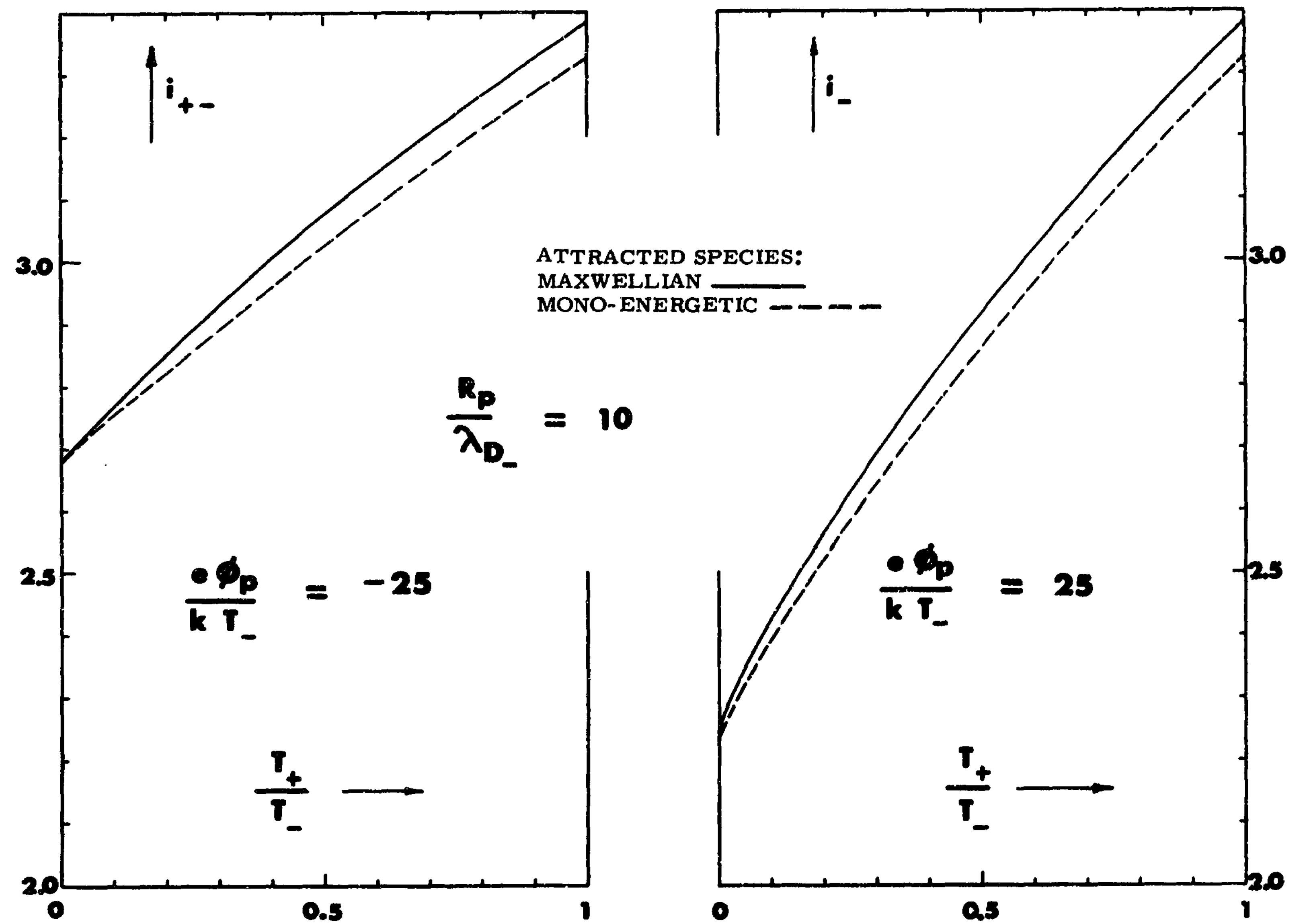

FIGURE 47 ION AND ELECTRON CURRENTS COLLECTED BY ION- AND ELECTRON-ATTRACTING CYLINDRICAL PROBES, RESPECTIVELY, AS FUNCTIONS OF T_+/T_-, FOR $R_p/\lambda_{D_-} = 10$ AND VALUES OF $e\phi_p/kT_-$ OF -25 AND +25. RESULTS FOR MONO-ENERGETIC ATTRACTED SPECIES SHOWN FOR COMPARISON.

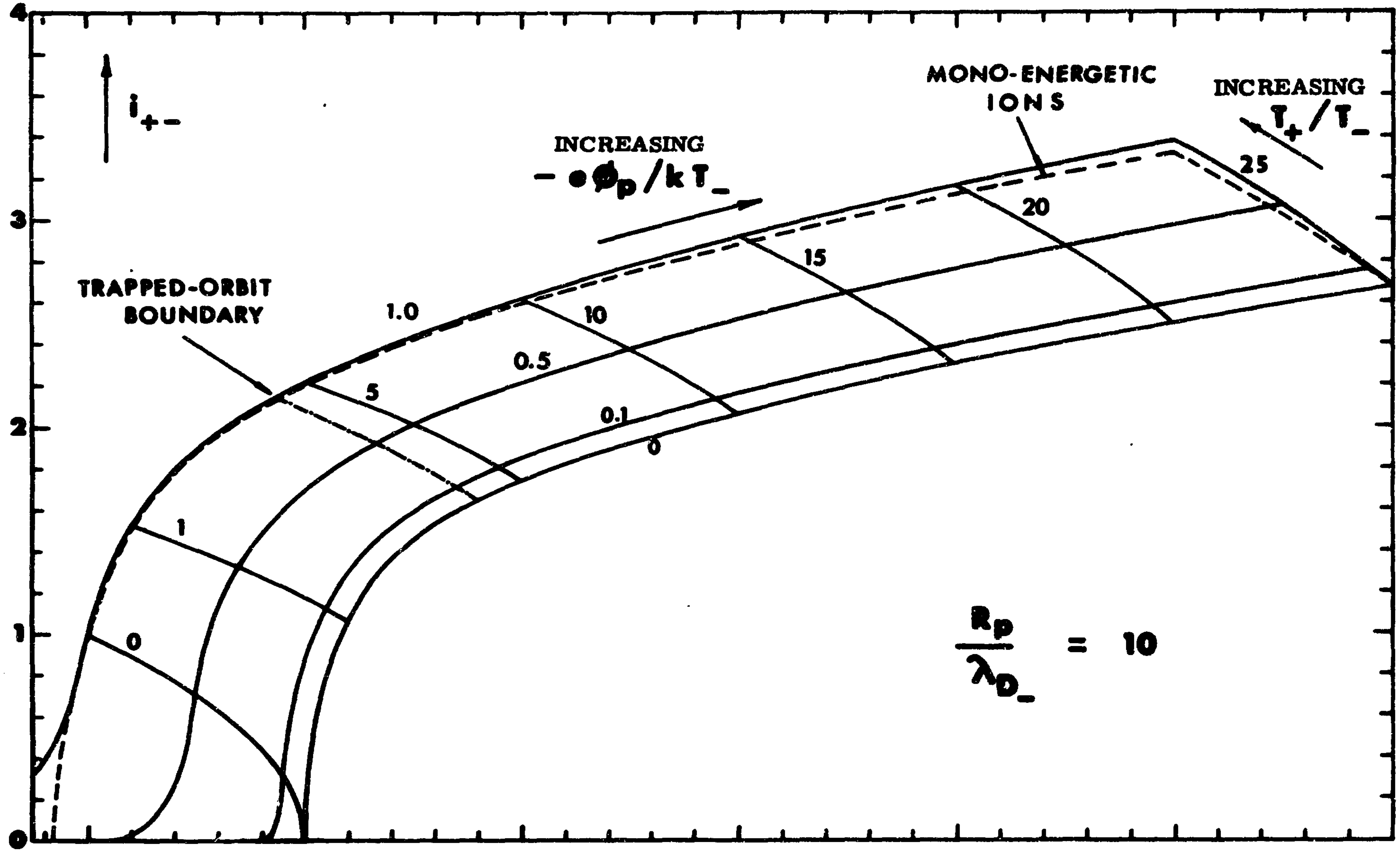

FIGURE 48 ION CURRENT i_{+-} AS A FUNCTION OF $e\phi_p/kT_-$ AND T_+/T_- FOR A CYLINDRICAL PROBE WITH $R_p/\lambda_{D_-} = 10$. MONO-ENERGETIC RESULT SHOWN FOR $T_+/T_- = 1$ AND FOR $e\phi_p/kT_- = -25$ FOR COMPARISON.

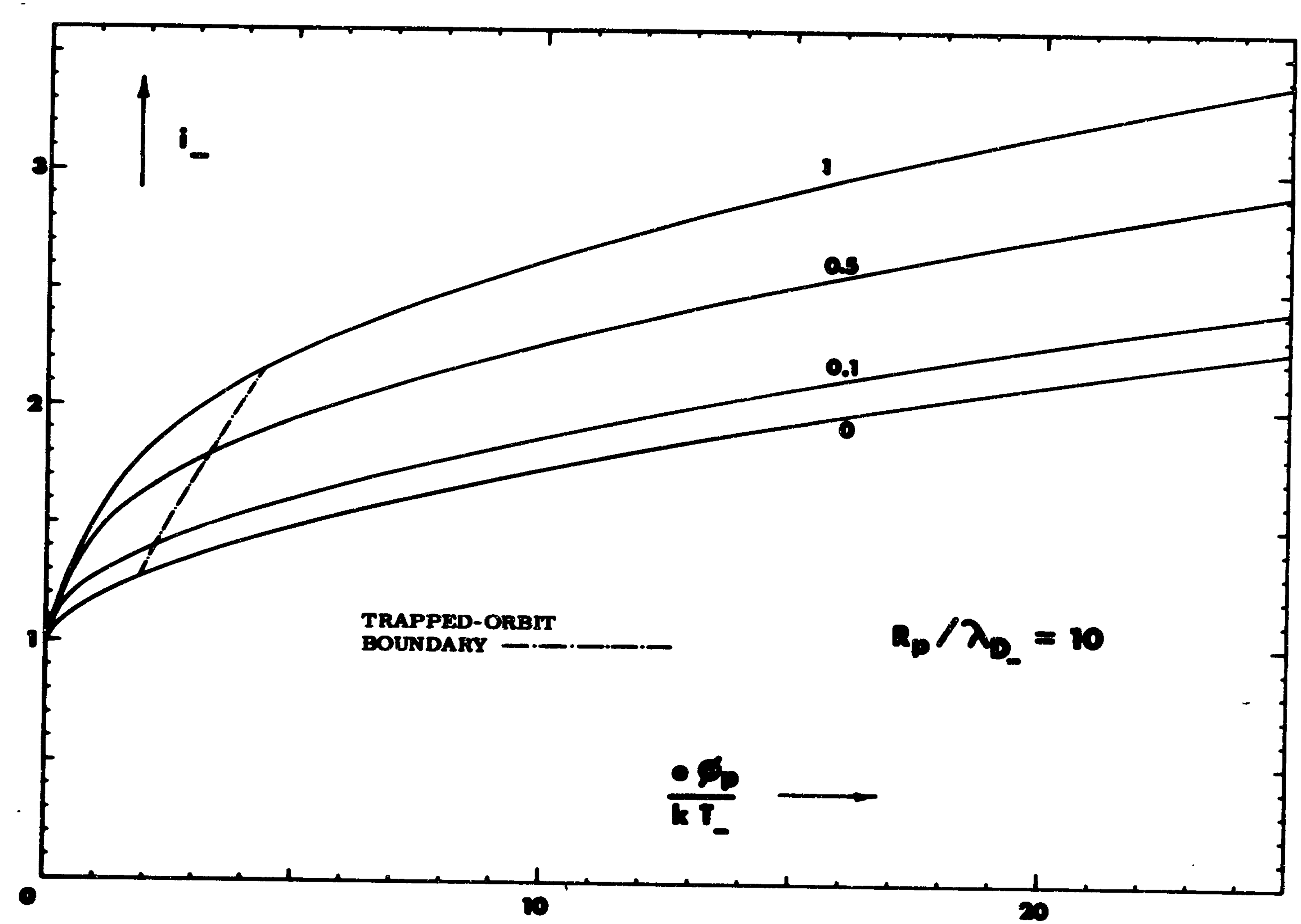

FIGURE 49 ELECTRON CURRENT i_- AS A FUNCTION OF $e\phi_p/kT_-$; PLOTTED FOR VALUES OF T_+/T_- FROM 0 to 1. CYLINDRICAL PROBE; $R_p/\lambda_{D_-} = 10$.

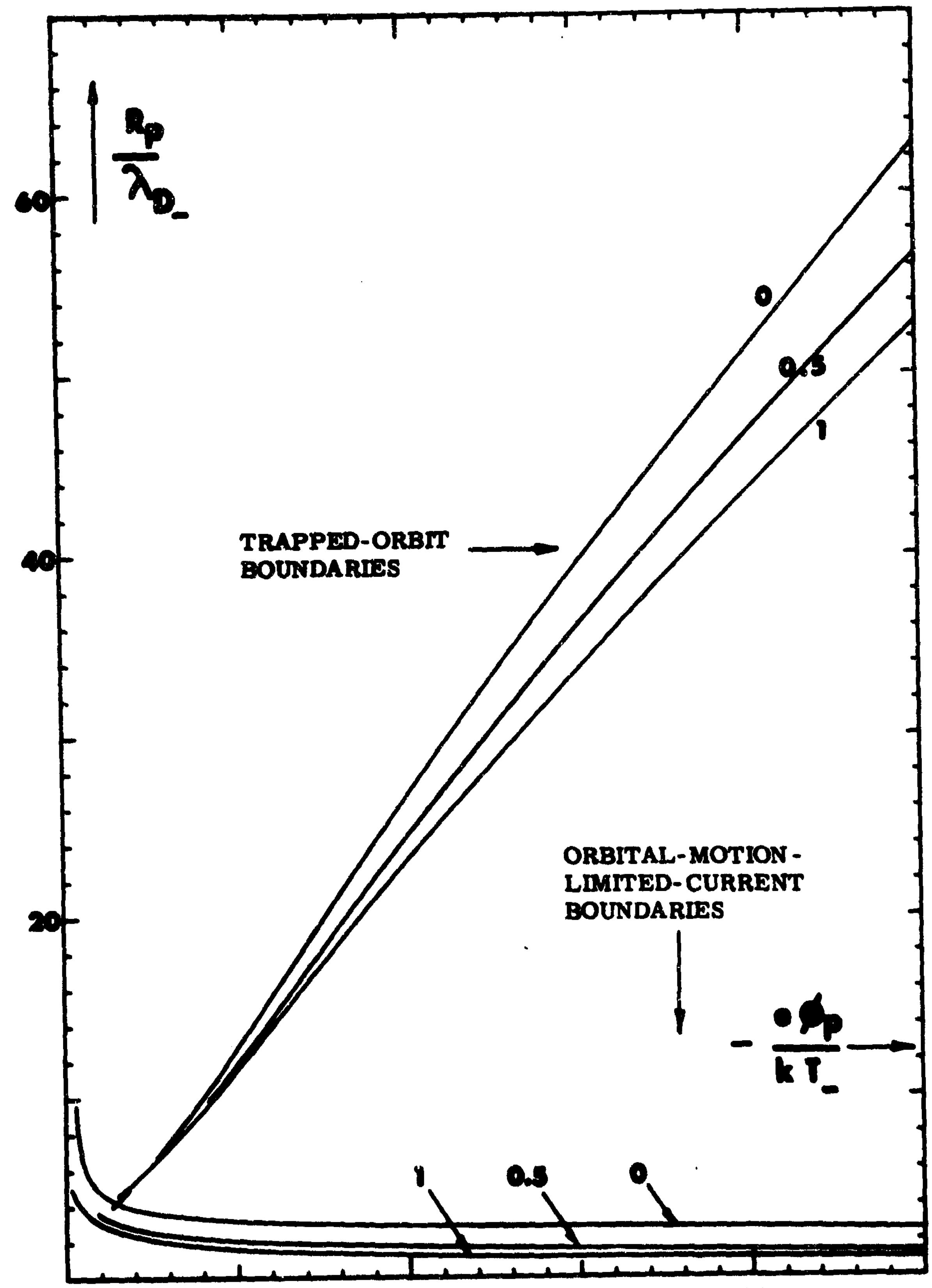

FIGURE 50a TRAPPED-ORBIT AND ORBITAL-MOTION-LIMITED-CURRENT BOUNDARIES PLOTTED AS FUNCTIONS OF PROBE POTENTIAL FOR AN ION-ATTRACTING CYLINDRICAL PROBE FOR VALUES OF T_+/T_- OF 0, 0.5 AND 1.

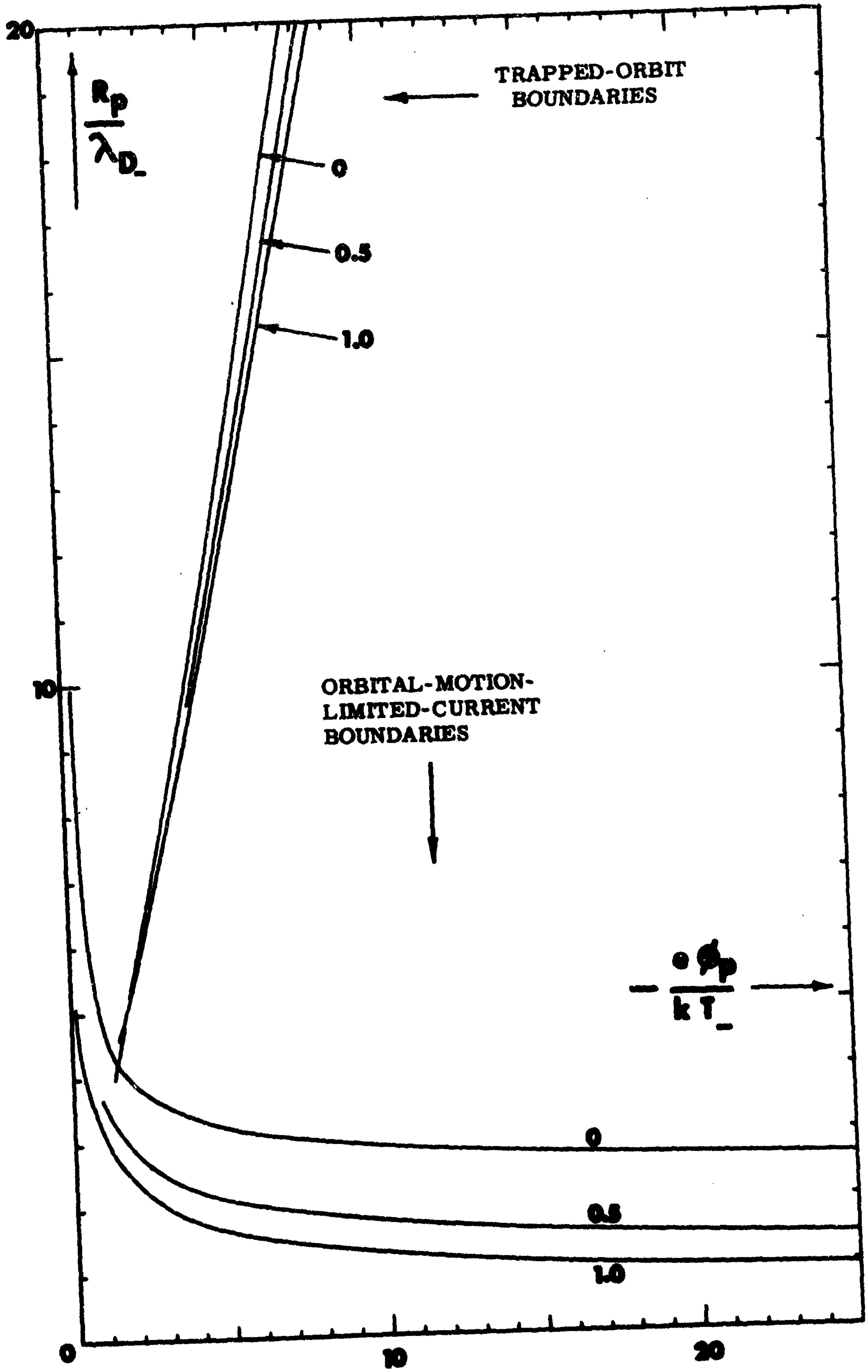

FIGURE 50b SAME QUANTITIES AS THOSE OF FIG. 50a PLOTTED ON A LARGER SCALE IN R_p/λ_{D_-}.

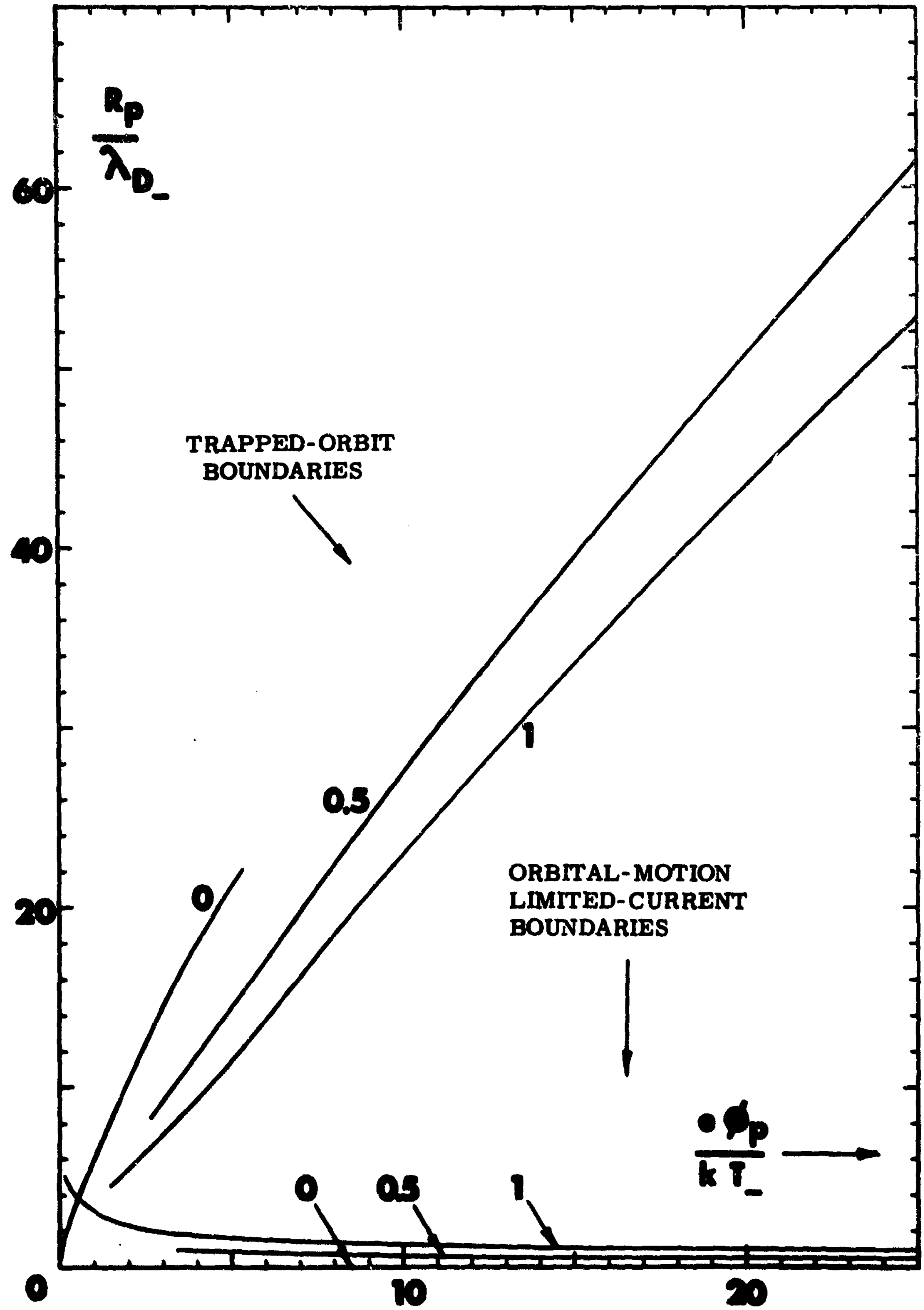

FIGURE 51 TRAPPED-ORBIT AND ORBITAL-MOTION-LIMITED-CURRENT BOUNDARIES PLOTTED AS FUNCTIQNS OF PROBE POTENTIAL FOR AN ELECTRON-ATTRACTING CYLINDRICAL PROBE FOR VALUES OF T_+/T_- OF 0, 0.5 AND 1.

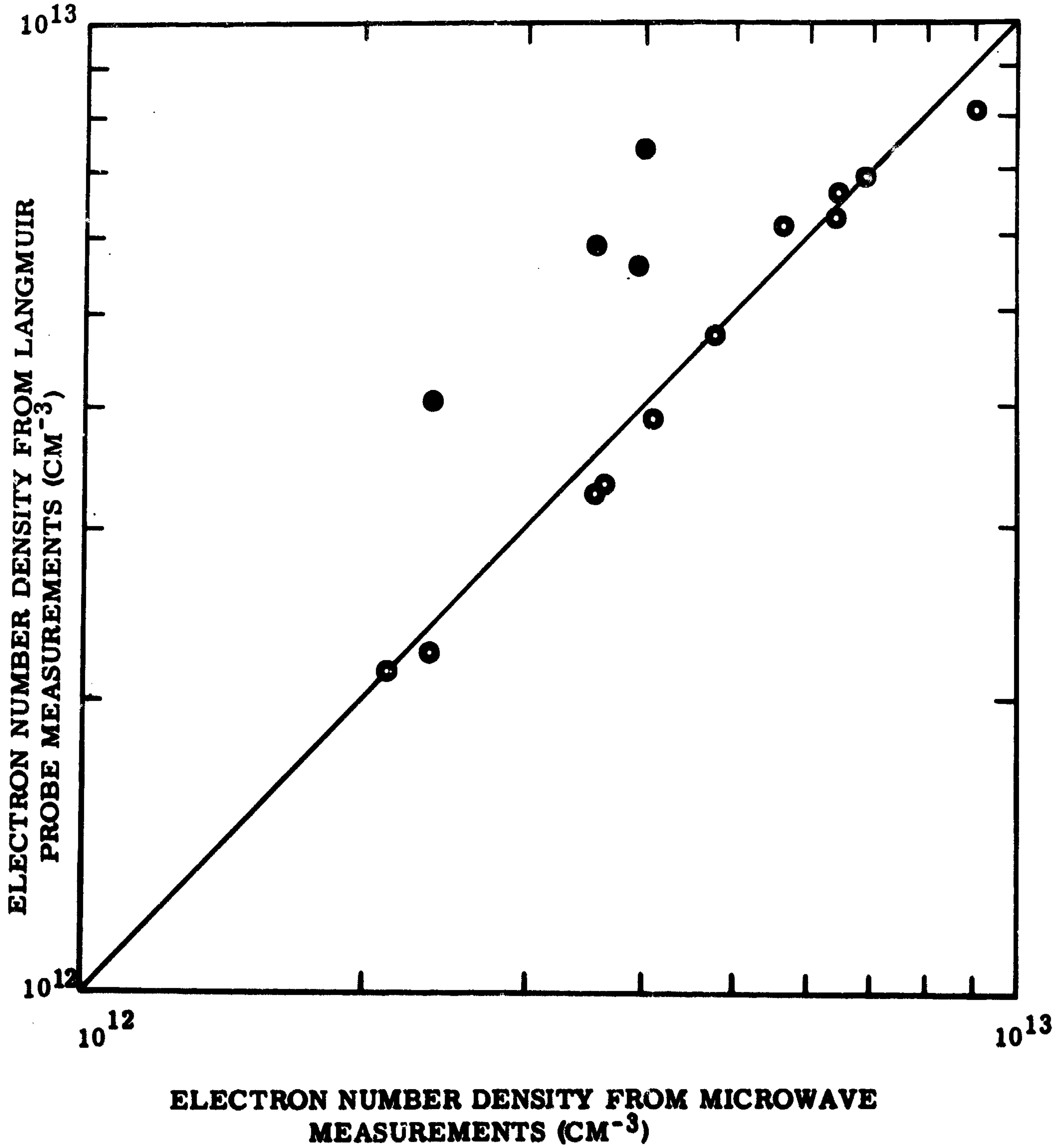

FIGURE 52 COMPARISON OF LANGMUIR PROBE AND MICROWAVE MEASUREMENTS, AFTER REFS. 3 AND 19.

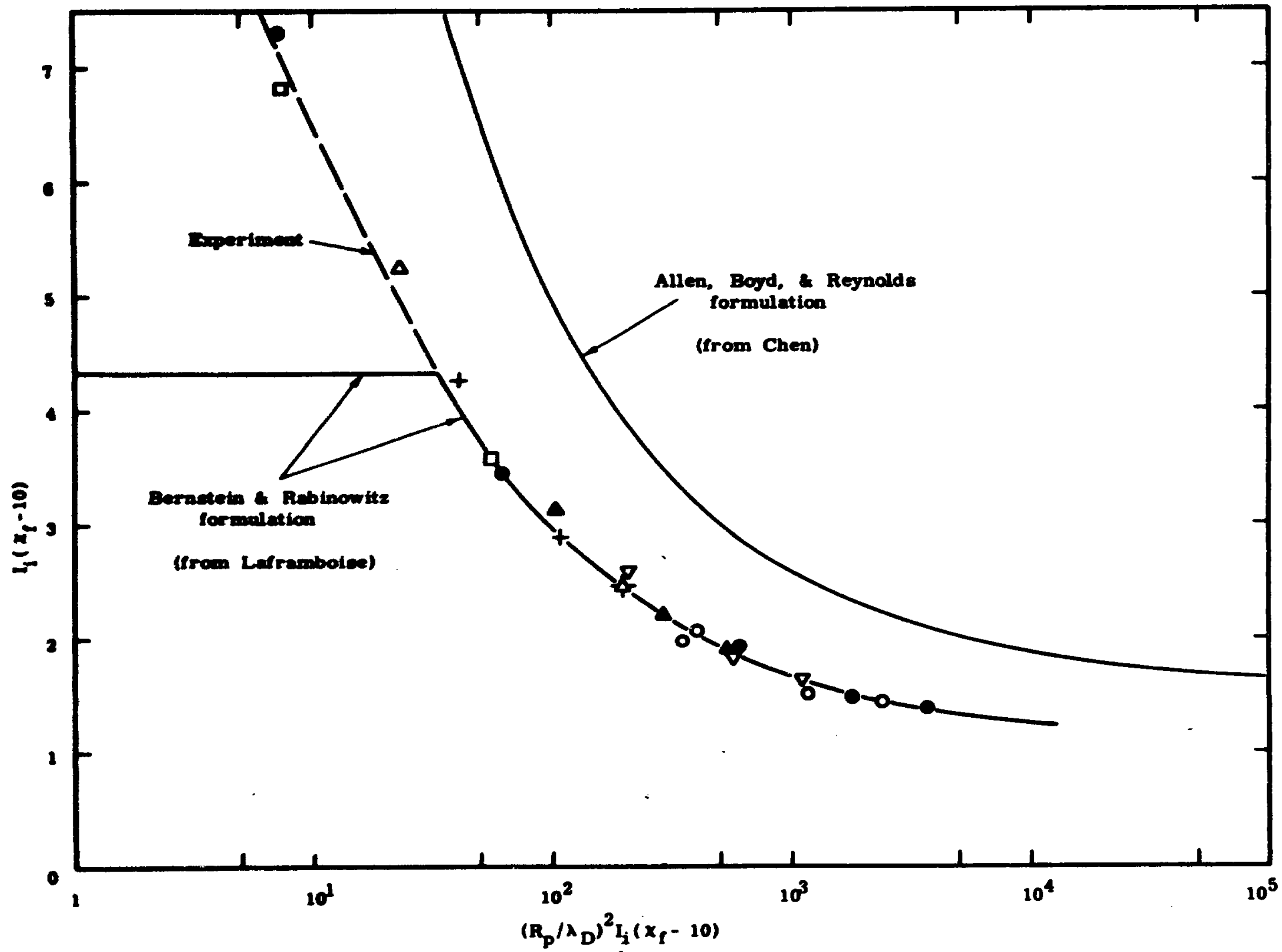

FIGURE 53 VARIATION OF DIMENSIONLESS ION CURRENT $I_i(\chi_f - 10)$ WITH $(R_p/\lambda_D)^2 I_i(\chi_f - 10)$, AFTER REFS. 4 AND 19. COMPARISON OF EXPERIMENT AND THEORY FOR $T_+/T_- \ll 1$. I_i IS EQUIVALENT TO THE CURRENT I_{+-} DEFINED IN SEC. IX: χ_f IS THE VALUE OF THE DIMENSIONLESS FLOATING POTENTIAL FOR AN ARGON PLASMA.

APPENDIX A

Limits on the Validity of the Collisionless Boltzmann-Vlasov Equation

The idealized collisionless plasma represented by the Vlasov equation is an abstraction which describes the behaviour of a more general plasma only in the limit as its number density N becomes small or its temperature becomes large. More precisely, it has been shown in a paper by Rostoker and Rosenbluth (Ref. 10) that the Vlasov equation is obtained from the full kinetic equation for the plasma in the limit as the number of particles in a Debye cube becomes large for each species in the plasma; i.e., as $g = 1/N\lambda_D^3 \rightarrow 0$. For a plasma which has a finite N and T, there exists a finite value of g, which is much smaller than unity in most cases of physical interest. It follows that in a hypothetical sequence of physical situations in which all relevant non-dimensional parameters are held constant except g, which is made to approach zero, the effect of collisions must in some manner become negligible. In particular, the distance traversed by a particle in the plasma before it is appreciably scattered from its collisionless trajectory by encounters with other individual particles must become large. We note again as in Sections I and III that the collisionless plasma obtained in the limit as $g \rightarrow 0$ still allows an individual particle to be influenced by the electric fields of others, but only by their collective macroscopic charge density rather than by their presence as individuals, which is the subject of concern here.

Spitzer (Ref. 13) has shown that in such a plasma, i.e. one having a small but non-zero value of g, corresponding to finite N and T, particles are scattered out of their collisionless trajectories by numerous small-deflection encounters with other particles, and that on the average, they are deflected much sooner by an accumulation of these distant encounters than by single close collisions.

These considerations serve to define a criterion which applies to situations wherein a probe of given size is present in a plasma having particular values of N and T. In such a situation, the results of a collisionless theory may be expected to be useful for predicting current collection if the average distance which the charged particles travel before being deflected appreciably from their collisionless trajectories is large compared to the diameter of the probe. Since the ions in the plasma have much greater mass than the electrons, the amounts of scattering accumulated by ions or by electrons as a result of encounters with ions or with electrons will, in general, be different for each of the four possible combinations of these particles. By considering separately each possible combination of scattered and scattering species, it is possible to derive a set of four scattering distances for the plasma; the smallest of these distances then becomes an upper limit on the probe size for which the collisionless theory will apply.

In order to consider these four scattering processes separately, it is here assumed that the scattering accumulated by a particle due to encounters with particles of each species may be added linearly to find the scattering due to simultaneous interaction with both.

In an incompletely ionized plasma, charged particles are also deflected by collisions with neutral atoms. This process has been treated elsewhere, for example in Chapters 3 and 5 of Ref. 14. Because of the short-range nature of the interaction potential between a charged and a neutral particle, collisions involving neutrals do not usually form the most severe limit on the collisionless theory if the degree of ionization of the plasma is greater than a few percent.

The derivation given by Spitzer (Ref. 13) assumes that a test particle moving through the plasma is deflected by a sequence of independent binary encounters with the unmodified Coulomb fields of nearby particles. This assumption is untrue since the test particle is under the influence of many other particles at any given time. However, Spitzer shows by a physical argument that his results may be expected to approximate usefully the actual behaviour of the test particle. It has also been shown by Sundaresan and Wu (Ref. 15) that expressions for the thermal conductivity of a plasma, obtained using Spitzer's assumption, are in good agreement with results obtained by a rigorous solution of a truncated form of the B-B-G-K-Y hierarchy.

We now consider the four scattering processes mentioned earlier. The ion-ion and electron-electron processes may be considered together. It may also be shown that in the limit of small deflections, and for a given impact parameter and initial velocity, an electron is scattered the same amount (except for sign) by an encounter either with a stationary ion or with a stationary electron. In the case of the encounter with an ion, the reduced mass (Ref. 13) for the encounter is nearly the electron mass, and the mass-center encounter coordinates coincide closely with the laboratory reference frame. For the electron-electron encounter, the reduced mass is one-half the electron mass. However, the transformation from mass-center to laboratory coordinates decreases the scattering angle by one-half (Ref. 11), and the two effects cancel. Therefore, a test electron moving much faster than the random thermal velocity experiences the same amount of scattering from ions as from other electrons.

Spitzer also shows that the dominant effect on a test particle moving at or above the random speed of the field particles is transverse scatter. In this situation the distance of interest is that in which it is scattered through a large angle; Spitzer uses as a reference an angle of 90°. In the fourth case to be considered, that of an ion test particle moving through electron field particles, the ion normally is moving much more slowly than the electrons and the dominant effect is to cause the ion to lose its forward momentum. In this case, the distance of interest is that in which it is effectively stopped.

In order to study the first three of these four types of scattering, we consider a test particle with velocity v and mass m traversing a plasma which consists of one species of charged particle having a Maxwellian velocity distribution. Let m_1 be the mass of each field particle in the plasma and let T_1 and N_1 be the temperature and number density of the field particles. Let q and q_1 be the charge on test particle and field particles, respectively. Let b_o be the impact parameter between test particle and field particle that would correspond to 90° deflection if the field particle were infinitely massive. Let t_c and t_d be the average time taken by the test particle to deflect through 90° by a single close encounter and by many small-angle encounters, respectively. Making use of Eq. (5.22) in Spitzer, we obtain

$$\frac{t_d}{t_c} = \frac{1}{8 \Psi \ln \Lambda}$$

where

$$\begin{aligned} \Lambda &= \lambda_D / b_o \\ \lambda_D^2 &= \epsilon k\, T_1 / q_1^2\, N_1 \\ t_c &= 1/\pi N_1\, v b_o^2 \\ b_o &= q\, q_1 / 4\pi\epsilon\, m v^2 \end{aligned} \tag{A.1}$$

Ψ is a function of the ratio of test particle speed to field particle thermal speed. When this ratio is large, $\Psi \rightarrow 1$. For ratios of order unity, Ψ is somewhat less than 1, so that esimates of deflection time based on $\Psi = 1$ form a lower bound on the actual value, and are therefore conservative.

In general, $t_d \ll t_c$, so that most particles are deflected from their collisionless trajectories by multiple small-angle encounters.

We assume that $\Psi = 1$, that $q_1 = q$, and that the test particle has the same energy as the average over field particles. We then have:

$$\frac{m}{2} v^2 = \frac{3}{2} k\, T_1 \tag{A.2}$$

$$b_o = q^2 / 12\pi\epsilon\, kT_1 = 1/12\pi N_1\, \lambda_D^2 \tag{A.3}$$

$$\Lambda = \lambda_D / b_o = 12\pi N_1 \lambda_D^3 = 12\pi/g \tag{A.4}$$

We define S_d as the distance travelled by the test particle while accumulating 90° deflection. We then obtain:

$$S_d = v t_d = \frac{1}{8\pi N_1\, b_o^2 \ln\Lambda} = \frac{18\pi\, \lambda_D}{g \ln\,(12\pi/g)} \tag{A.5}$$

We assume that the Vlasov solution will become invalid for probe diameters larger than the 90° deflection distance. We note that $S_d/2R_p$ is, in effect, a Knudsen number for each of the four scattering processes that we are discussing. The condition for validity of results obtained from the Vlasov equation is therefore:

$$R_p/\lambda_D \leq 9\pi / g \ln(12\pi/g) \tag{A.6}$$

This relation puts an upper limit on g. This limit becomes more severe as R_p/λ_D increases.

In order to study the fourth scattering case, that of a test ion being deflected by electron field particles, we make use of Eqs. (5.27) to (5.29) in Spitzer, to obtain the following expression for the rate of slowing down of the ion:

$$-\frac{v}{\dot{v}} = \frac{3\sqrt{\pi}m_-}{2m_+}\left(\frac{2kT_-}{m_-}\right)^{\frac{3}{2}}\left(\frac{2\pi\epsilon^2 m_+^2}{N_- q_+^2 q_-^2 \ln\Lambda}\right) = K \qquad (A.7)$$

K depends on v only through $\ln\Lambda$. ' ignore this dependence to obtain the following expression for the distance travelled by the ion before losing most of its forward velocity:

$$S_s = \int_{t=t_0}^{\infty} v dt = -\int_{v=v_0}^{0} K dv = Kv_0 \qquad (A.8)$$

We assume that the ion is initially moving at the mean ion thermal speed:

$$\frac{1}{2} m_+ v_0^2 = \frac{3}{2} kT_+ \qquad (A.9)$$

Substituting, and setting $q_+^2 = q_-^2$, we obtain:

$$S_s = (6\pi)^{\frac{3}{2}}\left(\frac{m_+ T_+}{m_- T_-}\right)^{\frac{1}{2}} \frac{\lambda_{D-}}{g_- \ln(\frac{12}{g_-}\frac{T_+}{T_-})} \qquad (A.10)$$

If $T_+ = T_-$, we obtain, from (A.5) and (A.10):

$$\frac{S_s}{S_d} = \left(\frac{2\pi}{3}\frac{m_+}{m_-}\right)^{\frac{1}{2}} \qquad (A.11)$$

For a hydrogen plasma, this ratio is 62; for an argon plasma it is 390. Therefore, unless the ratio T_+/T_- is extremely small, the ion-ion scattering distance S_d will always be smaller than the distance S_s

In C.G.S. units, we obtain, for the Debye length:

$$\lambda_D(\text{cm.}) = 6.90\sqrt{\frac{T(^\circ K)}{N(\text{cm.}^{-3})}} \qquad (A.12)$$

$$1/g = N\lambda_D^3 = 328\sqrt{\frac{(T(^\circ K))^3}{N(\text{cm.}^{-3})}} \qquad (A.13)$$

For any given R_p/λ_D, it is now possible to obtain a maximum allowable value of g from (A.6), and thence to obtain a maximum allowable number density for any given T, from (A.13). Table 1 gives a set of values of N_{max}. derived in this manner, for values of the ratio R_p/λ_D of 2.5, 10, and 100, and values of T of 10^3 and 2×10^4 °K.

It should be borne in mind that when the scattering of electrons in a plasma is being considered, N is the total number density $N_+ + N_-$, since, as has been shown, ions and electrons contribute equally to electron scattering. In this case it is also necessary to modify the definition of λ_r in Eq. (A.1) and hence the argument of the logarithmic term in subsequent expressions. This is because λ_D appears in the derivation of this expression as the effective penetration distance of the test particle electric field; the Debye length of the plasma as a whole is related to the ion and electron Debye lengths as follows:

$$\frac{1}{\lambda_D^2} = \frac{1}{\lambda_{D_+}^2} + \frac{1}{\lambda_{D_-}^2} \qquad (A.14)$$

If $T_+ = T_-$, the Debye length of the plasma as a whole is less than that for ions or electrons by the factor $\sqrt{2}$; if $T_+ \ll T_-$, the plasma Debye length is approximately equal to that of the ions.

Finally, it should be remembered that the criteria developed here are useful only for a qualitative estimate of the safety of using the results of the Vlasov solution in any given situation. To obtain a quantitative value of the error made by using the collisionless theory would require a solution of the more general problem including the effects of collisions.

APPENDIX B

Discussion of the Collisionless Boltzmann Equation

It can be shown that the Liouville equation (Ref. 11) that describes the statistical behaviour of a physical system is valid only when the system is described in terms of position coordinates r_i and momentum coordinates p_i which are canonical; that is, r_i and p_i satisfy Hamilton's equations:

$$\frac{\partial H}{\partial p_i} = \dot{r}_i \qquad \frac{\partial H}{\partial r_i} = -\dot{p}_i \tag{B.1}$$

H is a function of the r_i & p_i which can usually be identified with the energy of the system. The total number of position and momentum coordinates r_i and p_i is equal to the number of degrees of freedom of the system. For example, if the system consists of n interacting particles and each of these is free to move in three dimensions, then the values of 6n coordinates must be specified to determine completely the state of the system. In rectangular coordinates, the 3n position coordinates r_i then become $x_1, y_1, z_1, x_2, y_2, z_2, \ldots x_n, y_n, z_n$. In this case $p_i = mv_i = m\dot{r}_i$ and the p_i become $m\dot{x}_1, m\dot{x}_2, \ldots m\dot{z}_n$.

In the collisionless limit, the motion of each charged particle becomes independent of the individual positions of all the others and depends only on the macroscopic overall field resulting from their collective charge density (Sec. III). The Liouville equation that describes the motion of that particle then becomes independent of the coordinates of all others; in fact, it reduces to a form identical with the collisionless Boltzmann equation (4.1a or b). This fact, namely that the collisionless Boltzmann equation is in reality a one-particle form of the Liouville equation, is pointed out here in order to make clear that it is subject to the same restrictions, namely that it is only true when expressed in canonical coordinates. The Boltzmann equation is very often derived from elementary considerations rather than as a special case of the Liouville equation, and this restriction then does not appear explicitly. Such derivations are usually carried out in rectangular coordinates, in which case the position coordinates r_i, expressed in vector form, become $\underline{r} = (x,y,z)$, and the velocity coordinates v_i can be written as $\underline{v} = \dot{\underline{r}} = (v_x, v_y, v_z)$. The momentum coordinates p_i canonical to r_i are then expressible as $\underline{p} = (mv_x, mv_y, mv_z)$. It is then customary to write $\underline{p} = m\underline{v}$. If this vector relation is substituted into the collisionless Boltzmann equation (4.1a or b) the result is the form commonly seen, for instance in Ref. 5, as follows:

$$\frac{Df}{Dt} = \frac{\partial f}{\partial \underline{r}}\cdot\underline{v} + \frac{\partial f}{\partial \underline{v}}\cdot\frac{\underline{F}}{m} = 0 \tag{B.2}$$

However, the relation $\underline{p} = m\underline{v}$ itself is a formally incorrect statement, since the use of vector notation implies that this relation is true independently of its expression in a particular coordinate system; this is not the case if $\underline{p}$ is to fit the definition of Eqs. (B.1). For example, in cylindrical coordinates, where $\underline{r} = (r,\theta,z)$ and $\underline{v} = (v_r, v_\theta, v_z) = (\dot{r}, r\dot{\theta}, \dot{z})$, the momentum canonically conjugate to $\underline{r}$ by Eqs. (B.1) is $\underline{p} = (m\dot{r}, mr^2\dot{\theta}, m\dot{z})$; this expression is not equal to $m\underline{v}$ because the momentum p_θ canonical to the coordinate θ is the angular momentum $mr^2\dot{\theta}$ rather than the linear momentum $mr\dot{\theta}$. This warning is mentioned here because the Boltzmann equation is most often written in the form of Eq. (B.2) rather than that of Eqs. (4.1) and may therefore be a potential source of confusion. The fact that Eq. (B.2) can give incorrect results may be verified by substituting into Eqs. (4.1) and (B.2) the expressions for $\underline{r}$,$\underline{v}$ and $\underline{p}$ in cylindrical coordinates, and then solving these equations by standard methods to find the corresponding loci of constant value of f, i.e. particle trajectories. Examination of these resulting trajectories for the case of a central force field will indicate that those obtained from Eq. (B.2) do not show conservation of angular momentum as required. A similar situation holds for spherical coordinates. This anomaly was found during the early stages of this investigation when an attempt was made to use Eq. (B.2) to obtain explicit trajectory equations.

A related problem is the precise definition of the distribution function f which appears in both Eqs. (4.1) and (B.2) as well as in Sections VII and X. Since Eq. (4.1) is expressed in terms of canonical coordinates r_i and p_i, the distribution function f referred to in this equation must be a density in the space defined by these same coordinates. In other words, if $\tilde{N}$ is now the total number of particles in a 6-dimensional volume element in this space, whereas N has been defined as number density in physical space, then the definition of f is $f = d^6\tilde{N}/d^3\underline{r}d^3\underline{p} = d^3N/d^3\underline{p}$. However, both of the distribution functions given by Eqs. (7.12) and (7.13), for instance, are of the form implied by their appearance in Eq. (7.1) and therefore are given in terms of position-velocity rather than position-momentum space. In other words, f in these equations has the definition $f = d^6\tilde{N}/d^3\underline{r}d^3\underline{v} = d^3N/d^3\underline{v}$. This is in spite of the fact that f appears in these equations as a function of energy E. By way of further illustration, the density in (E,J^2) space (in spherical coordinates) i.e. $d^2N/dEdJ^2$, is given by a different expression, namely the integrand of Eq. (7.5), which is the quantity $\pi f(E,J)\ \partial(v_r,v_t^2)/\partial(E,J^2)$.

APPENDIX C

Behaviour of the Iterative Solution Method

We first examine Poisson's equation in its nondimensional form, Eqs. (9.6) or (11.3). We imagine that we have a net charge density $\eta_{net}(x)$ that differs from the solution of the problem by a small positive increment over a certain range of x. Because of the negative sign in the Poisson equation, the resulting effect will be to depress the second derivative of χ by a small increment over this range. This increment will be proportional to γ, the square of ratio of probe radius to the reference Debye length. Since we have a two-point boundary value problem involving a constraint on potential at either end of the range of x, a rise in potential will be produced over the entire range, with the maximum rise tending to occur near the region where the charge increment has been imposed. If the distribution of charged particles in position space is now calculated, and the result is compared to that for the true solution, there will be fewer ions but more electrons in this region. The result will be a net charge density that now differs from the true solution by a negative rather than a positive increment.

The magnitude of this increment will increase if either γ is increased or the range of x between end points is increased. If the process is repeated, the increment again changes sign. The result of repeating this process is therefore a sequence of functions $\eta_{net}(x)$ which oscillates about the true solution. If γ or the range of x is sufficiently large, the oscillations will diverge and must be damped by mixing the N'th and N + 1'th iterates at each step.

APPENDIX D

Integration of the Poisson Equation

From Eq. (9.6), the Poisson equation for the spherical probe is:

$$\frac{d^2\chi}{dx^2} = -\frac{\gamma\,\eta_{net}}{x^4} \tag{D.1}$$

We introduce a new radial variable s(x) which is zero at the probe surface (x = 1) and which increases as radius increases (x decreases). We arrange the radial dependence of s so that s is a steeply rising function near the probe surface and a less steeply rising function farther out. This is done in order to define a suitable computation net; points in this net will be placed at equal increments in s. Varying the form of s(x) allows us to place points in this net densely within the sheath region and sparsely outside it. The specific forms of s(x) that have been used in the computations are contained in the listing of Program 1 in Appendix I. We assume that dx/ds can be explicitly calculated everywhere. We then have:

$$\frac{ds}{dx}\frac{d}{ds}\left(\frac{d\chi}{ds}\frac{ds}{dx}\right) = -\frac{\gamma\,\eta_{net}(s)}{x^4(s)} = K_0(s) \tag{D.2}$$

$$\frac{d\chi}{ds} = \frac{dx}{ds}\left(\frac{d\chi}{ds}\frac{ds}{dx}\right)_{s=0} + \frac{dx}{ds}\int_0^s K_0(s')\,\frac{dx'}{ds'}\,ds' \tag{D.3}$$

Let:

$$K_1(s) = \frac{dx}{ds}\int_0^s K_0(s')\,\frac{dx'}{ds'}\,ds' \tag{D.4}$$

Integrating a second time, and noting that the bracketed quantity in Eq. (D.3) is equal to $(d\chi/dx)_{s=0}$, we obtain:

$$\chi(s) = \chi(0) + \left(\frac{d\chi}{dx}\right)_{s=0}(x(s) - x(0)) + \int_0^s K_1(s')ds' \tag{D.5}$$

Let:

$$K_2(s) = \chi(0) + \int_0^s K_1(s')\,ds' \tag{D.6}$$

Then:

$$\chi(s) = \left(\frac{d\chi}{dx}\right)_{s=0}(x(s)-1) + K_2(s) \tag{D.7}$$

From (D.3), we obtain:

$$\frac{d\chi}{dx}(s) = \left(\frac{d\chi}{dx}\right)_{s=0} + \frac{K_1(s)}{\frac{dx}{ds}(s)} \tag{D.8}$$

Equations (D.7) and (D.8) are now used together with appropriate boundary conditions at the outer edge of the computation net, to solve for $(d\chi/dx)_{s=0}$. Equations (8.9), expressed in non-dimensional form in terms of x, give in the spherical case the following boundary condition at $x = x_B$:

$$\left(\frac{d\chi}{dx}\right)_B = \frac{2\chi_B}{x_B} \qquad (D.9)$$

By setting $s = s_B$ in (D.7) and (D.8), and substituting the resulting two equations in (D.9), we obtain:

$$\left(\frac{d\chi}{dx}\right)_{s=0} = \frac{2K_2(s_B) - x_B K_1(s_B)\left(\frac{dx}{ds}\right)_B}{2 - x_B} \qquad (D.10)$$

This value of $(d\chi/dx)_{s=0}$ may now be substituted into (D.7) and (D.8) to compute χ , $d\chi/dx$, and thereby $d\chi/ds$, as functions of s. The quantities χ and $d\chi/ds$ are used in the subsequent calculation of charge densities as outlined in Appendix E.

In solving the boundary-value problem concerned with zero-temperature repelled particles (Sec. XII), the outer boundary of the computation net becomes the sheath edge, so that the required boundary condition becomes $\chi_B = 0$, Setting the left side of Eq. (D.7) equal to zero gives:

$$\left(\frac{d\chi}{dx}\right)_{s=0} = \frac{K_2(s_B)}{1 - x_B} \qquad (D.11)$$

In this case we choose a function $s(x)$ which places points densely near the sheath edge and less densely closer to the probe. The function actually used is indicated in the listing of Program 2 in Appendix I.

A similar procedure can be derived in the cylindrical case. Here the Poisson equation (11.3) becomes

$$\frac{d}{dx}\left(x\frac{d\chi}{dx}\right) = -\frac{\gamma\, \eta_{net}(s)}{x^3\,(s)} = K_o(s) \qquad (D.12)$$

Proceeding as before, we obtain:

$$\frac{d\chi}{ds} = \frac{1}{x}\,\frac{dx}{ds}\left(\frac{d\chi}{dx}\right)_{s=0} + \frac{1}{x}\,\frac{dx}{ds}\int_0^s K_o(s')\,\frac{dx'}{ds'}\,ds' \qquad (D.13)$$

We define:

$$K_1(s) = \frac{1}{x}\frac{dx}{ds}\int_0^s K_o(s')\,\frac{dx'}{ds'}\,ds' \qquad (D.14)$$

We integrate again, and use the definition of $K_2(s)$ in Eq. (D.6) to obtain:

$$\chi(s) = \left(\frac{d\chi}{dx}\right)_{s=0} \ln\ x(s) + K_2(s) \tag{D.15}$$

From (D.13), we obtain:

$$\frac{d\chi}{dx}(s) = \frac{\left(\frac{d\chi}{dx}\right)_{s=0}}{x(s)} + \frac{K_1(s)}{\frac{dx}{ds}(s)} \tag{D.16}$$

Using (8.9b), we obtain:

$$\left(\frac{d\chi}{dx}\right)_B = \frac{\chi_B}{x_B} \tag{D.17}$$

We proceed as in the spherical case and set $s = s_B$ in (D.15) and (D.16), then substitute in (D.17) to obtain:

$$\left(\frac{d\chi}{dx}\right)_{s=0} = \frac{K_2(s_B) - x_B\ K_1\ (s_B)/\left(\frac{dx}{ds}\right)_B}{1 - \ln x_B} \tag{D.18}$$

If we again use the boundary condition $\chi_B = 0$, we obtain:

$$\left(\frac{d\chi}{dx}\right)_{s=0} = - \frac{K_2\ (s_B)}{\ln\ x_B} \tag{D.19}$$

The numerical integrations required in calculations of the functions $K_1(s)$ and $K_2(s)$ involve integrands that are specified at n discrete values of s separated by equal intervals Δs. It is necessary to compute values of these functions corresponding to the same n values of s. If we let $y_i = y(s_i)$ represent the given integrand and $Y_i = Y(s_i)$ represent the required result for i = 1, 2, ... n, we then have:

$$Y_i = Y_{i-1} + \int_{s_{i-1}}^{s_i} y(s)\ ds \tag{D.20}$$

This integration process is approximated as follows: we pass a parabolic arc through the points y_1, y_2, and y_3 to find $Y_2 - Y_1$; a cubic arc through y_{i-2} to y_{i+1} to find $Y_i - Y_{i-1}$ for i = 3,4,...n-1, and another parabolic arc through y_{n-2}, y_{n-1}, and y_n to find $Y_n - Y_{n-1}$. The resulting formulae are:

$$Y_2 = Y_1 + (5y_1 + 8y_2 - y_3)\ \Delta s/12$$

$$Y_i = Y_{i-1} + (13\ (y_{i-1} + y_i) - y_{i-2} - y_{i+1})\ \Delta s/24;\ i=3,4,\ldots n-1$$

$$Y_n = Y_{n-1} + (5y_n + 8y_{n-1} - y_{n-2})\ \Delta s/12 \tag{D.21}$$

If we set $Y_1 = 0$ and sum expressions (D.21), we obtain the following approximation formulae for Y_n, for various values of n:

$$
\begin{aligned}
Y_3 &= (y_1 + 4y_2 + y_3)\ \Delta s/3 \\
Y_4 &= (3y_1 + 9y_2 + 9y_3 + 3y_4)\ \Delta s/8 \\
Y_5 &= (9y_1 + 28y_2 + 22y_3 + 28y_4 + 9y_5)\ \Delta s/24 \\
Y_6 &= (9y_1 + 28y_2 + 23y_3 + 23y_4 + 28y_5 + 9y_6)\ \Delta s/24 \\
Y_n &= (9y_1 + 28y_2 + 23y_3 + 24(y_4 + y_5 + \dots y_{n-3}) \\
&\quad + 23y_{n-2} + 28y_{n-1} + 9y_n)\ \Delta s/24;\ n > 6
\end{aligned}
\tag{D.22}
$$

These formulae have been used in evaluating the integrals (E.33), (E.36), (E.88), and (E.91). The major advantage of these expressions, in comparison with many other numerical integration formulae, is that they weigh equally all of the interior points $y_4 \dots y_{n-3}$. This feature is of particular importance in evaluating (E.33) and (E.88). These functions are evaluated successively, many times during each iteration of the computing program, for values of s differing by Δs, and with integrands $y(s,s')$ that are integrated over s' and change in a continuous manner from each value of s to the next. In many cases $y(s,s')$ is a rapidly varying function of s and s', and it was found that application of a standard numerical procedure having unequal weighting factors tended to cause unacceptable scatter in calculations of charge densities.

Another advantage of expressions (D.22) is that they do not restrict the integer n to multiples of other integers.

APPENDIX E

Expressions for Charge Density and Collected Current in the Case of a Maxwellian Velocity Distribution

We substitute expressions (9.11) to (9.14) and (12.2) for $\Omega_n(\beta)$, together with expressions (9.2) and (11.5) for the Maxwellian velocity distribution, into the charge density expressions (9.5) and (11.2) and the current collection expressions (9.9) and (11.4). By referring to Figs. 3, 5, 6, 8 and 10, we then define a set of integrals in terms of which charge density and collected current may be calculated.

For the sphere, we substitute Eqs. (9.13), (9.12), (12.2), (9.14) and (9.11), in that order, together with Eq. (9.2), into Eq. (9.5), to define the following integrals:

$$\eta_{1,s}(A) = - \frac{1}{\sqrt{\pi}} \int_A^\infty d\beta \; e^{-\beta} \; (\beta - \chi)^{\frac{1}{2}} \qquad (E.1)$$

where $A \geq \chi$. We note that the value of this integral depends on χ as well as on A although for conciseness in later expressions this dependence on χ is not indicated explicitly. The subscript s is defined as referring to the spherical probe; the subscript c will be used to refer to the cylindrical probe. It is important to note here that the subscript s does not correspond in any way with the radial net coordinate s, which has been used in Appendix D and is used again in this Appendix, beginning with Eq. (E.28).

$$\eta_{2,s}(A) = - \frac{1}{\sqrt{\pi}} \int_A^\infty d\beta \; e^{-\beta} \left\{ \beta - \chi - x^2 (\beta - \chi_p) \right\}^{\frac{1}{2}} \qquad (E.2)$$

where:

$$A \geq \kappa$$

and:

$$\kappa = \frac{\chi - x^2 \chi_p}{1 - x^2} \qquad (E.3)$$

κ is the value of β at which the lines $\beta = \chi_p + \Omega$ and $\beta = \chi + \Omega x^2$ intersect (Fig. 1b)

$$\eta_{3,s}(A) = - \frac{1}{\sqrt{\pi}} \int_A^{\beta_B} d\beta \quad e^{-\beta} \qquad \left\{ \beta - \chi - \beta \frac{x^2}{x_B^2} \right\}^{\frac{1}{2}} \qquad (E.4)$$

where: $0 \leq A \leq \beta_B$; β_B is the value of β at which the lines $\beta = \chi + \Omega x^2$ and $\beta = \Omega x_B^2$ intersect (point B in Fig. 10a); we obtain:

$$\beta_B = - \frac{\chi}{x^2/x_B^2 - 1} \qquad (E.5)$$

$$\eta_{4,s}(\beta_1, \beta_2) = - \frac{1}{\sqrt{\pi}} \int_{\beta_1}^{\beta_2} d\beta \; e^{-\beta} \left\{\beta - \chi - \Omega_G(\beta)\; x^2 \right\}^{\frac{1}{2}} \qquad (E.6)$$

Finally:

$$\eta_{5,s} = 0$$

We also substitute Eqs. (9.12), (12.2) and (9.14) into Eq. (9.9) to define integrals for expressing current collection:

$$i_{1,s}(A) = \int_A^\infty d\beta \; e^{-\beta} \; (\beta - \chi_p) \qquad (E.7)$$

where:

$$A \geq 0$$

$$i_{2,s}(A) = \int_0^A d\beta \; e^{-\beta} \; \frac{\beta}{x_B^2} \qquad (E.8)$$

where

$$0 \leq A \leq \beta_B$$

$$i_{3,s}(\beta_1,\beta_2) = \int_{\beta_1}^{\beta_2} d\beta \; e^{-\beta} \; \Omega_G(\beta) \qquad (E.9)$$

For the cylinder, substitution of Eqs. (9.13), (9.12), (12.2), (9.14) and (9.11), respectively, together with Eq. (11.5), into Eq. (11.2), allows us to define the following integrals for the expression of charge density:

$$\eta_{1,c} = 0$$

$$\eta_{2,c}(A) = \frac{1}{\pi} \int_A^\infty d\beta \; e^{-\beta} \; \text{arc sin} \left\{ \frac{x^2(\beta - \chi_p)}{\beta - \chi} \right\}^{\frac{1}{2}} \qquad (E.10)$$

where, once again, we require $A \geq \kappa$.

$$\eta_{3,c}(A) = \frac{1}{\pi} \int_A^{\beta_B} d\beta \quad e^{-\beta} \; \text{arc sin} \left\{ \frac{x^2}{x_B^2} \; \frac{\beta}{\beta - \chi} \right\}^{\frac{1}{2}} \qquad (E.11)$$

where, once again, we require $0 \leq A \leq \beta_B$.

$$\eta_{4,c}(\beta_1,\beta_2) = \frac{1}{\pi} \int_{\beta_1}^{\beta_2} d\beta \; e^{-\beta} \; \text{arc sin} \left\{ \frac{\Omega_G(\beta)\; x^2}{\beta - \chi} \right\}^{\frac{1}{2}} \qquad (E.12)$$

$$\eta_{5,c}(A) = \frac{1}{2}\int_A^{\infty} d\beta\ e^{-\beta} = \frac{e^{-A}}{2} \tag{E.13}$$

We also substitute Eqs. (9.12), (12.2) and (9.14), together with Eq. (11.5), into Eq. (11.4) to define integrals with which to express the current collection for the cylinder. We obtain:

$$i_{1,c}(A) = \frac{2}{\sqrt{\pi}}\int_A^{\infty} d\beta\ e^{-\beta}\ (\beta - \chi_p)^{\frac{1}{2}} \tag{E.14}$$

where:

$$A \geq 0$$

$$i_{2,c}(A) = \frac{2}{\sqrt{\pi}}\int_0^{A} d\beta\ e^{-\beta}\ \left(\frac{\beta}{x_B^2}\right)^{\frac{1}{2}} \tag{E.15}$$

where:

$$0 \leq A \leq \beta_B$$

$$i_{3,c}(\beta_1,\beta_2) = \frac{2}{\sqrt{\pi}}\int_{\beta_1}^{\beta_2} d\beta\ e^{-\beta}\ (\Omega_G(\beta)\ )^{\frac{1}{2}} \tag{E.16}$$

We define η_n and i_n as representing either $\eta_{n,s}$ and $i_{n,s}$ for the sphere or $\eta_{n,c}$ and $i_{n,c}$ for the cylinder. We are then able to express the charge density and collected current for either species of particle in terms of η_n and i_n.

For example, if the (Ω,β) plane has the appearance shown in Fig. 3a, we have:

$$\begin{aligned} \eta &= 2\ \eta_5(0) - \eta_2(0) - \eta_1(0) \\ i &= i_1(0) \end{aligned} \tag{E.17}$$

This situation corresponds to that of Fig. 8, case 5, in the eventthat the portions of the locus of extrema shown dotted in this diagram are not present.

If the (Ω,β) plane has the appearance shown in Fig. 3b, we then have:

$$\begin{aligned} \eta &= 2\ \eta_5(\chi) - 2\ \eta_1(\chi) + \eta_1(\chi_p) - \eta_2(\chi_p) \\ i &= i_1(\chi_p) \end{aligned} \tag{E.18}$$

This situation corresponds to that of Fig. 8, case 6, with the same qualification as above.

If the (Ω,β) plane has the appearance of Fig. 5b, we have:

$$\eta = 2\,\eta_5(\beta_E) + 2\,\eta_4(\beta_H,\beta_E) - \eta_2(\beta_H) + \eta_4(0,\beta_H) - \eta_1(0)$$
$$i = i_3(0,\beta_H) + i_1(\beta_H) \tag{E.19}$$

If the (Ω,β) plane has the appearance of Fig. 10b, we obtain:

$$\eta = 2\,\eta_5(\beta_B) + \eta_3(0) + \eta_3(\beta_C) - \eta_4(\beta_C,\beta_H) - \eta_2(\beta_H) - \eta_1(0)$$
$$i = i_2(\beta_C) + i_3(\beta_C,\beta_H) + i_1(\beta_H) \tag{E.20}$$

Numerous other combinations of these functions are produced by the various forms of locus of extrema shown in Fig. 8.

We now carry out the integrations indicated in the expressions for η_n and i_n.

We define the function $g(x)$ in terms of the well-known error integral $\mathrm{erf}(x)$ by the following equation:

$$g(x) = \frac{\sqrt{\pi}}{2}\, e^{x^2}\left(1 - \mathrm{erf}(x)\right) \tag{E.21}$$

where:

$$\mathrm{erf}(x) = \frac{2}{\sqrt{\pi}}\int_0^x e^{-t^2}\,dt$$

For large x, the following asymptotic expansion (Ref. 16) is useful:

$$\mathrm{erf}(x) \simeq 1 - \frac{e^{-x^2}}{x\sqrt{\pi}}\left(1 - \frac{1}{2x^2} + \frac{1.3}{(2x^2)^2} - \frac{1.3.5}{(2x^2)^3} + \ldots\right) \tag{E.22}$$

We now integrate (E.1) to obtain:

$$\eta_{1,s}(A) = -\frac{e^{-A}}{\sqrt{\pi}}\left(\sqrt{A-\chi} + g\left(\sqrt{A-\chi}\right)\right) \tag{E.23}$$

If $A = \chi$, we note that $g(0) = \sqrt{\pi}/2$ to obtain:

$$\eta_{1,s}(\chi) = -\frac{e^{-\chi}}{2} \tag{E.24}$$

Integrating (E.2), we obtain:

$$\eta_{2,s}(A) = -\sqrt{1-x^2}\,\frac{e^{-A}}{\sqrt{\pi}}\left(\sqrt{A-\kappa} + g\left(\sqrt{A-\kappa}\right)\right) \tag{E.25}$$

In order to integrate (E.4), we note that it can be transformed to:

$$\eta_{3,s}(A) = -\left(\frac{x^2/x_B^2 - 1}{\pi}\right)^{\frac{1}{2}} \int_A^{\beta_B} d\beta\, e^{-\beta} \sqrt{\beta_B - \beta} \tag{E.26}$$

Integrating by parts, we obtain:

$$\eta_{3,s}(A) = -\left(\frac{x^2/x_B^2 - 1}{\pi}\right)^{\frac{1}{2}} \left\{ \sqrt{\beta_B - A}\; e^{-A} - e^{-\beta_B} \int_0^{\sqrt{\beta_B - A}} e^{t^2}\, dt \right\} \tag{E.27}$$

Equation (E.6) must be integrated numerically, since $\Omega_G(\beta)$ is generated in tabular form by the numerical solution scheme. In order to carry out this integration, we make use of the radial variable s defined in Appendix D, and we note that the functional dependence $\Omega = \Omega_G(\beta)$ can be expressed parametrically as $\Omega = \Omega_G(s)$, $\beta = \beta_G(s)$. Equation (E.6) then becomes:

$$\eta_{4,s}(\beta_1,\beta_2) =$$

$$-\frac{1}{\sqrt{\pi}} \int_{s'=s_1}^{s'=s_2} ds' \, \frac{d\beta_G(s')}{ds'}\, e^{-\beta_G(s')} \left\{\beta_G(s') - \chi(s) - \Omega_G(s')\, x^2(s)\right\}^{\frac{1}{2}} \tag{E.28}$$

Making use of Eq. (9.8b), we define:

$$\alpha_G(s') = \frac{d\beta_G(s')}{ds'} = \left(\frac{1}{2}\frac{d\chi}{dx'} - \frac{x'}{2}\frac{d^2\chi}{dx'^2}\right)\frac{dx'}{ds} \tag{E.29}$$

Substituting Eq. (9.6), we obtain:

$$\alpha_G(s') = \frac{1}{2}\frac{d\chi}{ds'} + \frac{\gamma\eta_{net}(s')}{2\,x'^3}\,\frac{dx'}{ds'} \tag{E.30}$$

We also define:

$$\epsilon_G(s') = \alpha_G(s')\, e^{-\beta_G(s')} \tag{E.31}$$

$$\Psi_G(s,s') = \left\{\beta_G(s') - \chi(s) - \Omega_G(s')\, x^2(s)\right\}^{\frac{1}{2}} \tag{E.32}$$

(E.28) becomes:

$$\eta_{4,s}(\beta(s_1),\beta(s_2)) = -\frac{1}{\sqrt{\pi}} \int_{s'=s_1}^{s'=s_2} ds' \; \epsilon_G(s')\, \Psi_G(s,s') \tag{E.33}$$

This integral is now in a form suitable for numerical evaluation; the integrand has been reduced to a function of potential and its first two radial derivatives, enabling the integration to be carried out over the computation net in position space. The form of this integral means that the value of the density contribution $\eta_{4,s}$ at the position s depends on the form of the potential at every value of the radial coordinate s' between the locations s_1 and s_2, and not on conditions at s only.

This means that the overall problem is "global" rather than "local" in nature and cannot be reduced to an ordinary differential equation as long as the distribution function (which is contained in the expression for ϵ_G) is poly-energetic in form. This fact substantiates the statement made to this effect in Sec. V.

Equations (E.7) and (E.8) may be integrated to give:

$$i_{1,s}(A) = (A - \chi_p + 1)\, e^{-A} \tag{E.34}$$

$$i_{2,s}(A) = \frac{1}{x_B^{\,2}} \left(1 - (A + 1)\, e^{-A}\right) \tag{E.35}$$

(E.9) may be integrated in the same manner as (E.6) to yield:

$$i_{3,s}(\beta(s_1),\beta(s_2)) = \int_{s'=s_1}^{s'=s_2} ds'\ \epsilon_G(s')\ \Omega_G(s') \tag{E.36}$$

Equations (E.23) to (E.36) define all of the functions necessary to compute η and i for a spherical probe. As examples of their use, we substitute them in (E.17) and (E.18) to obtain expressions for η and i for the attracted and repelled species, respectively, in the cases where the locus of extrema does not enter the first quadrant of the (Ω,β) plane. We note once again that this condition is satisfied for the repelled species if the potential is a monotonically decreasing function of radius; this is usually the case. It is satisfied for the attracted species if the decay of potential with radius is nowhere steeper than that for an inverse square potential.

In the spherical case, the unshielded potential varies as the inverse of radius, whereas the asymptotic form of the shielded potential is an inverse square of radius (Sec. XIII). In the cylindrical case, the unshielded potential is logarithmic in radius, and the asymptotic shielded potential varies inversely with radius. In both cases, the effect of space charge on potential will be small out to a distance of many probe radii in the limit $R_p/\lambda_D \ll 1$. When this effect is present, it tends to steepen the potential gradient; for sufficiently large R_p/λ_D, there will exist regions steeper than an inverse square, and expressions (E.17) will not give correct values for η and i. It is not clear a priori whether these expressions are correct for a finite range of R_p/λ_D or only in the limit as $R_p/\lambda_D \to 0$. The former situation appears more likely in the cylindrical case than the spherical, because in the cylindrical case the potential tends to have a shallower form than for the sphere. The computed results (Sections XV and XVI) verify this expectation .

We first use (E.18a) to calculate η for a repelling probe ($\chi_p > 0$). Substituting (E.23), (E.24) and (E.25), we obtain:

$$\eta = e^{-\chi} - \frac{e^{-\chi_p}}{\sqrt{\pi}} \left(\sqrt{\chi_p - \chi} + g\left(\sqrt{\chi_p - \chi}\right)\right) + \sqrt{1-x^2}\ \frac{e^{-\chi_p}}{\sqrt{\pi}} \left(\sqrt{\chi_p - \kappa} + g\left(\sqrt{\chi_p - \kappa}\right)\right) \tag{E.37}$$

From(E.3) we note that:

$$(\chi_p - \kappa)\,(1 - x^2) = \chi_p - \chi \tag{E.38}$$

(E.37) becomes:

$$\eta = e^{-\chi} - \frac{e^{-\chi_p}}{\sqrt{\pi}} \left\{ g(\sqrt{\chi_p - \chi}) - \sqrt{1 - x^2}\; g\left(\sqrt{\frac{\chi_p - \chi}{1 - x^2}}\right) \right\} \tag{E.39}$$

If χ_p becomes large, this expression reduces to the familiar "Boltzmann factor" or thermodynamic equilibrium distribution. At the probe surface, $x \to 1$ and $\chi \to \chi_p$. We obtain:

$$\eta_p = \frac{e^{-\chi_p}}{2} \tag{E.40}$$

This expression corresponds to a distribution function which is zero for outward-moving particles and Maxwellian for inward-moving particles, as expected for the repelled species at the probe surface. We note that at sufficiently small probe potentials, the difference between this result and the Boltzmann factor becomes too large to be ignored. Lam (Ref. 7) has used an expression of the same form as (E.40) to derive a quasi-neutral solution which gives an approximate relation between current and probe potential when the latter is small enough that no sheath forms near the probe.

Far from the probe, $x \to 0$ and we again obtain from (E.39) the Boltzmann factor as a limit. In the field-free case, $\chi_p = \chi = 0$, we obtain the geometrical depletion factor due solely to the solid angle subtended by the probe at any radius:

$$\eta = \frac{1 + \sqrt{1 - x^2}}{2} \tag{E.41}$$

We next substitute (E.23) and (E.25) into (E.17a) to obtain the shallow-potential form of η for an attracting probe ($\chi_p < 0$) as follows:

$$\eta = \sqrt{\frac{1 - x^2}{\pi}} \left\{ \sqrt{-\kappa} + g(\sqrt{-\kappa}) \right\} + \frac{1}{\sqrt{\pi}} \left\{ \sqrt{-\chi} + g(\sqrt{-\chi}) \right\} \tag{E.42}$$

The requirement $\kappa \leq 0$ implies $\chi/\chi_p \geq x^2$. This condition is satisfied in the shallow-potential case.

If we again set $\chi_p = \chi = 0$, we recover the form (E.41).

We now substitute Eq. (E.34) into Eqs. (E.17b) and (E.18b) to obtain the currents collected by the probe when current collection is orbital-motion-limited (Sec. VIII). Substituting, we obtain the well-known results:

$$i = 1 - \chi_p \quad ; \quad \chi_p \leq 0$$
$$i = e^{-\chi_p} \quad ; \quad \chi_p \geq 0 \tag{E.43}$$

The cases of most interest and difficulty are those which depart from the above forms of η and i, and for which η and i must be calculated by one of a variety of expressions of which (E.19) is an example.

Functions analogous to those in Eqs. (E.23) to (E.36) are now developed for the cylindrical probe. In general, these expressions are considerably more complicated than those for the sphere.

We integrate Eq. (E.10) by parts to obtain:

$$\eta_{2,c}(A) = \frac{e^{-A}}{\pi} \arctan\left\{\frac{x^2}{1-x^2}\,\frac{A-\chi_p}{A-\kappa}\right\}^{\frac{1}{2}} + \frac{x}{\sqrt{1-x^2}}\,\frac{\chi_p-\chi}{2\pi}\int_A^{\infty} \frac{d\beta\, e^{-\beta}}{(\beta-\chi)(\beta-\chi_p)^{\frac{1}{2}}(\beta-\kappa)^{\frac{1}{2}}} \tag{E.44}$$

It is necessary to distinguish two cases: A is greater than either χ_p or κ , which usually occurs in the calculation of η for attracted particles, and $A = \chi_p$, which occurs for repelled particles.

We observe that the integrand in (E.44) has branch points at χ_p and κ on the β axis, and a simple pole at χ , which always lies between χ_p and κ . For the repelling probe, we usually have $\kappa < \chi_p$. For the attracting probe, this situation may be reversed. Since the range of integration never includes any of the interval between the two branch points, the pole $\beta = \chi$ is always outside the range of integration.

We replace the variable of integration β in (E.44) by a new coordinate which is so defined that the two branch points are located symmetrically about the origin. In order to do this, we define:

$$\begin{aligned} \tau &= (\kappa + \chi_p)/2 \\ \xi &= \beta - \tau \\ \mu &= \max(\kappa, \chi_p) - \tau \\ \theta &= \chi - \tau \\ B &= A - \tau \end{aligned} \tag{E.45}$$

We define the integral in Eq. (E.44) as H_1 and substitute (E.45) to obtain:

$$H_1(B,\infty) = e^{-\tau}\int_B^{\infty} \frac{e^{-\xi}\, d\xi}{(\xi - \theta)\,(\xi^2 - \mu^2)^{\frac{1}{2}}} \tag{E.46}$$

where: $B \geq \mu$ and $-\mu < \theta < \mu$; $B = \mu$ corresponds to the situation $A = \chi_p$.

In the situation $B > \mu$ we may expand the denominator of Eq. (E.46) as follows:

$$\left(1 - \frac{\theta}{\xi}\right)^{-1} = \left(1 + \frac{\theta}{\xi}\right) \sum_{j=0}^{\infty} \left(\frac{\theta}{\xi}\right)^{2j} \tag{E.47}$$

$$\left(1 - \frac{\mu^2}{\xi^2}\right)^{-\frac{1}{2}} = 1 + \sum_{i=0}^{\infty} \left(\frac{\mu}{\xi}\right)^{2i} \frac{1.3.5....2i-1}{2.4.6....2i} \tag{E.48}$$

$$\left(1 - \frac{\theta}{\xi}\right)^{-1}\left(1 - \frac{\mu^2}{\xi^2}\right)^{-\frac{1}{2}} = \left(1 + \frac{\theta}{\xi}\right)\sum_{k=0}^{\infty} \frac{P_k}{\xi^{2k}} \tag{E.49}$$

where:

$$P_0 = 1$$

$$P_k = \theta^{2k}\sum_{i=0}^{k} \left(\frac{\mu}{\theta}\right)^{2i} \frac{1.3.5....2i-1}{2.4.6....2i} \; ; \quad k > 0$$

Substituting:

$$H_1(B,\infty) = e^{-(\tau+B)}\sum_{m=2}^{\infty} T_m F_m(B) \tag{E.50}$$

where:

$$T_2 = 1$$

$$T_3 = \theta$$

$$T_{2k} = P_{k-1}$$

$$T_{2k+1} = P_{k-1} \cdot \theta$$

and:

$$F_m(B) = e^B \int_B^{\infty} \frac{e^{-\xi} d\xi}{\xi^m} \tag{E.51}$$

By integrating Eq. (E.51) by parts, we derive the following recursion formula for $m > 1$:

$$F_m(B) = \frac{1}{m-1}\left(\frac{1}{B^{m-1}} - F_{m-1}(B) \right) \tag{E.52}$$

$F_1(B)e^{-B}$ is a well-known transcendental function called the exponential integral of B, or Ei(B) (Ref. 16). From this reference, we have, for $B < 1$:

$$F_1(B) = e^B\left(-\ln B - C_E + B - \frac{B^2}{2.2!} + \frac{B^3}{3.3!} - \frac{B^4}{4.4!} \cdots\right) \tag{E.53}$$

where C_E is Euler's constant; $C_E = 0.57721566\ldots$. In the range $1 \le x < \infty$, Ei(B) may be numerically approximated by a formula given in Ref. 17, page 190.

The power series (E.48) fails to converge for $\xi = \mu$; therefore, the power series representation of the denominator in (E.46) is not uniformly convergent in any interval that includes μ, and the term-by-term integration derived above cannot be used to evaluate (E.46) if $B = \mu$. In fact, the series cannot be used to compute this integral for values of B within a certain neighbourhood of μ becuase convergence is too slow to be useful.

We therefore derive a procedure for integrating the integrand of (E.46) from μ to a larger finite value. We may then use this procedure to evaluate (E.46) as follows:

$$H_1(B,\infty) = H_1(\mu,B_o) - H_1(\mu,B) + H_1(B_o,\infty) \tag{E.54}$$

B_o is the smallest value of B for which the representation (E.50) converges with adequate speed. If $B \ge B_o$ we evaluate $I_1(B,\infty)$ using (E.50) only.

In order to derive this procedure, we let $\xi = \mu \cosh z$ to obtain, from (E.46):

$$H_1(\mu,B) = e^{-(\tau+\theta)}\int_0^K \frac{e^{-(\mu\cosh z - \theta)}}{\mu \cosh z - \theta}\, dz \tag{E.55}$$

where:

$$K = \cosh^{-1}\left(\frac{B}{\mu}\right) = \ln\left(\frac{B}{\mu} + \sqrt{\frac{B^2}{\mu^2} - 1}\right)$$

Expanding the exponential in series and noting that $\tau + \theta = \chi$, we obtain:

$$H_1(\mu,B) = e^{-\chi}\left\{\int_0^K \frac{dz}{\mu \cosh z-\theta} - \int_0^K dz + \sum_{n=1}^{\infty} \frac{(-1)^{n+1}}{(n+1)!}\int_0^K (\mu \cosh z-\theta)^n\, dz\right\} \tag{E.56}$$

$$= e^{-\chi}\left\{\left[\frac{2}{\mu\Phi}\ \text{arc tan}\left(\frac{L-\theta/\mu}{\Phi}\right) - \text{arc tan}\left(\frac{1-\theta/\mu}{\Phi}\right)\right] - K + \frac{1}{2}\left[\frac{\mu}{2}\left(L-\frac{1}{L}\right) - \theta K\right]\right.$$

$$\left. + \sum_{n=2}^{\infty} \frac{(-1)^{n+1}}{(n+1)!}\mu^n\left[R_n + R_0\left(\frac{-\theta}{\mu}\right)^n \sum_{i=1}^{n-1}\left(\frac{-\theta}{\mu}\right)^i R_{n-i}\ \frac{n!}{i!(n-i)!}\right]\right\} \tag{E.57}$$

where:

$$L = e^K$$

$$\Phi = 1 - \frac{\theta^2}{\mu^2}$$

$$R_n = \int_0^K \cosh^n z \, dz$$

By integrating by parts, we derive the following recursion formula for R_n:

$$R_n = \frac{1}{n} \left(\cosh^{n-1} K \sinh K + (n-1) R^{n-2} \right) \qquad (E.58)$$

For sufficiently large values of μ, it becomes impossible to find a value of B_0 such that the series in Eqs. (E.50) and (E.57) both converge sufficiently fast to be of use in numerical computation of $H_1(B,\infty)$. In such cases, a numerical quadrature routine is used.

In this case, Eq. (E.46) is transformed by use of the relation $\xi = -\ell n \omega$ to remove the infinite upper limit of integration. We obtain:

$$H_1(B,\infty) = e^{-\tau} \int_0^{e^{-B}} \frac{d\omega}{(-\ell n\omega - \theta)\left((\ell n\omega)^2 - \mu^2 \right)^{\frac{1}{2}}} \qquad (E.59)$$

In the case $A = \chi_p$, the first term on the right side of (E.44) vanishes; from (E.55), we obtain:

$$H_1(\mu,\infty) = \frac{e^{-\chi}}{\mu} \int_0^{\infty} \frac{e^{-\mu(\cosh z - 1 + 1/\lambda)}}{(\cosh z - 1 + 1/\lambda)} \, dz$$

$$= \frac{e^{-\chi}}{\mu} P(\mu,\lambda) \qquad (E.60)$$

where: $\lambda = \mu/(\mu - \theta)$; we note that if either μ or λ is large, the main contribution to the integral is for small z. Since $-\mu < \theta < \mu$, we always have $\lambda > 1/2$.

Differentiating P, we obtain:

$$\frac{\partial P}{\partial \mu} = -e^{\mu(1-1/\lambda)} \int_0^{\infty} e^{-\mu \cosh z} \, dz = -e^{\mu(1-1/\lambda)} K_0(\mu) \qquad (E.61)$$

$K_0(\mu)$ is the zero-order modified Bessel function of the second kind. For sufficiently large values of μ, the following asymptotic expansion is useful (Ref. 18):

$$K_o(\mu) = \sqrt{\frac{\pi}{2\mu}}\, e^{-\mu} \left\{ 1 - \frac{1^2}{8\mu} + \frac{1^2 . 3^2}{2!(8\mu)^2} - \frac{1^2 . 3^2 . 5^2}{3!(8\mu)^3} \ldots . \right\} \tag{E.62}$$

$$= \sqrt{\frac{\pi}{2}}\, e^{-\mu} \sum_n \frac{C_n}{\mu^{n+\frac{1}{2}}}$$

$$P(\infty,\lambda) = 0$$

$$\therefore \quad P(\mu,\lambda) = - \int_\mu^\infty \frac{\partial P}{\partial \mu'}\, d\mu' = \int_\mu^\infty e^{\mu'(1-1/\lambda)}\, K_o(\mu')\, d\mu'$$

$$= \sqrt{\frac{\pi}{2}} \sum_n C_n \int_\mu^\infty \frac{e^{-\mu'/\lambda} d\mu'}{(\mu')^{n+\frac{1}{2}}} \tag{E.63}$$

Let:

$$Q_n = \int_\mu^\infty \frac{e^{-\mu'/\lambda} d\mu'}{(\mu')^{n+\frac{1}{2}}} = e^{-\mu/\lambda}\, R_n \tag{E.64}$$

Then:

$$R_0 = 2\sqrt{\lambda}\ g\left(\sqrt{\frac{\mu}{\lambda}}\right)$$

$$R_n = \frac{1}{n - \frac{1}{2}} \left[\frac{1}{\mu^{n - \frac{1}{2}}} - \frac{R_{n-1}}{\lambda} \right] \tag{E.65}$$

The asymptotic series $\sum_n C_n R_n$ fails to give a result if either μ or λ is too small; however, the minimal value $\lambda = 1/2$ is sufficiently large to obtain a result.

Equations (E.45) to (E.65) define the method for numerical evaluation of Eq. (E.44).

The evaluation of $\eta_{3,c}(A)$ is carried out in a similar manner. We integrate Eq. (E.11) by parts, observing that the bracketed quantity in this equation is equal to unity at the upper limit of integration β_B. We obtain

$$\eta_{3,c}(A) = \frac{e^{-A}}{\pi} \arcsin \left\{ \frac{x^2}{x_B^2}\ \frac{A}{A - \chi} \right\}^{\frac{1}{2}} - \frac{e^{-\beta_B}}{2} - \frac{1}{2\pi} \frac{\chi}{\left(1 - \frac{x_B^2}{x^2}\right)} \int_A^{\beta_B} \frac{e^{-\beta}\, d\beta}{(\beta-\chi)\beta^{\frac{1}{2}}(\beta_B-\beta)^{\frac{1}{2}}} \tag{E.66}$$

We define the integral in Eq. (E.66) as $H_2(A)$. Once again, we make a change of variables in this integral, as follows:

$$\begin{aligned} \mu &= \frac{\beta_B}{2} \\ \xi &= \beta - \frac{\beta_B}{2} \\ \theta &= -\chi + \frac{\beta_B}{2} \end{aligned} \tag{E.67}$$

Substituting, we obtain:

$$H_2(A) = e^{-\mu} \int_{A-\mu}^{\mu} \frac{e^{-\xi}\, d\xi}{(\xi+\theta)(\mu^2-\xi^2)^{\frac{1}{2}}} \tag{E.68}$$

We observe that the integrand has branch points at $\xi = \pm \mu$ and a simple pole at $\xi = -\theta$, where $\theta > \mu$. Once again, the pole is always outside the range of integration.

As before, it is necessary to distinguish two cases: $0 < A \leq \beta_B$, and $A = 0$. We expand the integrand of Eq. (E.68) as follows:

$$\begin{aligned} e^{-\xi}(\xi+\theta)^{-1} &= \frac{1}{\theta} \sum_{i=0}^{\infty} \frac{(-\xi)^i}{i!} \sum_{j=0}^{\infty} \frac{(-\xi)^j}{\theta^j} \\ &= \frac{1}{\theta} \sum_{k=0}^{\infty} P_k\, (-\xi)^k \end{aligned} \tag{E.69}$$

where:

$$P_k = \sum_{i=0}^{k} \frac{1}{i!\,\theta^{k-i}}$$

Substituting, we obtain:

$$H_2 = \frac{e^{-\mu}}{\theta} \sum_{k=0}^{\infty} P_k \int_{A-\mu}^{\mu} \frac{(-\xi)^k d\xi}{(\mu^2 - \xi^2)^{\frac{1}{2}}} \tag{E.70}$$

We set $\xi = \mu \sin z$ to obtain:

$$H_2 = \frac{e^{-\mu}}{\theta} \sum_k (-1)^k P_k\, \mu^k \int_{\arcsin(\frac{A}{\mu} - 1)}^{\frac{\pi}{2}} \sin^k z\, dz \tag{E.71}$$

In the case A = 0, we obtain:

$$S_k = \int_{-\frac{\pi}{2}}^{\frac{\pi}{2}} \sin^k z \, dz \quad = \pi \;;\; k = 0$$

$$= 0 \;;\; k \text{ odd}$$

$$= \pi \left[\frac{1.3.5....k - 1}{2.4.6.... \quad k}\right]; \; k \text{ eve}$$

For $0 < A \leq \beta_B$, we may integrate Eq. (E.72) by parts to der ve the r formula:

$$S_k = \frac{\alpha^{k-1}\sqrt{1 - \alpha^2}}{k} + \frac{k - 1}{k} S_{k-2}$$

where $\alpha = \frac{A}{\mu} - 1$

If μ is large or nearly equal to θ , the series in Eq. fails to converge rapidly enough to be useful for numerical comput $A > 0$, numerical quadrature must then be used to evaluate Eq. (E 11). $A = 0$, we substitute $\xi = \mu \cos z$ in Eq. (E.68) and re-define $P(\mu,\lambda)$ to

$$H_2(0) = \frac{e^{\mu/\lambda}}{\mu} \int_0^{\pi} \frac{e^{-\mu(1/\lambda + 1 - \cos z)}dz}{\frac{1}{\lambda} + 1 - \cos z} = \frac{e^{\mu/\lambda}}{\mu} P(\mu,\lambda) \qquad \text{(E.74)}$$

where: $\lambda = \mu/(\theta-\mu)$; once again, we note that the integrand gives most of its contribution for small z if either μ or λ becomes large. In this case, we have $0 < \mu < \infty$ and $0 < \lambda < \infty$. Differentiating $P(\mu,\lambda)$ with respect to μ as before, we obtain:

$$\frac{\partial P}{\partial \mu} = -e^{-\mu(1/\lambda + 1)} \int_0^{\pi} e^{\mu \cos z} dz = -e^{-\mu(1/\lambda + 1)} I_o(\mu) \qquad \text{(E.75)}$$

$I_o(\mu)$ is the zero-order Bessel function of imaginary argument (Ref. 18, pages 162-163). This function has the following asymptotic expansion for large μ:

$$I_o(\mu) = \frac{e^{\mu}}{\sqrt{2\pi\mu}} \left[1 + \frac{1^2}{8\mu} + \frac{1^2 3^2}{2!(8\mu)^2} + \frac{1^2 3^2 5^2}{3!\,(8\mu)^3} + \ldots \right] \qquad \text{(E.76)}$$

$$= \frac{e^{\mu}}{\sqrt{2\pi\mu}} \sum_n \frac{C_n}{\mu^n}$$

Since $P(\infty,\lambda) = 0$ we have:

$$P(\mu,\lambda) = -\int_{\mu}^{\infty} \frac{\partial P}{\partial \mu'}\, d\mu' = \int_{\mu}^{\infty} e^{-\mu'(1/\lambda + 1)}\, I_o(\mu')\, d\mu'$$

$$= \int_{\mu}^{\infty} e^{-\mu/\lambda}\, \frac{\pi}{2\mu'} \left(\sum_n \frac{C_n}{\mu'^n} \right) d\mu' \tag{E.77}$$

$$\therefore H_2(0) = \frac{e^{\mu/\lambda}}{\mu} \sqrt{\frac{\pi}{2}} \sum_n C_n \int_{\mu}^{\infty} \frac{e^{-\mu'/\lambda} d\mu'}{\mu'^{\, n+\frac{1}{2}}} = \frac{1}{\mu} \sqrt{\frac{\pi}{2}} \sum_n C_n\, R_n \tag{E.78}$$

where R_n is defined in Eq. (E.64).

Here we must allow not only for the case of small μ but also for the case of small λ. In either situation the summation in Eq. (E.78) fails to produce a result because of the way in which μ and λ enter into the recursion formula (E.65).

We first study the case where λ is small compared to unity, but μ is not.

If we take the first term in Eq. (E.78), we obtain:

$$H_2(0) \simeq \frac{\lambda}{\mu} \sqrt{\frac{2\pi}{\lambda}}\, g\left(\sqrt{\frac{\mu}{\lambda}}\right) \tag{E.79}$$

In the case of small λ, we observe that the integrand in Eq. (E.74) depends mostly on the numerator in the region in which it gives most of its contribution to the integral, namely the region of small z. In other words, the width of the peak in the integrand depends primarily on μ; the influence of the denominator is small in comparison. We approximate the denominator, for $\lambda \ll 1$, as follows:

$$\frac{1}{\frac{1}{\lambda} + 1 - \cos z} = \frac{\lambda}{1 + \lambda(1 - \cos z)} \simeq \lambda e^{\lambda(\cos z - 1)} \tag{E.80}$$

Substituting in Eq. (E.74), we obtain:

$$H_2(0) \simeq \frac{\lambda e^{-\mu-\lambda}}{\mu} \int_0^{\pi} e^{(\mu+\lambda)\cos z}\, dz = \frac{\lambda e^{-\mu-\lambda}}{\mu}\, \pi\, I_o(\mu+\lambda) \tag{E.81}$$

$$= \frac{\lambda}{\mu} \sqrt{\frac{\pi}{2(\mu + \lambda)}} \left[1 + \frac{1^2}{8(\mu + \lambda)} + \frac{1^2 3^2}{2!(8(\mu + \lambda))^2} \cdots \right]$$

For large values of ξ, $g(\xi) \rightarrow 1/2$; for small λ and large μ, Eqs. (E.79) and (E.81) can be shown to approach the same limit. We combine them to obtain the following approximation formula:

$$H_2(0) \simeq \frac{\lambda}{\mu} \sqrt{\frac{2\pi}{\lambda}}\, e\left(\sqrt{\frac{\mu}{\lambda}}\right)\left[1 + \frac{1^2}{8(\mu+\lambda)} + \frac{1^2 3^2}{2!(8(\mu+\lambda))^2} \cdots\right] \quad (E.82)$$

If λ is large and μ is small, the Taylor expansion of $I_o(\mu)$ can be substituted into Eq. (E.77). This expansion is:

$$I_o(\mu) = 1 + \left(\frac{\mu}{2}\right)^2 + \frac{(\mu/2)^4}{(2!)^2} + \ldots. + \frac{(\mu/2)^{2n}}{(n!)^2} \ldots = \sum_n C_n \mu^{2n} \quad (E.83)$$

From Eq. (E.77) we have:

$$P(\mu,\lambda) = \left\{ \int_0^W - \int_0^\mu + \int_W^\infty \right\} e^{-\mu'(1/\lambda + 1)} \pi I_o(\mu')\, d\mu' \quad (E.84)$$

Evaluating the first integral term-by-term, we have:

$$\int_0^W e^{-\mu'(1/\lambda + 1)} I_o(\mu')\, d\mu' = e^{-AW} \sum_n C_n R_{2n} \quad (E.85)$$

where:

$$R_k = e^{AW} Q_k = e^{AW} \int_0^W e^{-A\xi} \xi^k\, d\xi$$

$$A = 1 + 1/\lambda$$

$$R_0 = \frac{e^{AW} - 1}{A}$$

$$R_k = \frac{k R_{k-1} - W^k}{A}$$

W is an experimentally obtained value of μ chosen such that the series representations (E.77) and (E.85) both converge rapidly enough to be useful. If both μ and λ are small, the series in Eq. (E.71) is used to compute H_2.

Equations (E.67) to (E.85) define the method for numerical evaluation of Eq. (E.66).

The expression for $\eta_{4,c}$ in Eq. (E.12) can be transformed into an integration over radius in the same manner as the expression for $\eta_{4,s}$ in Eqs. (E.6). This time, we substitute the cylindrical Poisson equation (11.3) into Eq. (E.29) to obtain:

$$\alpha_G(s') = \frac{d\chi}{ds'} + \frac{\gamma\eta_{net}(s')}{2x'^3} \quad \frac{dx'}{ds'} \tag{E.86}$$

We again define $\epsilon_G(s')$ as in Eq. (E.31); we define $\psi_G(s,s')$ as follows:

$$\psi_G(s,s') = \text{arc tan} \left\{ \frac{\Omega_G(s')x^2(s)}{\beta_G(s')-\chi(s)-\Omega_G(s')x^2(s)} \right\}^{\frac{1}{2}} \tag{E.87}$$

Substituting in Eq. (E.12), we obtain:

$$\eta_{4,c}(\beta(s_1),\beta(s_2)\ ) = \frac{1}{\pi}\int_{s'=s_1}^{s'=s_2} ds'\ \epsilon_G(s')\ \psi_G(s,s') \tag{E.88}$$

The current collection expressions (E.14) and (E.15) may be integrated by parts to obtain:

$$i_{1,c}(A) = \frac{2}{\sqrt{\pi}}\ e^{-A} \left\{ \sqrt{A - \chi_p} + g\left(\sqrt{A - \chi_p}\right) \right\} \tag{E.89}$$

$$i_{2,c}(A) = \frac{1}{x_B}\left[1 - \frac{2}{\sqrt{\pi}}\ e^{-A}\left(\sqrt{A} + g\left(\sqrt{A}\right) \right) \right] \tag{E.90}$$

Finally, Eq. (E.16) becomes:

$$i_{3,c}(\beta(s_1),\ \beta(s_2)\ ) = \frac{2}{\sqrt{\pi}}\int_{s'=s_1}^{s'=s_2} ds'\ \epsilon_G(s')\ \sqrt{\Omega_G(s')} \tag{E.91}$$

Equations (E.44) to (E.91) define all of the expressions necessary for computing η and i for a cylindrical probe. As in the spherical case, some special cases are of importance. We first calculate η for a repelling probe, once again under the assumption of a monotonic potential. Substituting Eqs. (E.10) and (E.13) into Eq. (E.18a), we obtain:

$$\eta = e^{-\chi} - \frac{1}{\pi}\int_{\chi_p}^{\infty} d\beta\ e^{-\beta}\ \text{arc sin}\left\{ \frac{x^2(\beta - \chi_p)}{\beta - \chi} \right\}^{\frac{1}{2}} \tag{E.92}$$

For large χ_p we again recover the Boltzmann factor; at the probe surface, $\chi \rightarrow \chi_p$, $x \rightarrow 1$, and we again obtain Eq. (E.40). In the field-free case, $\chi_p = \chi = 0$, we obtain, for the geometrical depletion factor:

$$\eta = 1 - \frac{1}{\pi}\ \text{arc sin x} \tag{E.93}$$

As before, we may also obtain this result by using the expression for η for attracted particles.

Using Eqs. (E.17b) and (E.18b) together with Eq . (E.89), we obtain, for the orbital-motion-limited currents:

$$
\begin{aligned}
i &= \frac{2}{\sqrt{\pi}} \left(\sqrt{-\chi_p} + g\left(\sqrt{-\chi_p}\right)\right) \; ; \; \chi_p \leq 0 \\
i &= e^{-\chi_p} \qquad\qquad ; \; \chi_p \geq 0
\end{aligned}
\tag{E.94}
$$

APPENDIX F

Current Collected by a Probe of Large Radius When Repelled Particles Are at Zero Temperature and Attracted Particles are Maxwellian

We define a radial coordinate x, measured inward from the sheath edge, and two transverse coordinates y and z. In the planar approximation, Poisson's equation reduces to:

$$\frac{d^2\phi}{dx^2} = - \frac{\rho}{\epsilon} \qquad \text{(F.1)}$$

At $x = 0$, $\phi = 0$ and $d\phi/dx = 0$. At the probe surface, $\phi < 0$. The distribution function at the sheath edge is a half-Maxwellian consisting only of particles moving into the sheath. Constants of the motion are E_x, v_y, and v_z.

$$\begin{aligned} E &= Ze\phi(x) + \frac{m}{2} v_x^2 + \frac{m}{2}(v_y^2 + v_z^2) \\ &= E_x + E_t \end{aligned} \qquad \text{(F.2)}$$

E_t is the energy associated with transverse motion. The distribution function is:

$$\begin{aligned} f &= N_\infty \left(\frac{m}{2\pi kT}\right)^{3/2} \cdot e^{-E_x/kT} \; e^{-E_t/kT} \quad ; \quad v_x > 0 \\ f &= 0 \quad ; \quad v_x < 0 \end{aligned} \qquad \text{(F.3)}$$

$$N = \int_0^\infty \int_{-\infty}^\infty \int_{-\infty}^\infty f_- \, dv_x \, dv_y \, dv_z = \int_0^\infty \int_{-\infty}^\infty \int_{-\infty}^\infty f_- \frac{dv_x}{dE_x} dE_x \, dv_y \, dv_z \qquad \text{(F.4)}$$

$$v_x = \sqrt{\frac{2}{m}\Big(E_x - Ze\phi(x)\Big)} \quad ; \quad \frac{dv_x}{dE_x} = \frac{1}{\sqrt{2m\Big(E_x - Ze\phi(x)\Big)}} \qquad \text{(F.5)}$$

$$\eta = \frac{N}{N_\infty} = \int_0^\infty \left(\frac{m}{2\pi kT}\right)^{\frac{1}{2}} \frac{e^{-E_x/kT}\, dE_x}{\sqrt{2m\,(E_x - Ze\phi(x))}} \int_{-\infty}^{\infty}\int_{-\infty}^{\infty} \left(\frac{m}{2\pi kT}\right) e^{-\frac{m}{2}\left(\frac{v_y^2 + v_z^2}{kT}\right)} dv_y \, dv_z$$

$$\begin{aligned} &= \frac{1}{2}\int_0^\infty \left(\frac{1}{\pi kT}\right)^{\frac{1}{2}} \frac{e^{-E_x/kT}\, dE_x}{\sqrt{E_x - Ze\phi(x)}} = \frac{1}{2\sqrt{\pi}} \int_0^\infty \frac{e^{-\beta}\, d\beta}{\sqrt{\beta - \chi}} \\ &= \frac{1}{\sqrt{\pi}}\, g\left(\sqrt{-\chi}\right) \end{aligned} \qquad \text{(F.6)}$$

The quantities β and χ are as defined in Sec. IX; g is as defined in Appendix E.

We note that $\rho = ZeN$ and define $s = x/\lambda_D$ and $y = -\chi$ to obtain, from Eqs. (F.1) and (F.6):

$$\frac{d^2y}{ds^2} = \eta(y) = \frac{1}{\sqrt{\pi}}\ g(\sqrt{y}) \tag{F.7}$$

Since y and dy/ds are both zero at s = 0, it can be shown that Eq. (F.7) has the solution:

$$s = \int_0^y \frac{dy'}{\sqrt{2\int_0^{y'} \eta(y'')dy''}} \tag{F.8}$$

We define $\sigma_1(y')$ as the square of the denominator in the integrand. Substituting into Eq. (F.8), we obtain:

$$\sigma_1(y') = \frac{2}{\sqrt{\pi}} \int_0^{y'} g(\sqrt{y''})\ dy''$$

$$= \int_0^{y'} e^{y''}\ (1 - \operatorname{erf} \sqrt{y''})\ dy''$$

$$= \frac{2}{\sqrt{\pi}} \left\{ g(\sqrt{y'}) - \left(\frac{\sqrt{\pi}}{2} - \sqrt{y'} \right) \right\} \tag{F.9}$$

Examination of the form of g shows that Eq. (F.9) is of order y'. When the square root of this expression is substituted into the denominator of (F.8), a singularity occurs in the integrand at y' = 0. We may eliminate this singularity by defining $\sigma_1(y') = y'\ \sigma_2(y')$ and setting $y' = z^2$. We then obtain:

$$s = \int_0^y \frac{dy'}{\sqrt{\sigma_1(y')}} = 2 \int_0^{\sqrt{y}} \frac{dz}{\sqrt{\sigma_2(z^2)}} \tag{F.10}$$

We may obtain a power series expansion for $g(\xi)$ as follows:

$$g(\xi) = \frac{\sqrt{\pi}}{2}\ e^{\xi^2}\ (1-\operatorname{erf} \xi)$$

$$= \frac{\sqrt{\pi}}{2}\ e^{\xi^2} - e^{\xi^2} \int_0^{\xi} e^{-t^2}\ dt \tag{F.11}$$

$$= \frac{\sqrt{\pi}}{2}\ e^{\xi^2} - h(\xi)$$

The second term, $h(\xi)$ may be written as a Taylor series:

$$h(\xi) = \sum_{m=0}^{\infty} \frac{h^{(m)}(0)\xi^m}{m!} \tag{F.12}$$

Repeated differentiation of $h(\xi)$ gives:

$$\begin{aligned} h^{(n+1)} &= 2(\xi h^{(n)} + nh^{(n-1)}) \\ h^{(n+1)}(0) &= 2nh^{(n-1)} \\ h^{(2n)}(0) &= 0 \\ h^{(2n+1)}(0) &= 2^{2n}n! \end{aligned} \tag{F.13}$$

Substituting in Eq. (F.12) gives:

$$h(\xi) = \xi + \frac{2}{3}\xi^3 + \frac{4}{15}\xi^5 \ldots\ldots = \sum_{n=0}^{\infty} \frac{\xi^{2n+1}\, 2^n}{1.3.5\ldots(2n-1)(2n+1)} \tag{F.14}$$

$$= \sum_{n=0}^{\infty} \xi^{2n+1} Q_n$$

For large $\xi, h(\xi) \rightarrow \frac{\sqrt{\pi}}{2} e^{\xi^2}$; the difference between these two quantities becomes small compared with their magnitudes, and Eq . (F.11) cannot be used to give numerical results because of round-off errors.

We therefore use the following form to compute $s(y)$:

$$s = 2\int_0^{\sqrt{y_1}} \frac{dz}{\sqrt{\sigma_2(z^2)}} + \int_{y_1}^{y} \frac{dy'}{\sqrt{\sigma_1(y')}} \tag{F.15}$$

y_1 is an experimentally obtained value of y for which neither Eq. (F.9) nor (F.11) suffers from round-off error. From the definition of σ_2, we obtain the following series form:

$$\sigma_2(z^2) = \frac{\sigma_1(z^2)}{z^2} = \sum_{n=1}^{\infty} \frac{z^{2n-2}}{n!} - \frac{2z}{\sqrt{\pi}} \sum_{n=1}^{\infty} z^{2n-2} Q_n \tag{F.16}$$

Equations (F.8) to (F.16) define the numerical solution of Eq . (F.7). The solution gives the number of attracted-species Debye lengths s between the probe surface and the sheath edge as a function of probe potential χ_p in the planar-sheath approximation. A program that has been used to compute s by means of the above expressions appears in Appendix I (Program 3). Numerical values of s for various χ_p appear in the output from this program which is shown in Appendix J.

Since in the planar-sheath approximation, all particles entering the sheath are collected, the increase in collected current as χ_p becomes larger depends only on the increase in sheath area. For the sphere, the area of the sheath edge varies as the square of its radius; for the cylinder, it varies directly as radius.

The collected current for the sphere is therefore given by the following expression:

$$i(\chi_p) = \frac{I}{I_0} = \left(1 + \frac{\lambda_D s(\chi_p)}{R_p}\right)^2 \tag{F.17}$$

For the cylinder:

$$i(\chi_p) = 1 + \frac{\lambda_D s(\chi_p)}{R_p} \tag{F.18}$$

In cases where λ_D is not small compared to R_p, the planar approximation will fail to give correct values for the collected current for three reasons. First, the planar form (F.1) of the Poisson equation will fail to closely approximate the spherical or cylindrical forms. Second, the orbital-motion-limited current will decrease below the values given by (F.17) and (F.18) in terms of sheath edge radius because some of the attracted particles will be able to enter the sheath and orbit out of it again without being collected by the probe. Finally, the orbital-motion-limited current itself will over-estimate the current because a certain class of particles entering the sheath will orbit out of it because of barriers created by the potential well itself.

APPENDIX G

Power Series Solution of the Allen, Boyd and Reynolds Equation

Numerical solution of the Allen, Boyd and Reynolds equation (Ref. 6) has been carried out here for reasons which are discussed in Sec.XIII. This differential equation expresses the dependence of potential on radius in the case of a spherical probe at large ion-attracting potential in the limit of zero ion temperature. The solution is carried out according to the method suggested in Ref. 5.

Combining Eqs. (13.12), (13.13) and (13.14), we obtain the Allen, Boyd, and Reynolds Equation:

$$\frac{1}{\xi^2}\frac{d}{d\xi}\left(\xi^2 \frac{d\chi_-}{d\xi}\right) = \frac{1}{2\sqrt{\pi}} \quad \frac{i^*}{\xi^2\sqrt{\chi_-}} - e^{-\chi_-} \qquad \text{(G.1)}$$

For convenience, we define new variables $s = 1/\xi$, $y = \chi_-$, $A = i^*/2\sqrt{\pi}$, and obtain:

$$x^4 \frac{d^2y}{dx^2} = \frac{Ax^2}{\sqrt{y}} - e^{-y} \qquad \text{(G.2)}$$

The boundary conditions at infinite radius become:

$$\left.\begin{aligned} y = \frac{dy}{dx} &= 0 \\ \frac{d^2y}{dx^2} &\text{ finite} \end{aligned}\right\} \text{at } x = 0 \qquad \text{(G.3)}$$

The condition that d^2y/dx^2 remains finite at $x = 0$ implies that the right-hand side of (G.2) must be of order x^4. As $y \to 0$, $e^{-y} \to 1$ and therefore $Ax^2/\sqrt{y} \to 1$.

Let: $$y = A^2x^4(1 + y') \;;\; y' \to 0 \text{ as } x \to 0$$

where: $$y' = \sum_{n=1}^{\infty} a_n x^n \qquad \text{(G.4)}$$

Therefore: $$y = \sum_{n=4}^{\infty} b_n x^n \qquad \text{(G.5)}$$

where: $$b_1 = b_2 = b_3 = 0$$

$$b_4 = A^2$$

$$b_n = A^2 \, a_{n-4} \;;\; n > 4$$

Substituting in the left side of Eq. (G.2), we obtain:

$$x^4 \frac{d^2y}{dx^2} = \sum_{k=6}^{\infty} b_{k-2} (k-2)(k-3)\, x^k \tag{G.6}$$

Also:

$$\begin{aligned} \frac{Ax^2}{\sqrt{y}} &= (1 + y')^{-\frac{1}{2}} \\ &= 1 + \sum_{i=1}^{\infty} c_i (y')^i \end{aligned} \tag{G.7}$$

where:

$$c_i = (-1)^i \ \frac{1.3.5....2i-1}{2.4.6....2i}$$

Substituting for y' in Eq. (G.7):

$$\begin{aligned} \frac{Ax^2}{\sqrt{y}} &= 1 + \sum_{i=1}^{\infty} c_i \left(\sum_{j=1}^{\infty} a_j\, x^j \right)^i \\ &= 1 + \sum_{k=1}^{\infty} e_k\, x^k \end{aligned} \tag{G.8}$$

where:

$$\begin{aligned} e_k &= c_1 a_k + \sum_{i=2}^{k} c_i \sum_{h=k-i+1} \delta(j_1 + 2j_2 + \ldots + hj_h - k) \left(\frac{i!}{j_1!j_2!\ldots j_h!} \right) a_1^{\,j_1} a_2^{\,j_2} \ldots a_h^{\,j_h} \\ &= c_1\, a_k + e_k^{*} \end{aligned} \tag{G.9}$$

and: $\delta(m) = 1$ for $m = 0$; $\delta(m) = 0$ for $m \neq 0$.

Also:

$$\begin{aligned} e^{-y} &= 1 + \sum_{i=1}^{\infty} d_i \left(\sum_{j=1}^{\infty} b_j x^j \right)^i \\ &= 1 + \sum_{k=1}^{\infty} f_k\, x^k \end{aligned} \tag{G.10}$$

where:

$$d_i = \frac{(-1)^i}{i!}$$

and f_k is given by an expression identical in form to Eq. (G.9).

Equating coefficients of like powers in Eq. (G.2), we obtain:

$$e_k = f_k \quad ; \quad k < 6$$
$$e_k = f_k + b_{k-2}\,(k-2)(k-3); \quad k \geq 6 \tag{G.11}$$

Since Eq. (G.2) is invariant upon change of sign of x, it follows that a_n and b_n must vanish for all odd values of n.

For k = 2, we obtain, from Eq. (G.11):

$$c_1\, a_2 = d_1\, b_2 + d_2\, b_1^2 - c_2\, a_1^2 = 0 \tag{G.12}$$

Therefore a_k and b_k both vanish for $k < 4$, and Eq. (G.9) reduces to:

$$e_k^* = \sum_{i=2}^{k/4} c_i \sum_{h=k-4i+4} \delta(4j_4 + 6j_6 + \ldots + hj_h - k) \left(\frac{i!}{j_4!\, j_6! \cdots j_n!} \right) a_4^{\,j_4} a_6^{\,j_6} \ldots a_h^{\,j_h} \tag{G.13}$$

We therefore obtain from Eqs. (G.5) and (G.11) a set of recursive relations for defining any b_k in terms of $b_1 \ldots b_{k-1}$ as follows:

$$b_k = A^2\, a_{k-4}$$
$$c_1\, a_k = d_1\, b_k + b_{k-2}(k-2)(k-3) + f_k^* - e_k^* \tag{G.15}$$

Equations (G.4) to (G.15) define the power series expansion required to begin the numerical integration of (G.2), according to the method suggested in Ref. 5; the Runge-Kutta numerical integration procedure is used to complete the integration.

APPENDIX H

Operation of Computer Programs

Programs 1 and 2, both of which are listed in Appendix I along with two smaller programs, constitute tested methods for carrying out the computation involved in this research for the general case and for the case of zero-temperature repelled particles, respectively. Either of these programs produces one result, corresponding to one given value of each of the input quantities $e\phi_p/kT_-$, T_+/T_-, and R_p/λ_{D-}, (where we have again assumed $Z_+=1$, $Z_-=-1$) in an average time of about two minutes on the IBM 7094 computer (depending on the values of these parameters), to a relative accuracy in all computed quantities of about 0.002 or better. Most of the results not involving extreme values of the input parameters have relative accuracies better than 0.001.

For program 1, these accuracies have been checked by running representative cases (a case consisting of one set of values of the three quantities mentioned above), each with several combinations of computation net spacing Δs and outer boundary position R_B/R_p, in order to find the innermost boundary position and coarsest net consistent with acceptable results. This procedure is usually carried out at a nondimensional probe potential of $\pm$ 25, the largest to be used, since it has been found that the demands by the program for large boundary radius and fine net become more severe as probe potential increases. It is then possible to compute with confidence all cases involving smaller probe potentials and the same values of T_+/T_- and R_p/λ_{D-} using the computation net thus determined.

In general, the program becomes more demanding of a large number of points in the computation net at both very large and very small values of R_p/λ_{D-}, and more demanding of a large number of Debye lengths between R_p and R_B for very large R_p/λ_{D-}. Since the rate of convergence of the program becomes slower as $(R_B-R_p)/\lambda_{D-}$ is increased, the cases of large R_p/λ_{D-} have therefore been the most expensive in computation time, particularly for the sphere. In fact, the case $e\phi_p/kT_- = \pm 25$, $T_+/T_- = 1$, $R_p/\lambda_{D-} = 100$ consumed about 20 minutes of computation time, the largest value for any case computed. Accordingly, no cases were attempted for the spherical probe at this value of R_p/λ_{D-} for any intermediate values of T_+/T_-.

When several cases were run for decreasing values of the repelled-species temperature, the attracted-species parameters being held constant, it was found that the program became more demanding of a fine computation net but it was possible to move R_B closer to the probe because of the contraction of the sheath as repelled-species temperature was decreased.

When a sequence of cases of decreasing attracted-species temperature was run with the repelled-species parameters held constant, only small changes in computation net requirements were noticed in the case of the cylinder, but in the case of the sphere, the required values of net fineness and outer boundary radius increased rapidly. At the same time, the collected current result was observed to become more and more sensitive to small changes in the form of the potential until a point was reached where computations [illegible]d to be practical. This restriction became more severe with increasing probe potential; for instance, it proved impossible to compute the ion current collected by the sphere for the case e[illegible] $T_- = -25$, $T_+/T_- = 0.1$, $R_p/\lambda_{D-} = 10$.

These findings are in accordance with the prediction deduced from analytical considerations in Sec. XIII. These restrictions proved less severe when calculations were made using the mono-energetic distribution for the attracted species.

Table 4 shows suggested computation net spacings and outer boundary radii to be used with program 1, as determined by experience using the program. It was found experimentally that in most cases the outer boundary was at a large enough radius to produce results of the desired accuracy if the net charge density $\eta_+ - \eta_-$ was smaller than 0.001 at the boundary.

Figure 11 shows ion and electron charge densities as functions of radius for a cylindrical probe for the case $e\phi_p/kT_- = 25$, $T_+/T_- = 1$, $R_p/\lambda_{D_-}=10$, for various positions of the outer boundary radius R_B. The significant feature of this diagram is the fact that in each instance charge separation is seen to occur near the outer boundary. This occurs because of the fact that the assumed relation (8.9) between the potential and its slope at $r = R_B$ is only an approximation to the relation that would actually exist at that radius in the infinite-plasma case; the potential adjusts its shape to compensate for this error by increasing its curvature near this boundary. Because Poisson's equation (4.3) is satisfied everywhere, this curvature implies a charge separation near $r = R_B$. Since these boundary conditions are derived from the leading term in the representation of the potential for large radii (Sec. XIII), they become more nearly correct as the boundary radius is increased; accordingly, the charge separation near $r = R_B$ may be expected to decrease as R_B is increased. This behaviour is in fact seen to occur in Fig. 11.

Because of this ability of the solution scheme to locally adjust the potential to compensate for errors in the boundary conditions at $r = R_B$, it may be expected that computed values of current collection will approach the limiting value corresponding to an infinite plasma very rapidly as R_B is increased. This is in fact the case, and it is of crucial importance in designing a practical solution scheme. Earlier trials with a boundary held at zero potential required R_B to equal to many probe radii before the current collection results were observed to approach a limit with increasing R_B. Placing R_B at such large distances from the probe resulted in unacceptably large expense in computation time per result; it was evident at that time that a better set of boundary conditions was required before the computation scheme could be made useful.

The remarkable insensitivity of the solution scheme to errors in the relation between the potential and its slope at $r = R_B$ was made use of in carrying out the computation for the cylindrical probe with zero temperature attracted particles, using the boundary conditions for the finite-temperature problem. It has been shown (Sec. XIII) that in the zero-temperature limit, the asymptotic form of the cylindrical-probe potential is no longer proportional to the inverse of the radius but to the inverse two-thirds power of the radius. When computations for this case were carried out using the finite-temperature boundary conditions, experimentation with various values of R_B proved the result to be so stable that it never became necessary to put the more exact boundary conditions into the program.

The key to this insensitivity to boundary conditions is the fact that the boundary potential is free to seek its own equilibrium value; the strong tendency of the plasma towards neutrality tends to fix the local potential a small distance from the boundary while a small amount of charge separation adjusts the derivative at the boundary; the disturbance in potential shape caused by the presence of the boundary is thus confined to the immediately adjacent region.

In order to initiate a calculation with any one of the programs listed in Appendix I, it is necessary to provide it with appropriate data as indicated by comments included with the program listing. In the case of Program 1, this data includes the values of the parameters π_3, π_6, and γ. Depending on which species is used as reference, there are two equivalent ways of specifying these quantities. For example, it is possible to carry out the calculation for the case $e\phi_p/kT_- = -25$, $T_+/T_- = 0.75$, $R_p/\lambda_{D-} = 10$, using as input values $\pi_3 = -33.33$, $\pi_6 = 0.75$, $\gamma = 133.3$. It is more convenient to interchange the roles of ions and electrons and use the values $\pi_3 = 25$, $\pi_6 = 1.333$, $\gamma = 100$.

It is also necessary to specify, as input quantities, two coefficients which determine the magnitude of the mixing function (Sec. V). Choosing values that are too large causes the computation to diverge in an oscillatory manner (Appendix C); choosing values that are too small causes excessive amounts of computation time to be used before adequate convergence is attained. The fortran subprogram ADJUST (Appendix I) monitors the convergence of the calculations and attempts to correct the mixing function accordingly, thus making some allowance for a poor initial guess.

This subprogram also ends the execution of a case when the accuracy of the computed attracted-species currents and net charge density is sufficient. It uses two criteria for making this decision. The first is the convergence of the current result to an asymptotic value; three computed current values, spaced 10 iterations apart, are stored and used to calculate an asymptotic result, based on an assumed exponential approach to equilibrium; if the third result differs from the asymptote by a relative amount less than 0.001, the first criterion is assumed satisfied.

It was found necessary to include a second criterion because of the non-monotonic nature of the approach of the current result to its final value. This behaviour is illustrated in Fig. 12, which shows computed current as a function of iteration number for a typical case. This behaviour caused a tendency for the calculation to be terminated prematurely by false indications of approach to an asymptotic result.

Accordingly, convergence is now also tested by comparing the quantity η_{net} computed at the end of a given iteration with the unmodified net charge density $\eta_+ - \eta_-$ produced by the next iteration. If the calculation has converged fully, these must agree by definition; the square of the relative difference between them is averaged over the interval R_B-R_p and iteration continues until this average is less than 0.01.

During early development of the program, an attempt was made to speed the calculations by storing values of the net charge density distribution over several iterations and projecting the entire distribution ahead to an estimated asymptotic result. This procedure failed because of the sensitivity of the program; it almost inevitably produced a fictitious system of potential barriers more complicated than any of those for which calculation of charge densities had been programmed.

The optimum method of generating each Maxwellian result is normally to begin by computing the corresponding case for mono-energetic attracted particles, and then to use the charge density distribution resulting from this case as an initial approximation for the Maxwellian case. Since the time per iteration for the mono-energetic case is much smaller than that for the Maxwellian, this procedure usually results in a smaller total expenditure of computer time and produces an extra (mono-energetic) result as a bonus. The first two examples of computer output shown in Appendix J illustrate this procedure.

Program 2, which is used in computing the case of zero-temperature repelled particles, has presented considerable difficulties in operation. This is apparently because as it converges toward a result, it often passes through a set of approximate configurations in which the calculation of a succeeding iterate is highly sensitive to the precise spacing of points in the computation net and resulting inaccuracies in the computation are capable of setting up stable oscillations which prevent convergence from being completed. These difficulties seem to be less severe in many cases if a very coarse or very fine net is used; however, these remedies have the disadvantages of inaccurate results and great expense in computation time, respectively.

In spite of these difficulties, this program has been successfully used to compute spherical and cylindrical probe characteristics for values of R_p/λ_{D_-} from 0.5 to about 20. Since in this case the planar-sheath approximation (Appendices F,I,J) gives the limiting form of the probe characteristics for large R_p/λ_{D_-}, results for values larger than 20 can be obtained by graphical interpolation to a high degree of accuracy.

Computations using Programs 3 and 4 are much simpler to carry out than those using Programs 1 and 2; the operation of these programs may be studied by examining the relevant equations in Appendices F and G, as well as the listing of these programs and samples of their output in Appendices I and J, respectively.

APPENDIX I

Computer Program Listing

The Fortran II Programs used to make the numerical calculations are as follows:

Main Program 1: used to carry out computations for the general case.

Main Program 2: used to carry out computations for the case of zero-temperature repelled particles.

Subprograms ADJUST, COOKIE, CHARGE, CUBIC, POLATE, CHAMON, CAL, COEFT: used by main programs 1 and 2; COEFT is also used by main program 3.

Subprograms FIRST, SECOND, THIRD, FOURTH, UNO, DUO, TRE, SDFN: used together with main programs 1 or 2 to carry out calculations for spherical geometry.

Subprograms FIRST, SECOND, THIRD, FOURTH, DYO, CDO, TRY, CORE: Used together with main programs 1 or 2 to carry out calculations for cylindrical geometry.

Main Program 3: used together with subprogram COEFT to calculate the planar-sheath limit of the case of zero-temperature repelled particles as described in Appendix F.

Main Program 4: used together with subprograms POWERS and CHASPH to obtain a numerical solution of the Allen, Boyd, and Reynolds equation (Ref. 6) as described in Appendix G.

A listing of each of these programs follows:

Page 1

```
C     MAIN PROGRAM 1
C     SPHERICAL OR CYLINDRICAL LANGMUIR PROBE CHARACTERISTIC
      DIMENSION A(8),YYY(10)
      DIMENSION X(401),XSQ(401),S(401),DXDS(401),ROP(401),SCOT(401),
     1 COOK(401),XI(401),DXIDS(401),ETA(401),ETAPS(401),ETANG(401),
     2 RHO(401),OMGAG(401),BETAG(401),ALFAG(401),PSIG(401),EPSG(401),
     3 V(401),Z(401),SH(401)
      COMMON X,XSQ,S,DXDS,ROP,SCOT,COOK,XI,DXIDS,ETA,ETAPS,ETANG,RHO,
     1 OMGAG,BETAG,ALFAG,PSIG,EPSG,V,Z,SH
      COMMON PI,SQTPI,VIPI,SAV,MODE,M,MP,DELTS,GAMMA,PI3,PI6,PI7,VPOS,
     1 VNEG,NPRINT,KT1,KT2,LL,KEND
      COMMON LINK,DETH,EXV,EDV,N2,N22,NW,SW,SWA,BETAW,BETAWA,MACK,MIKE,
     1 SCRIT,SCRITA,LK,LKA,CRISS,CROSS,VST,AMU,THETA,KBO,MCO,MZET

C     PI3 IS NONDIMENSIONAL PROBE POTENTIAL REFERRED TO IONS.
C     PI6 IS  EFFECTIVE ION-TO-ELECTRON TEMPERATURE RATIO.
C     GAMMA=(PROBE RADIUS/ION DEBYE DISTANCE)**2
C     P IS VALUE OF S AT OUTERMOST POINT IN COMPUTATION NET.
C     QT1 AND QT2 ARE COEFFICIENTS OF  DEBYE  TERM AND  FAR-FIELD  TERM
C          IN MIXING FUNCTION.

C     KT1 SPECIFIES AMOUNT OF OUTPUT FOR EACH ITERATION EXCEPT LAST.
C     KT2 SPECIFIES AMOUNT OF OUTPUT FOR LAST ITERATION.
C     KT3 SPECIFIES MANNER OF GENERATION OF FIRST ITERATION.
C          KT3=1 - POLYNOMIAL COEFFICIENTS ARE READ IN
C          KT3=2 - RE-USES ETA FROM PREVIOUS CASE
C          KT3=3 - USES PREPARED POLYNOMIAL
C          KT3=4 - USES POTENTIAL WHICH IS SUM OF DEBYE TERM AND
C                       POWER-LAW TERM
C          KT3=5 - READS ETA FROM CARDS AND INTERPOLATES
C     M IS NUMBER OF POINTS IN COMPUTATION NET.
C     NDUB IS ITERATION AT WHICH DENSITY OF POINTS IN COMPUTATION NET
C          IS DOUBLED.
C     NEND IS MAXIMUM NUMBER OF ITERATIONS.
C     NPRINT - OUTPUT WILL OCCUR AT EVERY NPRINT,TH NET POINT.
C     MODE SPECIFIES WHETHER COMPUTATION IS FOR SPHERICAL OR CYLINDRICAL
C          PROBE.
C     KWIT SPECIFIES HOW MUCH CONTROL IS EXERCISED OVER
C          CONVERGENCE OF THE CALCULATIONS BY SUBROUTINE ADJUST.
C     KBD SPECIFIES BOUNDARY CONDITIONS AT OUTER BOUNDARY.
C          KBD=1 - OUTER BOUNDARY IS AT ZERO POTENTIAL.
C          KBD=2 - LINEAR RELATION BETWEEN POTENTIAL AND ITS RADIAL
C                       DERIVATIVE IS SPECIFIED AT OUTER BOUNDARY.
C     MCD SPECIFIES PARTICLE DISTRIBUTION FUNCTIONS.

      KASE=1
    3 READ INPUT TAPE 5,4,PI3,PI6,GAMMA,P,QT1M,QT2M
    4 FORMAT(1P4E10.3,0P2F10.7)
      READ  INPUT  TAPE 5,5,KT1,KT2,KT3,M,NDUB,NEND,NPRINT,MODE,KWIT,KBD
     1 ,MCD
    5 FORMAT(14I5)

      IF(KT3-2)165,165,166
  166 IF(SENSE LIGHT 1)167,165
  167 IF(SENSE LIGHT 2)168,165
  168 SENSE LIGHT 1
      SENSE LIGHT 2
      GO TO 3

  165 KT1=KT1
      KT2=KT2
  222 PRINT 220,KASE
  220 FORMAT(12H0 BEGIN CASE I5)
```

Page 2

```
  221 KASE=KASE+1
      IF(QT1M)321,321,320
  320 QT1=QT1M
      QT2=QT2M
  321 GO TO (6,270),MODE
    6 WRITE OUTPUT TAPE 6,7
    7 FORMAT(32H1 SPHERICAL PROBE CHARACTERISTIC)
      GO TO 9
  270 WRITE OUTPUT TAPE 6,271
  271 FORMAT(34H1 CYLINDRICAL PROBE CHARACTERISTIC)
    9 WRITE OUTPUT TAPE 6,10,PI3,PI6,GAMMA,P,QT1,QT2
   10 FORMAT(8X3HPI3,7X3HPI6,5X5HGAMMA,9X1HP,7X3HQT1,7X3HQT2/
     1 1X1P4E10.3,0P2F10.7)
   81 WRITE OUTPUT TAPE 6,8,KT1,KT2,KT3,M,NDUB,NEND,NPRINT,MODE,KWIT,KBD
     1 ,MCD
    8 FORMAT(56H    KT1  KT2  KT3     M NDUB NEND NPRINT MODE KWIT KBD MCD
     1/1X14I5)

      TIME=CLOCK(0,0)

  101 PI=3.1415927
      SQTPI=1.7724539
      VIPI=1.0/PI
      SAV=1.0/SQTPI
      MAD=1
      MEW=0
      KINGS=1
      MZET=1
      GO TO (111,112,113,114,115),KT3

C     READ OR GENERATE QUANTITIES REQUIRED TO BEGIN FIRST ITERATION.

  111 GO TO (262,263),MODE
  262 READ INPUT TAPE 5,44,(A(I),I=2,8)
   44 FORMAT(1P7E10.3)
  182 WRITE OUTPUT TAPE 6,180,(A(I),I=2,8)
  180 FORMAT(53H  COEFFICIENTS IN INITIAL POTENTIAL APPROXIMATION ARE /
     1 1X1P7E10.3)
      GO TO 15
  263 READ INPUT TAPE 5,44,(A(I),I=1,7)
      WRITE OUTPUT TAPE 6,180,(A(I),I=1,7)
      GO TO 15

  112 N=MP-1
      NP=MP
      FACT=(GAM/GAMMA)*(PI3/PIOLD)
      DO 90 I=1,NP
   90 ETA(I)=ETA(I)*FACT
      IF(P-POLD)15,336,335
  335 KINGS=2
      GO TO 15
  336 IF(N-M)17,15,19
   17 M=N
      WRITE OUTPUT TAPE 6,22,M
   22 FORMAT(4H  M=I5)
      GO TO 15
   19 L=N/M
      MP=M+1
      DO 21 I=2,MP
      J=(I-1)*L+1
   21 ETA(I)=ETA(J)
      GO TO 15
```

Page 3

```
  113 DO 14 I=1,8
   14 A(I)=1.0
      GO TO 15

  114 READ INPUT TAPE 5,200,BEE
  200 FORMAT(1PE10.3)
      GO TO (206,290),MODE
  206 WRITE OUTPUT TAPE 6,208,BEE
  208 FORMAT (57H  COEFFICIENT OF SQUARE TERM IN INITIAL APPROXIMATION I
     1S  1PE10.3)
      GO TO 15
  290 WRITE OUTPUT TAPE 6,291,BEE
  291 FORMAT (57H  COEFFICIENT OF LINEAR TERM IN INITIAL APPROXIMATION I
     1S  1PE10.3)
      GO TO 15

  115 MP=M+1
      READ INPUT TAPE 5,116,L
  116 FORMAT(I5)
      READ INPUT TAPE 5,117,(ETA(I),I=1,MP,L)
  117 FORMAT(1P6E12.5)
  186 WRITE OUTPUT TAPE 6,118,L,(ETA(I),I=1,MP,L)
  118 FORMAT(4H  L=I2,27H  INITIAL VALUES OF ETA ARE/(1X1P6E12.5))
      GO TO 15

   15 SENSE LIGHT 0
      SENSE LIGHT 1
      KEND=0
      GAM=GAMMA
      PIOLD=PI3
      POLD=P

C     GENERATE ARRAYS S AND DXDS TO DEFINE COMPUTATION NET.
C     FORM OF THESE QUANTITIES DEPENDS ON WHETHER ROGA (RATIO OF PROBE
C     RADIUS TO LARGER DEBYE LENGTH) IS GREATER OR LESS THAN 2.6 OR 25.1

   16 FLM=M
      DELTS=P/FLM
      MP=M+1
      RATO=MIN1F(PI6,1.0)
      ROGA=SQRTF(GAMMA*RATO)
      IF(ROGA-25.1)253,253,254

  253 DO 18 I=1,MP
      FIE=I-1
      S(I)=DELTS*FIE
      IF(ROGA-2.6)360,360,361
  360 X(I)=EXPF(-S(I))
      DXDS(I)=-X(I)
      GO TO 362
  361 X(I)=1.0-S(I)
      DXDS(I)=-1.0
  362 ROP(I)=1.0/X(I)
      XSQ(I)=X(I)**2
      SCOT(I)=SQRTF(1.0-XSQ(I))
   18 COOK(I)=COOKIE(I,QT1,QT2)
      GO TO 260

  254 SNT=0.9
      ZNP=1.0/(1.0-SNT)
      ZPP=10.0/(SNT*ROGA)
      AVA=ZNP-1.0
      ENN=(ZNP-ZPP)/AVA
```

Page 4

```
      DO 255 I=1,MP
      FIE=I-1
      S(I)=DELTS*FIE
      X(I)=ZNP*(1.0-S(I))-AVA*(1.0-S(I))**ENN
      DXDS(I)=-ZNP+ENN*AVA*(1.0-S(I))**(ENN-1.0)
  256 ROP(I)=1.0/X(I)
      XSQ(I)=X(I)**2
      SCOT(I)=SQRTF(1.0-XSQ(I))
  255 COOK(I)=COOKIE(I,QT1,QT2)
      GO TO 260

C     SUPPLY FURTHER QUANTITIES REQUIRED TO BEGIN FIRST ITERATION.

  260 IF(KEND)20,20,23

   20 GO TO (25,294,25,207,187),KT3
  294 GO TO (337,338),KINGS
  338 NPP=NP+1
      POWR=4.990-FLOATF(MODE)
      DO 339 I=NPP,MP
  339 ETA(I)=ETA(NP)*(X(I)/X(NP))**POWR
      KINGS=1
  337 GO TO (26,280),MODE

   25 QUA1=0.0
  275 JAA=3-MODE
      JBB=9-MODE
      DO 24 J=JAA,JBB
   24 QUA1=QUA1+A(J)
      ERROR=PI3/QUA1
      DO 27 J=JAA,JBB
   27 A(J)=A(J)*ERROR
      DO 29 I=1,MP
      QUA1=0.0
      QUA2=0.0
      QUA3=0.0
      DO 30 J=JAA,JBB
      JCC=J-2+MODE
      QUA1=QUA1+A(J)*X(I)**J
      QUA2=QUA2+FLOATF(J)*A(J)*X(I)**(J-1)
   30 QUA3=QUA3-FLOATF(J*JCC)*A(J)*X(I)**(J+2)
      Z(I)=QUA1
      DXIDS(I)=QUA2*DXDS(I)
   29 ETA(I)=QUA3/GAMMA
      GO TO (37,283),MODE

  207 AVE=1.0-BEE
      AA=AVE*PI3
      BB=BEE*PI3
      GO TO (295,296),MODE

  295 DO 210 I=1,MP
      DVE=EXPF(ROGA*(1.0-1.0/X(I)))
      Z(I)=AA*X(I)*DVE+BB*XSQ(I)
      DXIDS(I)=(AA*DVE*(1.0+ROGA/X(I))+2.0*BB*X(I))*DXDS(I)
  210 ETA(I)=-AA*DVE*X(I)*RATO-2.0*BB*(XSQ(I)**2)/GAMMA
      GO TO 37

  296 DO 298 I=1,MP
      DVE=EXPF(ROGA*(1.0-1.0/X(I)))
      ROXI=SQRTF(X(I))
      Z(I)=AA*DVE*ROXI+BB*X(I)
      DXIDS(I)=(AA*DVE*(0.5/ROXI+ROXI*ROGA/XSQ(I))+BB)*DXDS(I)
```

Page 5

```
  298 ETA(I)=-(AA*DYE*ROXI*(XSQ(I)/4.0+ROGA*ROGA)+BB*XSQ(I)*X(I))/GAMMA
      GO TO 283

  187 KNO=M/L
      IF(L-1)999,999,998
  998 KNOM=KNO-1
      FLL=L
      K=L+1
      KPL=K+L
      KML=K-L
      UP=ETA(KPL)/2.0
      DN=ETA(KML)/2.0
      DA=UP-DN
      DB=UP-ETA(K)+DN
      DO 188 J=2,L
      DEL=FLOATF(J-K)/FLL
  188 ETA(J)=ETA(K)+DA*DEL+DB*DEL**2

      DO 190 KEY=2,KNOM
      K=KEY*L+1
      KM=K-L
      JS=KM+1
      JE=K-1
      KPL=K+L
      KML=K-L
      KMPL=KM+L
      KMML=KM-L
      UP=ETA(KPL)/2.0
      DN=ETA(KML)/2.0
      UPM=ETA(KMPL)/2.0
      DNM=ETA(KMML)/2.0
      DA=UP-DN
      DB=UP-ETA(K)+DN
      DAM=UPM-DNM
      DBM=UPM-ETA(KM)+DNM
      DO 191 J=JS,JE
      DEL=FLOATF(J-K)/FLL
      DELM=FLOATF(J-KM)/FLL
      ETC=ETA(K)+DA*DEL+DB*DEL**2
      ETCM=ETA(KM)+DAM*DELM+DBM*DELM**2
  191 ETA(J)=ETC*ABSF(DELM)+ETCM*ABSF(DEL)
  190 CONTINUE

      JS=KNOM*L+2
      JE=KNO*L
      DO 192 J=JS,JE
      DEL=FLOATF(J-K)/FLL
  192 ETA(J)=ETA(K)+DA*DEL+DB*DEL**2
  999 KAY=KNO*L+1
      KAZ=KAY+1
      IF(KAZ-MP)194,194,293
  194 POWR=4.990-FLOATF(MODE)
      DO 193 J=KAZ,MP
  193 ETA(J)=ETA(KAY)*(X(J)/X(KAY))**POWR

  293 GO TO (26,280),MODE

C     INTEGRATE ETA AND EMPLOY BOUNDARY CONDITIONS AT OUTER EDGE OF NET
C     TO OBTAIN ZI AND DXIDS.

   26 DO 33 I=1,MP
   33 Y(I)=-GAMMA*ETA(I)/(XSQ(I)**2)*DXDS(I)
      Z(1)=0.0
```

Page 6

```
      KINK=1
      GO TO 34

   36 DO 38 I=1,MP
      DXIDS(I)=Z(I)*DXDS(I)
   38 Y(I)=DXIDS(I)
      Z(1)=PI3
      KINK=2
      GO TO 34

  280 DO 281 I=1,MP
  281 Y(I)=-DXDS(I)*GAMMA*ETA(I)/(X(I)*XSQ(I))
      Z(1)=0.0
      KINK=3
      GO TO 34

  282 DO 284 I=1,MP
      DXIDS(I)=Z(I)*DXDS(I)/X(I)
  284 Y(I)=DXIDS(I)
      Z(1)=PI3
      KINK=4
      GO TO 34

   34 Z(2)=Z(1)+(5.0*Y(1)+8.0*Y(2)-Y(3))*DELTS/12.0
      DO 35 I=3,M
   35 Z(I)=Z(I-1)+(13.0*(Y(I-1)+Y(I))-Y(I-2)-Y(I+1))*DELTS/24.0
      Z(MP)=Z(M)+(5.0*Y(MP)+8.0*Y(M)-Y(M-1))*DELTS/12.0
      GO TO (36,37,282,283),KINK

   37 GO TO (325,326),KBD
  325 EDGE=Z(MP)/(1.0-X(MP))
      GO TO 327
  326 EDGE=(2.0*Z(MP)-X(MP)*DXIDS(MP)/DXDS(MP))/(2.0-X(MP))
  327 DO 39 I=1,MP
      DXIDS(I)=DXIDS(I)+EDGE*DXDS(I)
   39 XI(I)=Z(I)+EDGE*(X(I)-1.0)
      IF(MCO-1)199,199,340

  283 GO TO (330,331),KBD
  330 EDGE=-Z(MP)/LOGF(X(MP))
      GO TO 332
  331 EDGE=(Z(MP)-X(MP)*DXIDS(MP)/DXDS(MP))/(1.0-LOGF(X(MP)))
  332 DO 285 I=1,MP
      DXIDS(I)=DXIDS(I)+EDGE*DXDS(I)/X(I)
  285 XI(I)=Z(I)+EDGE*LOGF(X(I))
      IF(MCO-1)199,199,340

C     CALCULATE POSITIVE AND NEGATIVE CHARGE DENSITIES.

  199 CALL CHARGE
      GO TO 341

  340 CALL CHAMON
      GO TO 341

  341 IF(SENSE LIGHT 1)161,160
  161 IF(SENSE LIGHT 2)162,160
  162 SENSE LIGHT 1
      SENSE LIGHT 2
      GO TO 318

  160 KEND=KEND+1
      KT1=KT1
```

Page 7

```
      GO TO (41,300,71,71),KT1

C     OUTPUT AS SPECIFIED BY KT1.

  300 MYK=10
      LYM=1
  303 KYT=XMODF(KEND,MYK)
      IF(KYT)315,316,315
  316 KYT=10
  315 IF(PI3)304,304,305
  304 YYY(KYT)=YPOS
      GO TO 306
  305 YYY(KYT)=YNEG
      GO TO 306

  306 IF(KYT-MYK)310,307,310
  307 IF(PI3)308,308,309
  308 WRITE OUTPUT TAPE 6,302,KEND,YNEG,(YYY(I),I=1,MYK)
  302 FORMAT(5H KENDI4,6H YNEG=F9.6,6H YPOS=10F9.4)
      GO TO 310
  309 WRITE OUTPUT TAPE 6,301,KEND,YPOS,(YYY(I),I=1,MYK)
  301 FORMAT(5H KENDI4,6H YPOS=F9.6,6H YNEG=10F9.4)
      GO TO 310
  310 GO TO (41,311),LYM

   71 WRITE OUTPUT TAPE 6,45,YPOS,YNEG
   45 FORMAT(7H  YPOS=1PE14.7,7H  YNEG=1PE14.7)
   70 GO TO (41,41,41,42),KT1
   42 WRITE OUTPUT TAPE 6,43,(I,ROP(I),ETA(I),XI(I),ETAPS(I),ETANG(I),
     1 I=1,MP,NPRINT)
   43 FORMAT(2(12H   I   R(I)/RP,9X3HETA,10X2HXI,7X5HETAPS,7X5HETANG)/
     1 (2(1XI3,0PF8.4,1P4E12.5)))

C     CALCULATE NEW VALUES OF NET CHARGE DENSITY.

   41 DO 40 I=1,MP
   40 ETA(I)=(1.0-COOK(I))*ETA(I)+(ETAPS(I)-ETANG(I))*COOK(I)

      IF(PI3)350,350,351
  350 YUSE=YPOS
      GO TO 352
  351 YUSE=YNEG
      GO TO 352

  352 CALL ADJUST(NEND,MAD,MEW,DT1,DT2,KWIT,0.001,YUSE,YINY)

  228 IF(NEND-KEND-1)46,47,46
   47 GO TO (311,312,311,311),KT1
  312 MYK=XMODF(KEND,10)
      IF(MYK)311,311,313
  313 LYM=2
      GO TO 306

  311 KT1=KT2
   46 IF(NEND-KEND)99,99,48
   48 IF(NDUB-KEND)50,51,50

C     KEND = NEND. STOP ITERATING.

   99 IF(PI3)355,355,356
  355 YIN=YINY*SQRTF(PI6)
      GO TO 357
  356 YIN=YINY/SQRTF(PI6)
```

Page 8

```
  357 YPN=YPOS*SQRTF(PI6)
      YNP=YNEG/SQRTF(PI6)
      WRITE OUTPUT TAPE 6,98,YPN,YNP,YIN
   98 FORMAT(6H  YPN=1PE12.5,6H  YNP=1PE12.5,6H  YIN=1PE12.5)
  318 TOTAL=CLOCK(TIME)/100.0
      WRITE OUTPUT TAPE 6,319,TOTAL
  319 FORMAT(29H0 EXECUTION TIME IN MINUTES  F7.2)
      GO TO 3

C     KEND = NDUB. DOUBLE NUMBER OF POINTS IN NET.

   51 IF(400-2*M) 54,58,58
   58 DO 52 I=1,MP
      K=2*(MP-I)+1
      L=MP-I+1
   52 ETA(K)=ETA(L)
      M=2*M
      NPRINT=2*NPRINT
      GO TO 16

   23 DO 53 I=5,MP,4
      ETA(I-3)=(3.0*ETA(I-4)+6.0*ETA(I-2)-ETA(I))/8.0
   53 ETA(I-1)=(-ETA(I-4)+6.0*ETA(I-2)+3.0*ETA(I))/8.0
   54 WRITE OUTPUT TAPE 6,57,M
   57 FORMAT(2X2HM=I8)

   50 LITE=XMODF(KEND,4)+1
      SENSE LIGHT 0
      GO TO (61,62,63,64),LITE
   61 SENSE LIGHT 1
      GO TO (26,280),MODE
   62 SENSE LIGHT 2
      GO TO (26,280),MODE
   63 SENSE LIGHT 3
      GO TO (26,280),MODE
   64 SENSE LIGHT 4
      GO TO (26,280),MODE
      END
```

Page 9

```
C     MAIN PROGRAM 2
C     PROBE CHARACTERISTIC - REPELLED PARTICLES AT ZERO TEMPERATURE
      DIMENSION YYY(10)
      DIMENSION X(401),XSQ(401),S(401),DXDS(401),ROP(401),SCOT(401),
     1 COOK(401),XI(401),DXIDS(401),ETA(401),ETAPS(401),ETANG(401),
     2 RHO(401),OMGAG(401),BETAG(401),ALFAG(401),PSIG(401),EPSG(401),
     3 Y(401),Z(401),SH(401)
      COMMON X,XSQ,S,DXDS,ROP,SCOT,COOK,XI,DXIDS,ETA,ETAPS,ETANG,RHO,
     1 OMGAG,BETAG,ALFAG,PSIG,EPSG,Y,Z,SH
      COMMON PI,SQTPI,VIPI,SAY,MODE,M,MP,DELTS,GAMMA,PI3,PI6,PI7,YPOS,
     1 YNEG,NPRINT,KT1,KT2,LL,KEND
      COMMON LINK,WETH,EXY,EDY,N2,N22,NW,SW,SWA,BETAW,BETAWA,MACK,MIKE,
     1 SCRIT,SCRITA,LK,LKA,CRISS,CROSS,YST,AMU,THETA,KBD,MCD,MZET,MALT

C     PTEE = NONDIMENSIONAL PROBE POTENTIAL FOR ATTRACTED PARTICLES
C     PROBYE = PROBE RADIUS / DEBYE LENGTH OF ATTRACTED SPECIES
C     SHERAD = INITIAL VALUE OF SHEATH EDGE RADIUS / PROBE RADIUS
C          IF SHERAD +VE , SHEDGE = SHERAD.
C          IF SHERAD = 0, RE-USE SHEDGE FROM PREVIOUS CASE.
C          IF SHERAD -VE , GENERATE SHEDGE FROM CHILD-LANGMUIR RELATION.
C     QT1 AND QT2 ARE COEFFICIENTS OF .DEBYE. TERM AND .FAR-FIELD. TERM
C          IN MIXING FUNCTION.

C     KT1 SPECIFIES AMOUNT OF OUTPUT FOR EACH ITERATION EXCEPT LAST.
C     KT2 SPECIFIES AMOUNT OF OUTPUT FOR LAST ITERATION.
C     INITIA SPECIFIES WHETHER INITIAL CHARGE DENSITY FUNCTION ( ETA )
C          IS THAT FOR A CHILD-LANGMUIR SHEATH OR WHETHER PREVIOUS ETA
C          IS RE-USED.
C          INITIA = 1 - CHILD-LANGMUIR SHEATH ASSUMED.
C          INITIA = 2 - CHILD-LANGMUIR SHEATH ASSUMED TO BEGIN FIRST
C                       ITERATION. PREVIOUS ETA RE-USED WHEN SHEATH EDGE
C                       RADIUS IS RESET.
C          INITIA = 3 - PREVIOUS ETA RE-USED.
C     M IS NUMBER OF POINTS IN COMPUTATION NET.
C     NDUB IS ITERATION AT WHICH DENSITY OF POINTS IN COMPUTATION NET
C          IS DOUBLED.
C     NEND IS MAXIMUM NUMBER OF ITERATIONS.
C     NPRINT - OUTPUT WILL OCCUR AT EVERY NPRINT.TH NET POINT.
C     MODE SPECIFIES WHETHER COMPUTATION IS FOR SPHERICAL OR CYLINDRICAL
C          PROBE.
C     MCD SPECIFIES PARTICLE DISTRIBUTION FUNCTIONS.

      KASE=1
    3 READ  INPUT  TAPE 5, 4,PTEE,PROBYE,SHERAD,QT1M,QT2M
    4 FORMAT(1P3E10.3,0P2F10.7)
      READ  INPUT  TAPE 5,5,KT1,KT2,INITIA,M,NDUB,NEND,NPRINT,MODE,MCD
    5 FORMAT(14I5)

      IF(INITIA-2)165,165,166
  166 IF(SENSE LIGHT 1)167,165
  167 IF(SENSE LIGHT 2)168,165
  168 SENSE LIGHT 1
      SENSE LIGHT 2
      GO TO 3

  165 KT1=KT1
      KT2=KT2
  222 PRINT 220,KASE
  220 FORMAT(12H0 BEGIN CASE I5)
  221 KASE=KASE+1
      IF(QT1M)321,321,320
  320 QT1=QT1M
      QT2=QT2M
```

Page 10

```
  321 IF(SHERAD)400,401,402

  400 SHEDGE=1.0+1.121*(PTEE**0.75)/PROBYE
      GO TO 401

  402 SHEDGE=SHERAD
      GO TO 401

  401 GO TO (6,270),MODE
    6 WRITE OUTPUT TAPE 6,7
    7 FORMAT ( 73H1 SPHERICAL PROBE CHARACTERISTIC - REPELLED PARTICLES
     1AT ZERO TEMPERATURE)
      GO TO 9
  270 WRITE OUTPUT TAPE 6,271
  271 FORMAT(75H1 CYLINDRICAL PROBE CHARACTERISTIC - REPELLED PARTICLES
     1AT ZERO TEMPERATURE)
    9 WRITE OUTPUT TAPE 6,10,PTEE,PROBYE,SHEDGE,QT1,QT2
   10 FORMAT(7X4HPTEE,4X6HPROBYE,4X6HSHEDGE,7X3HQT1,7X3HQT2/
     1 1X1P3E10.3,0P2F10.7)
   81 WRITE OUTPUT TAPE 6,8,KT1,KT2,INITIA,M,NDUB,NEND,NPRINT,MODE,MCD
    8 FORMAT(47H   KT1  KT2 INITIA  M NDUB NEND NPRINT MODE MCD /1X14I5)

      TIME=CLOCK(0,0)

  101 PI=3.1415927
      SQTPI=1.7724539
      VIPI=1.0/PI
      SAY=1.0/SQTPI
      MAD=1
      MEW=0
      KUTY=1
      GAMMA=PROBYE**2
      PI6=1.0
      PTEE=-ABSF(PTEE)
      PI3=PTEE
      KBD=1
      MZET=2
      IF(INITIA-2)15,15,112

  112 N=MP-1
      NP=MP
      FACT=GAMOLD/GAMMA*PTEE/PTOLD
      DO 90 I=1,NP
   90 ETA(I)=ETA(I)*FACT
  316 IF(N-M)17,15,19
   17 M=N
      WRITE OUTPUT TAPE 6,22,M
   22 FORMAT(4H  M=I5)
      GO TO 15
   19 L=N/M
      MP=M+1
      DO 21 I=2,MP
      J=(I-1)*L+1
   21 ETA(I)=ETA(J)
      GO TO 15

   15 SENSE LIGHT 0
      SENSE LIGHT 1
      KEND=0
      GAMOLD=GAMMA
      PTOLD=PTEE
      KSET=1
```

Page 11

```
   16 FLM=M

      DELTS=1.0/FLM
      MP=M+1
      YZP=0.125

  253 DO 18 I=1,MP
      FIE=I-1
      S(I)=DELTS*FIE
      ROP(I)=SHEDGE-(SHEDGE-1.0)*(YZP*(1.0-S(I))+(1.-YZP)*(1.0-S(I))**2)
      X(I)=1.0/ROP(I)
      XSQ(I)=X(I)**2
      DXDS(I)=-XSQ(I)*(SHEDGE-1.0)*(YZP+2.0*(1.0-S(I))*(1.0-YZP))
      SCOT(I)=SQRTF(1.0-XSQ(I))
   18 COOK(I)=COOKIE(I,QT1,QT2)
      GO TO (20,23,20),KSET
   20 IF(2*INITIA+KSET-5)207,207,294

  207 DO 210 I=1,MP
      XI(I)=PTEE*((SHEDGE-1.0/X(I))/(SHEDGE-1.0))**1.3333333
  210 ETA(I)=0.5/SQRTF(1.0-2.0*XI(I))
      GO TO 294

  294 GO TO (370,370,228),KSET
  370 GO TO (26,280),MODE

C     COMPUTE POTENTIAL XI(1-MP) AND ITS GRADIENT DXIDS(1-MP) USING
C     CHARGE DENSITY ETA(1-MP)

   26 DO 33 I=1,MP
   33 Y(I)=-GAMMA*ETA(I)/(XSQ(I)**2)*DXDS(I)
      Z(1)=0.0
      KINK=1
      GO TO 34

   36 DO 38 I=1,MP
      DXIDS(I)=Z(I)*DXDS(I)
   38 Y(I)=DXIDS(I)
      Z(1)=PI3
      KINK=2
      GO TO 34

  280 DO 281 I=1,MP
  281 Y(I)=-DXDS(I)*GAMMA*ETA(I)/(X(I)*XSQ(I))
      Z(1)=0.0
      KINK=3
      GO TO 34

  282 DO 284 I=1,MP
      DXIDS(I)=Z(I)*DXDS(I)/X(I)
  284 Y(I)=DXIDS(I)
      Z(1)=PI3
      KINK=4
      GO TO 34

   34 Z(2)=Z(1)+(5.0*Y(1)+8.0*Y(2)-Y(3))*DELTS/12.0
      DO 35 I=3,M
   35 Z(I)=Z(I-1)+(13.0*(Y(I-1)+Y(I))-Y(I-2)-Y(I+1))*DELTS/24.0
      Z(MP)=Z(M)+(5.0*Y(MP)+8.0*Y(M)- [illegible]M-1))*DELTS/12.0
      GO TO (36,325,282,330),KINK

  325 EDGE=Z(MP)/(1.0-X(MP))
  327 DO 39 I=1,MP
      DXIDS(I)=DXIDS(I)+EDGE*DXDS(I)
```

Page 12

```
   39 XI(I)=Z(I)+EDGE*(X(I)-1.0)
      GO TO (199,340,340),MCD

  330 EDGE=-Z(MP)/LOGF(X(MP))
  332 DO 285 I=1,MP
      DXIDS(I)=DXIDS(I)+EDGE*DXDS(I)/X(I)
  285 XI(I)=Z(I)+EDGE*LOGF(X(I))
      GO TO (199,340,340),MCD

C     COMPUTE NEW CHARGE DENSITY ETAPS(1-MP)

  199 CALL CHARGE
      GO TO 341

  340 CALL CHAMON
      GO TO 341

  341 IF(SENSE LIGHT 1)161,160
  161 IF(SENSE LIGHT 2)162,160
  162 SENSE LIGHT 1
      SENSE LIGHT 2
      GO TO 318

  160 KEND=KEND+1
      KT1=KT1
      GO TO (41,300,71,71),KT1

  300 MYK=10
      LYM=1
  313 KYT=XMODF(KEND,MYK)
      IF(KYT)315,316,315
  316 KYT=10
  315 YYY(KYT)=YPOS

  306 IF(KYT-MYK)310,307,310
  307 WRITE OUTPUT TAPE 6,302,KEND,(YYY(I),I=1,MYK)
  302 FORMAT(5H KENDI4,3H Y=10F10.4)
  310 GO TO (41,311),LYM

   71 WRITE OUTPUT TAPE 6,45,YPOS
   45 FORMAT(3H Y=1PE14.7)
   70 GO TO (41,41,41,42),KT1
   42 WRITE OUTPUT TAPE 6,43,(I,ROP(I),ETA(I),XI(I),ETAPS(I),
     1 I=1,MP,NPRINT)
   43 FORMAT(2(7X1HI,3X7HR(I)/RP,11X3HETA,12X2HXI,7X7HETA NEW)/
     1 (2(4XI4,0PF10.5,1P3E14.7)))

   41 DO 40 I=1,MP
      ETANG(I)=0.0
   40 ETA(I)=(1.0-COOK(I))*ETA(I)+ETAPS(I)*COOK(I)

      PTERR=(X(MP)-XSQ(MP))*DXIDS(MP)/DXDS(MP)
      NHALT=NEND
      CALL ADJUST(NHALT,MAD,MEW,QT1,QT2,3.0,35,PTERR,PTINY)

      IF(NHALT-KEND-8)228,380,228
  380 IF(KEND-(KEND/10)*10)228,371,228
  371 ERROR=PTINY/PTEE
      IF(ABSF(ERROR)-0.0002)366,345,345

C     SHEATH EDGE POTENTIAL GRADIENT IS SMALL ENOUGH. END EXECUTION.

  366 NEND=XMINOF(KEND+8,NEND)
```

Page 13

```
      WRITE OUTPUT TAPE 6,363,ERROR
      GO TO 228

C     USE CURRENT VALUE OF SHEATH EDGE POTENTIAL GRADIENT TO RESET
C         SHEATH EDGE RADIUS.

  345 ERDD=ERD
      SHDD=SHD
      ERD=ERROR
      SHD=SHEDGE
      KUTY=KUTY+1
      IF(KUTY-3)385,386,386
  386 SHEDGE=SHD-ERD*(SHD-SHDD)/(ERD-ERDD)
      IF(SHEDGE-1.0)350,350,360

  385 IF(DXI(S(MP))351,350,352

  352 DXI=-XSO(MP)*DXIDS(MP)/DXDS(MP)
      D2XI=-ETA(MP)*GAMMA
      IF(D2XI)349,350,350

  350 WRITE OUTPUT TAPE 6,369,KUTY,ERDD,ERD,SHDD,SHD,SHEDGE
  369 FORMAT(29H TROUBLE IN SHEATH EDGE RESET I4,1P5E12.5)
      WRITE OUTPUT TAPE 6,43,(I,ROP(I),ETA(I),XI(I),ETAPS(I),I=1,MP)
      SENSE LIGHT 1
      SENSE LIGHT 2
      GO TO 318

  349 SHEDGE=SHEDGE-DXI/D2XI
      GO TO 360

  351 DO 353 L=1,M
      I=MP-L
      IF(DXIDS(I+1))354,354,350
  354 IF(DXIDS(I))353,353,355
  353 CONTINUE
      GO TO 350
  355 X(MP)=X(I)+(X(I+1)-X(I))/(-DXIDS(I+1)+DXIDS(I))*DXIDS(I)
      SHEDGE=1.0/X(MP)
      GO TO 360

  360 GO TO (361,362,362,362),KT1
  362 WRITE OUTPUT TAPE 6,363,ERROR,SHEDGE
  363 FORMAT(50H RELATIVE ERROR IN SHEATH EDGE POTENTIAL GRADIENT F11.6,
     1 24H NEW SHEATH EDGE RADIUS 1PE10.3)
  361 KSET=3
      GO TO 16

  228 IF(NENO-KEND-1)46,47,46
   47 GO TO (311,312,311,311),KT1
  312 MYK=XMODF(KEND,10)
      IF(MYK)311,311,313
  313 LYM=2
      GO TO 306

  311 KT1=KT2
   46 IF(NENO-KEND)318,318,48
   48 IF(NDUB-KEND)50,51,50

  318 TOTAL=CLOCK(TIME)/100.0
      WRITE OUTPUT TAPE 6,319,TOTAL
  319 FORMAT(29H0 EXECUTION TIME IN MINUTES  F7.2)
      GO TO 3
```

Page 14

```
C     DOUBLE NUMBER OF POINTS IN COMPUTATION NET.

   51 IF(400-2*M)54,58,58
   58 DO 52 I=1,MP
      K=2*(MP-I)+1
      L=MP-I+1
   52 ETA(K)=ETA(L)
      M=2*M
      NPRINT=2*NPRINT
      KSET=2
      GO TO 16

   23 DO 53 I=5,MP,4
      ETA(I-3)=(3.0*ETA(I-4)+6.0*ETA(I-2)-ETA(I))/8.0
   53 ETA(I-1)=(-ETA(I-4)+6.0*ETA(I-2)+3.0*ETA(I))/8.0
   54 WRITE OUTPUT TAPE 6,57,M
   57 FORMAT(2X2HM=I8)

C     RESET SENSE LIGHTS.

   50 LITE=XMODF(KEND,4)+1
      SENSE LIGHT 0
      GO TO (61,62,63,64),LITE
   61 SENSE LIGHT 1
      GO TO (26,280),MODE
   62 SENSE LIGHT 2
      GO TO (26,280),MODE
   63 SENSE LIGHT 3
      GO TO (26,280),MODE
   64 SENSE LIGHT 4
      GO TO (26,280),MODE
      END
```

Page 15

```
      SUBROUTINE ADJUST(NENO,MAD,MEW,QT1,QT2,KWIT,ACCY,YUSE,YINY)          ADJUST

C     SUBROUTINE ADJUST MONITORS CONVERGENCE OF THE CALCULATIONS AND
C         TAKES CORRECTIVE ACTION WHEN NECESSARY.

C     IF KWIT=1 ADJUST TAKES NO ACTION.
C     IF KWIT=2 ADJUST DAMPS ANY DIVERGENT OSCILLATIONS.
C     IF KWIT=3 ADJUST ALSO ENDS EXECUTION WHEN ACCURACY OF RESULTS
C        IS SUFFICIENT.
C     IF KWIT=4 ADJUST ALSO ATTEMPTS TO CORRECT FOR SLOW OSCILLATION
C         DAMPING AND SLOW CONVERGENCE.

      DIMENSION YCHEK(10),DCHEK(10),ZCHEK(10)
      DIMENSION X(401),XSO(401),S(401),DXDS(401),ROP(401),SCOT(401),
     1 COOK(401),XI(401),DXIDS(401),ETA(401),ETAPS(401),ETANG(401),
     2 RHO(401),OMGAG(401),BETAG(401),ALFAG(401),PSIG(401),EPSG(401),
     3 Y(401),Z(401),SH(401)
      COMMON X,XSO,S,DXDS,ROP,SCOT,COOK,XI,DXIDS,ETA,ETAPS,ETANG,RHO,
     1 OMGAG,BETAG,ALFAG,PSIG,EPSG,Y,Z,SH
      COMMON PI,SUTPI,VIPI,SAY,MODE,M,MP,DELTS,GAMMA,PI3,PI6,PI7,YPOS,
     1 YNEG,NPRINT,KT1,KT2,LL,KEND
      COMMON LINK,BETH,EXY,EDY,N2,N22,NW,SW,SWA,BETAW,BETAWA,MACK,MIKE,
     1 SCRIT,SCRITA,LK,LKA,CRISS,CROSS,YST,AMU,THETA,KBD,MCD,MZET,MALT

      IF(KWIT-1)228,228,21

C     IF KCHEK = 1 TO 9, STORE YCHEK(KCHEK) AND RETURN.

   21 KCHEK=XMODF(KEND,10)
      IF(KCHEK)251,250,251
  250 KCHEK=10
  251 YCHEK(KCHEK)=YUSE
  232 IF(KCHEK-8)228,121,122
  121 A8=B8
      B8=C8
      C8=YCHEK(8)
      GO TO 228
  122 IF(KCHEK-10)124,234,228
  124 A9=B9
      B9=C9
      C9=YCHEK(9)
      GO TO 228

C     IF KCHEK = 10, STORE YCHEK(10) AND LOOK FOR OSCILLATIONS IN
C     YCHEK(1-10).

  234 A10=B10
      B10=C10
      C10=YCHEK(10)
      DO 235 I=2,10
  235 DCHEK(I)=YCHEK(I)-YCHEK(I-1)
      DO 236 I=2,9
      IF(DCHEK(I))237,237,238
  237 IF(DCHEK(I+1))123,236,236
  238 IF(DCHEK(I+1))236,236,123
  236 CONTINUE
      DO 240 I=2,9
  240 ZCHEK(I)=(ABSF(DCHEK(I))+ABSF(DCHEK(I+1)))/2.0
      SMCHEK=0.0
      DO 262 I=2,8
  262 SMCHEK=SMCHEK+ZCHEK(I+1)/ZCHEK(I)
      IF(SMCHEK-6.3)123,123,242
```

Page 16

```
C     OSCILLATIONS HAVE BEEN OBSERVED. DECREASE MIXING AND RETURN.

  242 MEW=0
      MAD=2
  125 QT1=QT1*0.9
      QT2=QT2*0.9
      WRITE OUTPUT TAPE 6,127,KEND,QT1,QT2
  127 FORMAT(7H0 KEND=I4,27H  0.9 DECREASE IN MIX. QT1=F10.7,5H QT2=
     1 F10.7)
  128 DO 247 I=1,MP
  247 COOK(I)=COOK(I)*0.9
      GO TO 228

C     OSCILLATIONS FOUND TO BE ABSENT OR DECREASING.

  123 IF(KWIT-2)228,228,132

  132 GO TO (280,281),MZET

  280 MEW=MEW+1
      IF(MEW-2)228,134,134

  281 YMIN=YCHEK(1)
      YMAX=YCHEK(1)
      DO 282 I=1,9
      YMIN=MIN1F(YMIN,YCHEK(I+1))
  282 YMAX=MAX1F(YMAX,YCHEK(I+1))
      IF(ABSF(2.0*(YMAX-YMIN)/(YMAX+YMIN))-ACCY)283,283,228
  283 YINY=(C9+C10)/2.0
      GO TO 278

C     FIND OUT IF CONVERGENCE TOWARD AN ASYMPTOTIC RESULT IS YET
C     INDICATED. IF SO, GO TO 138.

  134 R10=(B10-C10)/(A10-B10)
      IF(R10)228,228,137
  137 IF(R10-1.0)138,228,228

C     ESTIMATE NUMBER OF ITERATIONS REMAINING BEFORE REQUIRED ACCURACY
C     IS ATTAINED. IF THIS EXCEEDS 40, GO TO 141. OTHERWISE GO TO 140.

  138 YINY=A10-(A10-B10)/(1.0-R10)
      ALPH=(C10-YINY)/(A10-YINY)
      FINS=20.0*(LOGF (ACCY*YINY/(C10-YINY))/LOGF(ALPH))
      KINS=FINS
      IF(KINS-40)140,140,141

C     CONVERGENCE IS TOO SLOW. IF MIXING FUNCTION HAS NOT ALREADY BEEN
C     DECREASED BECAUSE OF OSCILLATIONS, INCREASE IT.

  141 IF(KWIT-3)228,228,28
   28 GO TO (126,228),MAD

  126 FACT=1.111
      QTY=QT2*FACT
      QT2=MIN1F(QTY,0.7)
      FACT=FACT*QT2/QTY
      QTS=QT1
      ZIT=1.0-QT2
      ZAT=QT1*FACT
      QT1=MIN1F(ZIT,ZAT)
      MEW=0
      WRITE OUTPUT TAPE 6,142,KEND,QT1,QT2,C10,YINY
```

Page 17

```
142 FORMAT(4HOKND'4,13H SLO CONV QT1F10.7,4H QT2F10.7,2H Y1PE10.3,
   1 5H YINY1PE10.3)
 24 DO 143 I=1,MP
143 COOK(I)=COOKIE(I,QT1,QT2)
    GO TO 228

C      FIND OUT IF RESULT IS SUFFICIENTLY ACCURATE. IF SO, END EXECUTION.
C      IF NOT, GO TO 145.

140 IJJ=1
    IF(ABSF(C10-YINY)-AHSF(ACCY*YINY))144,144,275
144 IF(ABSF(C9-YINY)-ABSF(ACCY*YINY))146,146,275

275 IJJ=2
146 DO 266 I=1,MP
266 Y(I)=(2.*(ETAPS(I)-ETANG(I)-ETA(I))/(ETAPS(I)-ETANG(I)+ETA(I)))**2
    TOT=0.0
    DO 267 I=1,M
267 TOT=TOT+(Y(I+1)+Y(I))*(ROP(I+1)-ROP(I))*0.5
    AVGE=TOT/(ROP(MP)-1.0)
    IF(AVGE-0.0100)255,255,277

277 IJJ=2
255 GO TO (278,145),IJJ

278 WRITE OUTPUT TAPE 6,147,KEND,YINY
147 FORMAT(7HO KEND='4,36H RESULT SUFFICIENTLY ACCURATE. YINY=1PE10.3)
 26 NEND=XMINOF(KEND+8,NEND)
    GO TO 228

145 GO TO (228,228,151,34),KWIT

C      FIND OUT IF THERE ARE OSCILLATIONS DECREASING TOO SLOWLY TO ALLOW
C      ATTAINMENT OF REQUIRED ACCURACY WITHIN 40 ITERATIONS.
C      IF SO, GO TO 159. IF NOT, GO TO 151.

 34 IF(A8-A9)148,148,149
148 IF(A9-A10)151,151,150
149 IF(A9-A10)150,150,151

150 IF(B8-B9)152,152,153
152 IF(B9-B10)151,151,154
153 IF(B9-B10)154,154,151

154 IF(C8-C9)155,155,156
155 IF(C9-C10)151,151,157
156 IF(C9-C10)157,157,151

157 AMA=(ABSF(A8-A9)+ABSF(A9-A10))/2.0
    AMB=(ABSF(C8-C9)+ABSF(C9-C10))/2.0
    IF(AMB*(AMB/AMA)**2-ACCY*YINY)151,151,159

151 WRITE OUTPUT TAPE 6,170,KEND,C10,YINY,KINS,AVGE
170 FORMAT(7HC KEND=I4,3H Y=1PE10.3,6H YINY=1PE10.3,20H ESTD. CYCLES T
   1O END I3,6H AVGE=0PF8.4)
270 GO TO 228

C      DECREASE MIXING FUNCTION.

159 QT1=QT1*0.9
    QT2=QT2*0.9
    DO 171 I=1,MP
171 COOK(I)=COOK(I)*0.9
```

Page 18

```
    WRITE OUTPUT TAPE 6,172,KEND,QT1,QT2
172 FORMAT( 5HCKEND I4,38H OSCILLATIONS DAMPING TOO SLOWLY. QT1=F10.7,
   1 5H QT2=F10.7)
 31 MEW=0
    MAD=2
    GO TO 228

228 RETURN
    END
```

Page 19

```
      FUNCTION COOKIE(I,QT1,QT2)                                        COOKIE

C      FUNCTION COOKIE IS USED TO COMPUTE THE MIXING FUNCTION.
C      IT IS CALLED BY THE MAIN PROGRAM AND BY SUBROUTINE ADJUST.

      DIMENSION X(401),XSQ(401),S(401),DXDS(401),ROP(401),SCOT(401),
     1 COOK(401),XI(401),DXIDS(401),ETA(401),ETAPS(401),ETANG(401),
     2 RHO(401),OMGAG(401),BETAG(401),ALFAG(401),PSIG(401),EPSG(401),
     3 Y(401),Z(401),SH(401)
      COMMON X,XSQ,S,DXDS,ROP,SCOT,COOK,XI,DXIDS,ETA,ETAPS,ETANG,RHO,
     1 OMGAG,BETAG,ALFAG,PSIG,EPSG,Y,Z,SH
      COMMON PI,SQTPI,VIPI,SAY,MODE,M,MP,DELTS,GAMMA,P13,P16,P17,YPOS,
     1 YNEG,NPRINT,KT1,KT2,LL,KEND
      COMMON LINK,BETH,EXY,EDY,N2,N22,NW,SW,SWA,BETAW,BETAWA,MACK,MIKE,
     1 SCRIT,SCRITA,LK,LKA,CRISS,CROSS,YST,AMU,THETA,KBD,MCD,MZET

      ZAQ=SQRTF(GAMMA*MINIF(P16,1.0))
      GO TO (100,200),MODE
  100 COOKIE=QT1*X(I)*EXPF(ZAQ*(1.0-1.0/X(I))) +QT2*XSQ(I)
      RETURN
  200 ROXI=SQRTF(X(I))
      COOKIE=QT1*ROXI*EXPF(ZAQ*(1.0-1.0/X(I))) +QT2*X(I)
      RETURN
      END
```

Page 20

```
      SUBROUTINE CHARGE                                                 CHARGE

C      SUBROUTINE CHARGE USES XI(1-MP), DXIDS(1-MP), AND ETA(1-MP) TO
C      CAUSE GENERATION OF CHARGE DENSITIES ETAPS(1-MP) AND ETANG(1-MP),
C      AND CURRENTS YPOS AND YNEG. THIS SUBROUTINE ASSUMES MAXWELLIAN
C      PARTICLES AND FINITE COLLECTED CURRENTS. IT IS CALLED BY THE MAIN
C      PROGRAM WHEN MCD = 1.

      DIMENSION IKRIT(3),IW(3),LOFK(3),BBETAW(3),SSW(3),MONK(3),SKRIT(3)
      DIMENSION RKRIT(3),BKRIT(3)
      DIMENSION X(401),XSQ(401),S(401),DXDS(401),ROP(401),SCOT(401),
     1 COOK(401),XI(401),DXIDS(401),ETA(401),ETAPS(401),ETANG(401),
     2 RHO(401),OMGAG(401),BETAG(401),ALFAG(401),PSIG(401),EPSG(401),
     3 Y(401),Z(401),SH(401)
      COMMON X,XSQ,S,DXDS,ROP,SCOT,COOK,XI,DXIDS,ETA,ETAPS,ETANG,RHO,
     1 OMGAG,BETAG,ALFAG,PSIG,EPSG,Y,Z,SH
      COMMON PI,SQTPI,VIPI,SAY,MODE,M,MP,DELTS,GAMMA,P13,P16,P17,YPOS,
     1 YNEG,NPRINT,KT1,KT2,LL,KEND
      COMMON LINK,BETH,EXY,EDY,N2,N22,NW,SW,SWA,BETAW,BETAWA,MACK,MIKE,
     1 SCRIT,SCRITA,LK,LKA,CRISS,CROSS,YST,AMU,THETA,KBD,MCD,MZET

      KKEND=KEND
      JSIGN=1
  105 GO TO (101,102),JSIGN
  101 ZETA=GAMMA
      GO TO 103
  102 ZETA=GAMMA*P16
  103 DO 106 I=1,MP
      BETAG(I)=XI(I)-DXIDS(I)*X(I)/(2.0*DXDS(I))
      OMGAG(I)=-DXIDS(I)/(2.0*X(I)*DXDS(I))
      GO TO (334,335),KBD
  334 Y(I)=BETAG(I)-OMGAG(I)*XSQ(MP)
      GO TO 106
  335 Y(I)=BETAG(I)
  106 CONTINUE
      GO TO (480,481),KBD
  481 GO TO (720,721),MODE
  720 BETAG(MP)=0.0
  480 Y(MP)=0.0
  721 NW=0
      NKR=0
      NOMOK=0
      IGN=1
      KLASH=1
      MAR=1
      NAQ=1

C      SEARCH INWARD FOR A POINT WHERE THE LOCUS OF EXTREMA ENTERS THE
C      FIRST QUADRANT OF THE (OMEGA, BETA) PLANE. IF ONE IS FOUND, GO TO
C      203. IF NOT, GO TO 204.

      DO 107 J=2,MP
      I=MP+1-J
      IF(OMGAG(I))107,107,111
  111 IF(Y(I))107,107,112
  107 CONTINUE
      GO TO 204

  112 INIT=I
      GO TO (315,316),MODE

      DO 126 I
      ALFAG(I)=(( [illegible] (I)+ZETA*ETA(I)*DXDS(I)/(X(I)*XSQ(I)))/2.0
```

Page 21

```
126 EPSG(I)=ALFAG(I)*EXPF(-BETAG(I))
    GO TO 205

316 DO 317 I=1,MP
    ALFAG(I)=DXIDS(I)+ZETA*ETA(I)*DXDS(I)/(2.0*X(I)*XSQ(I))
    Z(I)=EXPF(-BETAG(I))
317 EPSG(I)=ALFAG(I)*Z(I)
    GO TO 205

205 DO 200 J=1,INIT
    I=INIT+1-J
    IF(OMGAG(I))200,200,201
201 IF(Y(I))200,200,202
202 IF(I-M)380,381,381
380 IF(OMGAG(I+1))381,381,382
382 IF(Y(I+1))381,381,200
381 IF(ALFAG(I))203,460,460
200 CONTINUE
    GO TO 204

460 ID=I
    DO 461 J=2,ID
    I=ID+1-J
    IF(Y(I))464,465,465
465 IF(OMGAG(I))464,463,463
463 IF(ALFAG(I))462,461,461
461 CONTINUE
    GO TO 462

464 INIT=XMINOF(I,M-1)
    GO TO 205

462 KLASH=2
    IVAR=XMINOF(I,M-1)
    I=ID
    GO TO 203

C     FIND THE LOCATION SSW(N) IN THE NET COORDINATE SYSTEM S,
C     CORRESPONDING TO THE NTH TIME THE LOCUS OF EXTREMA ENTERS THE
C     FIRST QUADRANT.

203 L=1
    GO TO (206,206,440),MAR
206 IW(MAR)=I
    INIT=I
    N=MAR
    LEAD=3
    IF(OMGAG(I+1))471,471,473
471 LEAD=1
    IF(Y(I+1))472,472,473
472 LEAD=2
473 IF(I-M)117,116,116
116 IF(ALFAG(MP))290,290,117
290 IF(OMGAG(MP))117,313,313
313 IF(Y(MP))117,312,312
312 SSW(N)=S(MP)
    MONK(N)=2
    GO TO (338,340),KBD
338 BBETAW(N)=BETAG(MP)
    GO TO 228
117 GO TO (122,122,121),LEAD
122 SOMA=S(I)+POLATE(DELTS,OMGAG(I),OMGAG(I+1),XSQ(I)*ALFAG(I),XSQ(I+1
   1 )*ALFAG(I+1),1,6)
```

Page 22

```
    SSW(N)=SOMA
121 GO TO (118,119,119),LEAD
119 GO TO (342,343),KBD
342 Y1P=ALFAG(I)*(1.0-XSQ(MP)/XSQ(I))
    Y2P=ALFAG(I+1)*(1.0-XSQ(MP)/XSQ(I+1))
    GO TO 344
343 Y1P=ALFAG(I)
    Y2P=ALFAG(I+1)
344 SBET = S(I)+POLATE(DELTS,Y(I),Y(I+1),Y1P,Y2P,1,1)
    SSW(N)=SBET
118 GO TO (474,475,474),LEAD
475 IF(SOMA-SBET)476,477,477
476 SSW(N)=SOMA
    LEAD=1
    GO TO 474
477 SSW(N)=SBET
    LEAD=3
474 MONK(N)=LEAD
    IF(LEAD+KBD-5)230,340,230
230 BBETAW(N)=CUBIC(DELTS,BETAG(I),BETAG(I+1),ALFAG(I),ALFAG(I+1),
   1 SSW(N)-S(I),1)
    BBETAW(N)=MAX1F(0.0,BBETAW(N))
    GO TO 228
340 BBETAW(N)=0.0
228 GO TO (296,467),KLASH
467 INIT=IVAR
    KLASH=1
    GO TO 296

C     SEARCH INWARD FOR A MAXIMUM IN THE LOCUS OF EXTREMA. IF ONE IS
C     FOUND, GO TO 211.

296 DO 210 J=1,INIT
    I=INIT+1-J
    IF(ALFAG(I))210,210,390
390 KTEST=XMINOF(I-1,3)
    IF(KTEST)211,211,391
391 DO 392 KV=1,KTEST
    KZ=I-KV
    IF(ALFAG(KZ))210,210,392
392 CONTINUE
    GO TO 211
210 CONTINUE
    BETH=BETAG(1)
    SCRIT=0.0
    SH(1)=0.0
    GO TO (223,297),NAQ

C     FOR ALL NET POINTS L SATISFYING THE APPROPRIATE CONDITIONS, FIND
C     THE POINTS SH(L) IN THE NET COORDINATE SYSTEM S WHERE THE TANGENT
C     TO THE LOCUS OF EXTREMA AT S(L) CROSSES THE LOCUS OF EXTREMA.

211 IKRIT(MAR)=I
    N=MAR
    CY=DELTS*ALFAG(I)/(ALFAG(I)-ALFAG(I+1))
    SKRIT(N)=S(I)+CY
    BKRIT(N)=CUBIC(DELTS,BETAG(I),BETAG(I+1),ALFAG(I),ALFAG(I+1),CY,1)
    XCRIT=X(I)+(X(I+1)-X(I))*ALFAG(I)/(ALFAG(I)-ALFAG(I+1))
234 RKRIT(N)=1.0/XCRIT
    ICRIT=I
    I=ICRIT+1
    DO 135 K=1,ICRIT
    L=ICRIT+1-K
```

Page 23

```
    JACK=1
138 PSIG(I)=BETAG(I)-XI(L)-OMGAG(I)*XSQ(L)
    IF(PSIG(I))136,136,137
136 I=I+1
    IF(I-IW(MAR)-1)138,138,215

137 IF(I-ICRIT-1)330,330,139
330 JACK=2
    GO TO 136

139 Y1=PSIG(I-1)
    Y2=PSIG(I)
    Y1P=ALFAG(I-1)*(1.0-XSQ(L)/XSQ(I-1))
    Y2P=ALFAG(I)*(1.0-XSQ(L)/XSQ(I))
    CSI=POLATE(DELTS,Y1,Y2,Y1P,Y2P,JACK,2)
320 SH(L)=S(I-1)+CSI
    SH(L)=MAX1F(SH(L),SKRIT(MAR))
    CSI=SH(L)-S(I-1)
    IF(SH(L)-SSW(MAR))716,215,215
716 GO TO (325,326),MODE
325 IF(L-1)327,326,327
326 BETYL=CUBIC (DELTS,BETAG(I-1),BETAG(I),ALFAG(I-1),ALFAG(I),CSI,1)
    Z(L)=EXPF(-BETYL)
327 IF(ALFAG(L))217,135,135
217 IF(OMGAG(L)-OMGAG(L+1))135,135,402

C     SEARCH INWARD ALONG THE LOCUS OF EXTREMA TO FIND OUT WHETHER IT
C     CROSSES ITSELF IN THE FIRST QUADRANT. IF SO, CALCULATE THE POINTS
C     CRISS AND CROSS IN THE NET COORDINATE SYSTEM.

402 KLUE=0
    LASH=0
    MASH=0
    NASH=0

401 IF(MASH+NASH-2)453,454,453
453 IF(KLUE-6)410,410,411

454 IVY=I-2+LASH
    BECR=BETAG(IVY)
    GO TO 455

411 WRITE OUTPUT TAPE 6,412,KLUE,KEND
412 FORMAT(36H TROUBLE IN SUBROUTINE CHARGE  KLUE=I4,11H ITERATION I5)
    BECR=(Y1+Y2)/2.0
    GO TO 455

410 X1=OMGAG(I)
    Y1=BETAG(I)
    Y1P=XSQ(I)
    X2=OMGAG(I-1)
    Y2=BETAG(I-1)
    Y2P=XSQ(I-1)
    X3=OMGAG(L+1)
    Y3=BETAG(L+1)
    Y3P=XSQ(L+1)
    X4=OMGAG(L)
    Y4=BETAG(L)
    Y4P=XSQ(L)
    DEL12=X2-X1
    DEL34=X4-X3
    DX4=X4-X1
403 DY4=Y4-CUBIC(DEL12,Y1,Y2,Y1P,Y2P,DX4,1)
```

Page 24

```
    IF(DY4)135,135,218

218 GO TO (295,440,440),MAR
295 IF(IGN-1)441,441,440
441 DX1=X1-X3
    DY1=Y1-CUBIC(DEL34,Y3,Y4,Y3P,Y4P,DX1,1)
    IF(DY1)404,404,405
404 I=I+1
    KLUE=KLUE+1
    LASH=1
    MASH=1
    GO TO 401

405 DX2=X2-X3
    DY2=Y2-CUBIC(DEL34,Y3,Y4,Y3P,Y4P,DX2,1)
    IF(DY2)407,406,406
406 I=I-1
    KLUE=KLUE+1
    LASH=2
    NASH=1
    GO TO 401

407 DX3=X3-X1
    DY3=Y3-CUBIC(DEL12,Y1,Y2,Y1P,Y2P,DX3,1)
    IF(DY3)408,409,409
409 KLUE=KLUE+8
    GO TO 401

135 I=I-1
    BETH=BETYL
    GO TO (224,301),NAQ

408 DY3P=Y3P-CUBIC(DEL12,Y1,Y2,Y1P,Y2P,DX3,2)
    DY4P=Y4P-CUBIC(DEL12,Y1,Y2,Y1P,Y2P,DX4,2)
    XCR=POLATE(DEL34,DY3,DY4,DY3P,DY4P,1,3)
    BECR=CUBIC(DEL34,Y3,Y4,Y3P,Y4P,XCR,1)
455 Y1=BETAG(L)-BECR
    Y2=BETAG(L+1)-BECR
    CRISS=S(L)+POLATE(DELTS,Y1,Y2,ALFAG(L),ALFAG(L+1),1,4)
    Y1=BETAG(I-1)-BECR
    Y2=BETAG(I)-BECR
    CROSS=S(I-1)+POLATE(DELTS,Y1,Y2,ALFAG(I-1),ALFAG(I),1,5)
395 IF(CROSS-SSW(MAR))715,215,215
715 MAR=2
    NAQ=2
    IW(2)=L
    INIT=L
    SSW(2)=CRISS
    GO TO 296

440 IGN=IGN+1
    IF(IGN-8)457,400,400
457 MAR=1
    NAQ=1
    INIT=L
    DO 450 I=1,MP
450 Z(I)=EXPF(-BETAG(I))
    GO TO 296

215 GO TO (300,440),NAQ
300 LOFK(MAR)=L
    NOMOK=MAR
    INIT=L
```

```
      MAR=MAR+1
      GO TO 209

  204 NW=MAR-1
      NKR=MAR-1
      IF(XI(1))220,221,221

  220 LINK=5
      GO TO (336,337),KBO
  336 BETH=-XI(1)/(1.0/XSQ(MP)-1.0)
      GO TO 225
  337 BETH=0.0
      GO TO 225

  221 LINK=6
      BETH=XI(1)
      GO TO 225

  223 LINK=1
      NW=MAR
      NKR=MAR-1
      GO TO 225

  224 LINK=2
      NW=MAR
      NKR=MAR
      GO TO 225

  237 LINK=7
      NW=1
      NKR=1
      GO TO 225

  301 LINK=8
      NW=1
      NKR=2
      GO TO 225

  225 IF(NW)226,226,470
  470 MACK=MONK(NW)
      MIKE=MONK(1)
      NZ=(MACK-4)*MACK+5
      NZ2=(MIKE-4)*MIKE+5
      IF(MACK-1)245,246,245
  246 GO TO (247,247,400,400,400,245,247,247,400,400),LINK
  247 LINK=LINK+2
  245 IF(NW-1)226,226,251
  251 IF(MIKE-1)226,310,226
  310 IF(LINK-3)400,226,311
  311 IF(LINK-4)400,226,400

  400 GO TO 282

  226 EXY=EXPF(-BETH)
      EDY=EXY/SQTPI
      IF(NW-1)265,261,262
  261 SW=SSW(1)
      SWA=S(MP)+1.0
      BETAW=BBETAW(1)
      GO TO 265
  262 SW=SSW(2)
      SWA=SSW(1)
      BETAW=BBETAW(2)
```



```
      BETAWA=BBETAW(1)
      GO TO (374,282,372),MACK

  374 GO TO (375,265,265),MIKE
  375 IF(BETAWA-BETAW)265,265,376
  376 BETAW=BETAWA
      GO TO 265

  372 GO TO (282,373,373),MIKE
  373 IF(BETAW-BETAWA)265,265,371
  371 BETAW=BETAWA
      GO TO 265

  265 GO TO (266,267,266,267,267,267,303,304,303,304),LINK

  266 SCRIT=0.0
      IF(NKR-1)270,281,282
  281 SCRITA=SKRIT(1)
      GO TO 270
  267 IF(NKR-1)285,286,287
  285 IF(LINK-5)282,270,270
  286 SCRIT=SKRIT(1)
      GO TO 270
  287 SCRIT=SKRIT(2)
      SCRITA=SKRIT(1)
      GO TO 270

  303 IF(NKR-1)282,305,282
  305 SCRIT=0.0
      SCRITA=SKRIT(1)
      GO TO 275
  304 IF(NKR-2)282,306,282
  306 SCRIT=SKRIT(2)
      SCRITA=SKRIT(1)
      GO TO 275

  282 WRITE OUTPUT TAPE 6,283,KEND,JSIGN,LINK,NW,NKR,MACK,MIKE,IGN,
     1 SCRIT,SCRITA
  283 FORMAT(52H  TROUBLE IN SUBROUTINE CHARGE. EXECUTION TERMINATED
     1 I6,7I4,1P2E12.5 )
      SENSE LIGHT 1
      SENSE LIGHT 2
      RETURN

  270 IF(NOMOK-1)271,272,273
  271 LK=MP+1
      GO TO 275
  272 LK=LOFK(1)
      LKA=MP+1
      GO TO 275
  273 LK=LOFK(2)
      LKA=LOFK(1)
      GO TO 275

  275 KT1=KT1
      IF(IGN-1)446,446,447
  447 WRITE OUTPUT TAPE 6,448,IGN,JSIGN,KEND
  448 FORMAT(33H LOCUS OF EXTREMA CROSSES ITSELF I3,19H TIMES DURING PAR
     1T I2,14H OF ITERATION I5)
  446 GO TO (160,160,156,156),KT1
  156 IF(NKR)236,236,237
  236 WRITE OUYPUT TAPE 6,240,LINK,BETAG(1)
  240 FORMAT(6H LINK=I2,12H   BETAG(1)=1PE12.5)
```



```
      GO TO 160
  237 WRITE OUTPUT TAPE 6,241,LINK , BETH , (RKRIT(I),BKRIT(I),I=1,NKR)
  241 FORMAT(6H LINK=I2,6H BETH=1PE12.5,(7H RTRAP=1PE12.5,7H BTRAP=
     1 1PE12.5))
      GO TO 160

  160 GO TO (171,171,173,173,175,175,308,308,308,308),LINK

  171 CALL FIRST
      GO TO 700
  173 CALL SECOND
      GO TO 700
  175 CALL THIRD
      GO TO 700
  308 CALL FOURTH
      GO TO 700

  700 GO TO (701,702),JSIGN

  701 DO 705 I=1,MP
  705 ETAPS(I)=RHO(I)
      YPOS=YST
      IF(MZET-1)713,713,714
  713 JSIGN=2
      SHIFT=-PI6
      DO 706 I=1,MP
      XI(I)=XI(I)*SHIFT
      DXIDS(I)=DXIDS(I)*SHIFT
  706 ETA(I)=-ETA(I)
      GO TO 105

  702 DO 710 I=1,MP
  710 ETANG(I)=RHO(I)
      YNEG=YST
      DO 712 I=1,MP
      XI(I)=XI(I)/SHIFT
      DXIDS(I)=DXIDS(I)/SHIFT
  712 ETA(I)=-ETA(I)
  714 RETURN
      END
```



```
      FUNCTION CUBIC(DELTS,Y1,Y2,Y1P,Y2P,CSI,N)                         CUBIC
C     IF N=1, THIS SUBPROGRAM FINDS Y FOR X = CSI, ASSUMING THAT Y IS A
C     CUBIC WITH Y = Y1 AND SLOPE = Y1P AT X = 0, AND Y = Y2 AND SLOPE =
C     Y2P AT X = DELTS. IF N=2, THE DERIVATIVE OF Y AT X = CSI IS
C     CALCULATED.

      A=(3.0*(Y2-Y1)-DELTS*(2.0*Y1P+Y2P))/DELTS**2
      B=(DELTS*(Y1P+Y2P)-2.0*(Y2-Y1))/DELTS**3
      GO TO (10,11),N
   10 CUBIC=Y1+CSI*(Y1P+CSI*(A+CSI*B))
      RETURN
   11 CUBIC=Y1P+CSI*(2.0*A+CSI*3.0*B)
      RETURN
      END
```

Page 29

```
      FUNCTION POLATE(DELTS,Y1,Y2,Y1P,Y2P,JACK,JOE)                     POLATE
C     POLATE GENERATES A CUBIC WITH Y=Y1 AND SLOPE=Y1P AT XS=0, AND Y=Y2
C     AND SLOPE=Y2P AT XS=DELTS. IT THEN USES NEWTONS METHOD TO FIND A
C     ROOT IN THE INTERVAL (0,DELTS) IF JACK=1, IN THE INTERVAL
C     (-DELTS,0) IF JACK=2.
      DIMENSION Q(2)
      DIMENSION X(401),XSQ(401),S(401),DXDS(401),ROP(401),SCOT(401),
     1 COOK(401),XI(401),DXIDS(401),ETA(401),ETAPS(401),ETANG(401),
     2 RHO(401),OMGAG(401),BETAG(401),ALFAG(401),PSIG(401),EPSG(401),
     3 Y(401),Z(401),SH(401)
      COMMON X,XSQ,S,DXDS,ROP,SCOT,COOK,XI,DXIDS,ETA,ETAPS,ETANG,RHO,
     1 OMGAG,BETAG,ALFAG,PSIG,EPSG,Y,Z,SH
      COMMON PI,SQTPI,VIPI,SAY,MODE,M,MP,DELTS,GAMMA,PI3,PI6,PI7,YPOS,
     1 YNEG,NPRINT,KT1,KT2,LL,KEND
      COMMON LINK,BETH,EXY,EDY,N2,N22,NA,SWA,BETA,BETAWA,MACK,MIKE,
     1 SCRIT,SCRITA,LK,LKA,CRISS,CROSS,XST,AMU,THETA,KBD,MCD,MZET
      K=1
      DUMP1=X(K)
      DUMP2=OMGAG(K)
      DUMP3=BETAG(K)
      DUMP4=ALFAG(K)
      DUMP5=PSIG(K)
      DUMP6=Y(K)
      DDELTS=DELTS
      DY1=Y1
      DY2=Y2
      DY1P=Y1P
      DY2P=Y2P
      JJACK=JACK
      JJOE=JOE
      CTEST=DELTS*FLOATF(JACK-1)
      GO TO (35,36),JACK
   35 IF(Y1/Y1P)37,36,39
   37 IF(Y2/Y2P)39,36,36
   38 IF(Y2/Y2P)36,36,40
   39 XN=-Y1/Y1P
      GO TO 41
   40 XN=DELTS-Y2/Y2P
   41 IF(XN)36,36,42
   42 IF(DELTS-XN)36,36,27
   36 XN=DELTS*Y1/(Y1-Y2)
      IF(Y1*Y2)51,17,51
   51 IF(XN+CTEST)25,25,26
   25 GO TO (21,27),JACK
   26 IF(XN+CTEST-DELTS)27,21,21
   21 WRITE OUTPUT TAPE 6,14,DELTS,Y1,Y2,Y1P,Y2P,XN,JACK,JOE
   14 FORMAT(16H POLATE TROUBLE,1P6E12.5,2I3)
      POLATE=MAX1F(-0.5*DELTS,MIN1F(XN,(1.5-2.0*FLOATF(JACK-1))*DELTS))
      RETURN
   27 XS=XN
      DO 10 I=1,10
      DO 50 J=1,2
   50 Q(J)=CUBIC(DELTS,Y1,Y2,Y1P,Y2P,XS,J)
      XT=XS-Q(1)/Q(2)
   13 IF(ABSF(XS-XT)/DELTS-1.0E-05)15,15,10
   10 XS=XT
```

Page 30

```
   15 IF(XT+CTEST)31,31,32
   31 GO TO (17,21),JACK
   32 IF(XT+CTEST-DELTS)34,17,17
   21 POLATE=-0.999*DELTS
      RETURN
   17 POLATE=XN
      RETURN
   34 POLATE=XT
      RETURN
      END
```

Page 31

```
      SUBROUTINE CHAMON                                                 CHAMON
C     SUBROUTINE CHAMON CARRIES OUT A COMPUTATION ANALOGOUS TO THAT OF
C     SUBROUTINE CHARGE IN THE CASE OF SIMPLIFIED PARTICLE DISTRIBUTIONS,
C     AS FOLLOWS.
C     MCD=2 - ATTRACTED PARTICLES MONO-ENERGETIC.
C     MCD=3 - SAME AS MCD=2 FOR ATTRACTED SPECIES. REPELLED PARTICLE
C             DENSITY DESCRIBED BY BOLTZMANN FACTOR.
C     MCD=4 - ATTRACTED PARTICLES AT ZERO ENERGY. CYLINDRICAL PROBE ONLY
C     MCD=5 - SAME AS MCD=4 FOR ATTRACTED SPECIES. SAME AS MCD=3 FOR
C             REPELLED SPECIES.
C     IF MCD = 4 OR 5, THIS SUBROUTINE MUST BE RUN WITH KBD=2 AND MODE=2
      DIMENSION OMEGA(2),SSW(2),XW(2),RW(2)
      DIMENSION X(401),XSQ(401),S(401),DXDS(401),ROP(401),SCOT(401),
     1 COOK(401),XI(401),DXIDS(401),ETA(401),ETAPS(401),ETANG(401),
     2 RHO(401),OMGAG(401),BETAG(401),ALFAG(401),PSIG(401),EPSG(401),
     3 Y(401),Z(401),SH(401)
      COMMON X,XSQ,S,DXDS,ROP,SCOT,COOK,XI,DXIDS,ETA,ETAPS,ETANG,RHO,
     1 OMGAG,BETAG,ALFAG,PSIG,EPSG,Y,Z,SH
      COMMON PI,SQTPI,VIPI,SAY,MODE,M,MP,DELTS,GAMMA,PI3,PI6,PI7,YPOS,
     1 YNEG,NPRINT,KT1,KT2,LL,KEND
      COMMON LINK,BETH,EXY,EDY,N2,N22,NA,SWA,BETA,BETAWA,MACK,MIKE,
     1 SCRIT,SCRITA,LK,LKA,CRISS,CROSS,XST,AMU,THETA,KBD,MCD,MZET
      KEND=KEND
      IF(KEND)330,401,330
  401 GO TO (330,404,405,521,522),MCD
  404 WRITE OUTPUT TAPE 6,406
  406 FORMAT(86X34HATTRACTED PARTICLES MONO-ENERGETIC)
      GO TO (535,536),MODE
  405 WRITE OUTPUT TAPE 6,407
  407 FORMAT(44X76HATTRACTED PARTICLES MONO-ENERGETIC, PROBE DOES NOT AB
     1SORB REPELLED PARTICLES)
      GO TO (535,536),MODE
  535 ENG=4.0/PI
      SONG=SQRTF(ENG)
      GO TO 330
  536 ENG=PI/4.0
      GO TO 330
  521 WRITE OUTPUT TAPE 6,523
  523 FORMAT(86X34HATTRACTED PARTICLES AT ZERO ENERGY)
      ENG=0.0
      GO TO 330
  522 WRITE OUTPUT TAPE 6,524
  524 FORMAT(44X76HATTRACTED PARTICLES AT ZERO ENERGY, PROBE DOES NOT AB
     1SORB REPELLED PARTICLES)
      ENG=0.0
      GO TO 330
  330 IF(P13)402,320,320
  320 BETH=XI(1)
      EXY=EXPF(-BETH)
      EDY=EXY/SQTPI
      CALL THIRD
```

Page 32

```
      GO TO 458
  402 DO 106 I=1,MP
      BETAG(I)=XI(I)-DXIDS(I)*X(I)/(2.0*DXDS(I))
      OMGAG(I)=-DXIDS(I)/(2.0*X(I)*DXDS(I))
      GO TO (505,506),KBD
  505 Y(I)=BETAG(I)-OMGAG(I)*XSQ(MP)
      GO TO 106
  506 Y(I)=BETAG(I)
  106 CONTINUE
      GO TO (315,316),MODE
  315 DO 126 I=1,MP
  126 ALFAG(I)=(DXIDS(I)+GAMMA*ETA(I)*DXDS(I)/(X(I)*XSQ(I)))/2.0
      GO TO 101
  316 DO 317 I=1,MP
  317 ALFAG(I)=DXIDS(I)+GAMMA*ETA(I)*DXDS(I)/(2.0*X(I)*XSQ(I))
      GO TO 101
  101 NKR=0
      INIT=M
  205 IF(INIT)204,204,206
  206 DO 600 J=1,INIT
      I=INIT+1-J
      IF(OMGAG(I))200,200,207
  207 IF(Y(I))200,200,202
  202 IF(BETAG(I)-ENG)200,200,413
  413 IF(BETAG(I+1)-ENG)201,201,200
  200 IF(OMGAG(I))600,600,601
  601 IF(OMGAG(I+1))602,602,600
  602 IF(BETAG(I)-ENG)600,600,603
  600 CONTINUE
      GO TO 204
  201 NKR=NKR+1
      INIT=I-2
      GO TO(415,415,416),NKR
  415 FRA=(ENG-BETAG(I+1))/(BETAG(I)-BETAG(I+1))
      OMEGA(NKR)=OMGAG(I+1)+(OMGAG(I)-OMGAG(I+1))*FRA
      GO TO 605
  603 NKR=NKR+1
      INIT=I-2
      GO TO (604,604,416),NKR
  604 FRA=-OMGAG(I+1)/(OMGAG(I)-OMGAG(I+1))
      OMEGA(NKR)=0.0
      GO TO 605
  605 SSW(NKR)=S(I+1)+(S(I)-S(I+1))*FRA
      XW(NKR)=X(I+1)+(X(I)-X(I+1))*FRA
      RW(NKR)=1.0/XW(NKR)
      GO TO (820,500),KBC
  820 SL=ENG/XSQ(MP)
      IF(OMEGA(NKR)-SL)500,500,501
  500 GO TO (205,417),NKR
  417 IF(OMEGA(1)-OMEGA(2))419,419,205
  419 NKR=1
```

```
      GO TO 205

  901 NKR=NKR-1
      GO TO 205

  416 WRITE OUTPUT TAPE 6,208
  208 FORMAT(66H  LOCUS OF MAXIMA AFFECTS COMPUTATION AT THREE OR MORE L
     1OCATIONS. EXECUTION TERMINATED)
      SENSE LIGHT 1
      SENSE LIGHT 2
      RETURN

  204 NTRAP=1
  482 INOY=INIT+1
      DO 483 J=1,INOY
      I=INOY+1-J
      IF(ALFAG(I))483,483,484
  484 IF(ALFAG(I+1))485,485,483
  485 IF(BETAG(I))541,541,540
  541 IF(BETAG(I+1))483,483,540
  483 CONTINUE
      GO TO 481

  540 NTRAP=2
      CY=DELTS*ALFAG(I)/(ALFAG(I)-ALFAG(I+1))
      BTRAP =  CUBIC(DELTS,BETAG(I),BETAG(I+1),ALFAG(I),ALFAG(I+1),CY,1)
      XTRAP=X(I)+(X(I+1)-X(I))*ALFAG(I)/(ALFAG(I)-ALFAG(I+1))
      RTRAP=1.0/XTRAP
      GO TO 481

  481 PL=ENG-XI(1)
      IF(NKR)489,489,490
  489 OMA=PL
      GO TO 491
  490 OMA=MIN1F(OMEGA(NKR),PL)
  491 OMA=MAX1F(OMA,0.0)
      GO TO (507,508),KHD
  507 SL=ENG/XSQ(MP)
      OMA=MIN1F(OMA,SL)

  508 KT1=KT1
      GO TO (160,160,156,156),KT1
  156 IF(NKR)236,236,237
  236 WRITE OUTPUT TAPE 6,241,PL,SL,BETAG(1)
  241 FORMAT(4H PL=1PE11.4,4H SL=1PE11.4,9H BETAG(1) 1PE11.4,
     1 (3H RW  1PE11.4,6H OMEGA 1PE11.4 ))
      GO TO (160,487),NTRAP
  237 WRITE OUTPUT TAPE 6,241,PL,SL,BETAG(1),(RW(I),OMEGA(I),I=1,NKR)
      GO TO (160,487),NTRAP

  487 WRITE OUTPUT TAPE 6,488,RTRAP,BTRAP
  488 FORMAT(76X8H  RTRAP=1PE14.7,8H  BTRAP=1PE14.7)
      GO TO 160

  160 DO 420 L=1,MP
      LL=L
      RL=(ENG-XI(L))/XSQ(L)
      IF(NKR-1)421,422,423
  421 OMB=RL
      GO TO 430

  422 IF(S(L)-SSW(1))424,421,421
  424 OMB=MIN1F(RL,OMEGA(1))
```



```
      GO TO 430

  423 IF(S(L)-SSW(2))425,422,422
  425 OMB=MIN1F(RL,OMEGA(2))
      GO TO 430

  430 OMB=MAX1F(OMB,0.0)
      GO TO (510,511),KBO
  510 OMB=MIN1F(OMB,SL)
  511 IF(OMA-OMB)431,432,433

  433 WRITE OUTPUT TAPE 6,480,OMA,OMB,LL,RL,NKR,KEND
  480 FORMAT(27H OMA GREATER THAN OMB, OMA=1PE14.7,5H OMB=1PE14.7,4H LL=
     1 I4,4H RL=1PE14.7,5H NKR=I2,6H KEND=I4)
      OMA=OMB
      GO TO 432

  431 IF(OMA)434,434,435

  434 IF(OMB-RL)436,437,437
  436 GO TO (438,439),MODE

  438 RHO(L) =(SQRTF(ENG-XI(L))-SQRTF(XSQ(L)*(RL-OMB)))/SQNG
      GO TO 420
  439 RHO(L) = 2.0*VIPI*ATANF(SQRTF(OMB/(RL-OMB)))
      GO TO 420

  437 GO TO (440,441),MODE

  440 RHO(L) = SQRTF(ENG-XI(L))/SQNG
      GO TO 420
  441 RHO(L) = 1.0
      GO TO 420

  435 IF(OMB-RL)442,443,443

  442 GO TO (444,445),MODE
  444 RHO(L) =(0.5*(SQRTF(ENG-XI(L))+SQRTF(XSQ(L)*(RL-OMA)))
     1 -SQRTF(XSQ(L)*(RL-OMB)) )/SQNG
      GO TO 420
  445 RHO(L) = VIPI*(2.0*ATANF(SQRTF(OMB/(RL-OMB)))-ATANF(SQRTF(OMA/(RL-
     1 OMA))))
      GO TO 420

  443 GO TO (446,447),MODE

  446 RHO(L) =(0.5*(SQRTF(ENG-XI(L))+SQRTF(XSQ(L)*(RL-OMA))))/SQNG
      GO TO 420
  447 RHO(L) = 1.0-VIPI*ATANF(SQRTF(OMA/(RL-OMA)))
      GO TO 420

  432 IF(OMA)448,449,449

  448 RHO(L) = 0.0
      GO TO 420

  449 IF(OMB-RL)450,451,451

  450 GO TO (452,453),MODE

  452 RHO(L) =(0.5*(SQRTF(ENG-XI(L))-SQRTF(XSQ(L)*(RL-OMA))))/SQNG
      GO TO 420
  453 RHO(L) = VIPI*ATANF(SQRTF(OMA/(RL-OMA)))
```



```
      GO TO 420

  451 GO TO (454,455),MODE

  454 RHO(L) = 0.5*SQRTF(ENG-XI(L))/SQNG
      GO TO 420
  455 RHO(L) = 0.5
      GO TO 420

  420 CONTINUE
      GO TO (456,457),MODE

  456 YST =0.5*SQTPI*OMA/SQNG
      GO TO 321
  457 IF(MCD-3)530,530,531
  530 YST =2.0*SAY*SQRTF(OMA)
      GO TO 321
  531 YST=2.0*SAY*SQRTF(OMA*PI6)
      GO TO 321

  321 IF(PI3)458,322,322

  458 DO 325 I=1,MP
  325 ETAPS(I)=RHO(I)
      YPOS=YST
      IF(MZET-1)331,331,332
  331 DO 326 I=1,MP
      XI(I)=-XI(I)*PI6
      DXIDS(I)=-DXIDS(I)*PI6
  326 ETA(I)=-ETA(I)
      IF(PI3)323,402,402

  323 BETH=XI(1)
      EXY=EXPF(-BETH)
      EDY=EXY/SQTPI
      CALL THIRD
      GO TO 322

  322 DO 327 I=1,MP
  327 ETANG(I)=RHO(I)
      YNEG=YST
      DO 328 I=1,MP
      XI(I)=-XI(I)/PI6
      DXIDS(I)=-DXIDS(I)/PI6
  328 ETA(I)=-ETA(I)
  332 RETURN
      END
```



```
      FUNCTION CAL(JACK,SA,SB,N1,N2)                                    CAL
C       IF N1=1, INTEGRATION STARTS ON A NET POINT
C       IF N1=2, INTEGRATION MAY START OFF A NET POINT
C       IF N1=3, INTEGRATION MAY START OFF A NET POINT AND INTEGRAND
C            BECOMES IMAGINARY OUTSIDE LIMIT OF INTEGRATION.
C       SIMILARLY FOR N2.
C       IF JACK=1 THEN CONTRIBUTION IS TO CHARGE DENSITY
C       IF JACK=2 THEN CONTRIBUTION IS TO COLLECTED CURRENT
C       SA AND SB ARE LIMITS OF INTEGRATION

      DIMENSION X(401),XSQ(401),S(401),DXDS(401),ROP(401),SCOT(401),
     1 COOK(401),XI(401),DXIDS(401),ETA(401),ETAPS(401),ETANG(401),
     2 RHO(401),OMGAG(401),BETAG(401),ALFAG(401),PSIG(401),EPSG(401),
     3 Y(401),Z(401),SH(401)
      COMMON X,XSQ,S,DXDS,ROP,SCOT,COOK,XI,DXIDS,ETA,ETAPS,ETANG,RHO,
     1 OMGAG,BETAG,ALFAG,PSIG,EPSG,Y,Z,SH
      COMMON PI,SQTPI,VIPI,SAY,MODE,M,MP,DELTS,GAMMA,PI3,PI6,PI7,YPOS,
     1 YNEG,NPRINT,KT1,KT2,LL,KEND
      COMMON LINK,BETH,EXY,EDY,N2,N22,NW,SW,SWA,BETAW,BETAWA,MACK,MIKE,
     1 SCRIT,SCRITA,LK,LKA,CMISS,CROSS,YST,AMU,THETA,KBO,MCD

      SUM=0.0
      JJACK=JACK
      DSA=SA
      DSB=SB
      NN1=N1
  384 NN2=N2
      GO TO (385,386),MODE
  386 NN1=XMINOF(NN1,2)
      NN2=XMINOF(NN2,2)

  385 GO TO (201,202,203),NN1
  201 IA=SA/DELTS+1.1
      IAX=IA
      GO TO 205
  202 IA=SA/DELTS+1.0
      IAX=XMAXOF(IA-1,1)
      GO TO 205
  203 IA=SA/DELTS+2.0
      IAX=IA
      GO TO 205

  205 GO TO (206,207,208),NN2
  206 IB=SB/DELTS+1.1
      IBX=IB
      GO TO 210
  207 IB=SB/DELTS+2.0
      IBX=XMINOF(IB+1,MP)
      GO TO 210
  208 IB=SB/DELTS+1.0
      IBX=IB
      GO TO 210
  210 GO TO (211,225),JACK

  211 DO 212 I=IAX,IBX
      IF(I-LL)221,222,221
  221 PSIG(I)=BETAG(I)-XI(LL)-OMGAG(I)*XSQ(LL)
      IF(PSIG(I))213,214,214
  213 IF(S(I)-SA)215,216,216
  216 IF(SB-S(I))215,217,217

  217 IF(MKXX-KEND-1)320,321,320
```

Page 37

```
320 IF(XABSF(I-LL)-4)321,321,353
321 KCAJ=KCAJ+1
    GO TO 222
353 WRITE OUTPUT TAPE 6,218,I,LL,PSIG(I),KCAJ,KEND
218 FORMAT(39H BETAG VS OMGAG CROSSES ITS TANGENT  I= I3,4H LL=I3,
   1 9H PSIG(I)= 1PE14.7,6H KCAJ=I4,6H KEND=I4)
    MXXX=KEND+1
    KCAJ=0
    GO TO 222

215 GO TO (290,293),MODE
290 Y(I)=-EPSG(I)*SQRTF(-PSIG(I))
    GO TO 212

222 PSIG(I)=0.0
    GO TO (315,293),MODE
315 Y(I)=0.0
    GO TO 212

214 GO TO (292,293),MODE
292 Y(I)=EPSG(I)*SQRTF(PSIG(I))
    GO TO 212
293 IF(OMGAG(I))294,315,294
294 QTPI=ATANF(SQRTF(ABSF(PSIG(I)/(XSQ(LL)*OMGAG(I)))))
    Y(I)=SIGNF(1.0,OMGAG(I))*EPSG(I)*(1.5707963-SIGNF(QTPI,PSIG(I)))
    GO TO 212
212 CONTINUE
    GO TO 230

225 GO TO (296,297),MODE

296 DO 226 I=IAX,IBX
226 Y(I)=EPSG(I)*OMGAG(I)
    GO TO 230

297 DO 310 I=IAX,IBX
310 Y(I)=SIGNF(1.0,OMGAG(I))*EPSG(I)*SQRTF(ABSF(OMGAG(I)))
    GO TO 230

230 MIKY=1
    ARINA=0.0
    ARINB=0.0
    GO TO (231,232,233),NN1
231 YA=Y(IA)
    AREAA=0.0
    GO TO 234
232 IF(IBX-IA-1)360,360,326
360 IF(IBX-IA)325,325,362
362 IF(IA-IAX)325,325,363
325 YA=Y(IA)+(Y(IA+1)-Y(IA))*(SA-S(IA))/DELTS
    AREAA=(S(IA+1)-SA)*(YA+Y(IA+1))*0.5
    GO TO 327
363 CSI=(SA-S(IA))/DELTS
    CTA=0.5*(Y(IA+1)-Y(IA-1))
    CTB=0.5*(Y(IA+1)+Y(IA-1))-Y(IA)
    YA=Y(IA)+CSI*(CTA+CSI*CTB)
    AREAA=DELTS*(Y(IA)*(1.0-CSI)+CTA/2.0*(1.0-CSI**2)+CTB/3.0*(1.0-CSI
   1 **3))
    GO TO 327
326 CSI=(SA-S(IA+1))/DELTS
    CTA=0.5*(Y(IA+2)-Y(IA))
    CTB=0.5*(Y(IA+2)+Y(IA))-Y(IA+1)
    YA=Y(IA+1)+CSI*(CTA+CSI*CTB)
```

Page 38

```
    AREAA=-CSI*(Y(IA+1)+CSI*(CTA/2.0+CSI*CTB/3.0))*DELTS
    ARINA=(Y(IA+1)+CTA/2.0+CTB/3.0)*DELTS
    MIKY=MIKY+1
327 IA=IA+1
    GO TO 234
233 YA=0.0
    AREAA=(S(IA)-SA)*Y(IA)*0.5
    GO TO 234

234 GO TO (236,237,238),NN2
236 YB=Y(IB)
    AREAB=0.0
    GO TO 239
237 IF(IB-IAX-1)369,369,342
369 IF(IBX-IB)341,341,365
365 IF(IB-IAX)341,341,366
341 YB=Y(IB-1)+(Y(IB)-Y(IB-1))*(SB-S(IB-1))/DELTS
    AREAB=(SB-S(IB-1))*(Y(IB-1)+YB)*0.5
    GO TO 343
366 CSI=(SB-S(IB))/DELTS
    CTA=0.5*(Y(IB+1)-Y(IB-1))
    CTB=0.5*(Y(IB+1)+Y(IB-1))-Y(IB)
    YB=Y(IB)+CSI*(CTA+CSI*CTB)
    AREAB=DELTS*(Y(IB)*(CSI+1.0)+CTA/2.0*(CSI**2-1.0)+CTB/3.0*(CSI**3
   1 +1.0))
    GO TO 343
342 CSI=(SB-S(IB-1))/DELTS
    CTA=0.5*(Y(IB)-Y(IB-2))
    CTB=0.5*(Y(IB)+Y(IB-2))-Y(IB-1)
    YB=Y(IB-1)+CSI*(CTA+CSI*CTB)
    AREAB=CSI*(Y(IB-1)+CSI*(CTA/2.0+CSI*CTB/3.0))*DELTS
    ARINB=(Y(IB-1)-CTA/2.0+CTB/3.0)*DELTS
    MIKY=MIKY+1
343 IB=IB-1
    GO TO 239
238 YB=0.0
    AREAB=(SB-S(IB))*Y(IB)*0.5
    GO TO 239

239 IF(IB-IA)241,242,243
241 IF(SB-SA)246,247,248
246 ISA=SA/DELTS
    ISB=SB/DELTS
    IF(ISB-ISA)282,286,282

286 IF(NXXX-KEND-1)355,356,355
356 NNN=NNN+1
    GO TO 247
355 WRITE OUTPUT TAPE 6,249,SA,SB,LL,KEND,NNN
249 FORMAT(33H SB A LITTLE SMALLER THAN SA, SA= 1PE14.7,4H SB=1PE14.7,
   1 4H LL=I3,6H KEND=I4,5H NNN=I4)
    NXXX=KEND+1
    NNN=0
    GO TO 247

282 IF(LXXX-KEND-1)351,350,351
350 KKK=KKK+1
    GO TO 247
351 WRITE OUTPUT TAPE 6,284,SA,SB,LL,KEND,KKK
284 FORMAT(32H SB IS MUCH SMALLER THAN SA, SA=1PE14.7,4H SB=1PE14.7,
   1 4H LL=I3,6H KEND=I4,5H KKK=I4)
    LXXX=KEND+1
    KKK=0
```

Page 39

```
    GO TO 247

247 SUM=0.0
    GO TO 275

248 IF(IAX-IB)370,371,371
370 IV=IB
    GO TO 375
371 IF(IBX-IA)372,372,373
373 IV=IA
375 CTA=0.5*(Y(IV+1)-Y(IV-1))
    CTB=0.5*(Y(IV+1)+Y(IV-1))-Y(IV)
    CSI1=(SA-S(IV))/DELTS
    CSI2=(SB-S(IV))/DELTS
    SUM=DELTS*(Y(IV)*(CSI2-CSI1)+CTA/2.0*(CSI2**2-CSI1**2)+CTB/3.0*(
   1 CSI2**3-CSI1**3))
    GO TO 275
372 SUM=(YA+YB)*(SB-SA)/2.0
    GO TO 275

242 SUM=AREAA+AREAB
    GO TO 275

243 SUM=AREAA+AREAB
    IF(IB-IA-2)251,261,261
251 GO TO (345,346,347),MIKY
345 SUM=SUM+0.5*(Y(IA)+Y(IB))*DELTS
    GO TO 275
346 SUM=SUM+ARINA+ARINB
    GO TO 275
347 SUM=SUM+0.5*(ARINA+ARINB)
    GO TO 275

261 NUM=IB-IA
    IF(NUM-3)332,333,340
340 IF(NUM-5)334,335,335

332 SUM=SUM+(Y(IA)+4.0*Y(IB-1)+Y(IB))*DELTS/3.0
    GO TO 275

333 SUM=SUM+(Y(IA)+Y(IB)+3.0*(Y(IA+1)+Y(IB-1)))*DELTS*0.375
    GO TO 275

334 SUM=SUM+(9.0*(Y(IA)+Y(IB))+28.0*(Y(IA+1)+Y(IB-1))+22.0*Y(IB-2))*
   1 DELTS/24.0
    GO TO 275

335 SUM=SUM+(9.0*(Y(IA)+Y(IB))+28.0*(Y(IA+1)+Y(IB-1))+23.0*(Y(IA+2)+Y(
   1 IB-2)))*DELTS/24.0
    IF(NUM-5)275,275,336

336 IAP=IA+3
    IBP=IB-3
    STA=0.0
    DO 337 I=IAP,IBP
337 STA=STA+Y(I)
    SUM=SUM+STA*DELTS

275 GO TO (271,272),JACK
271 GO TO (300,301),MODE
300 CAL=-SUM/SQTPI
    RETURN
301 CAL=-SUM/PI
```

Page 40

```
    RETURN
272 GO TO (302,303),MODF
302 CAL=-SUM
    RETURN
303 CAL=-SUM*2.0/SQTPI
    RETURN

C     REASON FOR NEGATIVE SIGNS IN STATEMENTS 300 TO 303  IS THAT
C     INTEGRATION ALONG S IS IN OPPOSITE SENSE TO INTEGRATION ALONG BETA

      END
```

Page 41

```
      FUNCTION COEFT(EX)                                                COEFT

C     COEFT(EX) = 0.5 * ROOT OF PI * EXPF(EX*EX) * (1.0-ERF(EX))
C     ERF(EX) = 2.0/ROOT OF PI * INTEGRAL FROM 0 TO EX OF EXPF(-T*T)*DT
C     APPROXIMATION USED FOR ERF(EX) IS GIVEN ON PAGE 169 OF HASTINGS
C     (REF. 17).

C     THIS SUBPROGRAM GIVES A RESULT WHICH HAS A RELATIVE ACCURACY OF
C     .00002 OR BETTER, DEPENDING ON ARGUMENT.
C     IF EX IS LESS THAN 2.21, HASTINGS APPROXIMATION IS USED.
C     OTHERWISE, ASYMPTOTIC SERIES IS USED.
C     IF EX IS BETWEEN 1.72 AND 2.82, A CORRECTION TERM IS ADDED.

      DEX=EX
      IF(EX-1.72)9,9,11
    9 CORT=0.0
      GO TO 15

   11 IF(EX-2.82)13,10,10
   10 SUM=0.5/EX
      TERM=SUM
      PROD=-2.0*EX**2
      DO 12 N=1,50
      TERMO=TERM
      TERM=TERM*FLOATF(2*N-1)/PROD
      IF(ABSF(TERM)-ABSF(TERMO))40,40,41
   40 SAM=SUM+TERM
      IF(SUM-SAM)12,16,12
   12 SUM=SAM
   41 SUM=SUM-0.5*TERMO
   16 COEFT=SUM
      RETURN

   13 IF(EX-2.21)20,21,21
   20 CORT=(EX-1.72)*(-.00000804-.00004920*(EX-1.72))

   15 QA=1.0/(1.0+.3275911*EX)
   99 COEFT=CORT+((((.94064607*QA-1.2878225)*QA+1.2596951)*QA-.25212867)
     1 *QA+.22583685)*QA
      RETURN

   21 VIN=0.5/EX
      V=VIN/EX
      IF(EX-2.345)25,26,26
   25 CENT=472.5
      CORT=-.00001401+(EX-2.28)*(-.00030640+.00165700*(EX-2.28))
      GO TO 30

   26 IF(EX-2.55)27,28,28
   27 CENT=945.-V*5197.5
      CORT=-.00000197+(EX-2.44)*(.00017400-.00087900*(EX-2.44))
      GO TO 30

   28 IF(EX-2.738)29,31,31
   29 CENT=945.-V*(10395.-V*67567.5)
      CORT=.00000040+(EX-2.64)*(-.00005370+.00029000*(EX-2.64))
      GO TO 30

   31 CENT=945.-V*(10395.-V*(135135.-V*1013512.5))
      CORT=.00002630*(EX-2.82)

   30 COEFT=CORT+(((((-CENT*V+105.0)*V-15.0)*V+3.0)*V-1.0)*V+1.0)*VIN
      RETURN
      END
```

Page 43

```
      SUBROUTINE SECOND                                                 SECOND
                                                                         SPHERE

C     THIS SUBROUTINE COMPUTES CHARGE DENSITY RHO(1-MP) AND COLLECTED
C     CURRENT YST, FOR A  SPHERICAL  PROBE, UNDER THE FOLLOWING
C     CONDITIONS.
C     LOCUS OF EXTREMA ENTERS FIRST QUADRANT BY CROSSING  BETA AXIS, AND
C     DOES NOT CROSS ITSELF IN THIS QUADRANT. LINK = 3 OR 4.

      DIMENSION X(401),XSQ(401),S(401),DXDS(401),ROP(401),SCOT(401),
     1 COOK(401),XI(401),DXIDS(401),ETA(401),ETAPS(401),ETANG(401),
     2 RHO(401),OMGAG(401),BETAG(401),ALFAG(401),PSIG(401),EPSG(401),
     3 Y(401),Z(401),SH(401)
      COMMON X,XSQ,S,DXDS,ROP,SCOT,COOK,XI,DXIDS,ETA,ETAPS,ETANG,RHO,
     1 OMGAG,BETAG,ALFAG,PSIG,EPSG,Y,Z,SH
      COMMON PI,SQTPI,VIPI,SAY,MODE,M,MP,DELTS,GAMMA,PI3,PI6,PI7,YPOS,
     1 YNEG,NPRINT,KT1,KT2,LL,KEND
      COMMON LINK,BETH,EXY,EDY,N2,N22,NW,SW,SWA,BETAW,BETAWA,MACK,MIKE,
     1 SCRIT,SCRITA,LK,LKA,CRISS,CROSS,YST,AMU,THETA,KBD
      GO TO (171,72),MODE
   72 WRITE OUTPUT TAPE 6,73
   73 FORMAT(49H0 WRONG SUBROUTINES BEING USED. EXECUTION DELETED )
      CALL EXIT
  171 GO TO (173,565),NW
  565 GO TO (566,173,173),MIKE
  566 EMAA=EXPF(-BETAWA)/SQTPI
  173 EMA=EXPF(-BETAW)/SQTPI
      N1=LINK-2
      DO 540 L=1,MP
      LL=L
      RHO(L)=DUO(BETH,EDY)
      IF(S(L)-SW)541,541,536
  541 RHO(L)=RHO(L)+UNO(BETAW,EMA)
      IF(S(L)-SH(1))543,544,544
  544 RHO(L)=RHO(L)+CAL(1,SH(1),S(L),N1,1)-CAL(1,S(L),SW,1,2)
      GO TO 540
  543 RHO(L)=RHO(L)-CAL(1,SH(1),SW,2,2)
      IF(S(L)-SCRIT)545,546,546
  545 RHO(L)=RHO(L)-2.0*CAL(1,SH(L),SH(1),3,2)
      GO TO 540
  546 RHO(L)=RHO(L)-2.0*CAL(1,S(L),SH(1),1,2)
      GO TO 540

  536 RHO(L)=RHO(L)-UNO(BETAW,EMA)+CAL(1,SH(1),SW,N1,2)
      GO TO (548,549),NW
  548 IF(XI(L))538,537,537
  537 RHO(L)=RHO(L)+EXPF(-XI(L))
      GO TO 540
  538 RHO(L)=RHO(L)+2.0*UNO(0.0,SAY)-2.0*TRE(0.0)
      GO TO 540

  549 GO TO (550,556,556),MIKE
  550 IF(L-LK)537,537,552
  552 IF(S(L)-SWA)553,548,548
  553 RHO(L)=RHO(L)+2.0*UNO(BETAWA,EMAA)
      GO TO 554

  556 IF(L-LK)548,548,557
  557 IF(S(L)-SWA)558,538,538
  558 RHO(L)=RHO(L)+2.0*UNO(0.0,SAY)-2.0*TRE(0.0)+2.0*TRE(BETAWA)
      GO TO 554

  554 IF(S(L)-SCRITA)524,525,525
```

Page 43

```
      SUBROUTINE FIRST                                                  FIRST
                                                                         SPHERE

C     THIS SUBROUTINE COMPUTES CHARGE DENSITY RHO(1-MP) AND COLLECTED
C     CURRENT YST, FOR A  SPHERICAL  PROBE, UNDER THE FOLLOWING
C     CONDITIONS.
C     LOCUS OF EXTREMA ENTERS FIRST QUADRANT BY CROSSING OMEGA AXIS, AND
C     DOES NOT CROSS ITSELF IN THIS QUADRANT. LINK = 1 OR 2.

      DIMENSION X(401),XSQ(401),S(401),DXDS(401),ROP(401),SCOT(401),
     1 COOK(401),XI(401),DXIDS(401),ETA(401),ETAPS(401),ETANG(401),
     2 RHO(401),OMGAG(401),BETAG(401),ALFAG(401),PSIG(401),EPSG(401),
     3 Y(401),Z(401),SH(401)
      COMMON X,XSQ,S,DXDS,ROP,SCOT,COOK,XI,DXIDS,ETA,ETAPS,ETANG,RHO,
     1 OMGAG,BETAG,ALFAG,PSIG,EPSG,Y,Z,SH
      COMMON PI,SQTPI,VIPI,SAY,MODE,M,MP,DELTS,GAMMA,PI3,PI6,PI7,YPOS,
     1 YNEG,NPRINT,KT1,KT2,LL,KEND
      COMMON LINK,BETH,EXY,EDY,N2,N22,NW,SW,SWA,BETAW,BETAWA,MACK,MIKE,
     1 SCRIT,SCRITA,LK,LKA,CRISS,CROSS,YST,AMU,THETA,KBD
      GO TO (171,72),MODE
   72 WRITE OUTPUT TAPE 6,73
   73 FORMAT(49H0 WRONG SUBROUTINES BEING USED. EXECUTION DELETED )
      CALL EXIT
  171 N1=LINK
      DO 560 L=1,MP
      LL=L
      RHO(L)=UNO(0.0,SAY)+DUO(BETH,EDY)-TRE(0.0)
      IF(S(L)-SH(1))552,554,554
  552 RHO(L)=RHO(L)-CAL(1,SH(1),SW,2,N2)
      IF(S(L)-SCRIT)551,553,553
  551 RHO(L)=RHO(L)-2.0*CAL(1,SH(L),SH(1),3,2)+TRE(BETAW)
      GO TO 560
  553 RHO(L)=RHO(L)-2.0*CAL(1,S(L),SH(1),1,2)+TRE(BETAW)
      GO TO 560
  554 IF (S(L)-SW)555,555,556
  555 RHO(L)=RHO(L)+CAL(1,SH(1),S(L),N1,1)-CAL(1,S(L),SW,1,N2)
     1 +TRE(BETAW)
      GO TO 560
  556 RHO(L)=RHO(L)+CAL(1,SH(1),SW,N1,2)-TRE(BETAW)
      IF(L-LK)560,560,542
  542 IF(S(L)-SWA)543,560,560
  543 RHO(L)=RHO(L)+2.0*TRE(BETAWA)
      IF(S(L)-SCRITA)544,545,545
  544 RHO(L)=RHO(L)-2.0*CAL(1,SH(L),SWA,3,N22)
      GO TO 560
  545 RHO(L)=RHO(L)-2.0*CAL(1,S(L),SWA,1,N22)
      GO TO 560
  560 CONTINUE
      YST=(BETH-XI(1)+1.0)*EXY+CAL(2,SH(1),SW,N1,N2)
      GO TO (562,561),KBD
  562 YST=YST+(1.0-(BETAW+1.0)*EXPF(-BETAW))/XSQ(MP)
  561 RETURN
      END
```

Page 44

```
  524 RHO(L)=RHO(L)-2.0*CAL(1,SH(L),SWA,3,N22)
      GO TO 540
  525 RHO(L)=RHO(L)-2.0*CAL(1,S(L),SWA,1,N22)
      GO TO 540
  540 CONTINUE
      YST=CAL(2,SH(1),SW,N1,2)+(BETH-XI(1)+1.0)*EXY
      RETURN
      END
```

```
      SUBROUTINE THIRD                                          THIRD
                                                                 SPHERE
C     SUBROUTINE THIRD COMPUTES THE CHARGE DENSITY RHO(1-MP) AND THE
C     COLLECTED CURRENT YST FOR AN ATTRACTING SPHERICAL PROBE (LINK = 5)
C     OR A REPELLING SPHERICAL PROBE (LINK = 6) IN THE CASE WHERE ANY
C     POTENTIAL BARRIERS WHICH MAY EXIST DO NOT AFFECT THE AMOUNT OF
C     COLLECTED CURRENT ( DO NOT AFFECT THE SHAPE OF THE JI VS. E CURVE)

      DIMENSION X(401),XSQ(401),S(401),DXDS(401),ROP(401),SCOT(401),
     1 COOK(401),XI(401),DXIDS(401),ETA(401),ETAPS(401),ETANG(401),
     2 RHO(401),OMGAG(401),BETAG(401),ALFAG(401),PSIG(401),EPSG(401),
     3 Y(401),Z(401),SH(401)
      COMMON X,XSQ,S,DXDS,ROP,SCOT,COOK,XI,DXIDS,ETA,ETAPS,ETANG,RHO,
     1 OMGAG,BETAG,ALFAG,PSIG,EPSG,Y,Z,SH
      COMMON PI,SQTPI,VIPI,SAY,MODE,M,MP,DELTS,GAMMA,PI3,PI6,PI7,YPOS,
     1 YNEG,NPRINT,KT1,KT2,LL,KEND
      COMMON LINK,BETH,EXY,EDY,N2,N22,NW,SW,SWA,BETAW,BETAWA,MACK,MIKE,
     1 SCRIT,SCRITA,LK,LKA,CRISS,CROSS,YST,AMU,THETA,KBD,MCD,MZET

  760 GO TO (175,72),MODE
   72 WRITE OUTPUT TAPE 6,73
   73 FORMAT(49H0 WRONG SUBROUTINES BEING USED. EXECUTION DELETED )
      CALL EXIT

  175 GO TO (586,585,585),MACK
  586 EMA=EXPF(-BETAW)/SQTPI
  585 DO 730 L=1,MP
      LL=L
      RHO(L)=0.0
      GO TO (200,177,575,177,575),MCD
  200 IF(LINK-5)176,176,177

  176 RHO(L)=UNO(0.0,SAY)+DUO(BETH,EDY)-TRE(0.0)-TRE(BETH)
      GO TO 178

  177 SKIT=SQRTF(MAX1F(0.0,(XI(1)-XI(L))))
      RHO(L)=EDY*(SCOT(L)*COEFT(SKIT/SCOT(L))-COEFT(SKIT))
      IF(MCD-1)201,201,575
  201 GO TO (576,575,575),MACK
  576 IF(L-LK)571,571,577
  577 IF(S(L)-SW)578,575,575

  578 RHO(L)=RHO(L)+2.0*UNO(BETAW,EMA)
      IF(S(L)-SCRIT)580,580,581
  580 RHO(L)=RHO(L)-2.0*CAL(1,SH(L),SW,3,2)
      GO TO 730
  581 RHO(L)=RHO(L)-2.0*CAL(1,S(L),SW,1,2)
      GO TO 730

  575 IF(XI(L))572,571,571
  571 RHO(L)=RHO(L)+EXPF(-XI(L))
      GO TO 730
  572 RHO(L)=RHO(L)+2.0*UNO(0.0,SAY)-2.0*TRE(0.0)
      IF(MCD-1)202,202,730
  202 GO TO (720,178,179),MACK

  178 IF(L-LK)730,730,742
  742 IF(S(L)-SW)732,720,720
  732 RHO(L)=RHO(L)+2.0*TRE(BETAW)
      IF(S(L)-SCRIT)736,737,737
  736 RHO(L)=RHO(L)-2.0*CAL(1,SH(L),SW,3,N2)
      GO TO 730
```



```
  737 RHO(L)=RHO(L)-2.0*CAL(1,S(L),SW,1,N2)
      GO TO 730
  720 IF(L-LKA)730,730,722
  722 IF(S(L)-SWA)723,730,730
  723 RHO(L)=RHO(L)+2.0*TRE(BETAWA)
      IF(S(L)-SCRITA)726,727,727
  726 RHO(L)=RHO(L)-2.0*CAL(1,SH(L),SWA,3,N22)
      GO TO 730
  727 RHO(L)=RHO(L)-2.0*CAL(1,S(L),SWA,1,N22)
      GO TO 730
  730 CONTINUE

      GO TO (181,204,205,204,205),MCD
  181 IF(LINK-5)180,180,204
  180 GO TO (750,751),KBD
  750 YST=(1.0-(BETH+1.0)*EXY)/XSQ(MP)+(BETH-XI(1)+1.0)*EXY
      RETURN
  751 YST=1.0-XI(1)
      RETURN
  204 YST=EXY
      RETURN
  205 YST=0.0
      RETURN
      END
```



```
      SUBROUTINE FOURTH                                         FOURTH
                                                                 SPHERE
C     THIS SUBROUTINE COMPUTES CHARGE DENSITY RHO(1-MP) AND COLLECTED
C     CURRENT YST, FOR A  SPHERICAL  PROBE, UNDER THE FOLLOWING
C     CONDITIONS.
C     LOCUS OF EXTREMA CROSSES ITSELF IN THE FIRST QUADRANT OF THE
C     (OMEGA,BETA) PLANE.

      DIMENSION X(401),XSQ(401),S(401),DXDS(401),ROP(401),SCOT(401),
     1 COOK(401),XI(401),DXIDS(401),ETA(401),ETAPS(401),ETANG(401),
     2 RHO(401),OMGAG(401),BETAG(401),ALFAG(401),PSIG(401),EPSG(401),
     3 Y(401),Z(401),SH(401)
      COMMON X,XSQ,S,DXDS,ROP,SCOT,COOK,XI,DXIDS,ETA,ETAPS,ETANG,RHO,
     1 OMGAG,BETAG,ALFAG,PSIG,EPSG,Y,Z,SH
      COMMON PI,SQTPI,VIPI,SAY,MODE,M,MP,DELTS,GAMMA,PI3,PI6,PI7,YPOS,
     1 YNEG,NPRINT,KT1,KT2,LL,KEND
      COMMON LINK,BETH,EXY,EDY,N2,N22,NW,SW,SWA,BETAW,BETAWA,MACK,MIKE,
     1 SCRIT,SCRITA,LK,LKA,CRISS,CROSS,YST,AMU,THETA,KBD
      GO TO (308,72),MODE
   72 WRITE OUTPUT TAPE 6,73
   73 FORMAT(49H0 WRONG SUBROUTINES BEING USED. EXECUTION DELETED )
      CALL EXIT
  308 IF(LINK-8)360,360,361
  360 NI=LINK-6
      GO TO 362
  361 NI=LINK-8
      EMA=EXPF(-BETAW)/SQTPI
  362 DO 320 L=1,MP
      LL=L
      IF(LINK-8)365,365,366

  365 RHO(L)=UNO(0.0,SAY)+DUO(BETH,EDY)-TRE(0.0)
      IF(S(L)-SW)321,321,322
  321 RHO(L)=RHO(L)+TRE(BETAW)
      GO TO 323
  322 RHO(L)=RHO(L)-CAL(1,SH(1),CRISS,NI,2)+CAL(1,CROSS,SW,2,2)
     1 -TRE(BETAW)
      GO TO 320

  366 RHO(L)=DUO(BETH,EDY)
      IF(S(L)-SW)381,381,382
  381 RHO(L)=RHO(L)+UNO(BETAW,EMA)
      GO TO 323
  382 RHO(L)=RHO(L)-UNO(BETAW,EMA)+CAL(1,SH(1),CRISS,NI,2)
     1 +CAL(1,CROSS,SW,2,2)
      IF(XI(L))385,386,385
  386 RHO(L)=RHO(L)+EXPF(-XI(L))
      GO TO 320
  385 RHO(L)=RHO(L)+2.0*UNO(0.0,SAY)-2.0*TRE(0.0)
      GO TO 320

  323 IF(S(L)-CROSS)328,328,326
  328 RHO(L)=RHO(L)-CAL(1,CROSS,SW,2,N2)
      GO TO 320
  326 RHO(L)=RHO(L)+CAL(1,SH(1),CRISS,NI,2)+CAL(1,CROSS,S(L),2,1)
     1 -CAL(1,S(L),SW,1,N2)
      GO TO 320
  328 IF(S(L)-SH(1))330,332,332
  330 RHO(L)=RHO(L)-CAL(1,SH(1),CRISS,2,2)
      IF(S(L)-SCRIT)329,331,331
  329 RHO(L)=RHO(L)-2.0*CAL(1,SH(L),SH(1),3,2)
      GO TO 320
```



```
  331 RHO(L)=RHO(L)-2.0*CAL(1,S(L),SH(1),1,2)
      GO TO 320
  332 IF(S(L)-CRISS)334,334,335
  334 RHO(L)=RHO(L)+CAL(1,SH(1),S(L),NI,1)-CAL(1,S(L),CRISS,1,2)
      GO TO 320
  335 RHO(L)=RHO(L)+CAL(1,SH(1),CRISS,NI,2)
      IF(S(L)-SCRITA)337,338,338
  337 RHO(L)=RHO(L)-2.0*CAL(1,SH(L),CROSS,3,2)
      GO TO 320
  338 RHO(L)=RHO(L)-2.0*CAL(1,S(L),CROSS,1,2)
      GO TO 320
  320 CONTINUE
      YST=(BETH-XI(1)+1.0)*EXY+CAL(2,SH(1),CRISS,NI,2)
     1 +CAL(2,CROSS,SW,2,N2)
      IF(LINK-8)367,367,700
  367 GO TO (370,700),KBD
  370 YST=YST+(1.0-(BETAW+1.0)*EXPF(-BETAW))/XSQ(MP)
  700 RETURN
      END
```

```
      FUNCTION UNO (A,EMA)                                              UNO
C     UNO = (1.0/ROOT OF PI)* INTEGRAL FROM A TO INFINITY OF
C        DBETA*EXPF(-BETA)*SQRTF(BETA-XI)
C     EMA=EXPF(-A)/SQTPI
      DIMENSION X(401),XSQ(401),S(401),DXDS(401),ROP(401),SCOT(401),
     1 COOK(401),XI(401),DXIDS(401),ETA(401),ETAPS(401),ETANG(401),
     2 RHO(401),OMGAG(401),BETAG(401),ALFAG(401),PSIG(401),EPSG(401),
     3 Y(401),Z(401),SH(401)
      COMMON X,XSQ,S,DXDS,ROP,SCOT,COOK,XI,DXIDS,ETA,ETAPS,ETANG,RHO,
     1 OMGAG,BETAG,ALFAG,PSIG,EPSG,Y,Z,SH
      COMMON PI,SQTPI,VIPI,SAY,MODE,M,MP,DELTS,GAMMA,PI3,PI6,PI7,YPOS,
     1 YNEG,NPRINT,KT1,KT2,LL,KEND
      COMMON LINK,BETH,EXY,EDY,N2,N22,NW,SW,SWA,BETAW,BETAWA,MACK,MIKE,
     1 SCRIT,SCRITA,LK,LKA,CRISS,CROSS,YST,AMU,THETA,KBD,MCD,MZET,HALT
      DUMMY=OMGAG(1)
      DUMMY=BETAG(1)
      DUMMY=ALFAG(1)
      AA=A
      TEST=A-XI(LL)
      IF(TEST)503,304,504
  503 IF(TEST/XI(LL)+1.0E-06)213,213,212
  213 IF(LXXX-KEND-1)210,211,210
  211 KKK=KKK+1
      GO TO 212
  210 WRITE OUTPUT TAPE 6,505,XI(LL),A,LL,KKK,KEND
  505 FORMAT(20H UNO NEG SQRT XI(LL)1PE14.7,3H A=1PE14.7,4H LL=I3,
     1 5H KKK=I4,6H KEND=I5)
      LXXX=KEND+1
      KKK=1
      GO TO 212
  212 TEST=0.0
  304 UNO=0.88622695*EMA
      RETURN
  504 EX=SQRTF(TEST)
  305 UNO=(EX+COEFT(EX))*EMA
      RETURN
      END
```



```
      FUNCTION DUO(A,EDY)                                               DUO
C     DUO = (1.0/ROOT OF PI)* INTEGRAL FROM A TO INFINITY OF
C        DBETA*EXPF(-BETA)*SQRTF(BETA-XI-XSQ*(BETA-XI(1)))
C     EDY=EXPF(-A)/SQTPI
      DIMENSION X(401),XSQ(401),S(401),DXDS(401),ROP(401),SCOT(401),
     1 COOK(401),XI(401),DXIDS(401),ETA(401),ETAPS(401),ETANG(401),
     2 RHO(401),OMGAG(401),BETAG(401),ALFAG(401),PSIG(401),EPSG(401),
     3 Y(401),Z(401),SH(401)
      COMMON X,XSQ,S,DXDS,ROP,SCOT,COOK,XI,DXIDS,ETA,ETAPS,ETANG,RHO,
     1 OMGAG,BETAG,ALFAG,PSIG,EPSG,Y,Z,SH
      COMMON PI,SQTPI,VIPI,SAY,MODE,M,MP,DELTS,GAMMA,PI3,PI6,PI7,YPOS,
     1 YNEG,NPRINT,KT1,KT2,LL,KEND
      COMMON LINK,BETH,EXY,EDY,N2,N22,NW,SW,SWA,BETAW,BETAWA,MACK,MIKE,
     1 SCRIT,SCRITA,LK,LKA,CRISS,CROSS,YST,AMU,THETA,KBD,MCD,MZET,HALT
      AA=A
      DUMMY=OMGAG(1)
      DUMMY=BETAG(1)
      DUMMY=ALFAG(1)
      IF(LL-1)501,502,501
  502 DUO=0.0
      RETURN
  501 DENOM=1.0-XSQ(LL)
      CAPPA=(XI(LL)-(XSQ(LL) *XI(1)))/DENOM
      TEST=A-CAPPA
      IF(TEST)503,304,504
  503 IF(TEST/CAPPA+1.0E-06)213,213,212
  213 IF(LXXX-KEND-1)210,211,210
  211 KKK=KKK+1
      GO TO 212
  210 WRITE OUTPUT TAPE 6,505,CAPPA,A,LL,KKK,KEND
  505 FORMAT(20H DUO NEG SQRT CAPPA=1PE14.7,3H A=1PE14.7,4H LL=I3,
     1 5H KKK=I4,6H KEND=I5)
      LXXX=KEND+1
      KKK=1
      GO TO 212
  212 TEST=0.0
  304 DUO=SCOT(LL)*0.88622695*EDY
      RETURN
  504 EX=SQRTF(TEST)
  306 DUO=SCOT(LL)*(EX+COEFT(EX))*EDY
      RETURN
      END
```



```
      FUNCTION TRE(A)                                                   TRE
C     TRE=(1.0/ROOT OF PI)*INTEGRAL FROM A TO AMDA OF
C        DBETA*EXPF(-BETA)* SQRTF(BETA-XI-BETA*XSQ/XSQ(MP))
      DIMENSION X(401),XSQ(401),S(401),DXDS(401),ROP(401),SCOT(401),
     1 COOK(401),XI(401),DXIDS(401),ETA(401),ETAPS(401),ETANG(401),
     2 RHO(401),OMGAG(401),BETAG(401),ALFAG(401),PSIG(401),EPSG(401),
     3 Y(401),Z(401),SH(401)
      COMMON X,XSQ,S,DXDS,ROP,SCOT,COOK,XI,DXIDS,ETA,ETAPS,ETANG,RHO,
     1 OMGAG,BETAG,ALFAG,PSIG,EPSG,Y,Z,SH
      COMMON PI,SQTPI,VIPI,SAY,MODE,M,MP,DELTS,GAMMA,PI3,PI6,PI7,YPOS,
     1 YNEG,NPRINT,KT1,KT2,LL,KEND
      COMMON LINK,BETH,EXY,EDY,N2,N22,NW,SW,SWA,BETAW,BETAWA,MACK,MIKE,
     1 SCRIT,SCRITA,LK,LKA,CRISS,CROSS,YST,AMU,THETA,KBD
      AA=A
  413 GO TO (414,404),KBD
  414 IF(MP-LL)405,404,405
  404 TRE=0.0
      RETURN
  405 IF(XI(LL))401,401,402
  402 WRITE OUTPUT TAPE 6,403,A,LL
  403 FORMAT(19H TRE XI POSITIVE A=1PE14.7,4H LL=I3)
      GO TO 404
  401 EMU=(XSQ(LL)/XSQ(MP))-1.0
      AMDA=-XI(LL)/EMU
      TEST=AMDA-A
      IF(TEST)410,411,411
  410 WRITE OUTPUT TAPE 6,412,LL,AMDA,A,EMU
  412 FORMAT(16H TRE NEG SQRT LLI3,5H AMDA1PE14.7,2H A1PE14.7,4H EMU1PE1
     14.7)
      GO TO 404
  411 SM=SQRTF(TEST)
  406 TRE=(SQRTF(EMU)/SQTPI)*(SM*EXPF(-A)-EXPF(-AMDA)*SDFN(SM))
      RETURN
      END
```



```
      FUNCTION SDFN(T)                                                  SDFN
C     SDFN(T)=INTEGRAL FROM 0 TO T OF EXPF(X**2)*DX
C     IF T IS BETWEEN 0 AND 4.5, TERM-BY-TERM INTEGRATION ON TAYLOR
C          SERIES IS CARRIED OUT.
C     IF T IS BETWEEN 4.5 AND 9, ASYMPTOTIC SERIES IS USED.
C     IF T IS LESS THAN 0 OR GREATER THAN 9, EXECUTION IS TERMINATED.
C     THIS SUBPROGRAM IS CALLED BY FUNCTION TRE.
      DT=T
      IF(T-9.0)10,10,11
   11 WRITE OUTPUT TAPE 6,12,T
   12 FORMAT(42H EXECUTION TERMINATED BY FUNCTION SDFN. T=1PE14.7)
      SENSE LIGHT 1
      SENSE LIGHT 2
      RETURN
   10 IF(T-4.5)13,13,14
   13 IF(T)11,16,16
   16 TSQ=T**2
      SUM=T
      QEY=T
      DO 15 M=2,100
      MM=2*M
      QEY=QEY*TSQ*FLOATF(MM-3)/FLOATF((M-1)*(MM-1))
      SAM=SUM+QEY
      IF(SAM-SUM)15,21,15
   15 SUM=SAM
      GO TO 11
   14 TSQ=T**2
      TOT=2.0*TSQ
      SUM=1.0
      QEY=1.0
      LIMIT=0.5*TSQ
      DO 30 M=1,LIMIT
      QEY=QEY*FLOATF(2*M-1)/TOT
      SUM=SUM+QEY
      IF(SUM*1.0E-07-QEY)30,30,32
   30 CONTINUE
      GO TO 11
   32 RT=EXPF(TSQ)*SUM/(2.0*T)
      SUM=RT
      GO TO 21
   21 SDFN=SUM
      RETURN
      END
```

Page 53

```
      SUBROUTINE FIRST                                                  FIRST
                                                                        CYLINDER
C     THIS SUBROUTINE COMPUTES CHARGE DENSITY RHO(1-MP) AND COLLECTED
C     CURRENT YST, FOR A CYLINDRICAL PROBE, UNDER THE FOLLOWING
C     CONDITIONS.
C     LOCUS OF EXTREMA ENTERS FIRST QUADRANT BY CROSSING OMEGA AXIS, AND
C     DOES NOT CROSS ITSELF IN THIS QUADRANT, LINK = 1 OR 2.

      DIMENSION X(401),XSQ(401),S(401),DXDS(401),ROP(401),SCOT(401),
     1 COOK(401),XI(401),DXIDS(401),ETA(401),ETAPS(401),ETANG(401),
     2 RHO(401),OMGAG(401),BETAG(401),ALFAG(401),PSIG(401),EPSG(401),
     3 Y(401),Z(401),SH(401)
      COMMON X,XSQ,S,DXDS,ROP,SCOT,COOK,XI,DXIDS,ETA,ETAPS,ETANG,RHO,
     1 OMGAG,BETAG,ALFAG,PSIG,EPSG,Y,Z,SH
      COMMON PI,SQTPI,VIPI,SAY,MODE,M,MP,DELTS,GAMMA,PI3,PI6,PI7,YPOS,
     1 YNEG,NPRINT,KT1,KT2,LL,KEND
      COMMON LINK,BETH,EXY,EDY,N2,N22,NW,SW,SWA,BETAW,BETAWA,MACK,MIKE,
     1 SCRIT,SCRITA,LK,LKA,CRISS,CROSS,YST,AMU,THETA,KBD
      GO TO (72,171),MODE
   72 WRITE OUTPUT TAPE 6,73
   73 FORMAT(49H0 WRONG SUBROUTINES BEING USED, EXECUTION DELETED )
      CALL EXIT
  171 NI=LINK
      ECY=EXY/PI
      DO 560 L=1,MP
      LL=L
      RHO(L)=-DYO(BETH,ECY)+TRY(0.0)
      IF(S(L)-SH(1))552,554,554

  552 RHO(L)=RHO(L)+CAL(1,SH(1),SW,2,N2)
      IF(S(L)-SCRIT)551,553,553
  551 RHO(L)=RHO(L)+2.0*CAL(1,SH(L),SH(1),3,2)-TRY(BETAW)+Z(L)
      GO TO 560
  553 RHO(L)=RHO(L)+2.0*CAL(1,S(L),SH(1),1,2)-TRY(BETAW)+Z(L)
      GO TO 560

  554 IF (S(L)-SW)555,555,556
  555 RHO(L)=RHO(L)-CAL(1,SH(1),S(L),NI,1)+CAL(1,S(L),SW,1,N2)
     1 -TRY(BETAW)+Z(L)
      GO TO 560

  556 RHO(L)=RHO(L)-CAL(1,SH(1),SW,NI,2)+TRY(BETAW)
      IF(L-LK)570,570,542
  542 IF(S(L)-SWA)543,570,570
  570 GO TO (572,573),KBD
  572 IF(L-MP)571,560,560
  571 RHO(L)=RHO(L)+EXPF(-XI(L)/(1.0-XSQ(L)/XSQ(MP)))
      GO TO 560
  573 RHO(L)=RHO(L)+1.0
      GO TO 560

  543 RHO(L)=RHO(L)-2.0*TRY(BETAWA)+Z(L)
      IF(S(L)-SCRITA)544,545,545
  544 RHO(L)=RHO(L)+2.0*CAL(1,SH(L),SWA,3,N22)
      GO TO 560
  545 RHO(L)=RHO(L)+2.0*CAL(1,S(L),SWA,1,N22)

  560 CONTINUE

      RH=SQRTF(BETH-XI(1))
      YST=2.0*EDY*(RH+COEFT(RH))+CAL(2,SH(1),SW,NI,N2)
      GO TO (575,576),KBD
```

Page 54

```
  575 RW=SQRTF(BETAW)
      YST=YST+(1.0-2.0*EXPF(-BETAW)*SAY*(RW+COEFT(RW)))/X(MP)
  576 RETURN
      END
```

Page 55

```
      SUBROUTINE SECOND                                                 SECOND
                                                                        CYLINDER
C     THIS SUBROUTINE COMPUTES CHARGE DENSITY RHO(1-MP) AND COLLECTED
C     CURRENT YST, FOR A CYLINDRICAL PROBE, UNDER THE FOLLOWING
C     CONDITIONS.
C     LOCUS OF EXTREMA ENTERS FIRST QUADRANT BY CROSSING  BETA AXIS, AND
C     DOES NOT CROSS ITSELF IN THIS QUADRANT, LINK = 3 OR 4.

      DIMENSION X(401),XSQ(401),S(401),DXDS(401),ROP(401),SCOT(401),
     1 COOK(401),XI(401),DXIDS(401),ETA(401),ETAPS(401),ETANG(401),
     2 RHO(401),OMGAG(401),BETAG(401),ALFAG(401),PSIG(401),EPSG(401),
     3 Y(401),Z(401),SH(401)
      COMMON X,XSQ,S,DXDS,ROP,SCOT,COOK,XI,DXIDS,ETA,ETAPS,ETANG,RHO,
     1 OMGAG,BETAG,ALFAG,PSIG,EPSG,Y,Z,SH
      COMMON PI,SQTPI,VIPI,SAY,MODE,M,MP,DELTS,GAMMA,PI3,PI6,PI7,YPOS,
     1 YNEG,NPRINT,KT1,KT2,LL,KEND
      COMMON LINK,BETH,EXY,EDY,N2,N22,NW,SW,SWA,BETAW,BETAWA,MACK,MIKE,
     1 SCRIT,SCRITA,LK,LKA,CRISS,CROSS,YST,AMU,THETA,KBD
      GO TO (72,171),MODE
   72 WRITE OUTPUT TAPE 6,73
   73 FORMAT(49H0 WRONG SUBROUTINES BEING USED, EXECUTION DELETED )
      CALL EXIT
  171 ECY=EXY/PI
      NI=LINK-2
      DO 540 L=1,MP
      LL=L
      RHO(L)=-DYO(BETH,ECY)
      IF(S(L)-SW)541,541,536

  541 RHO(L)=RHO(L)+Z(L)
      IF(S(L)-SH(1))543,544,544
  544 RHO(L)=RHO(L)-CAL(1,SH(1),S(L),NI,1)+CAL(1,S(L),SW,1,2)
      GO TO 540
  543 RHO(L)=RHO(L)+CAL(1,SH(1),SW,4,2)
      IF(S(L)-SCRIT)545,546,546
  545 RHO(L)=RHO(L)+2.0*CAL(1,SH(L),SH(1),3,2)
      GO TO 540
  546 RHO(L)=RHO(L)+2.0*CAL(1,S(L),SH(1),1,2)
      GO TO 540

  536 RHO(L)=RHO(L)-CAL(1,SH(1),SW,NI,2)
      GO TO (548,549),NW
  548 IF(XI(L))538,537,537
  537 RHO(L)=RHO(L)+EXPF(-XI(L))
      GO TO 540

  538 GO TO (560,561),KBD
  560 RHO(L)=RHO(L)+2.0*TRY(0.0)
      IF(L-MP)539,540,540
  539 RHO(L)=RHO(L)+EXPF(-XI(L)/(1.0-XSQ(L)/XSQ(MP)))
      GO TO 540
  561 RHO(L)=RHO(L)+1.0
      GO TO 540

  549 GO TO (550,556,556),MIKE

  550 IF(L-LK)537,537,552
  552 IF(S(L)-SWA)553,548,548
  553 RHO(L)=RHO(L)+Z(L)
      GO TO 554

  556 IF(L-LK)548,548,557
```

Page 56

```
  557 IF(S(L)-SWA)558,538,538
  558 RHO(L)=RHO(L)+2.0*(TRY(0.0)-TRY(BETAWA))+Z(L)
      GO TO 554

  554 IF(S(L)-SCRITA)524,525,525
  524 RHO(L)=RHO(L)+2.0*CAL(1,SH(L),SWA,3,N22)
      GO TO 540
  525 RHO(L)=RHO(L)+2.0*CAL(1,S(L),SWA,1,N22)

  540 CONTINUE

      RH=SQRTF(BETH-XI(1))
      YST=CAL(2,SH(1),SW,NI,2)+2.0*EDY*(RH+COEFT(RH))
      RETURN
      END
```

SUBROUTINE THIRD — THIRD CYLINDER

```
      SUBROUTINE THIRD
C       SUBROUTINE THIRD COMPUTES THE CHARGE DENSITY RHO(1-MP) AND THE
C       COLLECTED CURRENT VST FOR AN ATTRACTING CYLINDRICAL PROBE (LINK=8)
C       OR A REPELLING CYLINDRICAL PROBE (LINK=6) IN THE CASE WHERE ANY
C       POTENTIAL BARRIERS WHICH MAY EXIST DO NOT AFFECT THE AMOUNT OF
C       COLLECTED CURRENT ( DO NOT AFFECT THE SHAPE OF THE JI VS. E CURVE)

      DIMENSION X(401),XSQ(401),S(401),DXDS(401),ROP(401),SCOT(401),
     1 COOK(401),XI(401),DXIDS(401),ETA(401),ETAPS(401),ETANG(401),
     2 RHO(401),OMGAG(401),BETAG(401),ALFAG(401),PSIG(401),EPSG(401),
     3 Y(401),Z(401),SH(401)
      COMMON X,XSQ,S,DXDS,ROP,SCOT,COOK,XI,DXIDS,ETA,ETAPS,ETANG,RHO,
     1 OMGAG,BETAG,ALFAG,PSIG,EPSG,Y,Z,SH
      COMMON PI,SCTPI,VIPI,SAY,MODE,M,MP,DELTS,GAMMA,PI3,PI6,PI7,YPOS,
     1 YNEG,NPRINT,KT1,KT2,LL,KEND
      COMMON LINK,BETH,EXY,EDY,N2,N22,NW,SW,SA,BETAW,BETAWA,MACK,MIKE,
     1 SCRIT,SCRITA,LK,LKA,CRISS,CROSS,VST,AMU,THETA,KBD,MCD,MZET

  750 GO TO (72,175),MODE
   72 WRITE OUTPUT TAPE 6,73
   73 FORMAT(49H0 WRONG SUBROUTINES BEING USED. EXECUTION DELETED )
      CALL EXIT

  175 ECY=EXY/PI
  585 DO 730 L=1,MP
      LL=L
      RHO(L)=0.0
      GO TO (200,177,575,177,575),MCD
  200 IF(LINK-5)176,176,177

  176 RHO(L)=-DYO(BETH,ECY)+TRY(0.0)+TRY(BETH)
      GO TO 178

  177 RHO(L)=-DYO(BETH,ECY)
      IF(MCD-1)201,201,575
  201 GO TO (576,575,575),MACK
  576 IF(L-LK)571,571,577
  577 IF(S(L)-SW)578,575,575

  578 IF(S(L)-SCRIT)580,580,581
  580 RHO(L)=RHO(L)+2.0*CAL(1,SH(L),SW,3,2)+Z(L)
      GO TO 730
  581 RHO(L)=RHO(L)+2.0*CAL(1,S(L),SW,1,2)+Z(L)
      GO TO 730

  575 IF(XI(L))572,571,571
  571 RHO(L)=RHO(L)+EXPF(-XI(L))
      GO TO 730
  572 RHO(L)=RHO(L)+2.0*TRY(0.0)
      IF(MCD-1)202,202,740
  202 GO TO (720,178,178),MACK

  178 IF(L-LK)740,740,742
  742 IF(S(L)-SW)732,720,720
  732 RHO(L)=RHO(L)-2.0*TRY(BETAW)+Z(L)
      IF(S(L)-SCRIT)736,737,737
  736 RHO(L)=RHO(L)+2.0*CAL(1,SH(L),SW,3,N2)
      GO TO 730
  737 RHO(L)=RHO(L)+2.0*CAL(1,S(L),SW,1,N2)
      GO TO 730
```



```
  720 IF(L-LKA)740,740,722
  722 IF(S(L)-SWA)723,740,740
  723 RHO(L)=RHO(L)-2.0*TRY(BETAWA)+Z(L)
      IF(S(L)-SCRITA)726,727,727
  726 RHO(L)=RHO(L)+2.0*CAL(1,SH(L),SWA,3,N22)
      GO TO 730
  727 RHO(L)=RHO(L)+2.0*CAL(1,S(L),SWA,1,N22)
      GO TO 730

  740 GO TO (744,745),KBD
  744 IF(L-MP)741,730,730
  741 RHO(L)=RHO(L)+EXPF(-XI(L)/(1.0-XSQ(L)/XSQ(MP)))
      GO TO 730
  745 RHO(L)=RHO(L)+1.0

  730 CONTINUE

      GO TO (181,204,205,204,205),MCD
  181 IF(LINK-5)180,180,204
  180 RH=SQRTF(BETH-XI(1))
      VST=2.0*EDY*(RH+COEFT(RH))
      GO TO (746,747),KBD
  746 RW=SQRTF(BETH)
      VST=VST+(1.0-2.0*EDY*(RW+COEFT(RW)))/X(MP)
  747 RETURN
  204 VST=EXY
      RETURN
  205 VST=0.0
      RETURN
      END
```


SUBROUTINE FOURTH — FOURTH CYLINDER

```
      SUBROUTINE FOURTH
C       THIS SUBROUTINE COMPUTES CHARGE DENSITY RHO(1-MP) AND COLLECTED
C       CURRENT VST, FOR A CYLINDRICAL PROBE, UNDER THE FOLLOWING
C       CONDITIONS.
C       LOCUS OF EXTREMA CROSSES ITSELF IN THE FIRST QUADRANT OF THE
C       (OMEGA,BETA) PLANE.

      DIMENSION X(401),XSQ(401),S(401),DXDS(401),ROP(401),SCOT(401),
     1 COOK(401),XI(401),DXIDS(401),ETA(401),ETAPS(401),ETANG(401),
     2 RHO(401),OMGAG(401),BETAG(401),ALFAG(401),PSIG(401),EPSG(401),
     3 Y(401),Z(401),SH(401)
      COMMON X,XSQ,S,DXDS,ROP,SCOT,COOK,XI,DXIDS,ETA,ETAPS,ETANG,RHO,
     1 OMGAG,BETAG,ALFAG,PSIG,EPSG,Y,Z,SH
      COMMON PI,SCTPI,VIPI,SAY,MODE,M,MP,DELTS,GAMMA,PI3,PI6,PI7,YPOS,
     1 YNEG,NPRINT,KT1,KT2,LL,KEND
      COMMON LINK,BETH,EXY,EDY,N2,N22,NW,SW,SA,BETAW,BETAWA,MACK,MIKE,
     1 SCRIT,SCRITA,LK,LKA,CRISS,CROSS,VST,AMU,THETA,KBD
      GO TO (72,171),MODE
   72 WRITE OUTPUT TAPE 6,73
   73 FORMAT(49H0 WRONG SUBROUTINES BEING USED. EXECUTION DELETED )
      CALL EXIT
  171 ECY=EXY/PI
  350 IF(LINK-8)360,360,361
  360 NI=LINK-6
      GO TO 362
  361 NI=LINK-8
  362 DO 322 L=1,MP
      LL=L
      IF(LINK-8)365,365,366

  365 RHO(L)=-DYO(BETH,ECY)+TRY(0.0)
      IF(S(L)-SW)321,321,322
  321 RHO(L)=RHO(L)-TRY(BETAW)+Z(L)
      GO TO 323
  322 RHO(L)=RHO(L)-CAL(1,SH(L),CRISS,NI,2)-CAL(1,CROSS,SW,2,2)
     1 +TRY(BETAW)
      GO TO 370

  366 RHO(L)=-DYO(BETH,ECY)
      IF(S(L)-SW)391,391,392
  391 RHO(L)=RHO(L)+Z(L)
      GO TO 323
  392 RHO(L)=RHO(L)-CAL(1,SH(L),CRISS,NI,2)-CAL(1,CROSS,SW,2,2)
      IF(XI(L))395,396,396
  396 RHO(L)=RHO(L)+EXPF(-XI(L))
      GO TO 370
  395 RHO(L)=RHO(L)+2.0*TRY(0.0)
      GO TO 370

  370 GO TO (371,372),KBD
  371 IF(L-MP)340,372,340
  340 RHO(L)=RHO(L)+EXPF(-XI(L)/(1.0-XSQ(L)/XSQ(MP)))
      GO TO 320
  372 RHO(L)=RHO(L)+1.0
      GO TO 320

  323 IF(S(L)-CROSS)325,326,326
  325 RHO(L)=RHO(L)+CAL(1,CROSS,SW,2,N2)
      GO TO 320
  326 RHO(L)=RHO(L)-CAL(1,SH(L),CRISS,NI,2)-CAL(1,CROSS,S(L),2,1)
     1 +CAL(1,S(L),SW,1,N2)
```



```
      GO TO 320

  323 IF(S(L)-SH(L))337,332,332
  337 RHO(L)=RHO(L)+CAL(1,SH(L),CRISS,2,2)
      IF(S(L)-SCRIT)329,331,331
  329 RHO(L)=RHO(L)+2.0*CAL(1,SH(L),SH(L),3,2)
      GO TO 320
  331 RHO(L)=RHO(L)+2.0*CAL(1,S(L),SH(L),1,2)
      GO TO 320

  332 IF(S(L)-CRISS)334,334,335
  334 RHO(L)=RHO(L)+CAL(1,SH(L),S(L),NI,1)+CAL(1,S(L),CRISS,1,2)
      GO TO 320
  335 RHO(L)=RHO(L)+CAL(1,SH(L),CRISS,NI,2)
      IF(S(L)-SCRITA)337,338,338
  337 RHO(L)=RHO(L)+2.0*CAL(1,SH(L),CROSS,3,2)
      GO TO 320
  338 RHO(L)=RHO(L)+2.0*CAL(1,S(L),CROSS,1,2)
      GO TO 320
  320 CONTINUE
      RH=SQRTF(BETH-XI(1))
      VST=2.0*EDY*(RH+COEFT(RH)+CAL(2,SH(1),CRISS,NI,2)
     1 +CAL(2,CROSS,SW,2,N2))
      IF(LINK-8)367,367,770
  367 GO TO (379,770),KBD
  379 RW=SQRTF(BETAW)
      VST=VST+(1.0-2.0*EDY*(RW+COEFT(RW)))/X(MP)
  770 RETURN
      END
```

Page 61

```
      FUNCTION DYO(AA,ECCY)                                              DYO

C     DYO=(1.0/PI)*INTEGRAL FROM A TO INFINITY OF
C        DBETA*EXPF(-BETA)*ARC SIN(SQRTF(XSQ*(BETA-XI(1))/(BETA-XI)))

      DIMENSION THAMU(3),AMIN(30),R(30),AMAR(15),COE(15),VIB(30),FM(31)
      EQUIVALENCE (THAMU(1),AMAR(1)),(THAMU(16),COE(1)),(BIN(1),VIB(1)),
     1 (R(1),FM(1))
      DIMENSION X(40),XSQ(40),S(40),OXDS(40),ROP(40),SCOT(40),
     1 COOK(40),XI(40),OXIDS(40),ETA(40),ETAPS(40),ETANG(40),
     2 RHO(40),OMGAG(40),BETAG(40),ALFAG(40),PSIG(40),EPSG(40),
     3 Y(40),Z(40),SH(40)
      COMMON X,XSQ,S,OXDS,ROP,SCOT,COOK,XI,OXIDS,ETA,ETAPS,ETANG,RHO,
     1 OMGAG,BETAG,ALFAG,PSIG,EPSG,Y,Z,SH
      COMMON PI,SQTPI,VIPI,SAY,MODE,M,N,DELTS,GAMMA,PI3,PI6,PI7,YPOS,
     1 YNEG,NPRINT,KT,KT2,LL,KEND
      COMMON LINK,METH,EXY,EOY,N2,N22,N,S,A,BETA,BETAA,MACK,MIKE,
     1 SCRIT,SCRITA,LK,LKA,CHISS,CROSS,YST,AMU,THETA,KBD,MCO,MZET,HALT

      I=1
      DUM=OMGAG(I)
      DUMM=BETAG(I)
      DUMMY=ALFAG(I)
      A=AA
      ECY=ECCY
      IF(LL-1)40,41,40
   41 DYO=0.5*EXY
      RETURN

   40 IF(A-17.7212 9)206,206,2.6
  206 DYO=0.0
      RETURN

  2.6 DENOM=1.0-XSQ(LL)
      CAPPA=(XI(LL)-XSQ(LL)*XI(1))/DENOM
      GAMMA=(CAPPA-XI(1))*0.5
      AMU=ABSF(CAPPA-GAMMA)
  195 THETA=XI(LL)-GAMMA
      IF(CAPPA-XI(1))31,3.,32

   32 IF(A-CAPPA)13.,13.,33
   33 IF(CAPPA-XI(LL))13.,130,34
   34 IF(XI(LL)-XI(1))13 ,130,1.3

  130 IF(LKKK-KEND-1)210,211,21.
  211 KKK=KKK+1
      GO TO 212
  210 WRITE OUTPUT TAPE 6,37,A,CAPPA,XI(LL),XI(1),LL,KEND,KKK
      LKKK=KEND+1
      KKK=1
      GO TO 212

  212 A=1.  [illegible]*CAPPA
      ECY=EXPF(-A)/PI
      GO TO 1.3

   31 IF(XI(LL)-CAPPA)3.,3.,35
   35 IF(XI(1)-XI(LL))3.,3.,36
   36 IF(A-XI(1))3.,1.2,1.3

   3. WRITE OUTPUT TAPE 6,37,A,CAPPA,XI(LL),XI(1),LL,KEND
   37 FORMAT(1H  [illegible]
     1 [illegible]
```

Page 62

```
      CALL EXIT

  1.2 BNOT=A-GAMMA
      IF(AMU-2.0)198,198,199

  199 FLAM=AMU/(AMU-THETA)
      SQM=SQRTF(AMU)
      SQL=SQRTF(FLAM)
      DEE=SQM
      C=1.0
      AR=2.0*SQL*COEFT(SQM/SQL)
      TERM=C*AR
      SUM=TERM

      DO 215 N=1,20
      FLN=N
      DEE=DEE/AMU
      C=-C/8.0*FLOATF((2*N-1)**2)/FLN
      AR=(DEE-AR/FLAM)/(FLN-0.5)
      TERMO=TERM
      TERM=C*AR
      IF(ABSF(TERM)-ABSF(TERMO))216,216,217
  216 SUM=SUM+TERM
      IF(ABSF(SUM)*1.0E-06-ABSF(TERM))215,215,218
  215 CONTINUE
      GO TO 218

  217 SUM=SUM-0.5*TERMO
  218 BKT=EXPF(BNOT-AMU)/AMU*1.2533141*SUM
  200 DYO=(ECY*(XI(1)-XI(LL))*0.5*Y(LL)/SCOT(LL)*BKT
      RETURN

  198 V=2.6*AMU
      AL=5.0
      AK=1.6094379
      FI=SQRTF(1.0-(THETA/AMU)**2)
      MAD=3
      GO TO 129

  103 BNOT=A-GAMMA
      IF(AMU-4.1-1.5*THETA/AMU)201,201,202

  202 TLIM=EXPF(-BNOT)
      AIND=QUAD( [illegible] )/TLIM
      C30
      ALT=0.0
      GO TO 83

  201 IF(BNOT-1.25*AMU)104,1.4,129

  104 V=2.6*AMU
      AL=5.0
      AK=1.6094379
      QNOT=BNOT/AMU
      ALNOT=QNOT+SQRTF(QNOT**2-1.0)
      AKNOT=LOGF(ALNOT)
      FI=SQRTF(1.0-(THETA/AMU)**2)
      MAD=1
      GO TO 129

  121 AIND=STR
      AL=ALNOT
      AK=AKNOT
```

Page 63

```
      MAD=2
      GO TO 129

  129 [illegible]
      [illegible]
      [illegible]
      [illegible]
     1 [illegible]
      [illegible]
      [illegible]
      [illegible]
      [illegible]
      [illegible]
      [illegible]
      [illegible]
      [illegible]
      [illegible]
      [illegible]

      DO 11. [illegible]
      [illegible]
      [illegible]
      [illegible]
      [illegible]
      [illegible]

      [illegible]
      DO 118 [illegible]
      [illegible]
      [illegible]
  117 [illegible]
      GO TO 118
  116 [illegible]
  118 [illegible]
  116 [illegible]
      [illegible]

      [illegible]
      [illegible]
      DO 112 [illegible]
      [illegible]
  112 [illegible]
      [illegible]
      [illegible]
      [illegible]
  115 CONTINUE

  119 GO TO (121,122,123),MAD

  122 AIND=[illegible]
      GO TO 127

  123 AIND=[illegible]
      GO TO 127

  129 AIND=[illegible]
      [illegible]
      [illegible]
      GO TO 127

  127 E=[illegible]
      IF([illegible])91,91
```

Page 64

```
   90 [illegible]
     1 [illegible]
     2 [illegible]
      GO TO 10

   91 [illegible]
      [illegible]
      [illegible]
      GO TO 10

   10 [illegible]
      [illegible]
      DO 63 [illegible]
      [illegible]
   63 [illegible]
      [illegible]
      [illegible]
      [illegible]
      [illegible]
      [illegible]
      [illegible]

      DO 1. [illegible]
      [illegible]
      [illegible]
      [illegible]
      [illegible]
      [illegible]
      [illegible]
      [illegible]
      [illegible]
      [illegible]
      [illegible]
      [illegible]
      [illegible]
      [illegible]
   14 CONTINUE

   71 GO TO (10.,101,101,10C),MAD
  101 [illegible]
  102 GO TO (83,83,84,83),MAD
   83 [illegible]
  100 DYO=[illegible]
      RETURN
   84 DYO=[illegible]
      RETURN
      END
```

```
      FUNCTION COO(XL)                                                  COO
C     THIS FUNCTION SUBPROGRAM IS USED BY FUNCTION DYO AND IS CALLED
C     THROUGH UNIVERSITY OF TORONTO FORTRAN II NUMERICAL QUADRATURE
C     SUBPROGRAM QUAD.

      DIMENSION X(401),XSQ(401),S(401),DXDS(401),ROP(401),SCOT(401),
     1 COOK(401),XI(401),DXIDS(401),ETA(401),ETAPS(401),ETANG(401),
     2 RHO(401),OMGAG(401),BETAG(401),ALFAG(401),PSIG(401),EPSG(401),
     3 Y(401),Z(401),SH(401)
      COMMON X,XSQ,S,DXDS,ROP,SCOT,COOK,XI,DXIDS,ETA,ETAPS,ETANG,RHO,
     1 OMGAG,BETAG,ALFAG,PSIG,EPSG,Y,Z,SH
      COMMON PI,SQTPI,V2PI,SAY,MODE,M,MP,DELTS,GAMMA,PI3,PI6,PI7,YPOS,
     1 YNEG,NPRINT,KT1,KT2,LL,KEND
      COMMON LINK,BETH,EXY,EDY,N2,N22,NW,SW,SB,[illegible]TAW,BETAWA,MACK,MIKE,
     1 SCRIT,SCRITA,LK,LKA,CRISS,CROSS,YST,AMU,[illegible]TA,KBO

      IF(XL)101,101,102
  101 COO=0.0
      RETURN
  102 FLN=LOGF(XL)
      COO=-1.0/((FLN+THETA)*SQRTF(FLN**2-AMU**2))
      RETURN
      END
```



```
      FUNCTION TRY(AA)                                                  TRY
C     TRY=(1.0/PI)*INTEGRAL FROM A TO BH OF
C        DBETA*EXPF(-BETA)*[illegible] SIN(SQRTF(XSQ*BETA/(XSQ(MP)*(BETA-XI)))))
C     WARNING - FUNCTION TRY [illegible] NOT GIVE CORRECT RESULT IF MAGNITUDE OF
C     XI(LL) IS GREATER THAN [illegible]

      DIMENSION X(401),[illegible](401),ROP(401),SCOT(401),
     1 COOK(401),XI(401),[illegible],ETAPS(401),ETANG(401),
     2 RHO(401),OMGAG(401),BETAG(401),[illegible] PSIG(401),EPSG(401),
     3 Y(401),Z(401),SH(401)
      COMMON X,XSQ,S,DXDS,ROP,SCOT,COOK,X[illegible],ETAPS,ETANG,RHO,
     1 OMGAG,BETAG,ALFAG,PSIG,EPSG,Y,Z,SH
      COMMON PI,SQTPI,VIPI,SAY,MODE,M,MP,DELTS,GAMMA,PI3,PI6,PI7,YPOS,
     1 YNEG,NPRINT,KT1,KT2,LL,KEND
      COMMON LINK,BETH,EXY,EDY,N2,N22,NW,SW,SBA,[illegible],BETAWA,MACK,MIKE,
     1 SCRIT,SCRITA,LK,LKA,CRISS,CROSS,YST,AMU,TH[illegible],KBO,NCO,MZET

      DUMMY=OMGAG(1)
      DUMMY=BETAG(1)
      DUMMY=ALFAG(1)
      A=AA
      GO TO (65,66),KBO
   66 TRY=0.0
      RETURN

   65 IF(LL-MP)35,36,35
   36 TRY=0.5*EXPF(-A)
      RETURN

   35 DOM=XSQ(LL)/XSQ(MP)-1.0
      DRT=SQRTF(DOM)
      BH=-XI(LL)/DOM
      AMU=BH/2.0
      EXPA=EXPF(-AMU)
      THETA=AMU-XI(LL)
      IF(THETA-AMU)75,75,61

   75 WRITE OUTPUT TAPE 6,76,LL,KEND,AMU,THETA,AA
   76 FORMAT(18H FCN TRY, TROUBLE, 2I5,1P3E15.7 )
      CALL EXIT

   61 IF(BH-A)30,30,31

   30 WRITE OUTPUT TAPE 6,76,LL,KEND,AMU,THETA,AA
   70 TRY=0.0
      RETURN

   31 CERN=(AMU/24.0*A/(1.95*AMU))**3+(AMU/(0.92*THETA))**3-1.0
      IF(A)10,11,12
   10 WRITE OUTPUT TAPE 6,76,LL,KEND,AMU,THETA,AA
      A=0.0

   11 IF(CERN)40,40,41

   40 COE=0.5
      AMOK=(AMU/THETA)**2
      AMSK=AMOK
      TSO=THETA
      TSN=0.5*THETA**2
      P=1.0+TSO+TSN
```



```
      DO 16 K=4,200,2
      KIM=K-1
      TSO=TSN*THETA/FLOATF(KIM)
      TSN=TSO*THETA/FLOATF(K)
      AMSK=AMSK*AMOK
      COE=COE*FLOATF(KIM)/FLOATF(K)
      P=P+TSO+TSN
      TERM=P*AMSK*COE
      SUM=SUM+TERM
      IF(SUM*1.0E-07-TERM)16,19,19
   16 CONTINUE

   19 TRY=-0.5*(EXPA**2+X(LL)/X(MP)*XI(LL)/DRT*EXPA/THETA*SUM)
      RETURN

   41 FLAM=-AMU/XI(LL)
      W=MAX1F(AMU,8.3)
      SQW=SQRTF(W)
      SQL=SQRTF(FLAM)
      DEE=SQW
      C=1.0
      COO=COEFT(SQW/SQL)
      R=2.0*SQL*COO
      TERM=C*R
      SUM=TERM

      DO 500 N=1,20
      FLN=N
      DEE=DEE/W
      C=C/8.0*FLOATF((2*N-1)**2)/FLN
      R=(DEE-R/FLAM)/(FLN-0.5)
      TERMO=TERM
      TERM=C*R
      IF(ABSF(TERM)-ABSF(TERMO))501,501,498
  501 SAM=SUM+TERM
      IF(SAM-SUM)500,504,500
  500 SUM=SAM
      GO TO 502

  498 SUM=SUM-0.5*TERMO
  502 IF(ABSF(SUM)*1.0E-05-ABSF(TERMO))503,503,504

  503 MISS=1
      N=-1
      IF(AMU-FLAM)513,513,499
  499 IF(AMU-8.3)513,508,508

  508 FACT=1.0+0.125/(AMU+FLAM)+.0703125/(AMU+FLAM)**2
  509 SIM=FLAM/AMU*SQRTF(2.0*PI/FLAM)*COO*FACT
      GO TO 72

  513 WRITE OUTPUT TAPE 6,512,SUM,TERM,AMU,FLAM,MISS
  512 FORMAT(23H FCN TRY NONCONVERGENCE 1P4E12.5,I2)
      GO TO (504,511),MISS

  504 ASYC=PI/AMU*EXPF((AMU-W)/FLAM)*SUM/2.5066282
      TAYC=0.0
      IF(AMU-8.3)529,526,526

  529 AE=1.0+1.0/FLAM
      EXMU=EXPF(-AE*AMU)
      EXW=EXPF(-AE*W)
```



```
      C=1.0
      WN=EXW
      UN=EXMU
      Q2N=(EXMU-EXW)/AE
      TERM=C*Q2N
      SUM=TERM

      DO 510 N=1,18
      C=C/FLOATF(2*N)**2
      UN=UN*AMU
      WN=WN*W
      Q2NM=(FLOATF(2*N-1)*Q2N+WN-UN)/AE
      UN=UN*AMU
      WN=WN*W
      Q2N=(FLOATF(2*N)*Q2NM-WN+UN)/AE
      TERM=C*Q2N
      SAM=SUM+TERM
      IF(SAM-SUM)510,511,510
  510 SUM=SAM

      MISS=2
      IF(ABSF(SUM)*1.0E-05-ABSF(TERM))513,513,511

  511 TAYC=PI/AMU*EXPF(AMU/FLAM)*SUM

  526 SIM=ASYC+TAYC
   72 TRY=-0.5*(EXPA**2+X(LL)/X(MP)*XI(LL)/DRT*SIM/PI)
      RETURN

   12 EXMINA=EXPF(-A)
      IF(CERN)45,45,48
   48 IF(EXMINA-EXPA**2-2.0E-06)49,49,46
   49 TRY=0.0
      RETURN

   45 ALF=A/AMU-1.0
      COSS=SQRTF(1.0-ALF**2)
      SN=0.5*PI-ATANF(ALF/COSS)
      SNA=COSS
      SNB=0.5*(ALF*COSS+SN)
      ALKIM=ALF
      TSK=0.5*THETA**2
      AMSK1=-AMU/THETA
      AMSKK=AMSK1**2
      P=1.0+THETA
      SUM=SN+P*AMSK1*SNA
      P=P+TSK
      SUM=SUM+P*AMSKK*SNB

      DO 22 K=3,200
      TSK=TSK*THETA/FLOATF(K)
      AMSKK=AMSKK*AMSK1
      ALKIM=ALKIM*ALF
      SNC=(ALKIM*COSS+FLOATF(K-1)*SNA)/FLOATF(K)
      SNA=SNB
      SNB=SNC
      P=P+TSK
      TERM=P*AMSKK*SNC
      SUM=SUM+TERM
      IF(SUM*1.0E-07-ABSF(TERM))22,26,26
   22 CONTINUE

   26 SIM=EXPA*SUM/THETA
```

```
      GO TO 90

   46 ALF=A/AMU-1.0
      ALIM=ATANF(ALF/SQRTF(1.0-ALF**2))
      BLIM=0.5*PI
   99 SIM=EXPA*QUAD(ALIM,BLIM,CORE, 0.0 ,0.2,1)
F     CORE
      GO TO 90

   90 ARG=SQRTF(XSQ(LL)*A/((XSQ(LL)-XSQ(MP))*(BM-A)))
   73 TRY = EXM(MAPATANF(ARG)/PI - 0.5*EXPA**2
     1               - 0.5/PI*X(LL)/X(MP)*X1(LL)/ARTSIM
      RETURN
      END
```



```
      FUNCTION CORE(XL)                                                 CORE
C     THIS FUNCTION SUBPROGRAM IS USED BY FUNCTION TRY AND IS CALLED
C     THROUGH UNIVERSITY OF TORONTO FORTRAN II NUMERICAL QUADRATURE
C     SUBPROGRAM QUAD.

      DIMENSION X(401),XSQ(401),S(401),OXDS(401),ROP(401),SCOT(401),
     1 COOK(401),XI(401),OXIDS(401),ETA(401),ETAPS(401),ETANS(401),
     2 RHO(401),OMGAG(401),BETAG(401),ALFAG(401),PSIG(401),EPSG(401),
     3 Y(401),Z(401),SM(401)
      COMMON X,XSQ,S,OXDS,ROP,SCOT,COOK,XI,OXIDS,ETA,ETAPS,ETANS,RHO,
     1 OMGAG,BETAG,ALFAG,PSIG,EPSG,Y,Z,SM
      COMMON PI,SQTPI,VIPI,SAY,MODE,M,MP,DELTS,GAMMA,PI3,PI6,PI7,YPOS,
     1 YNEG,NPRINT,KT1,KT2,LL,KEND
      COMMON LINK,BETH,EXY,EDY,M2,M22,NU,SU,SMA,BETAU,BETAUA,MACK,MIKE,
     1 SCRIT,SCRITA,LK,LKA,CRISS,CROSS,YST,AMU,THETA,KBO

      SAMXL=AMU*SINF(XL)
      CORE=EXPF(-SAMXL)/(SAMXL+THETA)
      RETURN
      END
```



```
C     MAIN PROGRAM 3

C     SOLUTION OF    Y DOUBLE PRIME = EXPF(Y)*(1.0-ERF(SQRTF(Y)))/2.0
C                                   = COEFT(SQRTF(Y))/SQTPI

      DIMENSION ST(400)),X(50)),Y(50)),ETA(50)),S(50)),YP(400)),
     1 ETTA(400)),SS(400)),RPTRAP(400))

   10 READ INPUT TAPE 5,11,YMAX,Y1,NX,KXPRIN,NYP,KYPRIN
   11 FORMAT(1P2E10.3,4I5)
      WRITE OUTPUT TAPE 6,12
   12 FORMAT(64H1 SOLUTION OF    Y DOUBLE PRIME = EXPF(Y)*(1.0-ERF(SQRTF(
     1Y)))/2.0)
      WRITE OUTPUT TAPE 6,13,YMAX,Y1,NX,KXPRIN,NYP,KYPRIN
   13 FORMAT(10H0      YMAX,8X2HY1,8X2HNX,4X6HKXPRIN,7X3HNYP,4X6HKYPRIN /
     1 1P2E10.3,4I10 )

      SQTPI=1.7724539
      DELX=SQRTF(Y1)/FLOATF(NX)
      NXP=NX+1

      DO 15 I=1,NXP
      X(I)=DELX*FLOATF(I-1)
      XSQ=X(I)**2
      Y(I)=XSQ

      SUMA=1.0
      TERM=1.0
      DO 16 J=2,50
      TERM=TERM*XSQ/FLOATF(J)
      SAM=SUMA+TERM
      IF(SAM-SUMA)16,17,16
   16 SUMA=SAM

      WRITE OUTPUT TAPE 6,18
   18 FORMAT(10H NONCONV 1)
      GO TO 10

   17 TSQ=2.0*XSQ
      SUMB=0.66666667
      TERM=SUMB
      DO 20 K=2,50
      TERM=TERM*TSQ/FLOATF(2*K+1)
      SAM=SUMB+TERM
      IF(SAM-SUMB)20,23,20
   20 SUMB=SAM

      WRITE OUTPUT TAPE 6,24
   24 FORMAT(10H NONCONV 2)
      GO TO 10

   23 G=SUMA-2.0*X(I)*SUMB/SQTPI
      ST(I)=2.0/SQRTF(G)
   15 ETA(I)=COEFT(X(I))/SQTPI

      S(1)=0.0
      S(2)=(5.0*ST(1)+8.0*ST(2)-ST(3))*DELX/12.0
      DO 25 I=3,NX
   25 S(I)=S(I-1)+(13.0*(ST(I-1)+ST(I))-ST(I-2)-ST(I+1))*DELX/24.0
      S(NXP)=S(NX)+(5.0*ST(NXP)+8.0*ST(NX)-ST(NX-1))*DELX/12.0

      DELY=(YMAX-Y1)/FLOATF(NYP)
      NYPP=NYP+1
```



```
      DO 30 I=1,NYPP
      YP(I)=Y1+DELY*FLOATF(I-1)
      SKY=SQRTF(YP(I))
      COE=COEFT(SKY)
      ETTA(I)=COE/SQTPI
      FY=(SKY+COE)*2.0/SQTPI-1.0
   30 ST(I)=1.0/SQRTF(FY)

      SS(1)=S(NXP)
      SS(2)=SS(1)+(5.0*ST(1)+8.0*ST(2)-ST(3))*DELY/12.0
      DO 32 I=3,NYP
   32 SS(I)=SS(I-1)+(13.0*(ST(I-1)+ST(I))-ST(I-2)-ST(I+1))*DELY/24.0
      SS(NYPP)=SS(NYP)+(5.0*ST(NYPP)+8.0*ST(NYP)-ST(NYP-1))*DELY/12.0

      DO 41 I=1,NYPP
   41 RPTRAP(I)= 2.0*YP(I)*ST(I)

      WRITE OUTPUT TAPE 6,40
   40 FORMAT(1H0,2(9X1HY,11X3HETA,13X1HS,12X),6X6HRPTRAP)
      I=1
      J=1
      ISTEP=NX/KXPRIN
      JSTEP=NYP/KYPRIN
      MAXP=XMAX0F(ISTEP,JSTEP)+1
      DO 36 K=1,MAXP
      WRITE OUTPUT TAPE 6,35,Y(I),ETA(I),S(I),YP(J),ETTA(J),SS(J),RPTRAP
     1 (J)
   35 FORMAT(1H ,2(F11.8,F14.5,F14.4,11X),F12.4)
      I=I+KXPRIN
   36 J=J+KYPRIN
      GO TO 10
      END
```

Page 73

```
C       MAIN PROGRAM 4
C       SPHERICAL PROBE - ATTRACTED PARTICLES AT ZERO TEMPERATURE

C       ALLEN, BOYD, AND REYNOLDS EQUATION
C       (1.0/S**2)*D/DS(S**2*DY/DS) = AA/(S*S*SQRTF(Y)) - EXPF(-Y)
C            WHERE AA = NONDIMENSIONAL ION CURRENT / (2.0*SQRTF(PI))

C       REFERENCE ION CURRENT IS THAT COLLECTED BY A SPHERE OF RADIUS ONE
C       ELECTRON DEBYE LENGTH , IF IONS ARE MAXWELLIAN AND THEIR EFFECTIVE
C       TEMPERATURE IS EQUAL TO THAT OF THE ELECTRONS.

C       SOLUTION VIA METHOD OUTLINED BY BERNSTEIN AND RABINOWITZ.

C       IF LSET = 1, CURRNT IS READ IN. IF LSET = 2, AA IS READ IN.

D       DIMENSION A(200),B(200),C(200),D(200)
        DIMENSION KA(200),KB(200),KC(200),KD(200),SS(2000),ALPHA(2000),
       1 YY(2000),ETAP(2000),ETAN(2000),Y(2),YPRIME(2),Q(2),SFINAL(6),
       2 YFINAL(6),AVIR(2000),NFINAL(6)
        DIMENSION EMPTY(10)
        COMMON EMPTY,AA

        KAYSE=1
     10 READ INPUT TAPE 5,11,QUANT,LSET
     11 FORMAT(1PE10.3,I5)
        GO TO (110,111),LSET
    110 CURRNT=QUANT
        AA=CURRNT/3.5449078
        GO TO 112
    111 AA=QUANT
        CURRNT=AA*3.5449078
    112 WRITE OUTPUT TAPE 6,12,CURRNT,AA
     12 FORMAT(67H1 SPHERICAL PROBE - ATTRACTED PARTICLES AT ZERO TEMPERAT
       1URE - NONDIMENSIONAL CURRENT = 1PE12.5,6H , AA=1PE12.5)
        PRINT 175,KAYSE
    175 FORMAT(12H0 BEGIN CASE I5)
        KAYSE=KAYSE+1

        KSTOP=38
D   101 FIXY=2.0**8
D       VFIXY=1.0/FIXY
        DO 136 K=1,KSTOP
        KA(K)=0
        KB(K)=0
        KC(K)=0
    136 KD(K)=0

D       C(1)=-0.5
D       D(1)=-1.0
        DO 13 K=2,KSTOP
D       C(K)=-C(K-1)*FLOA  (2*K-1)/FLOATF(2*K)
D       D(K)=-D(K-1)/FLOATF(K)
        KD(K)=KD(K-1)
        IF(ABSF(D(K))-VFIXY)135,13,13
D   135 D(K)=D(K)*FIXY
        KD(K)=KD(K)-1
     13 CONTINUE

        IF QUOTIENT OVERFLOW 162,162
    162 IF ACCUMULATOR OVERFLOW  131,131
D   131 A(1)=0.0
D       A(2)=0.0
D       A(3)=0.0
```

Page 74

```
D       B(1)=0.0
D       B(2)=0.0
D       B(3)=0.0
D       B(4)=AA*AA
        DO 19 K=4,KSTOP,2
        IF(K-4)151,151,24
D    24 B(K)=AA*AA*A(K-4)
        KB(K)=KA(K-4)
    151 IF(ABSF(B(K))-FIXY)23,23,137
D   137 B(K)=B(K)*VFIXY
        KB(K)=KB(K)+1
        GO TO 151
     23 FLK=K
        KMAX=XMAXOF(KB(K),KB(K-2))
        DO 140 I=2,K
        DO 140 J=4,K,2
        IF(I+J-K)140,142,140
    142 KMAX=XMAXOF(KMAX,KD(I)+KB(J)+1,KA(J)+1)
    140 CONTINUE
D       SUM=D(1)*B(K)*VFIXY**(KMAX-KB(K))+(FLK-2.0)*(FLK-3.0)*B(  -2)*VFIXY
       1 **(KMAX-KB(K-2))
D       ZEE=0.0
D       ZOO=0.0
        CALL POWERS(ZEE,K,KMAX,VFIXY,B,KB,D,KD)
        CALL POWERS(ZOO,K,KMAX,VFIXY,A,KA,C,KC)
D   145 SUM=SUM+ZEE-ZOO
D       A(K)=SUM/C(1)
        KA(K)=KMAX
    152 IF(ABSF(A(K))-FIXY)143,143,144
D   144 A(K)=A(K)*VFIXY
        KA(K)=KA(K)+1
        GO TO 152
    143 IF QUOTIENT OVERFLOW 130,163
    163 IF ACCUMULATOR OVERFLOW 130,19
     19 CONTINUE
        GO TO 166

    130 KSTOP=K-1

    166 KP=1
        STEP=1.0
        S=100.0
        SSIZE=STEP
        LINK=1
        MARK=0
        KTRAP=0

     26 YOLD=Y(1)
        YPLD=Y(2)
        Y(1)=0.0
D       V1=0.0
        Y(2)=0.0
D       V2=0.0
D       SIA=1.0/S**2
D       SI=SIA
D       SI1=SIA*SIA
        DO 95 I=4,KSTOP,2
        FLI=I
D       FACTR = FIXY**(KB(I)-KB(I-2))*SIA
D       SI=SI*FACTR
D       SI1=SI1*FACTR
D       TERM=B(I)*SI
D       TERM1=-FLI*B(I)*SI1)
```

Page 75

```
D       VT=V1+TERM
D       VT1=V2+TERM1
        IF(B(I))127,25,127
    127 IF(V1-VT)25,21,25
     21 IF(V2-VT1)25,27,25
D    25 V1=VT
        IF QUOTIENT OVERFLOW 125,164
    164 IF ACCUMULATOR OVERFLOW 125,95
D    95 V2=VT1
    125 Y(1)=V1
        Y(2)=V2
        GO TO (26,29),LINK

     28 MARK=MARK+1
        S=S*2.0
        IF(MARK-5)26,31,31

     31 WRITE OUTPUT TAPE 6,32,S,VT,TERM,KSTOP
     32 FORMAT(32H UNABLE TO SUM POWER SERIES, S= 1PE10.3,4H VT=1PE10.3,
       1 6H TERM=1PE10.3,7H KSTOP=I3)
        GO TO 10

     27 Y(1)=V1
        Y(2)=V2
D       ETAPSD=AA/(S*S*SQRTF(Y(1)))
D       ETANGD=EXPF(-Y(1))
D       ALPHD=0.5*(S*(ETAPSD-ETANGD)+Y2)
        ETAPS=ETAPSD
        ETANG=ETANGD
    190 ALPH=ALPHD
        GO TO (96,97),LINK
     97 IF(ALPH)98,96,96
     98 IF(ALFOLD)76,99,99

     99 STRAPD=STRAP
        STRAP=S-(SOLD-S)*ALPH/(ALFOLD-ALPH)
        KTRAP=KTRAP+1

     96 SOLD=S
        ALFOLD=ALPH
        IF(S-100.0)35,35,36
     35 IF(Y(1)-20.0)36,171,171

    171 SS(KP)=S
        YY(KP)=Y(1)
        AVIR(KP)=CURRNT/S**2
        ETAP(KP)=ETAPS
        ETAN(KP)=ETANG
        ALPHA(KP)=ALPH
        KP=KP+1

     36 LINK=2
        IF(S-16.001)190,190,191
    191 ZTEP=STEP
        GO TO 200
    190 IF(S-4.0001)192,192,193
    193 ZTEP=STEP/2.0
        GO TO 200
    192 ZTEP=STEP/4.0
    200 S=S-ZTEP
        IF(S-0.499)158,158,26

     29 S=S+ZTEP
```

Page 76

```
        STYP=STEP
        SSTART=S
        MARK=0
        KPST=KP
        FNBR=MIN1F(80.0,1.2*SSTART)
        NBR=FNBR
        JEND=4
        IF(SSTART-8.0)183,183,184
    183 JEND=6
    184 JARK=0

    153 Y(1)=YOLD
        Y(2)=YPLD
        S=SSTART
        CALL DEQST(S,STYP,2,Y,YPRIME,Q,CHASPH)
F       CHASPH
D       ETAPS=AA/(S*S*SQRTF(YOLD))
D       ETANG=EXPF(-YOLD)
        EPOLD=ETAPS
        ENOLD=ETANG

     42 DO 40 N=1,NBR
        CALL DEQ(S,STYP,2,Y,YPRIME,Q,CHASPH)
D       VZ=0.0
D       SIA=1.0/S**2
D       SI=SIA
        DO 46 I=4,KSTOP,2
D       SI = SI*FIXY**(KB(I)-KB(I-2))*SIA
D       TERM=B(I)*SI
D       VT=VZ+TERM
        IF(TERM)157,46,157
D   157 TEST= ABSF(2.0*(VZ-VT)/(VZ+VT))-1.0E-11
        IF(TEST)47,46,46
D    46 VZ=VT
     47 KYB=1
        IF(ABSF(Y(1)-VZ)-0.001)48,48,49
     49 KYB=KYB+1
D    48 ETAPS=AA/(S*S*SQRTF(YT))
D       ETANG=EXPF(-YT)
D       TEST=ETAPS-ETANG-1.0E-09
        IF(TEST)50,50,91
     50 KYB=KYB+2
     91 GO TO (40,52,54,54),KYB
     40 CONTINUE
        GO TO 93

     54 IF(N-3*2**JARK)52,52,93

     52 IF(JARK-JEND)156,155,156
    156 JARK=JARK+1
        NBR=2*NBR
        STYP=STYP/2.0
        GO TO 153

    155 KSTOP=KSTOP-5
        IF(KSTOP-6)167,167,166
    167 WRITE OUTPUT TAPE 6,55,SSTART,YOLD,EPOLD,ENOLD,S,Y(1),YT,ETAPS,
       1 ETANG,N,JARK,KSTOP
     55 FORMAT(111HOATTEMPT TO RETRACE POWER SERIES SOLUTION USING RUNGE-K
       1UTTA PRODUCES INCONSISTENT RESULTS. THIS CASE DELETED.   /
       2 1X1P9E12.5,I5,2I3 )
        GO TO 10
```

Page 77

```
 53 WRITE OUTPUT TAPE 6,56,SSTART,YOLD,EPOLD,ENOLD,S,Y(1),YZ,ETAPS,
   1 ETANG,N,JARK,KSTOP
 56 FORMAT(37H0RUNGE-KUTTA AGREES WITH POWER SERIES // 7X6HSSTART,
   1 8X4HYOLD,6X5HEPOLD,6X5HENOLD,11X1HS,8X4HY(1),10X2HYZ,6X5HETAPS,
   2 6X19HETANG   N JARK KSTOP / 1X1P2E12.5,0P2F11.7,1P3E12.5,0P2F11.7,
   3 I6,I3,I5 )
    KKTRAP=KTRAP
    STEP=0.5
    KAT=2
    GO TO 60

 60 KTRAP=KKTRAP
    S=SSTART
    SSIZE=-STEP
    Y(1)=YOLD
    Y(2)=YPLD
    CALL DEQST(S,SSIZE,2,Y,YPRIME,Q,CHASPH)

    DO 61 I=1,4000
    SOLD=S
    ALFOLD=ALPH

    IF(S-16.0001) 75,261,261
275 IF(S-8.0001)2  ,277,278
278 SSIZE=-STEP/
    GO TO 261
277 IF(S-4.0001)279,279,280
280 SSIZE=-STEP/4.0
    GO TO 261
279 IF(S-2.0001)281,281,282
282 SSIZE=-STEP/8.0
    GO TO 261
281 SSIZE=-STEP/16.0
261 CONTINUE

    CALL DEQ(S,SSIZE,2,Y,YPRIME,Q,CHASPH)
    Y1=Y(1)
    Y2=Y(2)
    IF(Y(1))176,176,177

176 WRITE OUTPUT TAPE 6,178,S,Y(1),STEP,MARK
178 FORMAT(36H0 Y(1) NEGATIVE. TRY SMALLER STEPS.  1P3E14.5,I4)
    MARK=MARK+1
    GO TO 87

D 177 ETAPS=AA/(S*S*SQRTF(Y1))
D     ETANG=EXPF(-Y1)
D     ALPH=0.5*(S*(ETAPS-ETANG)+Y2)
      IF(I-(I/KAT)*KAT)63,62,63
   62 IF(S-130.1)104,104,63
  104 IF(Y(1)-0.01)63,172,172

  172 SS(KP)=S
      YY(KP)=Y(1)
      AVIR(KP)=CURRNT/S**2
      ETAP(KP)=ETAPS
      ETAN(KP)=ETANG
      ALPHA(KP)=ALPH
      KP=KP+1

   63 IF(ALPH)64,65,65
   64 IF(ALFOLD)65,66,66
```

Page 78

```
 66 STRAPO=STRAP
    STRAP=S-(SOLD-S)*ALPH/(ALFOLD-ALPH)
    KTRAP=KTRAP+1

 65 IF(KP-1)159,159,170
170 IF(YY(KP-1)-30.0)70,70,71
 70 IF(SS(KP-1)-.8001)71,159,159
159 IF(Y(1)-80.0)61,61,71

 61 CONTINUE

 91 WRITE OUTPUT TAPE 6,85,MARK,STEP,S,Y(1),(NFINAL(I),SFINAL(I),
   1 YFINAL(I),I=1,MARK )
 85 FORMAT(65H0UNABLE TO ACHIEVE SUFFICIENT ACCURACY WITH RUNGE-KUTTA
   1PROCEDURE // 1XI4,1P3E14.5 // (4(1XI5,1P2E12.5)) )
    GO TO 10

 71 MARK=MARK+1
    IF(KP-1)161,161,160
161 IF(Y(1)-80.0)160,160,165
165 SS(1)=0.0
    YY(1)=0.0
    AVIR(1)=0.0
    ETAP(1)=0.0
    ETAN(1)=0.0
    ALPHA(1)=0.0
160 KPM1=XMAXOF(1,KP-1)
    SFINAL(MARK)=SS(KPM1)
    YFINAL(MARK)=YY(KPM1)
    NFINAL(MARK)=KP-1
    IF(MARK-1)87,87,103
103 IF(ABSF(SFINAL(MARK)-SFINAL(MARK-1))-0.001)86,86,87
 86 IF(ABSF(YFINAL(MARK)-YFINAL(MARK-1))-0.001)88,88,87
 88 IF(NFINAL(MARK)-NFINAL(MARK-1))87,158,87

158 KPT=KP-1
    NCOL=(KPT+1)/2
    IF(KTRAP-1)115,116,116
116 WRITE OUTPUT TAPE 6,117,STRAP
117 FORMAT(20HCTRAPPING RADIUS IS  1PE14.5, 15H  DEBYE LENGTHS  )
115 WRITE OUTPUT TAPE 6,89
 89 FORMAT(1H /2(15X1HS,8X1HY,5X4HAVIR,3X4HETAP,3X4HETAN,5X7HALPHA   )/
   1 1H )
    DO 105 I=1,NCOL
105 WRITE OUTPUT TAPE 6,106,(SS(J),YY(J),AVIR(J),ETAP(J),ETAN(J),
   1 ALPHA(J),J=I,KPT,NCOL )
106 FORMAT(2(8XF10.4,2F9.4,2F7.4,F10.4))
    GO TO 10

 87 IF(MARK-5)90,91,91
 90 STEP=STEP/2.0
    KP=KPST
    KAT=2*KAT
    GO TO 60
    END
```

Page 79

```
      SUBROUTINE CHASPH(S,M,Y,YPRIME)                              CHASPH

C     THIS SUBPROGRAM IS USED BY MAIN PROGRAM 4, AND IS CALLED THROUGH
C     UNIVERSITY OF TORONTO FORTRAN II SUBPROGRAMS DEQ AND DEQST, WHICH
C     TOGETHER CARRY OUT A RUNGE-KUTTA NUMERICAL INTEGRATION PROCEDURE.

      DIMENSION Y(2),YPRIME(2)
      DIMENSION EMPTY(10)
      COMMON EMPTY,AA

      NIL=M
      YPRIME(1)=Y(2)
      Y1=Y(1)
      Y2=Y(2)
D     YP2=AA/(S*S*SQRTF(Y1))-EXPF(-Y1)-2.0*Y2/S
      YPRIME(2)=YP2
      RETURN
      END
```

Page 80

```
      SUBROUTINE POWERS(EFS,KV,KMAXV,VFIXYV,AV,KAV,CV,KCV)         POWERS

D     DIMENSION A(200),C(200),AV(200),CV(200)
      DIMENSION KA(200),KC(200),KAV(200),KCV(200)

D     EFS=0.0
D     STT=0.0
      K=KV
      KMAX=KMAXV
D     VFIXY=VFIXYV
      DO 299 I=1,K
D     A(I)=AV(I)
D     C(I)=CV(I)
      KA(I)=KAV(I)
  299 KC(I)=KCV(I)

      IF(K-8)300,301,301
  300 RETURN

  301 KM=K-4
      DO 302 I1=4,KM,2
      I2=K-I1
D 302 STT=STT+A(I1)*A(I2)*VFIXY**(KMAX-KA(I1)-KA(I2))
D     EFS=STT*C(2)*VFIXY**(-KC(2))
D     STT=0.0

      IF(K-12)300,303,303

  303 KM=K-8
      DO 304 I1=4,KM,2
      DO 304 I2=4,KM,2
      I3=K-I1-I2
      IF(I3-4)304,305,305
  305 IF(KM-I3)304,306,306
D 306 STT=STT+A(I1)*A(I2)*A(I3)*VFIXY**(KMAX-KA(I1)-KA(I2)-KA(I3))
  304 CONTINUE
D     EFS=EFS+STT*C(3)*VFIXY**(-KC(3))
D     STT=0.0

      IF(K-16)300,307,307

  307 KM=K-12
      DO 308 I1=4,KM,2
      DO 308 I2=4,KM,2
      DO 308 I3=4,KM,2
      I4=K-I1-I2-I3
      IF(I4-4)308,309,309
  309 IF(KM-I4)308,310,310
D 310 STT=STT+A(I1)*A(I2)*A(I3)*A(I4)*VFIXY**(KMAX-KA(I1)-KA(I2)-KA(I3)-
     1 KA(I4))
  308 CONTINUE
D     EFS=EFS+STT*C(4)*VFIXY**(-KC(4))
D     STY=0.0

      IF(K-20)300,317,317

  317 KM=K-16
      DO 318 I1=4,KM,2
      DO 318 I2=4,KM,2
      DO 318 I3=4,KM,2
      DO 313 I4=4,KM,2
      I5=K-I1-I2-I3-I4
      IF(I5-4)318,319,319
```

```
  319 IF(KM-I5)318,320,320
D 320 STT=STT+A(I1)*A(I2)*A(I3)*A(I4)*A(I5)*VFIXY**(KMAX-KA(I1)-KA(I2)-
     1 KA(I3)-KA(I4)-KA(I5))
  318 CONTINUE
D     EFS=EFS+STT*C(5)*VFIXY**(-KC(5))
D     STT=0.0

      IF(K-24)300,327,327

  327 KM=K-20
      DO 328 I1=4,KM,2
      DO 328 I2=4,KM,2
      DO 328 I3=4,KM,2
      DO 328 I4=4,KM,2
      DO 328 I5=4,KM,2
      I6=K-I1-I2-I3-I4-I5
      IF(I6-4)328,329,329
  329 IF(KM-I6)328,330,330
D 330 STT=STT+A(I1)*A(I2)*A(I3)*A(I4)*A(I5)*A(I6)*VFIXY**(KMAX-KA(I1)-
     1 KA(I2)-KA(I3)-KA(I4)-KA(I5)-KA(I6))
  328 CONTINUE
D     EFS=EFS+STT*C(6)*VFIXY**(-KC(6))
D     STT=0.0

      IF(K-28)300,337,337

  337 KM=K-24
      DO 338 I1=4,KM,2
      DO 338 I2=4,KM,2
      DO 338 I3=4,KM,2
      DO 338 I4=4,KM,2
      DO 338 I5=4,KM,2
      DO 338 I6=4,KM,2
      I7=K-I1-I2-I3-I4-I5-I6
      IF(I7-4)338,339,339
  339 IF(KM-I7)338,340,340
D 340 STT=STT+A(I1)*A(I2)*A(I3)*A(I4)*A(I5)*A(I6)*A(I7)*VFIXY**(KMAX-
     1 KA(I1)-KA(I2)-KA(I3)-KA(I4)-KA(I5)-KA(I6)-KA(I7))
  338 CONTINUE
D     EFS=EFS+STT*C(7)*VFIXY**(-KC(7))
D     STT=0.0

      IF(K-32)300,347,347

  347 KM=K-28
      DO 348 I1=4,KM,2
      DO 348 I2=4,KM,2
      DO 348 I3=4,KM,2
      DO 348 I4=4,KM,2
      DO 348 I5=4,KM,2
      DO 348 I6=4,KM,2
      DO 348 I7=4,KM,2
      I8=K-I1-I2-I3-I4-I5-I6-I7
      IF(I8-4)348,349,349
  349 IF(KM-I8)348,350,350
D 350 STT=STT+A(I1)*A(I2)*A(I3)*A(I4)*A(I5)*A(I6)*A(I7)*A(I8)*VFIXY**(
     1 KMAX-KA(I1)-KA(I2)-KA(I3)-KA(I4)-KA(I5)-KA(I6)-KA(I7)-KA(I8))
  348 CONTINUE
D     EFS=EFS+STT*C(8)*VFIXY**(-KC(8))
D     STT=0.0

      IF(K-36)300,357,357
```



```
  357 KM=K-32
      DO 358 I1=4,KM,2
      DO 358 I2=4,KM,2
      DO 358 I3=4,KM,2
      DO 358 I4=4,KM,2
      DO 358 I5=4,KM,2
      DO 358 I6=4,KM,2
      DO 358 I7=4,KM,2
      DO 358 I8=4,KM,2
      I9=K-I1-I2-I3-I4-I5-I6-I7-I8
      IF(I9-4)358,359,359
  359 IF(KM-I9)358,360,360
D 360 STT=STT+A(I1)*A(I2)*A(I3)*A(I4)*A(I5)*A(I6)*A(I7)*A(I8)*A(I9)*
     1 VFIXY**(KMAX-KA(I1)-KA(I2)-KA(I3)-KA(I4)-KA(I5)-KA(I6)-KA(I7)-KA(
     2 I8)-KA(I9))
  358 CONTINUE
D     EFS=EFS+STT*C(9)*VFIXY**(-KC(9))
D     STT=0.0

      RETURN
      END
```

APPENDIX J

Sample Output From Computer Programs

Pages 1 and 2 contain sample output from program 1

Pages 3 and 4 contain sample output from program 2

Page 5 contains the output from program 3

Page 6 contains sample output from program 4

Page 1

CYLINDRICAL PROBE CHARACTERISTIC

PI3	PI6	GAMMA	P	QT1	QT2
2.000E 01	1.000E 01	1.000E 02	7.200E-01	0.6000000	0.0600000

KT1	KT2	KT3	M	NCUB	NEND	NPRINT	MODE	KWIT	KBD	MCD
1	4	4	72	400	300	4	2	4	2	3

COEFFICIENT OF LINEAR TERM IN INITIAL APPROXIMATION IS 2.500E-02

ATTRACTED PARTICLES MONO-ENERGETIC. PROBE DOES NOT ABSORB REPELLED PARTICLES

KEND= 10 0.9 DECREASE IN MIX. QT1= 0.3600000 QT2= 0.0360000

KEND= 30 0.9 DECREASE IN MIX. QT1= 0.3240000 QT2= 0.0324000

KEND= 50 Y= 8.362E 00 YINY= 8.312E 00 ESTD. CYCLES TO END 12 AVGE= 1.2132

KEND= 60 Y= 8.292E 0C YINY= 8.241E 00 ESTD. CYCLES TO END 21 AVGE= 0.8461

KEND= 80 Y= 8.208E 0C YINY= 8.173E 00 ESTD. CYCLES TO END 23 AVGE= 0.1390

KEND= 90 Y= 8.190E 00 YINY= 8.160E 0C ESTD. CYCLES TO END 27 AVGE= 0.0831

KEND= 130 RESULT SUFFICIENTLY ACCURATE. YINY= 8.140E 00

PL= 2.0070540E 02 SL= 0. RW= 2.5575903E 00 OMEGA= 5.2076754E 01

YPOS= 0. YNEG= 8.1428607E 00

I	R(I)/RP	ETA	XI	ETAPS	ETANG	I	R(I)/RP	ETA	XI	ETAPS	ETANG
1	1.0000	-1.70099E-01	2.00000E 01	2.06115E-09	1.70088E-01	5	1.0617	-1.69691E-01	1.85083E 01	9.16100E-09	1.69670E-01
9	1.0870	-1.69745E-01	1.69859E 01	4.19889E-08	1.69702E-01	13	1.1364	-1.70397E-01	1.54346E 01	1.98080E-07	1.70304E-01
17	1.1905	-1.71926E-01	1.38576E 01	9.58557E-07	1.71665E-01	21	1.2500	-1.75453E-01	1.22610E 01	4.73281E-06	1.73961E-01
25	1.3158	-1.81715E-01	1.06529E 01	2.36316E-05	1.77593E-01	29	1.3889	-1.87690E-01	9.04784E 00	1.17645E-04	1.83046E-01
33	1.4706	-1.92076E-01	7.46643E 00	5.71967E-04	1.91101E-01	37	1.5625	-1.96781E-01	5.93809E 00	2.63706E-03	2.03015E-01
41	1.6667	-2.01171E-01	4.50607E 0C	1.10418E-02	2.20847E-01	45	1.7857	-1.97312E-01	3.23300E 00	3.94390E-02	2.47823E-01
49	1.9231	-1.70053E-01	2.19649E 00	1.11192E-01	2.88233E-01	53	2.0833	-1.14224E-01	1.45699E 00	2.32937E-01	3.45135E-01
57	2.2727	-5.47593E-02	1.00541E 00	3.65894E-01	4.14844E-01	61	2.5000	-1.87369E-02	7.56617E-01	4.69251E-01	4.84697E-01
65	2.7778	-5.80902E-03	6.11868E-01	5.42337E-01	5.47863E-01	69	3.1250	-2.04686E-03	5.12644E-01	5.53030E-01	6.01170E-01
73	3.5714	-3.49413E-03	4.35321E-01	6.47057E-01	6.49746E-01						

YPN= 0. YNP= 2.57500E 00 YIN= 2.57413E 00

EXECUTION TIME IN MINUTES 0.18

Page 2

CYLINDRICAL PROBE CHARACTERISTIC

PI3	PI6	GAMMA	P	QT1	QT2
2.000E 01	1.000E 01	1.000E 02	7.200E-01	0.3240000	0.0324000

KT1	KT2	KT3	M	NCUB	NEND	NPRINT	MODE	KWIT	KBD	MCD
2	4	2	72	400	100	4	2	3	2	1

KEND 10 YPOS= 0.000000 YNEG= 8.2036 8.1691 8.2012 8.1705 8.1994 8.1719 8.1979 8.1732 8.1967 8.1745

KEND= 10 0.9 DECREASE IN MIX. QT1= 0.2916000 QT2= 0.0291600

KEND 20 YPOS= 0.000000 YNEG= 8.1958 8.1776 8.1915 8.1811 8.1890 8.1830 8.1876 8.1842 8.1869 8.1849

KEND 30 YPOS= 0.000000 YNEG= 8.1864 8.1853 8.1861 8.1855 8.1860 8.1856 8.1859 8.1857 8.1858 8.1857

KEND= 30 RESULT SUFFICIENTLY ACCURATE. YINY= 8.186E 00

KEND 37 YPOS= 0.000000 YNEG= 8.1858 8.1857 8.1857 8.1856 8.1856 8.1856 8.1855

LINK= 6 DETAG(1)= 1.49653E 00

LINK= 2 RETH= 4.52297E 01 RTRAP= 1.55663E 00 ETRAP= 6.08234E 01

YPOS= 2.0611536E-09 YNEG= 8.1854517E 00

I	R(I)/RP	ETA	XI	ETAPS	ETANG	I	R(I)/RP	ETA	XI	ETAPS	ETANG
1	1.0000	-1.71089E-01	2.00000E 01	1.03058E-09	1.71085E-01	5	1.0417	-1.70677E-01	1.85039E 01	9.20117E-09	1.70675E-01
9	1.0870	-1.70717E-01	1.69771E 01	4.23578E-08	1.70720E-01	13	1.1364	-1.71315E-01	1.54215E 01	2.00690E-07	1.71344E-01
17	1.1905	-1.72631E-01	1.38404E 01	9.75372E-07	1.72716E-01	21	1.2500	-1.75092E-01	1.22393E 01	4.83661E-06	1.75078E-01
25	1.3158	-1.79688E-01	1.06265E 01	2.42642E-05	1.78703E-01	29	1.3889	-1.85374E-01	9.01540E 00	1.21524E-04	1.84360E-01
33	1.4706	-1.91927E-01	7.42635E 00	5.93357E-04	1.92630E-01	37	1.5625	-1.99498E-01	5.88990E 00	2.76725E-03	2.04915E-01
41	1.6667	-2.06306E-01	4.45200E 00	1.15553E-02	2.23360E-01	45	1.7857	-2.03142E-01	3.17916E 00	4.16208E-02	2.51283E-01
49	1.9231	-1.73237E-01	2.15223E 00	1.16225E-01	2.92902E-01	53	2.0833	-1.13130E-01	1.42961E 00	2.39403E-01	3.50600E-01
57	2.2727	-5.22845E-02	9.91330E-01	3.70342E-01	4.19220E-01	61	2.5000	-1.77837E-02	7.51012E-01	4.71869E-01	4.88731E-01
65	2.7778	-5.76523E-03	6.07254E-01	5.44845E-01	5.50533E-01	69	3.1250	-2.05098E-03	5.08305E-01	6.01515E-01	6.03539E-01
73	3.5714	-3.26230E-03	4.31533E-01	6.49253E-01	6.52039E-01						

YPN= 6.51794E-03 YNP= 2.58847E 00 YIN= 2.58856E 00

EXECUTION TIME IN MINUTES 0.52

Page 3

SPHERICAL PROBE CHARACTERISTIC ' REPELLED PARTICLES AT ZERO TEMPERATURE

PTFF	PROBVF	SHEBDE	QT1	QT2
-1.900E 01	1.000E 00	9.544E 00	0.1000000	0.9000000

KT1	KT2	INITIA	M	NCUB	NFND	NPRINT	MODE	MCD
1	4	2	40	300	200	2	1	3

ATTRACTED PARTICLES MONO-ENERGETIC, PROBE DOES NOT ABSORB REPELLED PARTICLES

KFND= 10 RESULT SUFFICIENTLY ACCURATE, VINY= 6.170E 00

KFND= 30 RESULT SUFFICIENTLY ACCURATE, VINY= 3.380E 00

KFND= 40 RESULT SUFFICIENTLY ACCURATE, VINY=-5.349E 00

KFND= 60 RESULT SUFFICIENTLY ACCURATE, VINY= 1.136E 00

KFND= 80 RESULT SUFFICIENTLY ACCURATE, VINY= 4.990E-01

KFND= 90 RESULT SUFFICIENTLY ACCURATE, VINY=-2.868E-01

KFND= 100 RESULT SUFFICIENTLY ACCURATE, VINY= 5.119E-02

KFND= 120 RESULT SUFFICIENTLY ACCURATE, VINY= 1.799E-02

KFND= 140 RESULT SUFFICIENTLY ACCURATE, VINY=-3.966E-03

KFND= 160 RESULT SUFFICIENTLY ACCURATE, VINY= 1.950E-03

RELATIVE ERROR IN SHEATH EDGE POTENTIAL GRADIENT -0.000129 NEW SHEATH EDGE RADIUS

PL= 1.67717[illegible] 01 SL= 2.47917[illegible] 01 RW= 3.5566227E 00 OMEGA= [illegible]

RTRAP= 2.7600710E 00 ETRAP= 1.0484412E 00

V= 1.2700972E 01

I	R(I)/RP	ETA	XI	ETA NEW	I	R(I)/RP	ETA	XI	ETA NEW
1	1.00000	1.78752438 00	-1.50000000 01	1.78752438 00	3	[illegible]	[illegible]	[illegible]	[illegible]
5	1.60301	1.47902198 00	-6.40816398 00	1.47902238 00	7	[illegible]	[illegible]	[illegible]	[illegible]
9	[illegible]	[illegible]	[illegible]	[illegible]	11	[illegible]	[illegible]	[illegible]	[illegible]
13	2.62973	8.03501968-01	-1.60492798 00	8.03490268-01	15	2.86920	7.00107068-01	-1.20826[illegible]	7.00333078-01
17	3.05443	7.87969098-01	-8.55866918-01	7.87913368-01	19	3.24600	8.00227068-01	[illegible]	8.00126778-01
21	3.42060	8.13052158-01	-4.07606098-01	8.13000178-01	23	3.50172	7.89594168-01	-2.71431608-01	7.89650908-01
25	3.72001	7.66515428-01	-1.74952798-01	7.66503758-01	27	[illegible]	[illegible]	[illegible]	[illegible]
29	3.97619	7.97922998-01	-6.20833778-02	7.97000558-01	31	4.07000	7.00448118-01	-3.38660[illegible]	7.00070968-01
33	[illegible]	[illegible]	[illegible]	[illegible]	35	[illegible]	[illegible]	[illegible]	[illegible]
37	4.29610	7.77070978-01	-1.90340428-03	7.70903138-01	39	4.33900	7.03180038-01	-3.00487018-06	7.02976798-01
41	4.36701	7.06524798-01	-2.38418988-07	7.06836118-01					

EXECUTION TIME IN MINUTES 0.10

```
SPHERICAL PROBE CHARACTERISTIC * REPELLED PARTICLES AT ZERO TEMPERATURE
    PIFF       PROBVF     SHEDGE        DT1        DT2
-1.500E 01 1.000E 00 4.368E 00 0.1000000 0.9000000
  KT1 KT2 INITIA  M NOUB NEND NPRINT MODE MCT
   2   4    3  40  300  120    2    1    1
KEND  10 Y=   10.8585  10.9099  10.9418  10.9641  10.9808  10.9939  11.0045  11.0134  11.0209  11.0273
KEND  20 Y=   11.0329  11.0378  11.0420  11.0458  11.0492  11.0522  11.0549  11.0573  11.0595  11.0615

KEND=  20 RESULT SUFFICIENTLY ACCURATE. YINY=-3.298E-01
RELATIVE ERROR IN SHEATH EDGE POTENTIAL GRADIENT     0.021485 NEW SHEATH EDGE RADIUS  4.498E 00
KEND  30 Y=   11.1233  11.1261  11.1285  11.1306  11.1324  11.1339  11.1353  11.1365  11.1377  11.1386
KEND  40 Y=   11.1395  11.1403  11.1411  11.1417  11.1423  11.1429  11.1434  11.1438  11.1442  11.1446

KEND=  40 RESULT SUFFICIENTLY ACCURATE. YINY=-3.157E-02
RELATIVE ERROR IN SHEATH EDGE POTENTIAL GRADIENT     0.002104 NEW SHEATH EDGE RADIUS  4.512E 00
KEND  50 Y=   11.1457  11.1462  11.1465  11.1469  11.1472  11.1474  11.1477  11.1479  11.1480  11.1482
KEND  60 Y=   11.1484  11.1485  11.1486  11.1487  11.1488  11.1489  11.1490  11.1491  11.1492  11.1492
KEND  70 Y=   11.1493  11.1493  11.1494  11.1494  11.1495  11.1495  11.1496  11.1496  11.1496  11.1497

KEND=  70 RESULT SUFFICIENTLY ACCURATE. YINY=-1.184E-03
RELATIVE ERROR IN SHEATH EDGE POTENTIAL GRADIENT     0.000079 NEW SHEATH EDGE RADIUS
KEND  77 Y=   11.1497  11.1497  11.1497  11.1498  11.1498  11.1498  11.1498
LINK= 2 BETH= 8.94845E-01 RTRAP= 2.82175E 00 BTRAP= 1.46201E 00
Y= 1.1149826E 01
```

I	R(I)/RP	ETA	XI	ETA NEW	I	R(I)/RP	ETA	XI	ETA NEW
1	1.00000	1.3492968E 00	-1.5000000E 01	1.3492992E 00	3	1.32156	1.2891686E 00	-9.5534053E 00	1.2891754E 00
5	1.62775	1.0918986E 00	-6.4669521E 00	1.0919091E 00	7	1.91858	9.4994344E-01	-4.5279108E 00	9.4995816E-01
9	2.19405	8.5196165E-01	-3.2301171E 00	8.5198203E-01	11	2.45415	7.8436750E-01	-2.3251756E 00	7.8439504E-01
13	2.65888	7.3683794E-01	-1.6770283E 00	7.3886950E-01	15	2.92625	7.0933137E-01	-1.2049481E 00	7.0937660E-01
17	3.14226	6.9166106E-01	-8.5799348E-01	6.9170060E-01	19	3.34090	6.8247338E-01	-6.0237467E-01	6.8245326E-01
21	3.52418	6.7918116E-01	-4.1471386E-01	6.7902898E-01	23	3.69209	6.7960719E-01	-2.7823424E-01	6.7938551E-01
25	3.84464	6.8215932E-01	-1.8051171E-01	6.8187325E-01	27	3.98182	6.8763073E-01	-1.1210132E-01	6.8732761E-01
29	4.10364	6.9716205E-01	-6.5701723E-02	6.9691480E-01	31	4.21010	7.0922262E-01	-3.5597801E-02	7.0908830E-01
33	4.30119	7.2244216E-01	-1.7256737E-02	7.2247443E-01	35	4.37691	7.3558547E-01	-7.0657730E-03	7.3582311E-01
37	4.43727	7.4754656E-01	-2.1648407E-03	7.4800171E-01	39	4.48227	7.5737239E-01	-3.4713745E-04	7.5801964E-01
41	4.51190	7.6434233E-01	-2.3841858E-07	7.6507767E-01					

EXECUTION TIME IN MINUTES 0.46

SOLUTION OF Y DOUBLE PRIME = EXPF(Y)*(1.0-ERF(SQRTF(Y)))/2.0

YMAX	YI	NX	KXPRIN	NYP	KYPRIN
2.500E 01	5.000E-01	100	4	2450	50

Y	ETA	S	Y	ETA	S
0.	0.50000	0.	0.50000	0.26158	1.5937
0.00080	0.48443	0.0569	1.00000	0.21379	2.3522
0.00320	0.46962	0.1143	1.50000	0.18658	2.9705
0.00720	0.45551	0.1724	2.00000	0.16810	3.5152
0.01280	0.44206	0.2311	2.50000	0.15440	4.0122
0.02000	0.42924	0.2903	3.00000	0.14367	4.4750
0.02880	0.41700	0.3501	3.50000	0.13496	4.9117
0.03920	0.40532	0.4105	4.00000	0.12770	5.3274
0.05120	0.39416	0.4715	4.50000	0.12151	5.7259
0.06480	0.38349	0.5331	5.00000	0.11616	6.1099
0.08000	0.37328	0.5952	5.50000	0.11147	6.4813
0.09680	0.36351	0.6579	6.00000	0.10731	6.8418
0.11520	0.35415	0.7212	6.50000	0.10359	7.1926
0.13520	0.34518	0.7850	7.00000	0.10024	7.5348
0.15680	0.33659	0.8494	7.50000	0.09719	7.8692
0.18000	0.32834	0.9143	8.00000	0.09441	8.1966
0.20480	0.32043	0.9798	8.50000	0.09186	8.5175
0.23120	0.31283	1.0459	9.00000	0.08950	8.8326
0.25920	0.30552	1.1125	9.50000	0.08732	9.1422
0.28880	0.29850	1.1796	10.00000	0.08529	9.4467
0.32000	0.29175	1.2473	10.50000	0.08340	9.7465
0.35280	0.28526	1.3155	11.00000	0.08162	10.0420
0.38720	0.27900	1.3842	11.50000	0.07996	10.3333
0.42320	0.27298	1.4535	12.00000	0.07840	10.6207
0.46080	0.26717	1.5233	12.50000	0.07692	10.9045
0.50000	0.26158	1.5937	13.00000	0.07552	11.1848
0.	0.	0.	13.50000	0.07420	11.4618
0.	0.	0.	14.00000	0.07295	11.7358
0.	0.	0.	14.50000	0.07175	12.0068
0.	0.	0.	15.00000	0.07062	12.2750
0.	0.	0.	15.50000	0.06953	12.5405
0.	0.	0.	16.00000	0.06850	12.8034
0.	0.	0.	16.50000	0.06751	13.0639
0.	0.	0.	17.00000	0.06656	13.3220
0.	0.	0.	17.50000	0.06565	13.5779
0.	0.	0.	18.00000	0.06478	13.8316
0.	0.	0.	18.50000	0.06394	14.0832
0.	0.	0.	19.00000	0.06313	14.3328
0.	0.	0.	19.50000	0.06236	14.5804
0.	0.	0.	20.00000	0.06161	14.8262
0.	0.	0.	20.50000	0.06088	15.0702
0.	0.	0.	21.00000	0.06019	15.3124
0.	0.	0.	21.50000	0.05951	15.5529
0.	0.	0.	22.00000	0.05886	15.7918
0.	0.	0.	22.50000	0.05823	16.0291
0.	0.	0.	23.00000	0.05762	16.2648
0.	0.	0.	23.50000	0.05703	16.4991
0.	0.	0.	24.00000	0.05645	16.7319
0.	0.	0.	24.50000	0.05589	16.9633
0.	0.	0.	25.00000	0.05535	17.1934

SPHERICAL PROBE - ATTRACTED PARTICLES AT ZERO TEMPERATURE - NONDIMENSIONAL CURRENT = 1.2000E 03 , [illegible]

RUNGE-KUTTA ... WITH POWER SERIES

SSTART	VOLD	EPOLD	ENOLD	S	Y(1)	YZ	ETAPS	ETANS	N	JMAX	KSTOP
5.0000E 01	1.90423E-02	0.9812629	0.9811378	1.0400E 02	8.20376E-06	8.13115E-06	0.9991080	0.9991072	124	3	38

TRAPPING RADIUS IS 1.67??E 01 DEBYE LENGTHS

S	Y	AVIR	ETAP	ETAN	ALPHA	S	Y	AVIR	ETAP	ETAN	ALPHA
58.0000	0.0103	0.1367	0.9494	0.9897	0.0011	35.0000	0.0906	0.9796	0.9100	0.9136	0.0743
57.0000	0.0111	0.1693	0.9440	0.9890	0.0013	34.0000	0.1056	1.0301	[illegible]	[illegible]	[illegible]
56.0000	0.0119	0.1827	0.5407	0.9881	0.0314	33.0000	0.1233	1.1019	0.8893	0.8840	0.0121
55.0000	0.0128	0.1957	0.9471	0.9872	0.0015	32.0000	0.1439	1.1719	0.8716	[illegible]	0.0770
54.0000	0.0139	0.4115	0.4041	0.9862	0.0017	31.0000	0.1713	1.2407	0.8510	0.8429	0.1192
53.0000	0.0150	0.4277	0.5857	0.9851	0.0019	30.0000	0.2093	1.3335	0.8221	0.8111	0.1472
52.0000	0.0162	0.4418	0.9863	0.9839	0.0021	29.0000	0.2616	1.4269	0.7870	0.7600	0.2181
51.0000	0.0175	0.4614	0.9827	0.9826	0.0323	28.0000	0.3394	1.5306	[illegible]	[illegible]	0.3796
50.0000	0.0190	0.4809	0.9812	0.9811	0.0026	27.0000	0.4400	1.6461	0.6938	0.6309	0.6710
49.0000	0.0210	0.4993	0.9721	0.9792	-0.1765	26.0000	0.6271	1.7781	0.6324	0.5361	1.1631
48.0000	0.0226	0.5238	0.9770	0.9776	-0.0176	25.0000	0.9268	1.9200	0.5633	0.3907	1.0917
47.0000	0.0243	0.5632	0.5825	0.9760	0.1568	24.0000	1.5213	2.0619	[illegible]	[illegible]	2.7035
46.0000	0.0272	0.5871	0.9695	0.9731	-0.0062	23.0000	2.2210	2.2604	0.4293	0.1604	3.1904
45.0000	0.0297	0.5926	0.5694	0.9707	-0.0705	22.0000	3.5200	2.4701	0.3779	0.0121	[illegible]
44.0000	0.0321	0.6198	0.6735	0.9682	0.1046	21.0000	5.1035	2.7211	0.3390	0.0061	2.3391
43.0000	0.0346	0.6490	0.9591	0.9662	-0.1083	[illegible]	7.2385	[illegible]	0.3133	0.0007	1.8022
42.0000	0.0394	0.6803	0.9667	0.9614	0.1109	19.0000	10.0942	3.3251	0.2937	0.0000	1.2021
41.0000	0.0447	0.7134	0.9521	0.9561	-0.0870	18.0000	13.6200	3.7037	0.2651	0.0000	0.7115
40.0000	0.0489	0.7500	0.9577	0.9523	0.0096	17.0000	17.9031	4.1922	0.2000	0.0000	0.1912
39.0000	0.0550	0.7690	0.9424	0.9458	-0.0688	16.0000	22.3045	4.6875	0.2700	0.0000	-0.4205
38.0000	0.0617	0.8110	0.9441	0.9402	0.0700	15.5000	25.1706	4.9960	0.2000	0.0000	-0.7300
37.0000	0.0704	0.8766	0.9321	0.9320	-0.0070	[illegible]	[illegible]	[illegible]	0.2032	0.0000	-1.0976
36.0000	0.0802	0.9254	0.9226	0.9230	-0.0115	[illegible]	31.5570	5.7075	0.2067	0.0000	-1.4002